Eidgenössische Technische Hochschule Zürich
Swiss Federal Institute of Technology Zurich

Institute of Design, Materials and Fabrication
Laboratory of Composite Materials and
Adaptive Structures

Master Thesis No. 15-048

Adaptation and study of a filament winding machine for in-situ consolidation of thermoplastic composites

Javier Molina Blanco

Advisor: Dr. Joanna Wong

IDMF – Laboratory of Composite Materials and Adaptive Structures
Prof. Dr. Paolo Ermanni
ETH Zürich

28.09.15

ETH Zürich
IDMF - Laboratory of Composite Materials and Adaptive Structures
LEE O 203
Leonhardstrasse 21
8092 Zürich

Telefon: +41 (0)44 633 63 02

www.structures.ethz.ch

Abstract

This thesis studies the automated filament winding process. Its two objectives are: 1) The restauration of a filament winding system functionality and system adaptation for the manufacturing of thermoplastic materials using commingled yarns and 2) The study of the effect of the system parameters on the consolidation degree of the final parts, and defining the processing window for the studied material that optimize its consolidation.

In order to recommission the filament winding system the numeric control machine is restored and the necessary systems for the machine adaptation for manufacturing thermoplastic composite materials are designed. The newly implemented components are calibrated to obtain the systems work range and instrumental uncertainty.

In order to investigate the automated filament winding process, 5 different processing variables are investigated. The experiments aim to study the influence of: 1) The main heat source temperature, 2) The preheating system temperature, 3) The process feed rate, 4) The compaction force and 5) The fiber tension over the consolidation degree of the final parts. The consolidation degree is evaluated through the mechanical properties of the produced specimens. Two different test methods are carried out to characterize the mechanical properties, the cylinder radial compression and the short beam strength test. To double check the mechanical results the void content is also quantified on the specimens. The void content is characterized as follows: First the cylinder's density is compared with the theoretical composite density at 0% void content. Second the void content of some specimens is calculated analyzing the cross section of the cylinders with an image processing program. Finally the obtained results of the first method are corrected with the more accurate results of the second method. The material used during the experimental investigation is a Twaron – Polyamide 6 commingled yarn. The material I characterized in order to know the relevant properties.

It is shown that all the studied parameters have a significant effect on the final cylinders consolidation degree. The best consolidation degree is obtained for a process feed rate between 5 and 20 mm/s, a main heat source temperature between 450-460°C. The compaction force is set to its maximum value 200N and the fiber tension to the minimum value that lets to the proper filament control 4N. Finally the preheating temperature is set to a temperature where the yarn is molten during the travel through it. The mechanical and void content results match with a correlation of 93.47%. The optimal set of process parameters enable to manufacture a cylinder with 94% of interlaminar shear stress of a reference manufactured by compression molding and a difference in the measured void content of 0.1%. The same parameter set has been used to manufacture cylinders of different dimensions and those maintain the consolidation degree.

Zusammenfassung

Diese Thesis studiert das automatisierte Filament Winding Verfahren. Die zwei Objektive sind: 1) Die Restauration von einem Faserwickel Funktionssystem und der Systemanpassung für die Herstellung von thermoplastichen Materialen mit der Benutzung von vermischten Garne und 2) Die Studie von dem Effekt des Systemparameters in dem Konsolidierungsgrad von den Abschlussteilen, und die Definierung des Prozesses für das studierte Material, welches Ihre Festigung optimiert.

Um zu recommision Das Faserwickelsystem, die numerische Kontrollmaschine ist restauriert und die notwendigen Systeme für die Maschineanpassungen zur Herstellung von thermoplastischen Verbundmaterialen entworfen. Die neue implementierte Komponente sind kalibriert um den Arbeitsbereich zu bestimmen und Instrumente ungewissenheit zu kriegen.

Um die automatischen Prozesse der Faserwickel zu untersuchen, wurden 5 verschiedene Prozessvariabeln studiert. In den Experimenten wurde der Einfluss von: 1) Der Hauptwärmequelle, 2) Der Vorwärmungtemperatur, 3) Der Prozessversorgungsquote, 4) Die Verdichtungskraft und 5) Der Faserkraft des Konsolidationsgrad der Endprodukte. Der Konsolidationsgrad wird bewertet durch die mechanischen Eigenschaften von den hergestellten Proben. Zwei verschiedene Proben werden durchgeführt um die mechanische Eigenschaften, den radialen Kompressionswert des Zylinders, sowie die Stahlenfestigkeitsprüfung zu charakterisieren. Zum Überprüfen der mechanischen Ergebnisse, wird auch der Porengehalt auf den Proben quantifiziert. Der Porengehalt wird folgendermaßen charakterisiert: Zuerst wird die Zylinderdichte mit der theoretischen Kompositdichte, welche 0% Poren aufweist, verglichen. Danach wird der Porengehalt durch die Analyse des Querschnitts des Cylinders mittels eines Fotoprozessorprogramms bestimmt. Am Ende wurden die erhaltene Werte der ersten Methode durch die neuen und präziseren Werten der zweite Methode ersetzt. Das Material, welches bei dieser experimentellen Forschung verwendet wurde ist ein Twaron – Polyamide 6 Mischgarn. Das Material wird charakterisiert um die relevanten Eigenschaften zu kennen.

Es hat sich herausgestellt, dass die studierten Parameter einen signifikanten Effekt auf den hergestellten Cylinder Konsolidierungsgrad haben. Der optimale Konsolidierungsgrad wurde für ein Prozess zwischen 5 und 20 mm/s und einer Hauptwärmequellentemperatur von 450-460 ºC ermittelt. Die Verdichtungskraft wird im Maximalwert 200N fixiert und die Faserspannung im Minimumwert. Dies resultiert in der besten Filamentkontrolle 4N. Schließlich, wird die Vorwärmungtemperatur in einer Temperatur fixiert, bei der das Garn geschmolzen wird. Die mechanischen Eigenschaften und der Porengehalt stimmen in den Ergebnissen in einem Wert von 93.47% überein. Die optimalen Prozesse ermöglichen die Herstellung von einem Zylinder mit 94% interlaminare Schubspannung und einer Differenz im Porengehalt von 0.1%. Die gleichen Parameterstellungen wurden benutzt um verschiedene Zylindergrößen herzustellen und sind im Konsolidierungsgrad enthalten.

ETH
Eidgenössische Technische Hochschule Zürich

Department of Mechanical and Process Engineering
Laboratory of Composite Materials and Adaptive Structures

ETH Zurich
Leonhardstrasse 27
CH-8092 Zurich

Student:	Molina Blanco, Javier	
	ETH-Nr: 14-910-764	Departement: MAVT
	Hochschule (if external student): Universitat Politècnica de Catalunya	
Thesis:	Title: Restoring, Redesigning, and Testing of a Research Scale Filament Winding Machine for Thermoplastic Composites	
	Kind of Thesis: MA	Semester: FS 2015
Supervisor:	Prof. Dr P. Ermanni	
Advisor:	Wong, Joanna	

Start of the work:	16/02/2015
Intermediate presentation (Zwischenpräsentation):	22/05/2015
Final presentation (Endepräsentation):	16/09/2015
Deadline delivery final report:	30/09/2015

Introduction

(Framework for the project, problem statement, motivation)

Filament winding is an easily automated industrial process by which fibre tows can be impregnated with resin, moulded around a mandrel, consolidated, and demoulded to form hollow products such as pipes and pressure vessels.

In this Masters thesis project, a partial filament winder (including tensioners, transverse motor, rotary motor) and control system will be reinstated and redesigned for the filament winding of thermoplastic composites intermediate materials such as commingled yarns and bicomponent fibres. Figure 1 shows a schematic of typical filament winding process used for thermoplastic composites.

In this design project, a research scale filament winding machine is to be restored, missing composites designed and produced, and machine functionality demonstrated. Ideally, the machine should be designed to:

- accept a variety of fibre roving
- have the ability to adjust fibre tension
- apply consolidation pressure and temperature
- produce sheets and cylinders as end products

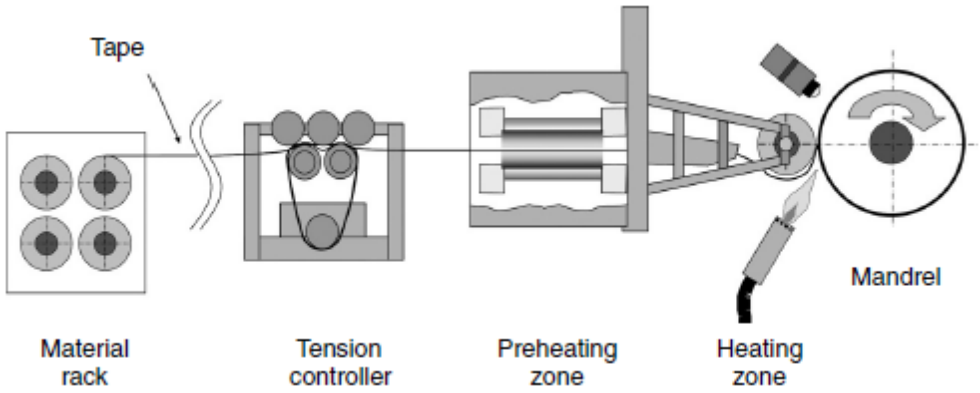

Figure 1 - Image taken from Advani et al.

The processing parameters of the filament winding machine will be investigated through their effects on the mechanical properties of the consolidated thermoplastic laminates.

Objectives

(Goals, Approach, expectations, deliverables)

The goal of this work is to restore functionality of the filament winder system, adapt the machine to the processing of thermoplastic composite intermediate materials, study the effects of processing parameters on the mechanical properties of a thermoplastic composite material and define a suitable processing window for the filament winding of this material on the restored equipment.

The approach of this project will be to setup an existing research scale filament winder, to design and build any missing components necessary for the filament winding of commingled yarns (including the fibre guide system, heating system, and mandrel), and test the mechanical properties of produced parts as a function of processing parameters.

Through this project, the student is expected to learn and demonstrate understanding of the filament winding machinery, the software used to control the filament winding system, the material properties of commingled yarns, and the effects of filament winding processing parameters on filament winded parts.

At the end of the project, detailed documentation on the hardware and software of the filament winder is to be delivered along with a recommended processing window for one type of thermoplastic commingled yarns.

Work breakdown

The work will be mainly subdivided in the following tasks:

1. **Initial setup of the filament winding machine from storage condition:** The 2-axes filament winding machine is to be reinstalled after long term storage and the basic functionalities of the control system and the mechanical parts tested and repaired, if necessary. Components required for the filament winding of commingled yarns and bicomponent fibres that have been lost or never acquired are to be identified.

2. **Design and fabrication of missing components:** The missing components identified in Task 1 are to be acquired, either by design and fabrication, or through purchase. These parts are likely to include the fibre guide system, the heating system, and mandrel.

3. **Design and implementation of control system software program for filament winding of a part:** The student will familiarize him/herself with the basic software needed to program the filament winder.

4. **Characterization of intermediate materials:** The melt and/or glass transition temperatures of available thermoplastic intermediate materials will be measured using DSC. Fibre volume content of these intermediate materials will be determined using TGA.

5. **Trouble shooting completed filament winding system:** Initial trials at filament winding will be attempted using commingled yarns and any unforeseen problems will be identified and sovled.

6. **Investigation of Process Parameters:** A design of experiment that examines the various parameters of consolidated temperature, roving tension, winding speed, will be undertaken for a chosen commingled yarn.

7. **Microstructural Study:** The void content of the produced samples will be studied using optical and scanning electron microscopy.

8. **Mechanical Testing:** The mechanical properties of the stamp formed samples will be tested.

The organization of the work is depicted in following table. The estimated deadlines are also shown.

Date	16-Feb-2015	23-Feb-2015	2-Mar-2015	9-Mar-2015	16-Mar-2015	23-Mar-2015	30-Mar-2015	6-Apr-2015	13-Apr-2015	20-Apr-2015	27-Apr-2015	4-May-2015	11-May-2015	18-May-2015	22-May-2015	25-May-2015	01-Jun-2015	08-Jun-2015	15-Jun-2015	22-Jun-2015	29-Jun-2015	06-Jul-2015	13-Jul-2015	20-Jul-2015	27-Jul-2015	03-Aug-2015	10-Aug-2015	17-Aug-2015	24-Aug-2015	31-Aug-2015	07-Sep-2015	14-Sept-2015	16-Sep=2015	21-Sept-2015	28-Sept-2015	30-Sep-2015
Week	1	2	3	4	5	6	7	8	9	10	11	12	13	14		15	16	17	18	19	20	21	22	23	24	25	26	27	28	29	30	31		32	33	
Task 1																																				
Task 2																																				
Task 3																																				
Mid-term presentation															**X**																					
Task 4																																				
Task 5																																				
Task 6																																				
Task 7																																				
Task 8																																				
Final presentation																																	**X**			
Writing Report																																				
Submit Report																																				**X**

Bibliography

Provide relevant publications, technical reports, Web-links… **and previous Student Thesis** to help the student getting started.

Koussios, S., (2004) *Filament Winding: A Unified Approach* . PhD Thesis, Technische Universiteit Delft, The Nederlands.

Zaniboni, C. (2010) *Oligomere Technologies for Cost-Effective Processing High-Performance Polyphthalamide Composite*, PhD Thesis, ETH Zurich, Switzerland.

Advani, S. G. and Hsiao, K-T, *Manufacturing techniques for polymer matrix composites (PMCs)*, Woodhead Publishing Limited, 2012.

Please consider

- Directives and useful information about Student Projects at the Centre of Structure Technology are available online at: https://www1.ethz.ch/structures/education/projects/Richtlinien.pdf
- Don't forget to register for the thesis under "My Studies" www.myStudies.ethz.ch at the begin of the semester
- A signed copy of this document has to be included in the final report

Zurich, 14/04/2015

Tutor:

Dr. J. Wong

Supervisor:

Prof. P. Ermanni

ETH

Eidgenössische Technische Hochschule Zürich
Swiss Federal Institute of Technology Zurich

Declaration of originality

The signed declaration of originality is a component of every semester paper, Bachelor's thesis, Master's thesis and any other degree paper undertaken during the course of studies, including the respective electronic versions.

Lecturers may also require a declaration of originality for other written papers compiled for their courses.

I hereby confirm that I am the sole author of the written work here enclosed and that I have compiled it in my own words. Parts excepted are corrections of form and content by the supervisor.

Title of work (in block letters):

ADAPTATION AND STUDY OF A FILAMENT WINDING MACHINE FOR IN-SITU CONSOLIDATION OF THERMOPLASTIC COMPOSITES

Authored by (in block letters):

For papers written by groups the names of all authors are required.

Name(s):	**First name(s):**
MOLINA BLANCO	JAVIER

With my signature I confirm that

- I have committed none of the forms of plagiarism described in the 'Citation etiquette' information sheet.
- I have documented all methods, data and processes truthfully.
- I have not manipulated any data.
- I have mentioned all persons who were significant facilitators of the work.

I am aware that the work may be screened electronically for plagiarism.

Place, date	**Signature(s)**
Zürich, 25/09/2015	

For papers written by groups the names of all authors are required. Their signatures collectively guarantee the entire content of the written paper.

Table of contents

Part 3. Appendix

List of Figures

List of Tables

List of Symbols

U_a	Error of the variable a.
S_a	Standard deviation of the variable a
$t_{(0.95;N-1)}$	Student's t- distribution coefficient for a confidence interval of 95%, and N-1 degrees of freedom.
F	Force
F_i	Minimum spring load
F_s	Maximum spring load
K	Spring constant.
ΔL	Compressed spring length
L_0	Spring free length
L	Spring length
δi	Minimum spring deformation value.
δs	Maximum spring deformation value
E_{pe}	Elastic potential energy
W_t	Torsion resistance
d	Spring wire diameter
D	Spring diameter.
N	Number of coils
τ	Shear stress
G	Stiffness modulus
q	Spring tension correction factor.
U	Spring buckling correction factor
d_{out}	Outer cylinder diameter
d_{in}	Inner cylinder diameter
e	Cylinder thickness

V	Cylinder volume
$Vf\%$	Fiber volume content
ρ_i	Density material i
ρ_{th}	Theoretical composite density
m	Cylinder mass
$V\%$	Void content %
N_{void}	Number of pixels digitalized as void on the cylinder section analyze
N_{total}	Total number of pixels on the image analyzed

Chapter 1

Introduction

1.1 Background

The technological progress of the different fields of engineering increasingly requires products that are more reliable, efficient, economical, as well as ecological. The new composite materials generation represents one of the tools to satisfy those society requisites when the optimization is looking for a solution in the weight - mechanical behaviour relationship, as well as abrasion resistance properties among others.

The demand for a lightweight solutions is growing in several areas, from lightening the mass of a microchip press structure in order to extend the life of its bearings, replacing the monocoque of a vehicle to reduce fuel consumption, or to produce a membrane for an artificial heart that deforms the desired proportion when tensed by the blood pressure in order to direct the blood flow in the desired paths and on the desired conditions.

However, most of the composite materials currently available cannot yet satisfy the economical requirements of the product, since they are expensive compared to conventional materials. As a result, high volume production has not increased as much as the variety of applications that they can be applied in. Due to this, improvement of the manufacturing techniques of these lightweight materials is still needed.

The use of thermoplastic composites is promising in overcoming the limitations of the tradition epoxy matrix composites. Thermoplastic composites offer noticeable advantages, such as the ability to process them in shorter cycles. They require just a phase transition from molten to solid state whereas the thermosetting requires a longer curing process to allow the chemical reaction. Thermoplastics also possess higher toughness, the possibility of pieces being reworked once they are manufactured and recyclability, an important fact in an increasingly environmentally aware society.

Nevertheless, the complicated impregnation of thermoplastics due to the high viscosity of the polymer and the fact that processing times are longer than the thermosets makes them still a difficult choice for the nowadays industry. Therefore thermosets are currently far more extensively produced in the industry than thermoplastics. The use of intermediate composite materials that are already impregnated (tapes) or non-impregnated materials as commingled yarns ease the thermoplastic impregnation, bringing a new opportunity to take profit of its material advantages.

Filament winding is a fabrication technique mainly used for manufacturing composite open or closed end structures. The process involves winding filaments under tension over a male mandrel. In a basic filament winding machine the mandrel rotates while the delivery head on a carriage moves horizontally laying down the filament in the desired pattern. The best mechanical performance of high performance composites is achieved when fibers are well aligned in the matrix. This makes filament winding a promising manufacturing process for composite thermoplastic materials, as it is a process that offers the possibility to build up the structure with a well desired fiber position and orientation, as well as alignment. Moreover it is a process that can be completely automated, bringing the possibility to adapt it into a production line for high volume production, reducing the produced parts cost. Figure 1.1 show a filament winding machine manufacturing a pressure vessel.

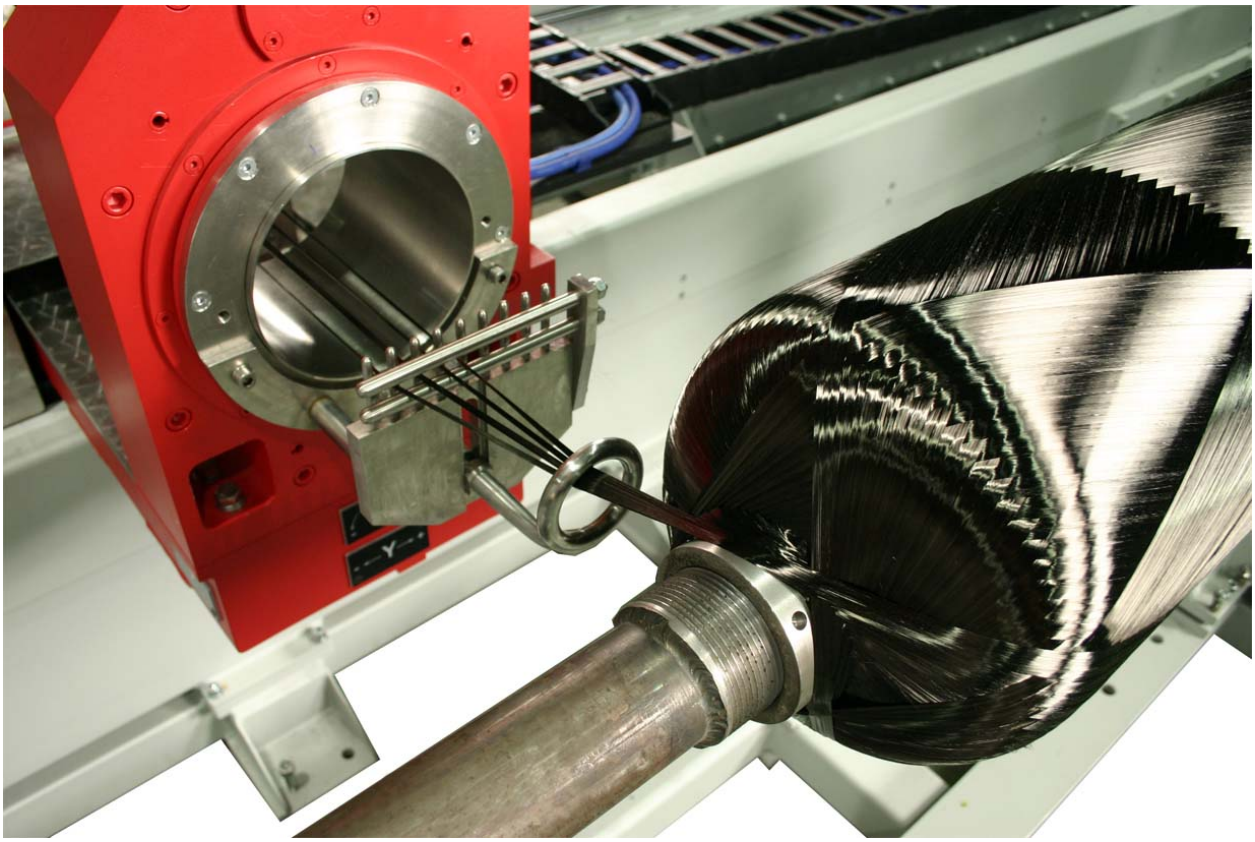

Figure 1.1. Filament winding machine. Carriage, multi-filament delivery head and mandrel included. Image property of MIKROSAM, control automation robotics

1.2 Examples of filament wound parts

Filament winding process is a manufacturing composite technique highly extended nowadays in different areas such as industry, marine or aerospace. It is normally used for manufacturing axially symmetrical open and close end structures, such as pipes, pressure vessels or tanks. Figure 1.2 and Figure 1.3 show some parts examples manufactured by the company Circomp. However filament winding with thermoplastics is not completely adapted in industry yet. The challenging manufacturing process for thermoplastics put them in a second place in comparison with the thermosets manufacturing, already fully stablished in the industry. The recyclability and reprocessing capability of the thermoplastic materials as well as the lack of curing time during the process together with the intermediate preimpregnated and non-impregnated materials available nowadays (commingled yarns,

bicomponent fibers and powder impregnated fibers) has revive the interest for the thermoplastic materials processing. Airbone Oil & Gas (AOG) in 2012 manufactured thermoplastic composite pipes installed in a pipe line at 2140 meter water deep in Brazil [22].

At any rate, the thermoplastic filament winding process keep being investigated. Some investigations has already focused in the thermoplastic filament winding manufacturing parts geometries such as S. K. Mazumdar and S. V. Hoa that manufacture non axisymmetric elliptical rings [33] or Gruber and Lamontia that manufacture thick cylinders combining filament winding and tape placement with two delivery heads, one of the produced parts is shown in Figure 1.4 [15]. Figure 1.5 show a bearing manufactured by the company Circomp of CF-PEEK by filament winding of thermoplastic composites.

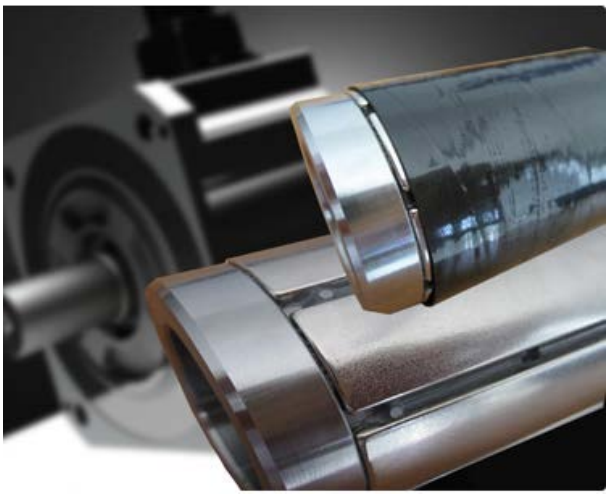

Figure 1.2. Composite sleeve for brushless DC electric motor. Image property of Circomp.

Figure 1.3. CFRP mast sunawning. . Image property of Circomp.

Figure 1.4. Thermoplastic cylinder of CF-PEEK. Image property of Accudyne systems, Inc.

Figure 1.5. Bearing CF-PEEK. Image property of Circomp.

1.3 State of the art

Today, established companies in different industries produce high performance composites using the filament winding process. Examples include high-grade composite tubes for aerospace and maritime structures among others. The majority of these companies are completely dedicated to the use of thermoset materials. Therefore the filament winding process using thermosets has been already highly investigated. That same situation is not happening with thermoplastic composites.

The difficulty of the thermoplastics processing (complicate impregnation, long cycles), reduced the adaptation of these materials to the nowadays industry. However, the generation of some intermediate materials, that are already impregnated or materials that ease the impregnation reopened the interest for the thermoplastic process.

Aiming the process improvement (cost reduction, short cycle times, process parameter set up) several studies have focuses on the optimization of the filament winding process with thermoplastics. They investigate the process working with preimpregnated material (tapes) or flexible intermediate materials such as powder impregnated fibers or commingled yarns. These studies investigated the influence of the process parameter in the quality of different final parts by using different materials, testing methods and reference manufacturing techniques. In 1992 Colton and Leach studied the influence of the process parameters over CF-PEEK open-ended cylinders, determining the quality of the parts from surface finish to void percentage [9]. In 1993 Lauke and Friedrich investigated the process parameters in ring specimens using GF-PA12 powder impregnated fiber. They tested mechanical properties of the specimens using axial beam flexure and double cantilever beam tensing. In 2001 Lee studied the thermoplastic filament winding process using GF-PP resin commingled yarn in ring specimens. The quality of the final part is quantified by measuring the void volume percentage of the polished cross sections of each specimen [9]. In 2011 Maffezzoli created a preliminary simulation of a heat transfer along the roving during the filament winding process using GF-PP commingled yarn comparing it with the experimental results [13].

Another of the important process points is to make it capable for manufacturing different geometries in order to adapt the producible products to the components necessities. Some researchers have focused on this point. Mazumdar and Hoa manufactured non-axisymmetric elliptical rings in 1995 [33]. Toso (2002) manufactured the reinforcement frames of a train coaches with tape winding process, using GF-PP tapes.

At the present time, some companies are already manufacturing high performance thermoplastic products. For example, Accudine System was, in 2002, able to produce thermoplastic rings for deep-sea pressures and different tubular profiles of CF-PEEK, which is manufactured with the combination of tape winding and the tape placement process. The mechanical results show higher properties than the reference postprocessed in autoclave [15, 24]. Other studies are focusing on the adaptation of thermoplastic materials for industry. Friedrick (2003) presented two technical ways for the production of self-lubricant slide bearings for severe environmental and load conditions [37]. Arhant, Davies, Burtin and Briançon (2015) presented the use of thermoplastic composites for underwater applications [2].

1.4 Objectives

This work will focus on the filament winding process of thermoplastic composites using commingled yarn intermediate materials.

There are two main objectives:

1. The restoration of the filament winding system functionality and system adaptation for the manufacturing of thermoplastic materials using commingled yarns.
2. The study of the effect of the system parameters on the consolidation degree of the final parts. Defining the processing window for the studied material that optimize its consolidation and providing the necessary data for the development of a consolidation model for the process.

1.5 Approach

The approaches of this thesis are the filament winding system recommissioning and the process experimental investigation.
In order to recommission the filament winding process, these actions are necessary: The Control Numeric Machine is restored; the control program that governs and coordinate the process axis is understood and different programs are created for the experimental investigation. The fiber guide system, the heating and preheating systems, the compaction system and the mandrel are designed and manufactured. The newly implemented components are calibrated. Finally the system functional parameters are set up for the machine to be capable of manufacturing cylinders laying down the yarn over the mandrel on the desired position, to obtain accurate parts geometry.

The goal of the experimental process investigation is to find the optimal processing window in order to process cylinders having the optimal consolidation degree and to demonstrate if the results can be maintained for different parts dimension. The consolidation degree is quantitatively judged in function of the mechanical properties and the void volume % of produced specimens.

1.6 Novelty of the research

In this investigation the filament winding process using Twaron-Polyamide 6 commingled yarn is investigated. This investigation provides information about the process parameters set up to manufacture the commingled yarn Twaron - PA6 and the material necessary characterization data.

The process parameters window has been investigated and defined for this material aiming to obtain the best consolidation degree of the cylinders manufactured. The parameters defined for the study are: heat source temperature, feed rate, compaction force, fiber tension and preheating temperature. This are the parameters remarked to be the more influential in previous investigations with similar intermediate materials as powder impregnated fibers [27] or commingled yarns using other materials [21].
However this investigation presents the experimental parameter investigation following a sequential order to obtain the best specimen consolidation degree. The specimen consolidation degree is quantified by mechanically testing the specimens. The mechanical results are later double checked with the void content analyze results.

As this is the first set-up of the CMAS Lab filament winding machine, a basic parameter investigation has been necessary to perform in order to obtain the elements range and effect of them over the material.
In addition to the standard investigation, the thickness and length variation of the specimens is investigated in function of the main source temperature variation and process feed rate variation.
A longer and a thicker specimen is manufactured with the same process parameters and the effect of the dimension variation over the consolidation degree of the specimens is observed.

1.7 Thesis overview

This thesis is organized in the following way:

In Chapter 2, an overview of the filament winding process for manufacturing thermoplastic materials is presented.

Chapter 3 includes the CMAS Lab filament winding machine layout and the design considerations of the implemented elements.

In Chapter 4, the implemented elements on the filament winding system are calibrated in order to know the work range, the magnitude applied and general error of each element.

Chapter 5 presents the studied material candidates for the experimental investigation, an outline of the filament winding of thermoplastic intermediate materials, and the methods and results of the material characterization.

Chapter 6 describes the process parameters investigated. The different experiments for the parameter study are explained. It also presents the methods and results for the two mechanical specimen tests, the radial cylinder compression and the short beam strength test and the methods and results of the void content characterization. Finally, the temperature measurements of the cylinders during the process is shown.

Chapter 7, includes the main achievements of this study and the outlook for the filament winding process of thermoplastic materials using commingled yarns.

Chapter 2

Introduction to automated filament winding with in-situ consolidation

This section gives and overview of the filament winding process for in-situ consolidation.

Thermoplastic filament winding is a continuous composite fabrication technique involving winding composite filaments under tension over a male support commonly called mandrel. During the process the thermoplastic polymer must be heated up over the melting temperature and compacted against the mandrel in order to achieve the composite consolidation. The high viscosity thermoplastics have to impregnate all the reinforcing material during the process, which represents a challenging issue for the winding parameters. To ease the material impregnation, intermediate materials already impregnated or post-impregnated materials (bicomponent fibers, commingled yarns,) with short flow distances to achieve during the wetting impregnation are used in the process. The process velocity, the temperature and the consolidation pressure (created by the fiber tension and the compaction force) are the main process parameters.

The working materials, the phenomena occurring during the process, the main process steps and the motion control system are described below.

2.1 Working materials

Composite materials for filament winding are delivered in spools as shown in Figure 2.1. The delivered filaments have a textile behaviour with the enough flexibility to be wound around the male mandrel.

In the thermoset process the reinforcing filaments are normally delivered on the spools and impregnated with the thermoset matrix during the process by using a resin bath or other different impregnating technology. The parts once wound need to be cured in a postprocess.

This thesis focus in the thermoplastic filament winding process. Thermoplastic materials for filament winding are delivered on spools which includes the thermoplastic material and the reinforcing fiber mixed in different preform states.

Figure 2.1. Filament winding spools, Twaron. Image property of TEIJIN

2.1.1 Commingled yarns

Due to the high viscosity of the thermoplastic materials, it is necessary to combine the matrix with the reinforcing fibers already in the preform stage in order to achieve very short flow paths during the impregnation. To achieve this short flow paths different preforms can be obtained for product manufacturing in filament winding [36].

The filament winding preforms can be divided in fully consolidated tapes, in which the micro and macro impregnation is done in the pre-form, and post-impregnated fibers. These last group is delivered just with a physical mixing of the reinforcing and thermoplastic materials. In the post-impregnated products the impregnation of the fiber by the matrix thermoplastic occurs during the winding process which requires and accurate parameters conditions. Some of the fibers included in this group are: powder impregnated fibers with and without shell, bicomponent fibers or commingled yarns between others. Figure 2.2 illustrate the different non-impregnated material preforms [29, 49].

As semi-finished materials the fiber volume content is fix therefore no variations can occur in the volume fiber % during the process [29] always that the process parameters are correct. It is possible to suffer some fiber % variations if the matrix is squeezed out by the consolidation pressure or there is material loses as the adhesion of the thermoplastic on the compaction cylinder.

Despite the fully impregnated materials or prepregs do not require to achieve the impregnation during the process, these preforms are relatively stiff and boardy, limiting the possible geometries to achieve and making them more suitable for the manufacturing of more simple and smooth parts or big components. The cost of the prepregs is also higher compared with the post-consolidated intermediate materials. In contrast the post-consolidated materials possess a textile behaviour until the material is consolidated what let to manufacture more complicate geometries and small parts. Also are cheaper than prepegs an important factor for large volume production. This make them an interesting focus of research for the nowadays industry.

Inside the family of post-impregnated intermediate materials, the powder impregnated fibers more known as FIT (Fiber Impregnated Thermoplastic) presents the reinforcing material in fiber form, this is coated with the thermoplastic material in powder form and covered with a thermoplastic shell. There is a large variety of thermoplastic materials presented in that preform state. Bicomponent fibers consist in a liquid crystalline polymer with a higher melting point and the matrix which is a polymer covering the

reinforcing fiber with a lower melting point. Bicomponent fibers are completely recyclable as they are a fully thermoplastic product.

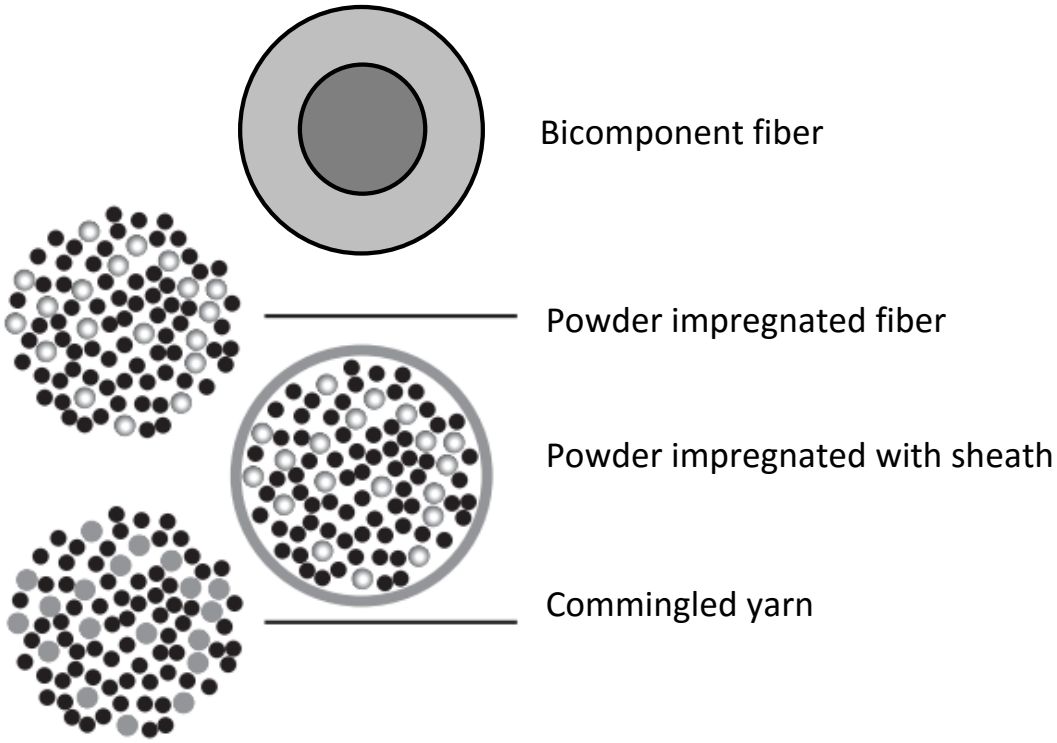

Figure 2.2. Intermediate materials for filament winding. Image modified property of ETHz 15302

This thesis study the filament winding process for in-situ consolidation using commingled yarns as raw material.

The commingled yarn is a semi-finished material that presents both the thermoplastic material and the reinforcing material in fiber form aligned and mingled in the tow.

As a post-impregnated preform the impregnation and rest of consolidation is achieved during the manufacturing process, right after the heat zone when the thermoplastic is heat up over the melting temperature [43]. A consolidation force is needed to distribute the thermoplastic around the fibers.

Commingled yarns are produced by hybrid yarn manufacturing, a cost effective process that makes the material more affordable than other prepregs. Additionally, they provide the capacity to address a number of challenging issues of traditional composites, including long term storage, shorter processing cycles, and the final part possess normally minor brittleness that some thermoset matrices because of the different polymer bonds [30]. They can be obtained in different preform states such as unidirectional layers, woven fabrics or braids [44].

One of the outstanding of the commingled yarns is his potential of intimate blending between the thermoplastic and reinforcing fiber while simultaneously maintaining the flexibility of the original fiber tow. As main drawback, the fiber can be damaged during the commingling process and the commingling degree is not always ideal [6, 21]. Moreover there is a limit of the available polymer fibers that can be

obtain in that preform state and the commingling process add an additional cost to the material compared with the direct impregnation.

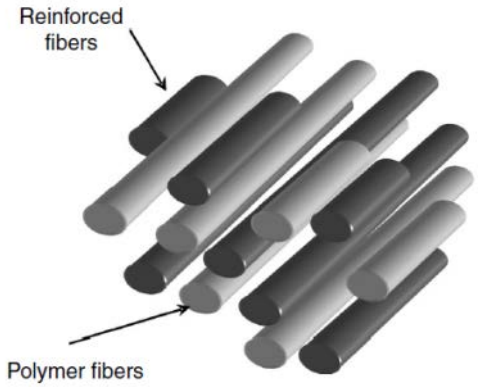

Figure 2.3. Commingled yarn. Image property of Manufacturing Techniques for Polymer Matrix Composites (PMCs). Woodhead Publishing

Some researchers also have investigated the thermoplastic filament winding process with online impregnation as Friedrich [16, 17] or W. Radford and M. Hedin that in 2015 achieved direct fiber impregnation using a 3D printer combined with a filament winder for the online consolidation of their cylinders of GF-PET [51]. As advenatges the direct impregnation do not require of the use of intermediate products which are more expensive than the raw materials, and the fiber volume content can be modified during the process. However this process add difficulties on the process parameters set up and the quality of the final parts need to be improved.

2.2 Phenomena occurring during the process

During the filament winding process the thermoplastic material has to achieve the complete composite consolidation. To reach that, the thermoplastic material must reach the melting temperature to later embed the reinforcing material on the matrix.

Different phenomena occur simultaneously during the consolidation. When the thermoplastic is molten, a compaction pressure is applied to achieve an intimate contact between the reinforcing fiber and the thermoplastic material, the resin flow across and in between the fibers forcing it to heal occurring the autoadhesion of the polymer flow fronts, the fiber deformation, the molecular interdifusion of the polymer molecules across the interface between tows and the diffusion of air and volatiles in the molten matrix. The voids are the result of the entrapped air [21, 29, 49].

If the exposure time or temperature of the material is exceeded, it will lead to the material degradation.

Those phenomena occur in a short time interval and in a very local area, the nip point. The nip point is the first contact point between the yarn and the mandrel surface. That leads to the necessity of an accurate process parameters selection. The parameter that influence in the consolidation are: the material viscosity; the consolidation pressure and heat exposure time [21]. The consolidation and impregnation time also depends on the on several material properties such as the polymer viscosity, the surface tension, the fiber permeability and the driving forces [29].

2.3 Winding Process

The filament winding process for in situ consolidation is divided in four main steps: The material supply, the tension application and control, the material heating and the material compaction (to achieve the material consolidation). The material is supplied by the material rack, the tension on the fiber is normally applied in the tension control unit, if it is installed a tension control, or it is naturally generated for the mandrel pulling the fiber in case of the lack of that tension unit (in that last case the tension is not controlled and vary during the process). The heating and consolidation of the material occur on the nip point. The nip point is the location where the incoming filament comes into contact with the mandrel. The material is heated by the main heater and the compaction is produced by the application of a compaction force through a roller on the nip point by a compaction device and also generated for winding the fiber under tension over the mandrel. Figure 2.4 shows the schematic of a filament winding process with thermoplastics. Figure 2.5 shows an image of the nip zone.

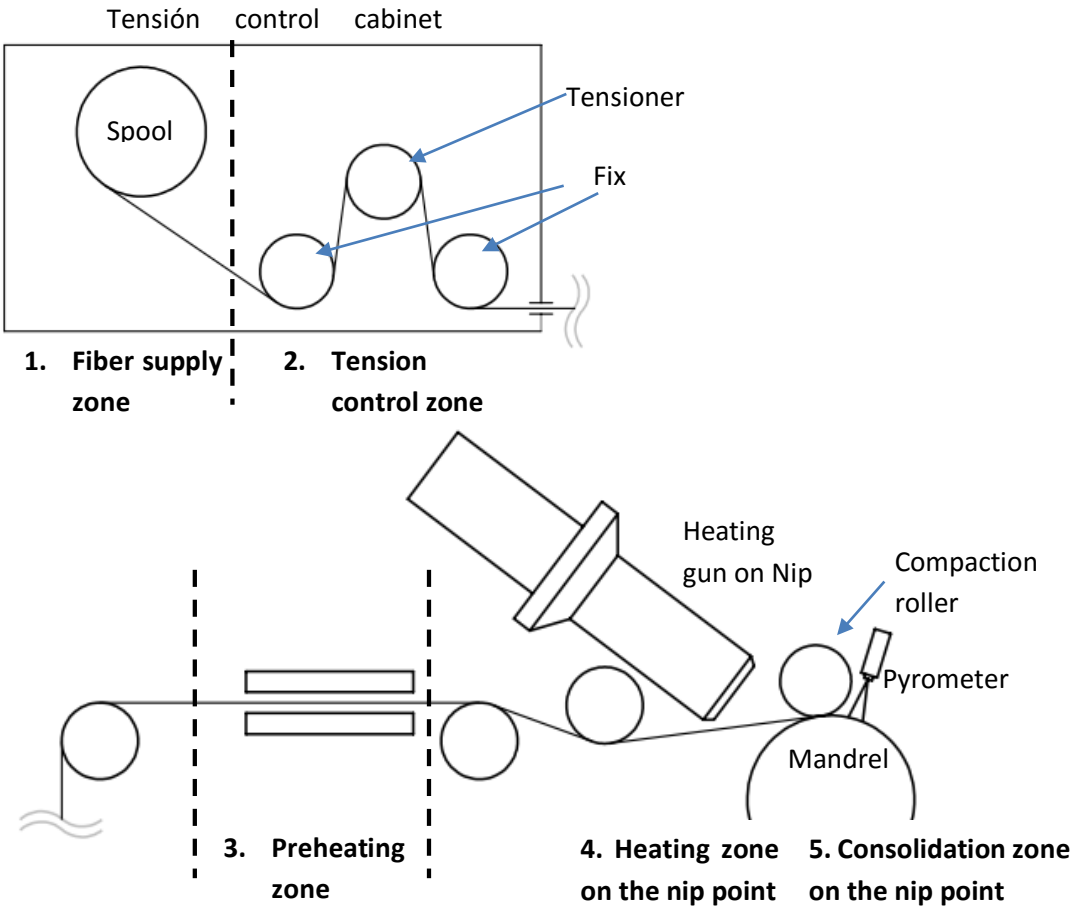

Figure 2.4. Schematic of filament winding process for in-situ consolidation

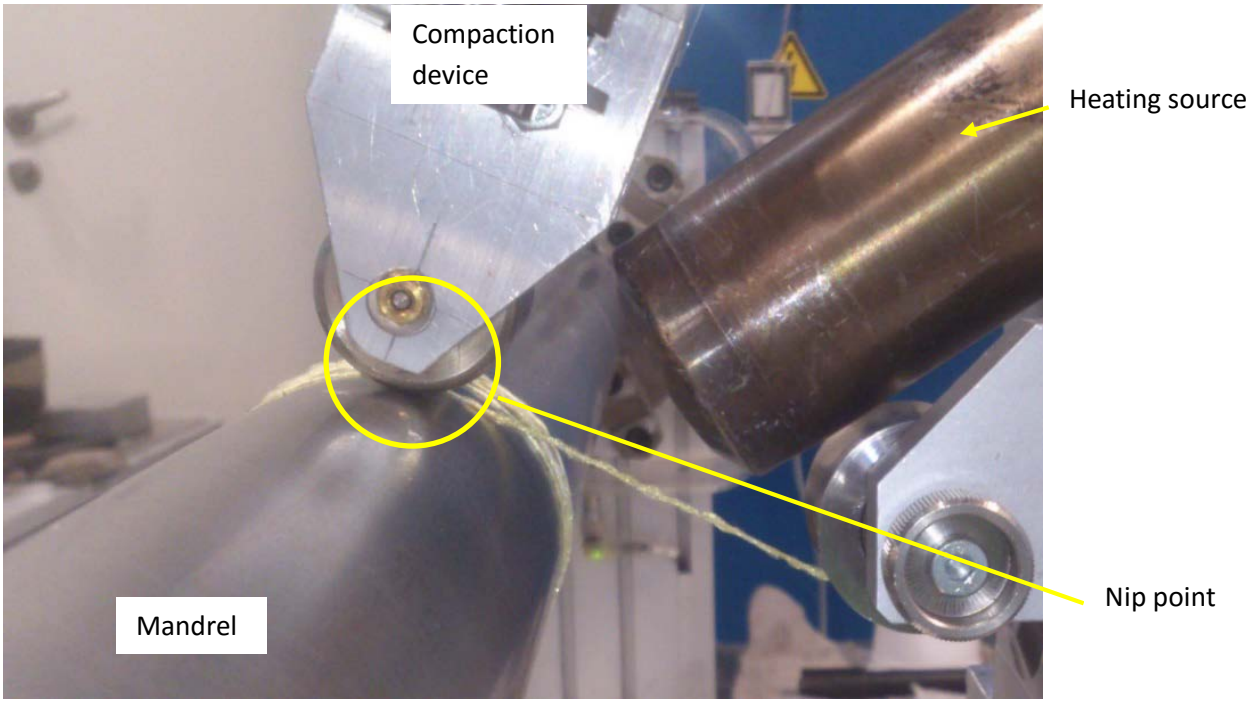

Figure 2.5. Compaction force and heating applied on the nip point

2.3.1 Material supply

The material supply is the first step on the filament winding process. The intermediate material, preimpregnated or not, is delivered in spools and mounted on the material rack. The number of spools can vary depending on the delivery head winding technology. The tensioner system and control can also be installed in the material rack, to set and control the desired tension for each spool. In that case the material rack could have a driven axis installed to control the process feed rate and with it the fiber tension.

2.3.2 Tension control system

A tension adjustment device applies the tensile force on the filament setting the tension. The tension can be controlled by mechanical adjustment devices or with a control system with a more accurate control. Figure 2.6 shows a spool creel with a fiber tension control system. The tension is applied by a dancer arm driven by a pneumatic cylinder. A tension control is normally installed on the process to set, measure and correct the tension maintaining it in the set desired value.

The filament tension induce a consolidation pressure on the fiber by being wound over the mandrel. That consolidation induce internal stress on the final part. An inhomogeneous tension conditions will generate and inhomogeneous residual stress on the manufactured part. To avoid it a tension control is normally installed to homogenise and maintain the tension during the process.

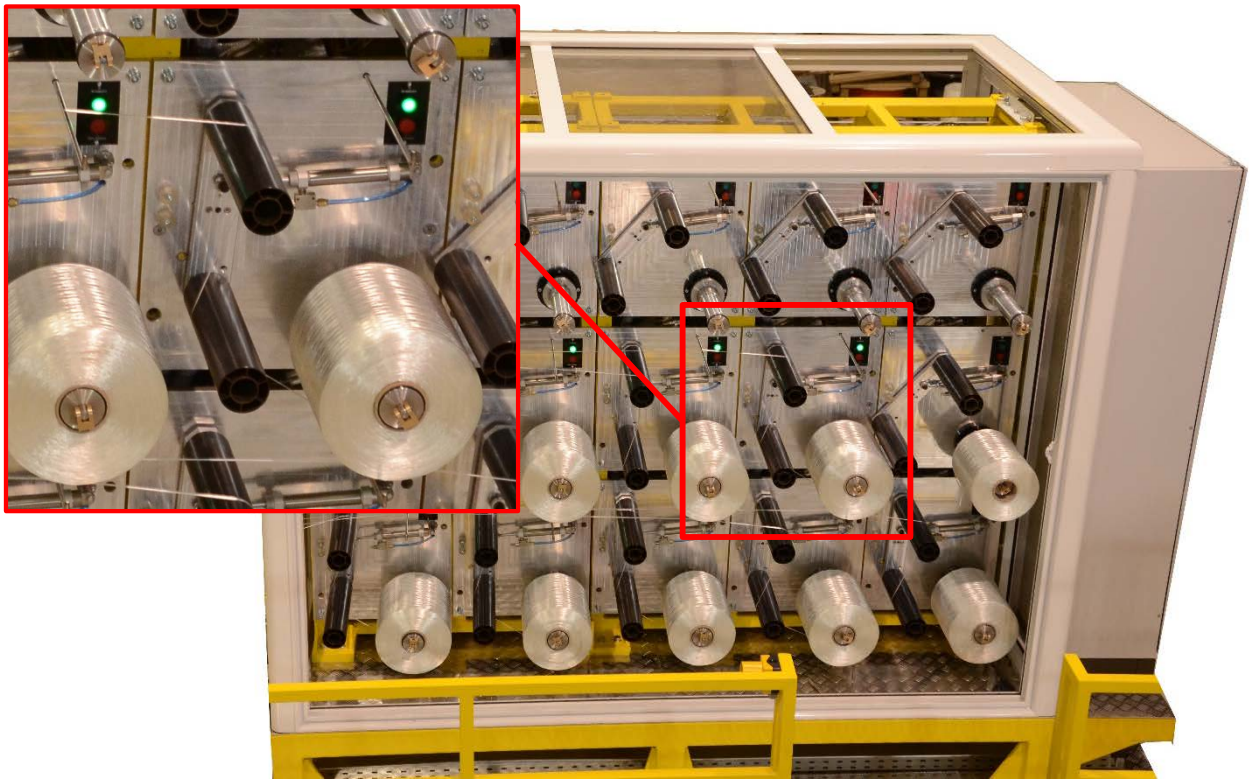

Figure 2.6. Fiber tensioner creel. Computer Controlled Electronic Tension System. Image property of Mikrosan.

2.3.3 Material heating

Main heat source

In filament winding for in situ consolidation the heat source applies the heat on the nip point. During the process the material is heated over the melting temperature to achieve the impregnation of the reinforcing fibers and consolidation of the final part. As the impregnation and consolidation of the thermoplastic is occurring in a very short time interval, the heating temperature and the exposure time of the thermoplastic composite has to be accurately controlled in order to maintain the temperature of the material over the melting point and under the degradation temperature to obtain a good final part quality. Being the exposure time of the fiber directly dependent of the winding velocity, the heat source highly affect on the consolidation quality and processing cost and can provoque process irregularities [9, 21, 27, 46].

Preheating source

The preheating source, as the name indicates, preheats the yarn before to arrive to the nip point. It is applied to support the main source to achieve the material consolidation in cases such as high process velocity, high thermoplastic melting temperature, low performance of the main force or thickness specimens [29]. On the preheating system the material is heated approximately at the melting temperature and the composite preconsolidates due to the fiber tension. The yarn cool down once is outside the preheating with the contact of the guiding elements. Figure 2.7 shows the temperature distribution along the process with the preheating influence [9].

Lauke and Friedrich (1993) demonstrate in their experimental investigation that the influence of the preheating has a positive effect in the specimen consolidation [27].

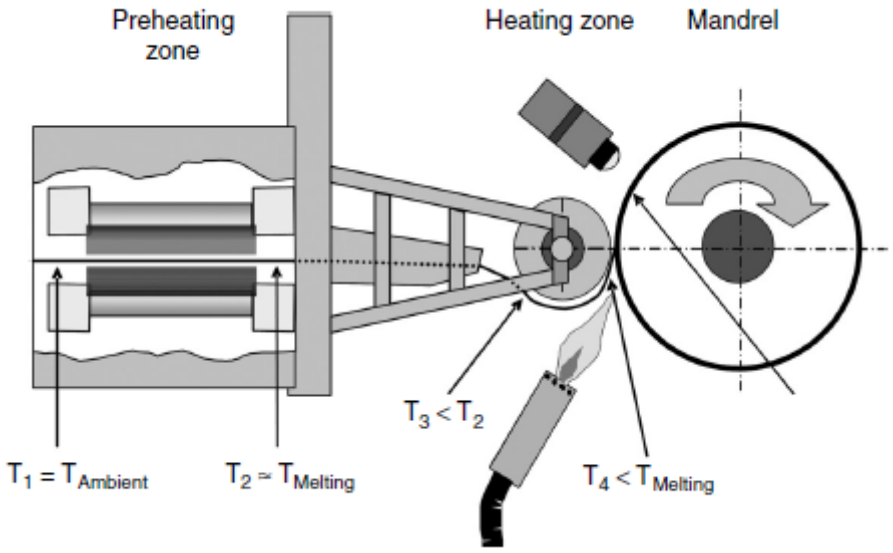

Figure 2.7. Preheating effect on the filament temperature. Image property of PMCs, Woodhead Publishing.

2.3.4 Material compaction

Once the material is heated up over the melting temperature, is wound around the mandrel while compacted to achieve the consolidation. The consolidation pressure is usually applied by a compaction system through a compaction roller on an adaptable compaction head, locally applied on the nip point. The fiber tension also applies a consolidation pressure on the filament but this pressure depends on several factors besides the fiber tension such as the material temperature and viscosity [27].

2.3.5 Mandrel

The mandrel is the male support in which the filament is laid on during the process producing hollow products as final parts. The mandrel provides the desired geometry for the wounds specimens. In filament winding for in-situ consolidation the compaction system must adapt to the mandrel geometry in order to maintain the compaction area and obtain and uniform consolidation.

There are different types of mandrel used depending on the geometry and finality of the manufacture component. For closed geometries as pressure vessels is impossible to extract the mandrel once the part is wound and consolidated if it is solid. There are different mandrel types to solve that problem. The most commonly used are [40]:

- The dissolvable cores, like sand mandrels where once the part is wound the mandrel is dissolved normally with water.
- Liners used as a mandrel, this component is never extract once the piece is finished, remains with it and it is considered in the part design.
- Comprehensible mandrels are used to ease or make possible the piece extraction without requiring the use of dissolvable mandrels.
- For big structures the mandrel is divided in different components to reduce the weight of the assembly and with it the process cost.

The mandrel can also have an additional heating system during the process to maintain the surface temperature control and to reduce the temperature difference between the yarn and the mandrel

surface. In a non-heated mandrel the surface temperature is not homogenous and increases during all the process due to the heater units.

2.4 Motion control

The motion control system include all the elements responsible for the regulation of the system behaviour. Normally the filament winding machines are controlled by a numerical controlled machine unit or similar. During the process all the machine axis are controlled for this elements determining the winding paths and the winding velocity of the yarn (created by the mandrel rotation and the carriage travel).

The filament winding operation can be performed by a winding machine or a standard industrial robotic with an adapted thermoplastic filament winding head.

The geometries that a winding machine is capable to produce depends on the number of axis installed [7]. The standard filament winding is a two axis machine, A the mandrel rotation, B the carriage travel (parallel to the mandrel). This machine is capable to wind pipes of all the dimensions. There are available on the market 4 and 6 axis machines. The 4 axis machine, C Distance between payout eye and mandrel, D payout eye rotation around the horizontal axis, is capable to properly manufacture pressure vessels and other concave structures such as bottles and tanks. The 6 axis machines, E payout eye rotation around the vertical axis, F change level of the payout eye, is capable to manufacture all kind of filament winding parts. There are winding machines with a greater number of axis on the market for more specific applications.

Figure 2.8. 6 axis filament winding machine. Image property of Engineering EHA (High-tech Assets).

Part 1

Design of filament winding for in-situ consolidation of thermoplastics composites

Chapter 3

System components description and design considerations

This section includes the description of the process layout and the Laboratory of Composite Material and Adaptive Structures (CMAS Lab) filament winding elements, as well as the design considerations to adapt the process to the manufacturing of composite materials for in-situ consolidation.

3.1 Machine layout description and elements description

The CMAS Lab filament winding machine layout is described in this section. The group consist of a WW2-0600-01450 winding machine belonging to Waltritsch & Wachter GmbH, the control unit, the fiber control cabinet and a pyrometer. Figure 3.1 shows the fiber tension control cabinet on the left side on the back and the winding machine at the front.

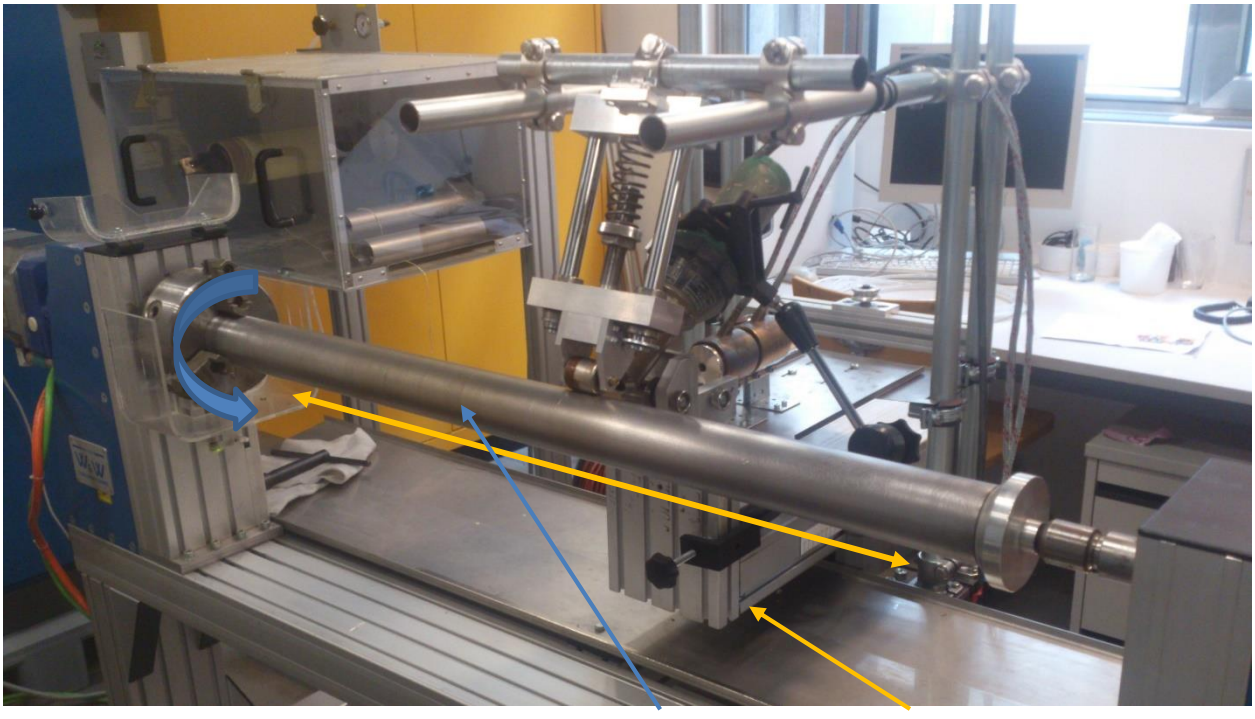

Figure 3.1. CMAS Lab filament winding machine

The WW2-0600-01450 winding machine is a two motion axis machine driven for the Numeric Control unit. One of the axis is the mandrel rotation and the other the carriage linear travel. As observed in Figure 3.1, the carriage moves parallel to the mandrel axis. Fixed to the carriage are all the elements that needs the transversal movement during the process. These elements are the heating and preheating system, the compaction force and the fiber guide system.

The maximum mandrel velocity is 185 rpm with a position accuracy of 0.04º. The maximum carriage velocity is 750mm/s with a position accuracy of 0.05mm. The machine is able to wind pipes up to 600mm diameter and 850 mm length. The machine technical data is included in APPENDIX A.1.

The control unit is a CNC module Sinumerik 840D NCU 571.3 and a PLC SIMATIK S7 with 32 inputs and 16 outputs from SIEMENS. The control unit controls two servo axis of the machine, the mandrel rotation and the carriage linear travel. It also power up and control the Servo Tension control (STC) module whose function is to maintain constant the set fiber tension. The CNC unit determines and controls the winding velocity and the winding paths during the process. The control system is prepared for 2 additional axis if it is desired.

The fiber control cabinet includes the spool axis and the dancer arm as shown in Figure 3.2. The spool axis is driven by the CNC unit which coordinates its rotation giving to the yarn the same linear velocity than the mandrel is requiring. The dancer arm cylinder applies through an air pressure arm a linear force over the yarn stabilising the winding tension. The air pressure arm is connected to the air pressure system through a regulator pneumatic valve that set the pressure of the pneumatic arm and with that the fiber tension. The tensions variations during the winding process are detected for the STC fiber control and corrected by increasing or decreasing the spool axis speed in order to free more or less fiber quantity until return to the set tension value.

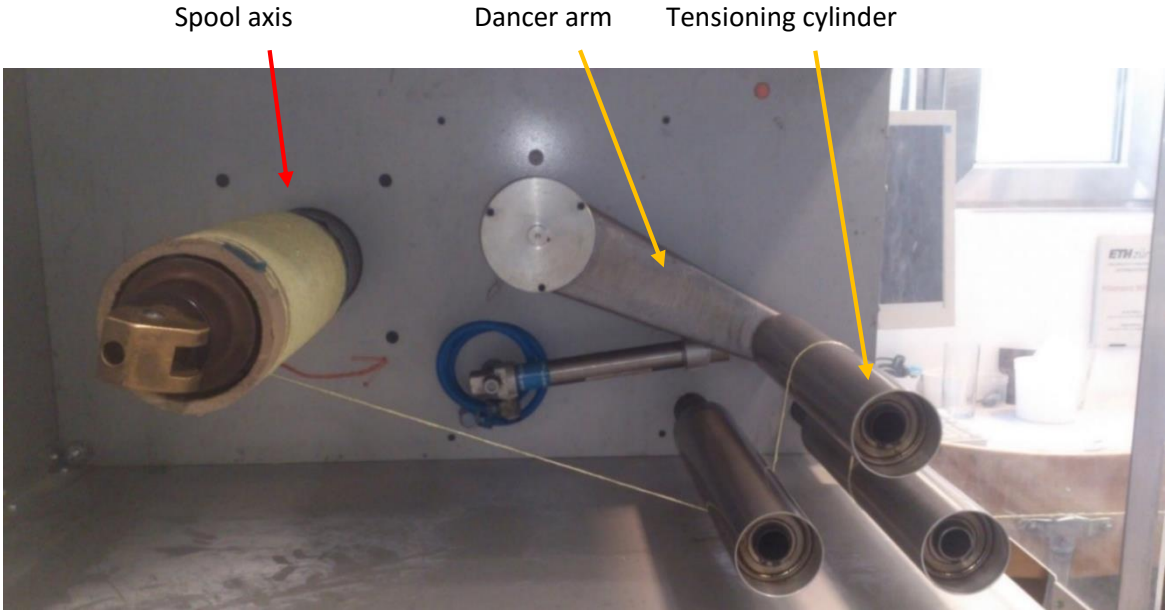

Figure 3.2. Tension control cabinet

Figure 3.3 shows the described and designed components of the CMAS Lab filament winding machine. It also shows the location of the pyrometer. The temperature on the yarn during the winding process is

measured with a pyrometer and the data are collected and controlled with the program INFRAWIN, from LUMASENSE technologies.

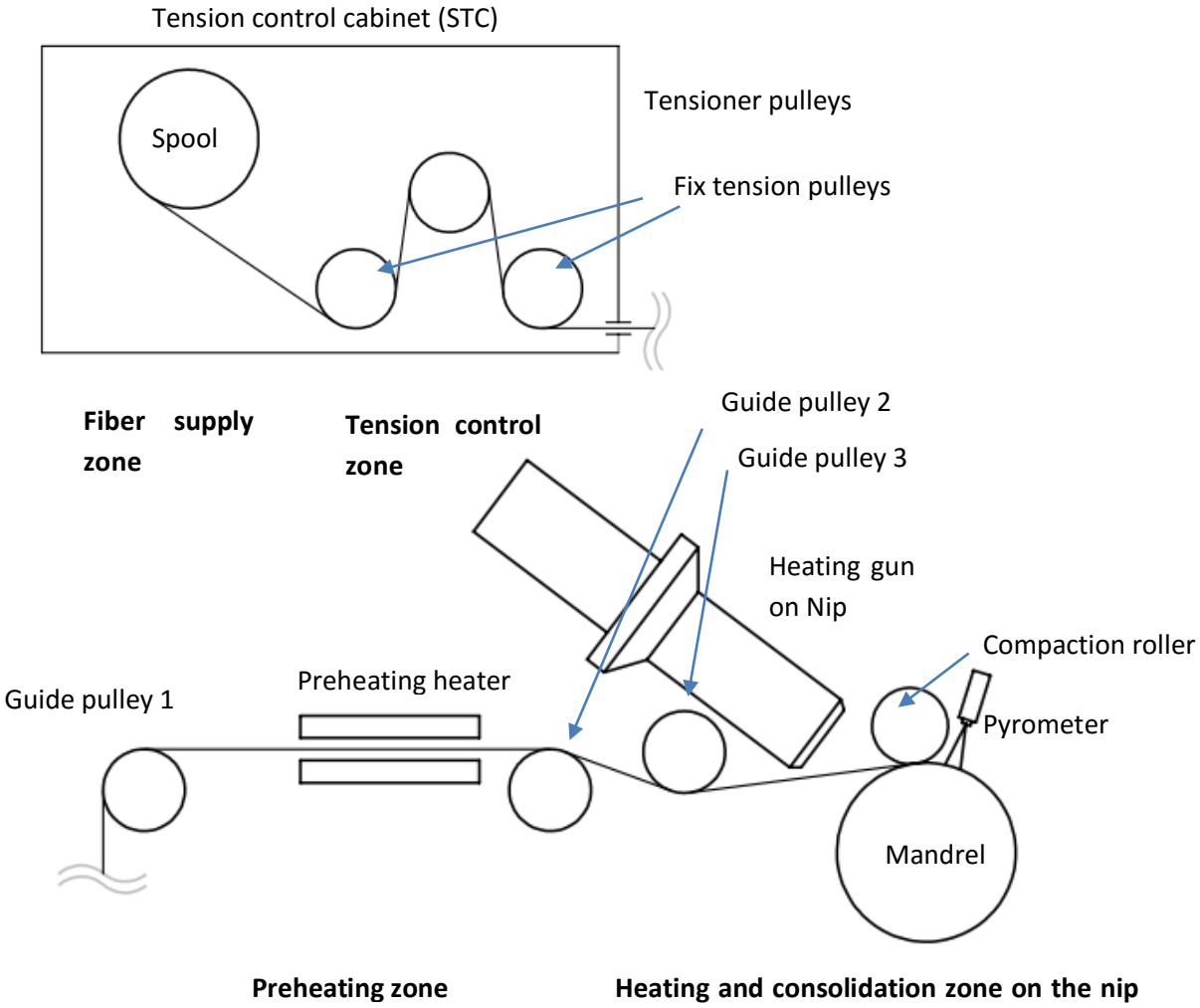

Figure 3.3. CMAS Lab Filament winding machine layout

The following systems are designed to adapt the machine for the manufacturing of thermoplastic composite materials [14, 42]:

- Fiber guiding system: A set of pulleys conducts the path of the yarn towards the mandrel.
- Heating system: A heat source to apply a local heat over the yarn on the nip point.
- Preheating system: A heat source to apply heat over the yarn before the nip point.
- Compaction force system: A system to apply the consolidation force on the nip point.
- Mandrel: Element with the desired part geometry.

3.2 Fiber guide system design

The fiber guide system is composed by the elements that conduce the fiber path from the fiber control cabinet until the mandrel. It is divided in two parts, the guiding inlet and the payout head. The guiding

inlet pulley is the first contact point of the yarn with the carriage (pulley 1 in Figure 3.3), it redirects the filament path thought the payout or delivery head. The delivery head is the last contact point between the fiber and the mandrel (pulley 2 and 3 in Figure 3.3), its function is to deliver the filament creating the desired winding paths.

The quality of the final parts depends on the fiber guide system precision, it prevents the creation of voids by twisted fibers or non-uniform layers. The discrepancies between the programmed yarn path and those in the fiber product are created on this system. Therefore an accurate design of the fiber guide system is fundamental for a proper final part quality.

The system has been designed with the objective of reducing the damage on the fiber created by the unavoidable friction forces caused by the contact of the guiding elements. To achieve that all the guiding elements are pulleys, minimizing the friction forces to avoid the yarn abrasion.

The guiding inlet consist in a polished steel pulley held by a structure of aluminum profiles from KANIA connected to the carriage. The pulley creates a 90º turn in the path of the fiber on the horizontal plane, in order to always maintain the same angle of path turning, independently of the carriage position as shown in Figure 3.4. If the contact angle between the fiber and the inlet pulley varies with the carriage movement, the friction created by the pulley and yarn contact will also vary causing a tension variation on the fiber during the process. With the 90º angle that variation is avoided [39].

The inlet pulley is positioned in the same horizontal plane as the control cabinet fiber outlet. If the cabinet outlet and the inlet pulley are at different heights the imbalanced friction forces induce a torque on the yarn twisting it during the process and consequently causing the fiber damage and void generation. [23, 39].

The fiber payout system or delivery head is positioned at the end of the carriage support. It consist in two pulleys that guide the yarn path through the yarn eye until the mandrel. The first (pulley 2) is a Teflon pulley with a guide machined on it to create a fix point between the inlet pulley (pulley 1) and the delivery head. Then the fiber path between the two pulleys will always have the same fixed trajectory and will able to position the preheating system. Pulley two is positioned in the same horizontal plain as the inlet pulley, again, to avoid the fiber twisting. The second pulley (pulley 3) is made of polished stainless steel to withstand the temperatures of the heating gun. This pulley will adapt the yarn path in function of the mandrel diameter making the angle transition as smooth as possible as shown in Figure 3.5.

Finally the yarn eye is the element positioned between the two pulleys made of stainless steel. Depending on the winding patterns desired if the movement of the carriage is too long and quick, the friction between the pulley 3 and the yarn is not sufficient to maintain the fiber in the correct trajectory. The function of the yarn eye is to deliver the yarn on those cases. It is completely polished in the entire inner surface to avoid the fiber damage. During the experimental work this element has not been used because the specimens are wound with radial winding. In radial winding the movement of the carriage is constant without sudden or contrary movements for what the friction on the yarn over the pulley is sufficient to deliver it in the correct position. Whenever possible, it is better to deliver the yarn just with the pulleys. The yarn eye increases the yarn friction and cause more damage on the fiber. Figure 3.5 shows the delivery head with the two pulleys installed. With this configuration there is no contact between the filament and the yarn eye.

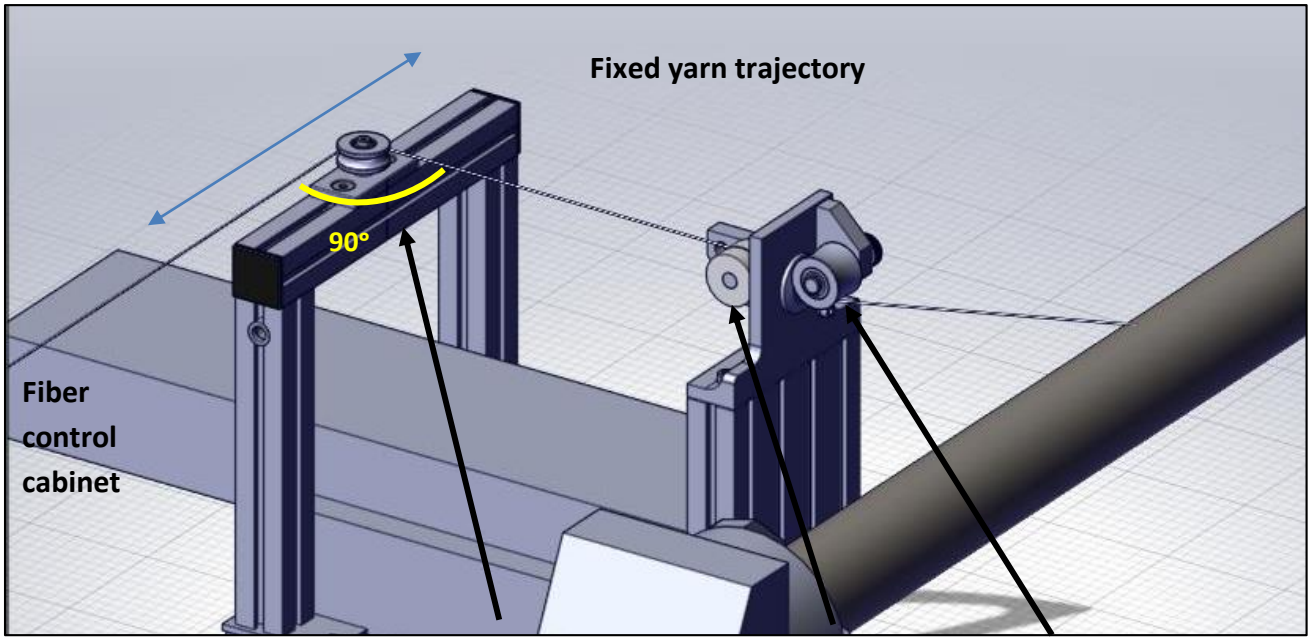

Figure 3.4. Fiber guide system

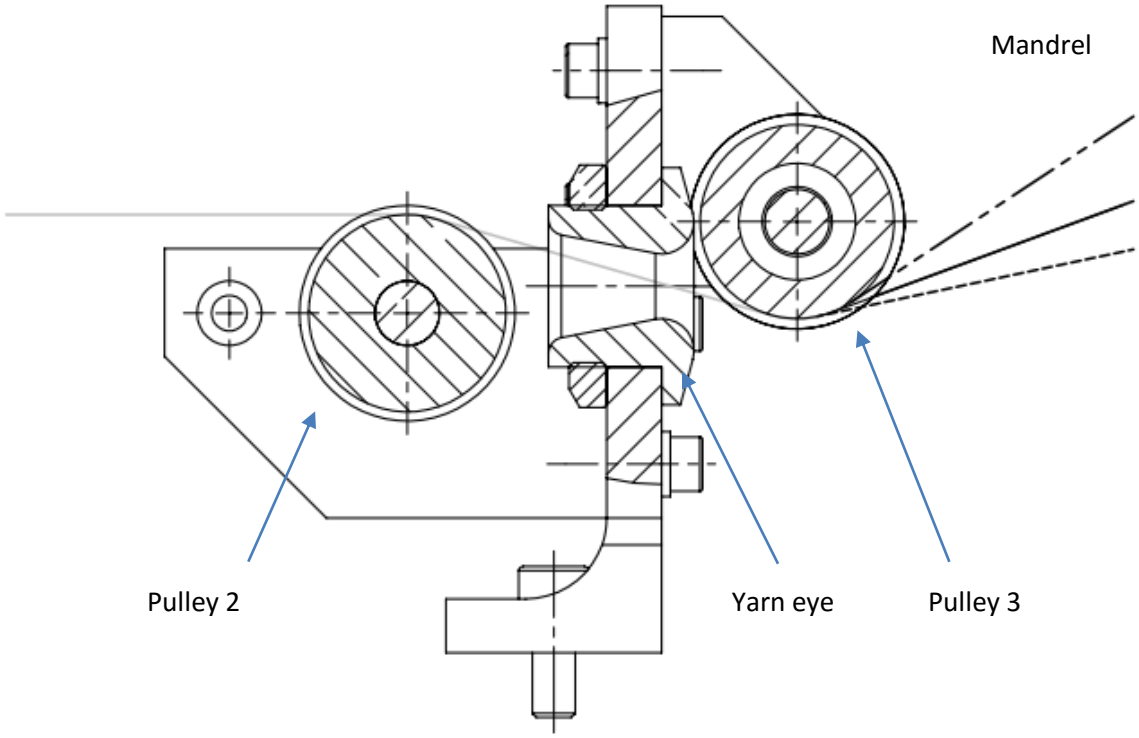

Figure 3.5. Fiber payout system with different yarn paths in function of the mandrel diameter.

3.3 Main heating system

The heat source influences notably on the final part properties and the processing cost. Each source and layout will cause a heat transfer and exposition time variation. There is a wide range of heating sources, R. Schledjewski and A. Miaris [47] offer a main source selection that evaluates the efficiency and cost processing for the tape placement process. The sources recommended are the laser, flame and hot gas torch. These sources are also the most commonly used in other researches for the commingled yarn manufacturing [8, 20, 21, 50].

The heat source selected is a heat air gun belonging to the CMAS Lab. The heat air gun is held by an articulated arm from FISSO. The articulated arm allows to position the heat gun in different layout positions. As shown in Figure 3.6 is positioned pointing the yarn on the upper part at the nip point. The calibration of the heat gun is explained in chapter 4.

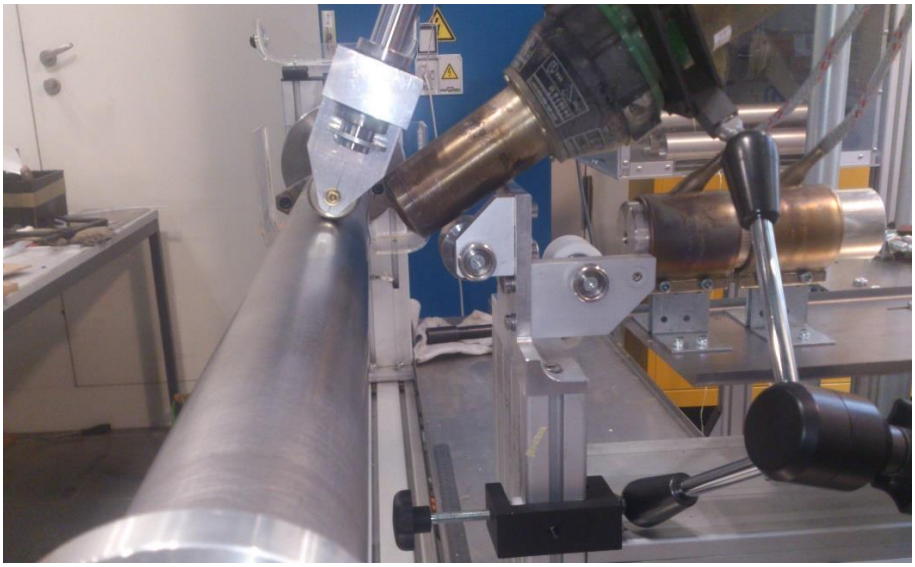

Figure 3.6. Heat gun and articulated arm.

3.4 Preheating system design

To preheat the yarn before arriving to the nip point a preheating system is designed. The preheating consist in two circular clamp heaters of 600W each one, with a maximum temperature of 400ºC. The heaters clamp an aluminium cylinder of 120mm length and an outer diameter of 50mm. The cylinder has a hole of 10mm diameter on the section centre.

The cylinder is heated by the electrical heaters power and it heats the yarn by convection and radiation when the yarn goes through it during the process. The resistance are hold by 4 L profiles of stainless steel, connected to a steel base of 1mm thickness. The base is clamped to the 4 legs of the compaction device structure as shown in Figure 3.7.

The power of the heaters is controlled with a variable phase angle regulator from United Automation, that enable to vary the voltage output from 0% to 98% of the input. Varying the power supplied to the resistance. The two heaters are connected in parallel to the variable tension regulator and the variable regulator is connected to a heatsink to dissipate the heat generated as shown in

Figure 3.8.

Due to the additional thermal inertia of the cylinder, once the temperature is established and arrives to the stationary conditions, the variation on the set up temperature is minimal.

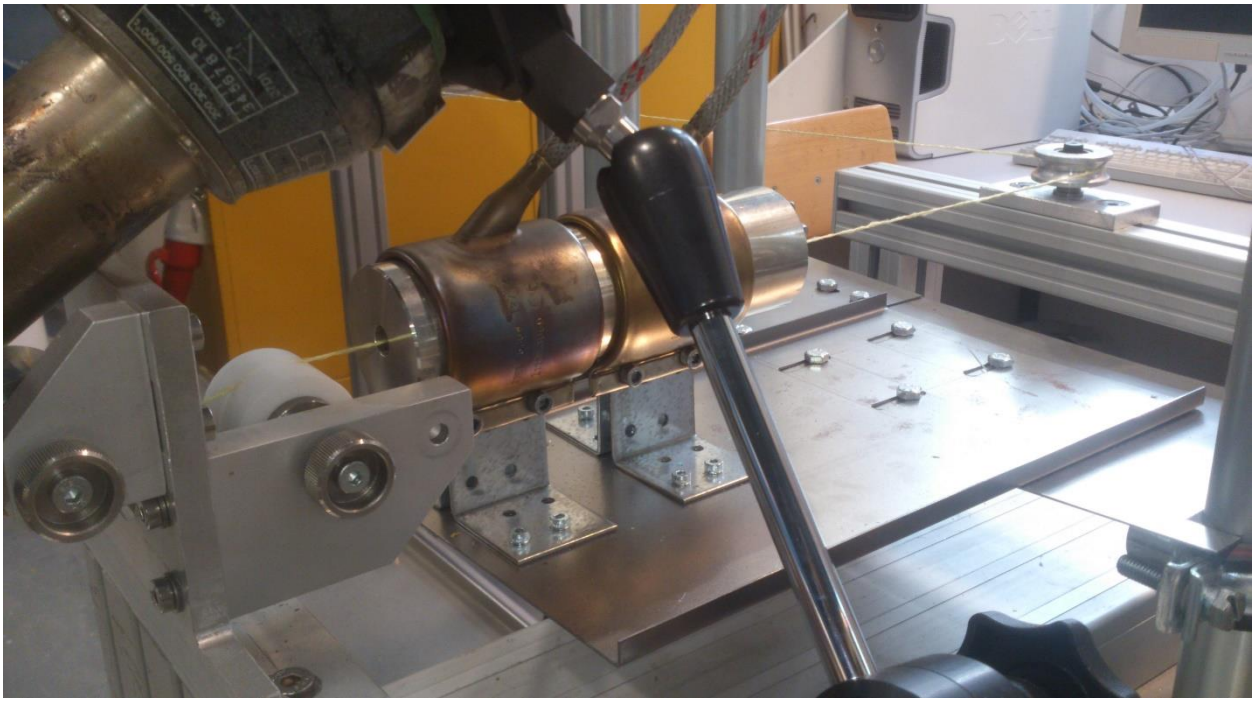

Figure 3.7. CMAS Lab filament winding machine. Preheating system

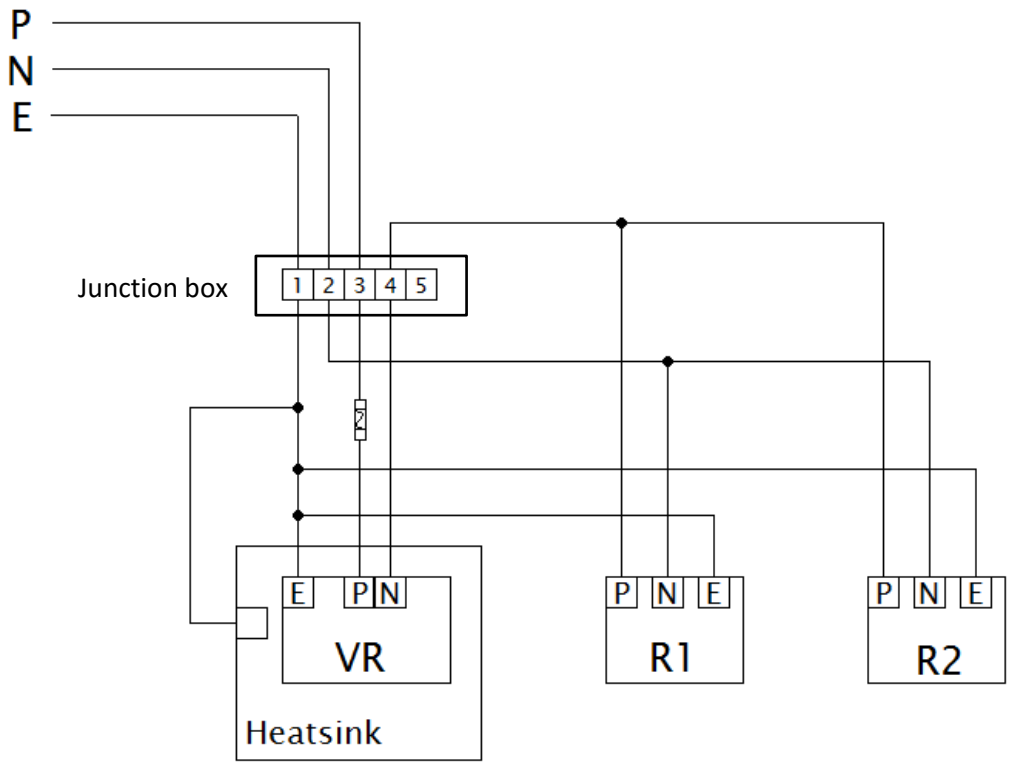

Figure 3.8. Preheating system connections.

3.5 Compaction force system design

To apply the consolidation force on the nip point a compaction system is designed. The system has been divided in two parts: The structure that hold the compaction device and the compaction device itself.

3.5.1 Compaction device

The designed device that applies the compaction force is shown in Figure 3.9. It consist on a support fixed to the structure, a spring that transmit the force, two guides and the compaction part.

The two guides are fixed to the support and their function is to guide and maintain equilibrated the compaction part. The compaction part can move freely through the guides. Two linear bushings connect the guides with the compaction part, allowing the movement of the compaction part through the guides without friction. A helical coil spring works in compression generating the force pushing away the compaction piece. The spring applies the force on the compaction piece through the spring base, it is connected to a nut that is connected to a thread axe fixed to the compaction part. The nut can be screwed up and down varying the spring length and with it the compaction force. The two outer circlips that close the guide's ends are just added to retain the compaction part when this is not applying the force over the mandrel.

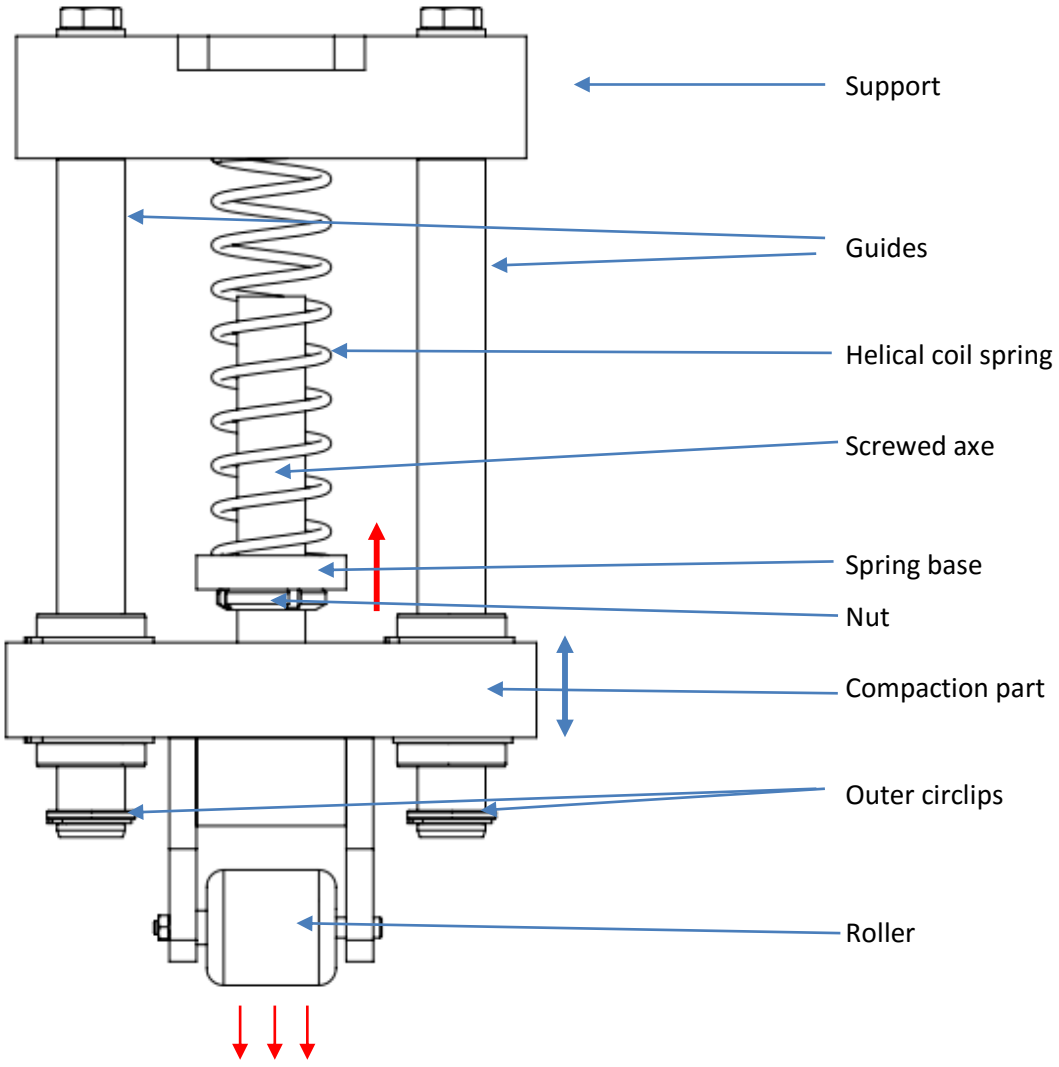

Figure 3.9. Compaction device schematic.

The compaction part includes the compaction roller that applies the compaction force over the yarn. The roller diameter is 32mm and the length is 28mm. It is made of stainless steel for the surface handle the applied forces. It can rotate freely with respect to the compaction part thanks to the two ball bearings installed.

As the mandrel is cylindrical the roller will have always the same contact area with the yarn during all the winding process. That will not happen for different geometries, the manufacturing of different geometries will make necessary the adaptation of the compaction device.

The compaction force applied by the compaction device to the yarn is transmitted to the mandrel and from this is transmitted to the support clamp bearings of the filament winding. The manufacturers of the machine do not recommend applying a force greater than 250N to the support clamps including the mandrel weight. This is taken as the limiting criteria to the spring dimensioning.

Despite the weight limitations on the support clamps the compaction system is designed to be able to apply a maximum compaction force of 300N. That way if in a future the bearings on the mandrel support are replaced the force can be increased.

To be able to easily control the applied force, the type of spring selected is a helical coil spring working in compression from Durovis. This type of spring has a linear behavior between the spring compression and the applied force. Moreover the force and spring deformation act in the same action line [41] what facilitates the design. The spring dimensioning method is included in APPENDIX A.2.

An adaptable structure is designed to position the compaction device in the desired position as shown in Figure 3.10. The force is applied in radial direction to the mandrel.

The compaction roller is coated with a semi-permanent releaser to avoid the thermoplastic adhesion to the surface.

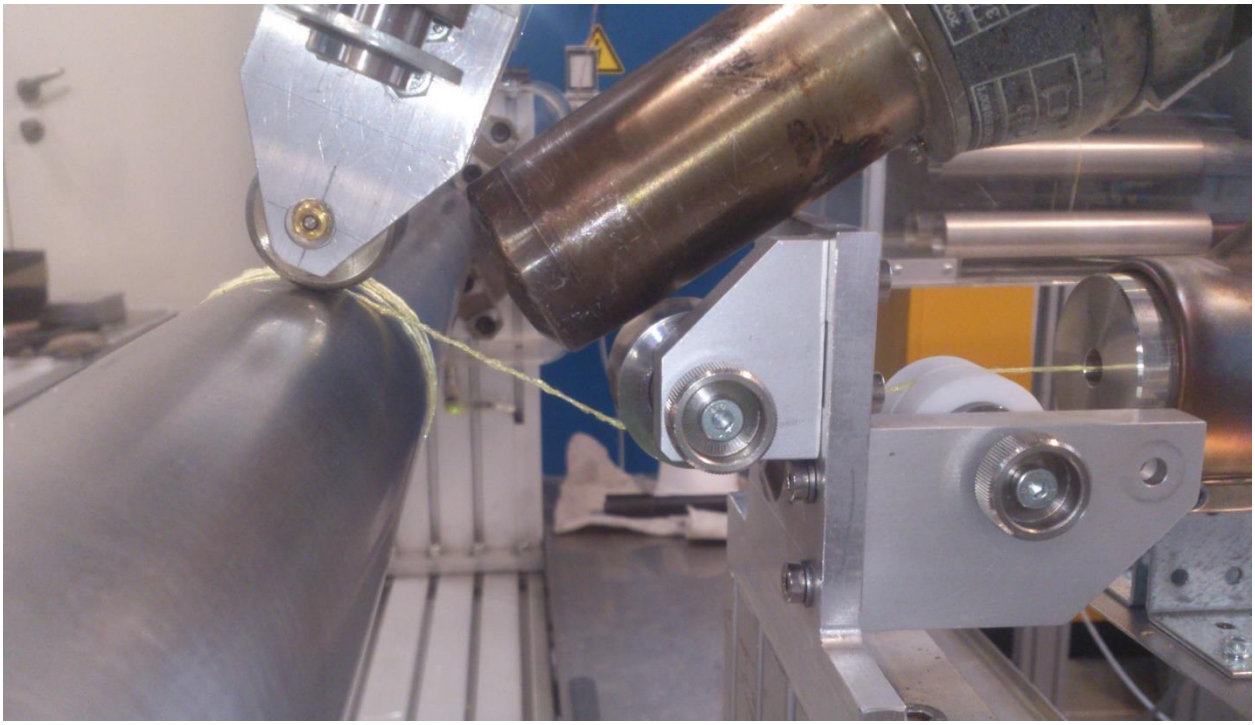

Figure 3.10. Compaction device, force application.

3.5.2 Compaction structure

The structure that hold the compaction device is designed with a tube profiles connection system. The tubes are connected by several clamps to the carriage base. The tubular structure can be adjusted increasing the height, the position and angle of the compaction device to adapt for different mandrel dimensions and geometries as shown in Figure 3.11. The separation of the 4 columns is fixed by the carriage base dimensions. The loads on the clamps are calculated in order to assure the clamps can hold the torque generated by the compaction force. A Finite Element Methods (FEM) analyse is carried out on the structure to assure the tubular profiles do not deform more than 1 mm under the maximum load. The deformation in this case would cause the length variation on the spring and a compaction force variation.

The structure has been dimensioned to handle the 300N load without deformations.

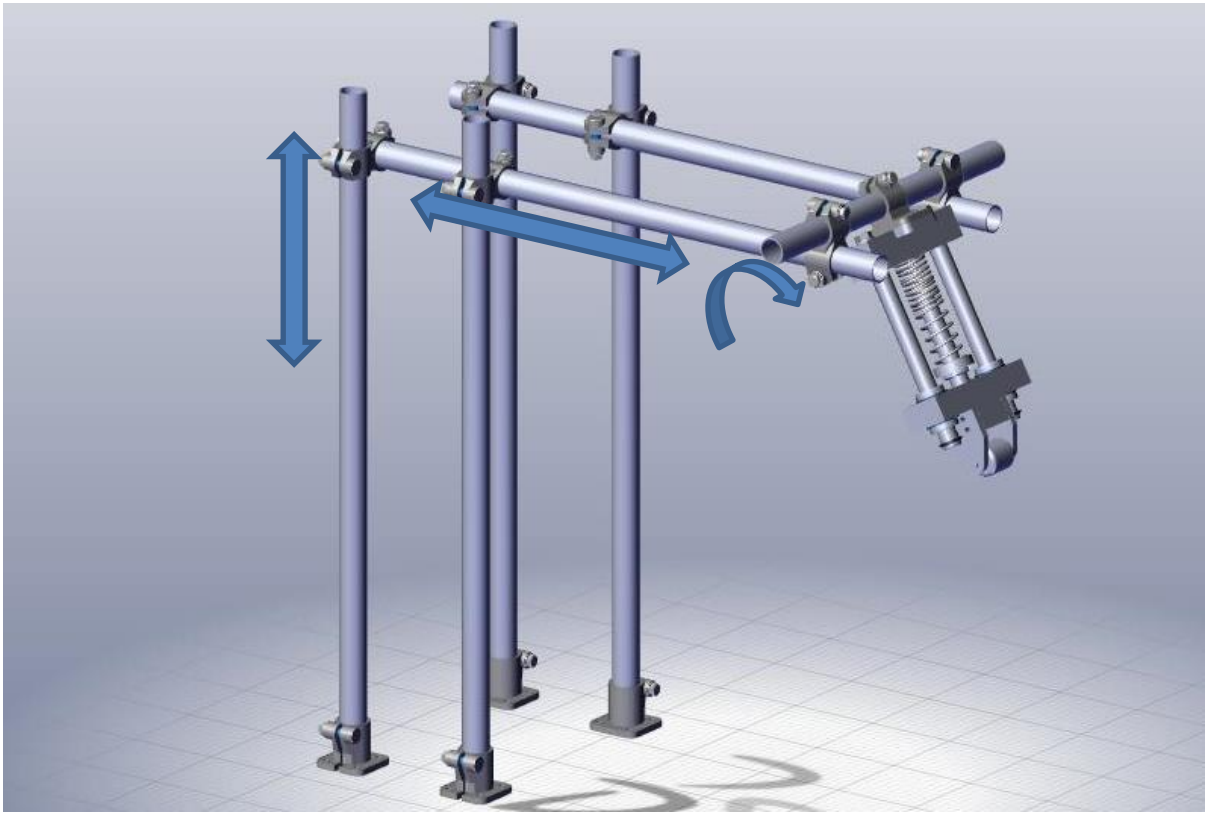

Figure 3.11. Compaction device adjustable structure

3.6 Mandrel design

The mandrel is clamped by the headstock and tailstock installed on the machine's bed. The headstock is connected to the servomotor through a planetary gearbox and transmit the rotational movement to the mandrel. It has installed a 3 jaw manual chuck able to clamp different mandrel diameters and pipes as shown in Figure 3.12. The other end of the mandrel is held by an adjustable tailstock that able to held several mandrel lengths by moving all the device as shown in Figure 3.13.

Figure 3.12. Headstock. 3 jaw manual chuck

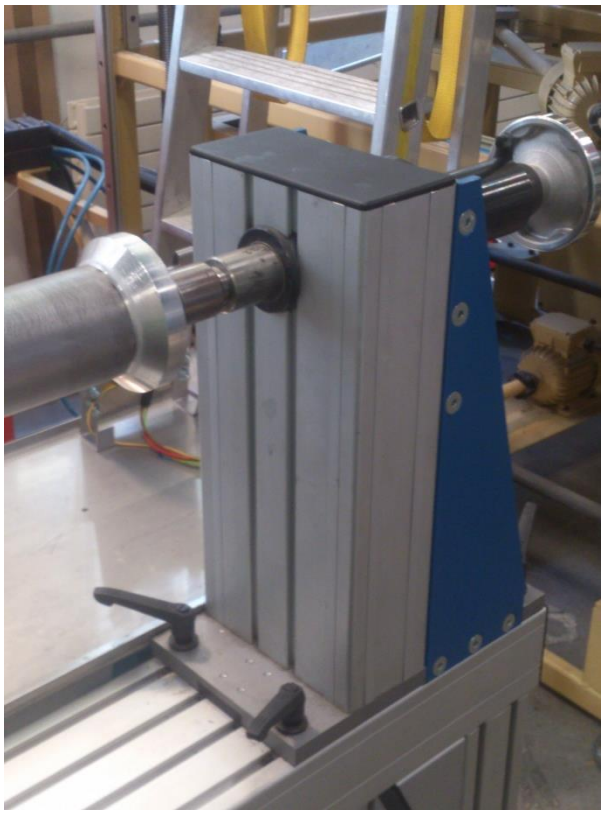

Figure 3.13. Adjustable tailstock

The selected mandrel is a non-heated solid pipe made of steel (St35) under DIN 2391, with and outer diameter of 65mm, 1.5mm thickness and 1010mm length. The selected length of the mandrel is 1010 mm to be able to wind several specimens along the length and accelerate the experimental process.

The maximum winding tension of the fiber is 12N and the maximum compaction force is 200N, neither the pressure nor the compaction force represents a risk for the material failure. The limiting factor in this case are the clamps of the machine. The compaction force is limited to 200N during the experiment to not surpass the manufacture recommended load for the clamps.

The mandrel surface is polished to ease the piece extraction once this is wound. It has been manufactured without exit angle. However during the experimental investigation, high fiber tension values have generated problems with the piece extraction. It is recommend working with a minimum exit angle or with a compressible mandrel for tensions greater than 5N.

To avoid adhesion of the thermoplastic material to the mandrel surface a semi-permanent releaser is applied. The applied product is XTENT 818 from the company Axel. The releaser ease the piece extraction avoiding the adhesion of the thermoplastic to the mandrel surface but it is observed that is necessary to replace it every 3 produced cylinders on the same area.

The components material list and the designed systems drawings are included in APPENDIX 1.3 and APPENDIX 1.4 respectively.

Chapter 4

Machine components calibration

This section includes the calibration of the elements incorporated to the CMAS Lab filament winding machine to adapt it to manufacture thermoplastic composites. This is a necessary step to obtain the exact work range of the different components and the instrument uncertainty.

4.1 Fiber tension system

The fiber tension instrument includes all the elements that apply and control the fiber tension on the yarn during the winding process. Those elements are the dancer arm and the spool axis, both elements positioned in the tension control cabinet. The tension control cabinet has installed a STC (Servo fiber tension control), element that controls the tension over the yarn by coordinating the movement of the creel axis and air pressure arm.

The fiber tension is applied over the yarn in the control cabinet during the winding process (Figure 4.1). The tension is applied by an air pressure cylinder, this one moves the arm connected to a cylinder which applies a lineal force over the yarn tensioning it. The pressure is set up at the beginning of the process by a pressure variable valve. By varying the pressure on the valve the fiber tension will vary proportionally.

As previously mentioned, during the winding process the set tension is controlled and maintained by an STC unit installed in the cabinet. The STC unit control both the air pressure arm and the roll axis. The moment there is a tension variation in the fiber during the process, the yarn will pull down the cylinder of the dancer arm varying the position of this and with it the pressure in the valve. The STC detect the position variation and drive the creel axis making it rotate to free more or less fiber in order to equal the tension and return the dancer arm to the initial position.

The aim of this section will be to stablish the relation between the air pressure set up on the cabinet and the tension on the fiber.

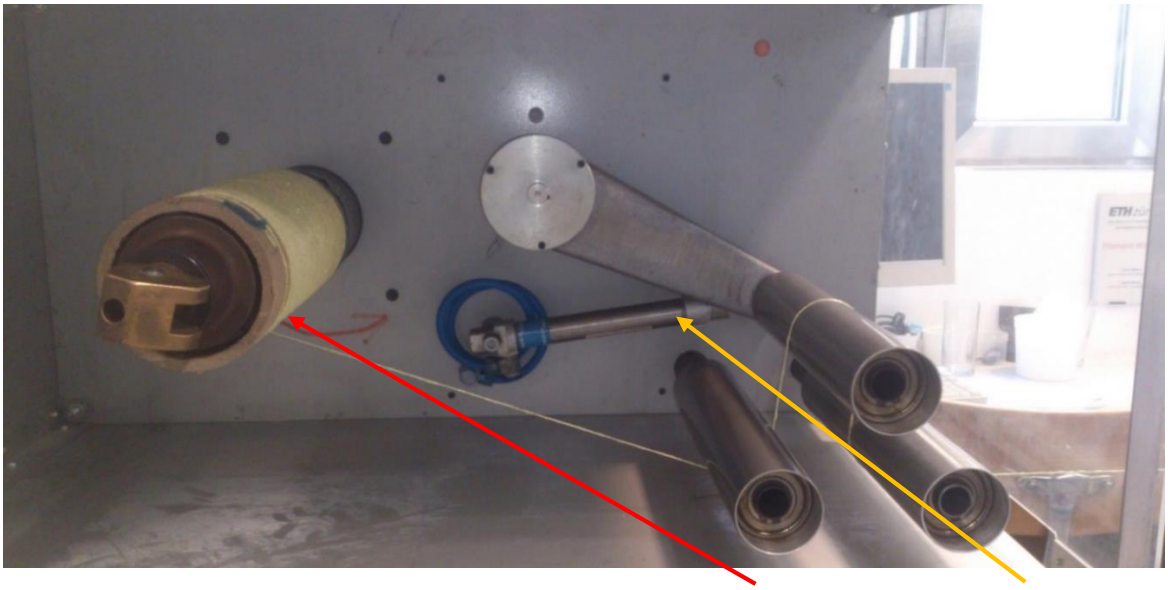

Figure 4.1. Control cabinet CMAS Lab filament winding machine

4.1.1 Experiment layout

In order to obtain the tension on the fiber (output) as a function of the pressure on the valve (input) the next test is assembled as follows.

1. A rope that hold tension until 20kg without deformations is wound by one of the ends around the creel axis, driven around the tension cylinders and direct outside of the cabinet as observed in Figure 4.2. The other end of the rope is tied to a weight of 14kg and positioned over a scale with resolution of 1g, Figure 4.3.
2. When the pressure is applied on the rope, the tension will create a weight variation on the scale measurement.
3. The variation on the weight is converted to the fiber tension.

Figure 4.2. Fiber tension calibration experiment layout 1

Figure 4.3. Fiber tension calibration experiment layout 2

4.1.2 Calibration process and results

A static calibration procedure is carried out as described in 'ANNEX B. Calibration Procedure to determine the overall system error [12, 32, 35].

Maintaining constant the conditions during the experiment, 28 input measurements are taken with the correspondence fiber tension values to estimate the linearity, hysteresis, sensitivity and zero shift error (19 upscale, 9 downscale). To estimate the repeatability error 14 additional measurement are obtained for the same input value (4 bar). The repeatability error is calculated for a high tension value what will consider a bigger error and assumed to be equal for all the input values.

Figure 4.4 shows the scatter diagram of the measured data between the system input and output. The system has a linear behaviour in the pressure input work range with a correlation of 0.999. Then is possible to adjust a linear regression between the input system (pressure), and output system (fiber tension).

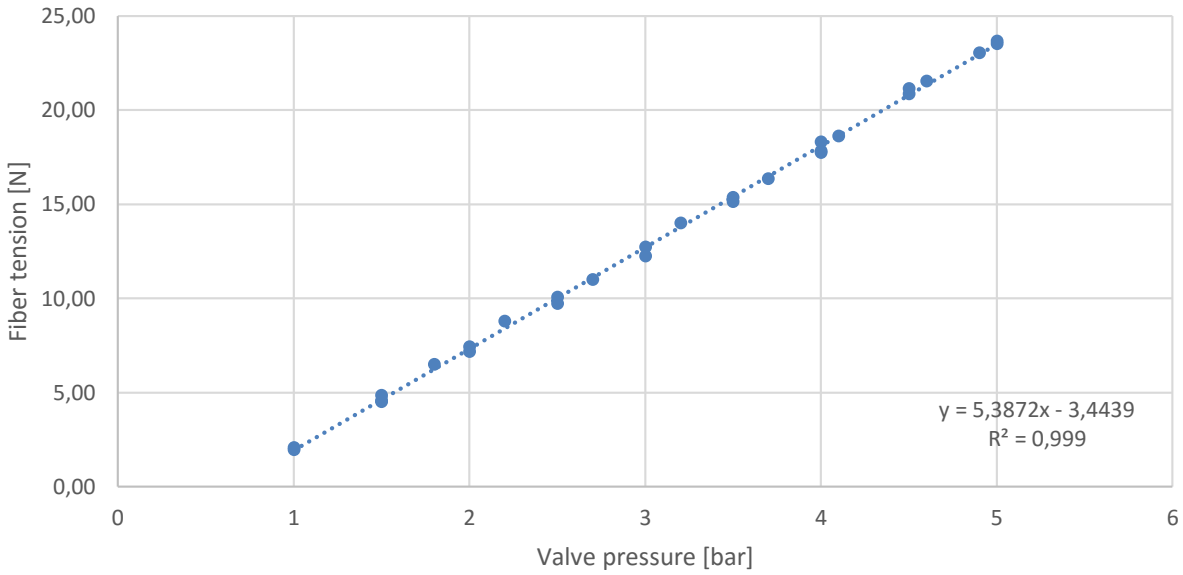

Figure 4.4. Linear regression Fiber tension-Valve pressure.

The estimated errors of the system and the general error (Uncertainty) are included on Table 4.1.

Table 4.1. Estimated fiber tension system errors. Sensitivity error calculated for a pressure of 4 bar.

Error type	Units	Value
Linearity	N	0.48
Hysteresis	N	0.49
Sensitivity	N/bar	0.07
Zero shift	N	0.23
Repeatability	N	0.04
General error	N	0.78

The fiber tension system of the CMAS Lab filament winding machine is able to apply a fiber tension between 2N to 30N with a general error of 0.8N.

-This experiment set up is static so the tension in the fiber created by the different rotation speed between the mandrel and the creel axis is not considered. As the STC maintains the tension constant equalling the velocities this assumption is accepted.

- The response time of the STC is not available.

4.2 Heating system

The objective of this calibration is to stablish the relationship between the switch position in the heating gun and the temperature on the tip of the nozzle, to calculate the error in the temperature set up and to calculate the temperature variation interval for a set up temperature. The temperature on the nozzle is measured with a thermocouple type k (Work range -270ºC to 1372ºC).

4.2.1 Experiment layout

The layout of the experiment is prepared as follow:

1. The heat gun is positioned in the same position that it has during the winding process in order to avoid possible air flow variations.
2. A thermocouple is fixed on the tip of the heat gun and maintained in the same position during all the experiment.
3. For each input position the temperature has been measured during 1 minute. The minimum, maximum and average values are annotated.

   Waiting 3 minutes before each measurement was necessary in order to achieve and stationary temperature.

4.2.2 Calibration process and results

The heating gun is calibrated following the calibration procedure described in ANNEX2. 'Calibration procedure'.

First 36 input points are measured in order to estimate the linearity, sensitivity, hysteresis and zero shift errors described in APPENDIX B.

Second 5 additional points are measured in the same input dial position to estimate the repeatability error.

The scatter diagram in Figure 4.5 shows the distribution between the dial position and the temperature of the gun. The system has a linear behaviour so a linear regression is adjusted to represent the system input and output.

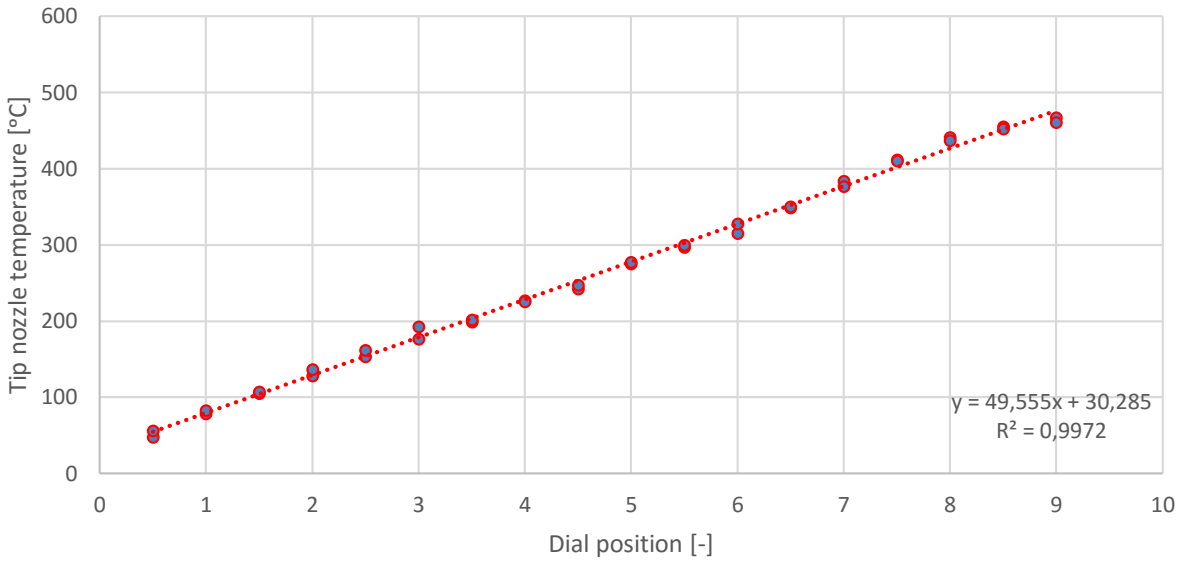

Figure 4.5. Scatter diagram Temperature heat gun nozzle – dial heat gun position

The estimated errors of the heat gun are shown in Table 4.2.

Table 4.2. Estimated errors for heat gun system. Hysteresis error calculated for position 9 maximum error.

Error type	Units	Value
Linearity	°C	23.9
Hysteresis	°C	16.2
Sensitivity	°C/position	0.9
Zero shift	°C	5.0
Repeatability	°C	4.6
General error	°C	30.8

A big amount of the error on the heat gun is due to the rudimentary dial switch that it is equipped. It creates difficulties to accurately position the switch to obtain the desired temperature. To decrease the temperature error and not take in consideration the influence on the dial switch while setting up the temperature, the temperature set up procedure is changed. The temperature on the heat gun is set up with a thermocouple instead of just the dial. That way the systematic errors (linearity, Hysteresis, Zero shift and sensitivity) are removed. So the considered error is the random one, repeatability.

The heat gun has a temperature range between 50°C and 460°C with a general error of 4.6°C.

4.2.3 Temperature variation interval for a set up value

The temperature during the process will vary around a maximum and minimum value. To estimate that interval, the variation between the maximum and minimum temperature of each data analysed in the previous experiment is calculated. The error of the variation calculation is obtained as follow:

$$U_{variation} = S_{variation} * t_{(0.95;N-1)} \tag{4.1}$$

The temperature variation interval is 2.8 +/- 1.6°C.

The temperature in the thermocouple is taken as the reference temperature, so is considered that has no error.

4.3 Preheating system

The preheating system is controlled by the power variation. The temperature in the device is set up using the thermocouple. The aim of the calibration is to quantify the temperature interval variation once the temperature is set up.

4.3.1 Experiment layout

To estimate the temperature variation a thermocouple type k is positioned on the centre of the preheating system cavity. All the measurements are made an hour after the temperature is set up on the preheating system, to assure the system is in stationary conditions.

4.3.2 Calibration process and results

Four data were measured for the same set up temperature. Each data was measured during half an hour, the maximum and minimum temperature during that time interval was annotated. The temperature variation then is calculated as the average of the difference between the maximum and minimum temperature for each point measured. The error of the measurement is calculated using equation 4.1.

Work temperature range = 0 to 400°C

Temperature variation interval = 0.6 +/- 0.3°C

4.4 Compaction instrument

The compaction instrument has been calibrated in order to obtain the relationship between the spring length and the force applied by the cylinder.

The force applied for the compaction instrument is caused by a helical spring working in compression. The force applied by a helical spring is linearly proportional to the compressed length as follow [41]:

$$F = k * \Delta L \tag{4.2}$$

Being known the initial spring length (L_0) the force applied for each screw length is calculated:

$$F = k * (L_0 - L) \tag{4.3}$$

The table Force-screw length relation is included on APPENDIX B. Machine systems conversion tables.

In order to confirm the theoretical force a test is carried out on the device.

4.4.1 Experiment Layout

The compaction device is positioned in a press to fix the distance between the two extremes as shown in Figure 4.6. A load cell (resolution of 5N) is added on top of the compaction device to measure the load applied. On top of the load cell a plate is positioned to distribute the load and to protect the load cell.

Once the layout is fix the spring length (input) is varied and the load annotate (output) in order to obtain the data points for the regresion.

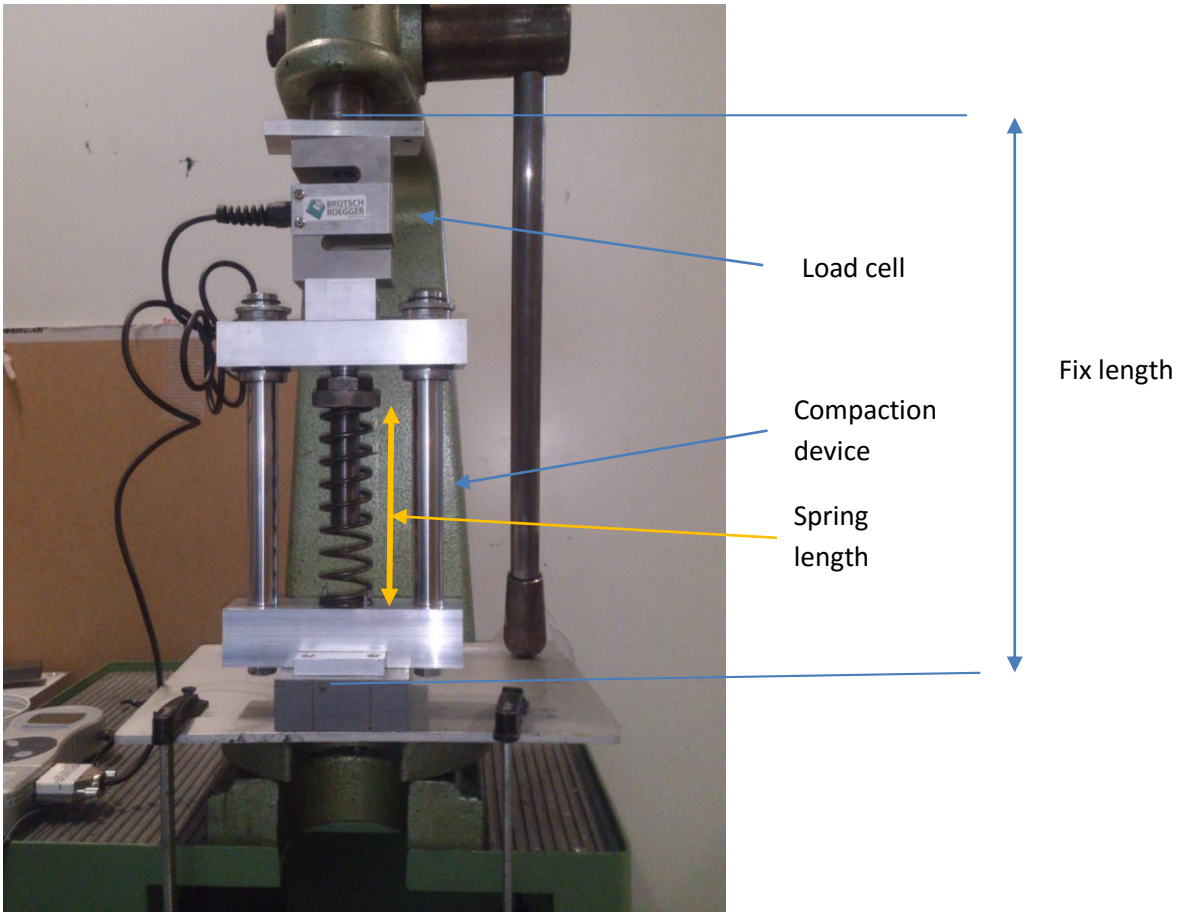

Figure 4.6. Compaction device test layout

In this test layout the weight of the free load part of the compaction device is working against the screw force, same as the load cell weight and plate weight. The mentioned elements are weighted separately on a scale and the load values are corrected.

4.4.2 Datas and results

36 different input points are measured with the load cell and for each input point 5 output values are taken. Figure 4.7 show the comparison between the theoretical and experimental curve. The calculated errors are shown in Table 4.3. It is necessary to comment that most of the error calculated is due to the measurement method. The resolution of the load cell is too low for the range analysed. There was no a more accurate load cell available. However is enough to obtain the application magnitude and confirm the theoretical values.

Table 4.3. Estimated errors for compaction device. Hysteresis error calculated for position 120 maximum error

Error type	Units	Value
Linearity	N	9,0
Sensitivity	N/mm	4,4
Zero shift	N	0,045
Repeatability	N	0,0
General error	N	10,0

The compaction device work range = 0N-350N +/- 10N.

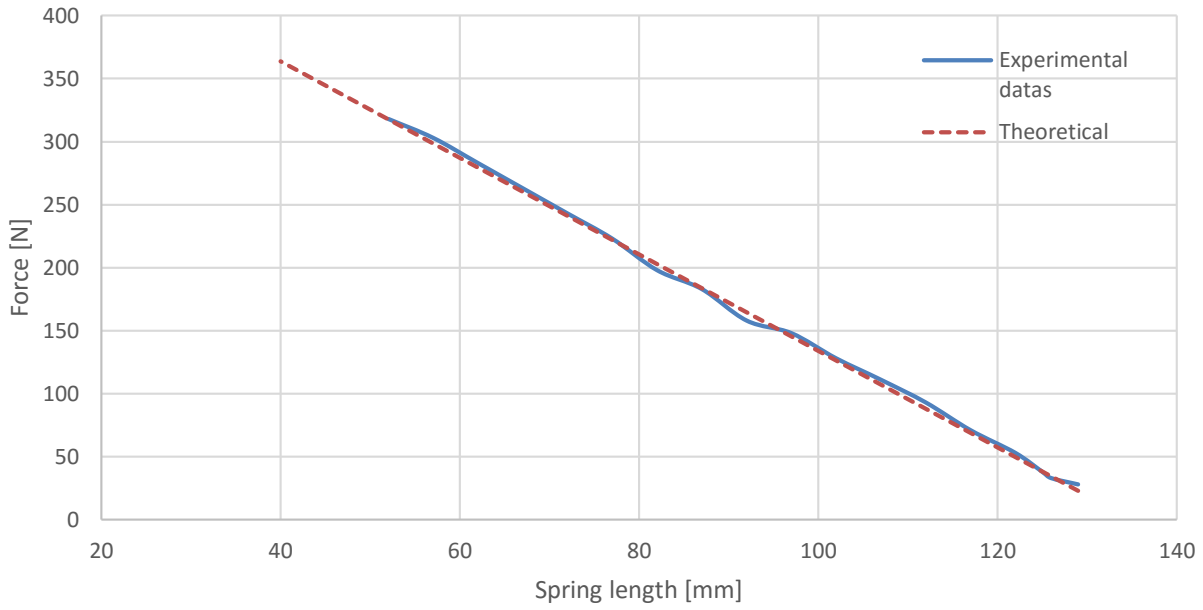

Figure 4.7. Comparison between theoretical and experimental curve of compaction device force-spring length relation.

Table 4.4 summarize the working range of the calibrated elements of the CMAS Lab filament winding machine. The heating gun and preheating data is given with the assumption the temperature is previously set up with the thermocouple as previously explained.

Table 4.4. Machine system elements work range and uncertainty.

Element	Work range	General error	Temperature variation interval for a set temperature	Time to stationary
Heat air gun	50-460 °C	4.6 °C	2.8 +/- 1.6 °C	3 min
Compaction device	0-360 N	+/-10 N	-	-
Fiber tension control	2 -30 N	+/-0.6 N	-	-
Mandrel feed rotation	185 rev/min	0.01 rev/min	-	-
Preheating system	0-400	-	0.6 +/- 0.3	45 min

- The conversion table between input and output of the fiber tension system and compaction force system are included in APPENDIX B.2.

Part 2

Experimental investigation of in-situ consolidation of thermoplastics composites

Chapter 5

Material characterization

In this section the intermediate materials considered for the cylinder manufacturing are characterized. All of the proposed materials are flexible intermediate materials, where the reinforcing and thermoplastic materials are physically mixed on the yarn in order to achieve shorter distances during the impregnation.

5.1 Proposed materials and analysed parameters

Four different materials stored in the CMAS Lab have been characterized.

Table 5.1. Intermediate materials characterized

Specimen	Fiber type	Thermoplastic Fiber	Reinforcing fiber
1	Powder impregnated fiber	Unknown	Glass fiber
2	Commingled yarn	Polyamide 6	Twaron
3	Commingled yarn	Polyamide 6	Carbon Fiber
4	Commingled yarn	Polyether ether ketone	Carbon Fiber

The specimen 1 is not a commingled yarn, it is a powder impregnated fiber manufactured in the university. Despite the fiber is not a commingled yarn it has been characterized in order to obtain the material information.

5.2 Material characterization methods

This section describes the different methods used to determine the material properties. For each one of the materials the next parameters has been determined:

5.2.1 Thermoplastic and reinforcing fiber area and diameters, comingling degree

The thermoplastic and reinforcing fiber area and diameters has been obtained by analysing the cross section and front view of the images taken with an electron microscope, a LEO 1530 Gemini from Zeiss (Germani).

During the sample preparation the fiber tows are cut and introduced in the microscope holders. Later the samples are frozen and a second cut in the cross section is done in order to make more fragile the yarns

and preserve the fibers without deformations. Finally the samples are coated with a 7 nm layer of platinum and analysed on a Scanning Electron Microscope.

Using an image processing and analyse program the diameter and area of the fibres is calculated. Five measurements of each material sample are taken to determine the magnitudes. Average and standard deviation is calculated.

The commingling degree is qualitatively evaluated observing the distribution of the thermoplastic and reinforcing fibers over the yarn

5.2.2 Glass transition and melting temperature of the thermoplastic matrix

The glass transition and the melting temperature of the thermoplastic matrix is determined using a differential scanning calorimetry analyse in a METLER TOLEDO, DSC 1 STARE System.

Each material is tested during 3 equal consecutive cycles, every cycle is adapt to surpass the material melting temperature. In each cycle the sample temperature is increased until surpass the melting temperature, later the sample temperature is decreased until the 0°C. The approximate starting temperature of the glass transition and the melting temperature are obtain of the curve Heat flow – Sample temperature for each of the specimens [52].

5.2.3 Degradation temperature and fiber weight content

The degradation temperature and fiber weight content of the 4 materials are determined using a thermogravimetric analyse in a Perkin Elmer Pyris 1 TGA machine.

The material samples are heated with a gradient of 30°C/min until 1000°C and maintained at the last temperature during 90 minutes to assure all the sample content is degraded.

The degradation temperature is obtained of the curve mass- sample temperature, indicates the moment when the mass of the material starts to decrease.

The fiber weight % is calculated by the relation between the mass volume fraction before and after the thermoplastic polymer degradation.

$$Fiber\ weight\ percentage = \frac{Fiber\ mass\ (after\ the\ thermoplastic\ degradation)}{Total\ mass\ (starting\ experiment)} \quad (3.1)$$

- Using the fiber weight % the fiber volume % is calculated as explained in section 5.3.5. page 48.

5.2.3.1 Fiber volume content for the selected material

For the selected material an image analyse of the polished fiber cross section has been carried out in order to more accurately determine the fiber volume % as this parameter is used for further calculations explained in the next section.

Sample preparation

Two parts of the semifinished material yarn are cut and introduced in a sample holder. The yarns are covered with aluminium foil in order to prevent the commingled yarn slice to lose the original structure. The holder with the sample is positioned in a mold and this is filled with a resin (Specifix resin). Once the resin has hardened the samples are extracted of the mold and polished. The polished samples are analysed and photographed in a standard microscope under 20 times magnification.

The calculation procedure of the volume content calculation is explained in section 5.3.5.1. Figure 5.1 shows an image of the sample holders and the hardened resin. The fiber samples are not included on the image.

Figure 5.1. Polished cross section samples. Commingled yarn tows not included include on the example.

5.3 Selected material and results

The selected material is the Twaron- PA6 commingled yarn. This material has been no previously studied in filament winding process and the melting temperature of the PA6 is suitable for the work temperature range of the CMAS Lab filament winding machine.

5.3.1 Material summary results

Table 5.2 show a summary of all the quantitative measured properties of the studied materials.

Table 5.2. Selected material properties. Twaron – PA6 commingled yarn

Twaron -PA6		
Yarn type	-	Commingled yarn
Theoretical Matrix density	[g/cm^3]	1.13
Theoretical Reinforcement density	[g/cm^3]	1.44
Fiber weight %	[-]	66.43%
Fiber volume %	[-]	60.83%
Fiber density	[g/cm^3]	1,31
Matrix fiber diameter	[µm]	55 +/- 5.4
Reinforcement fiber diameter	[µm]	15 +/- 1.2
Glass transition temperature	[^{o}C]	50
Melting matrix temperature	[^{o}C]	220
Temperature of degradation Matrix	[^{o}C]	320
Temperature of degradation Reinforcement	[^{o}C]	500

The data shown in this section are the Twaron-PA6 commingled yarn. The rest of the material characterization data is included in Annex C.

5.3.2 Fiber diameter and qualitative commingling degree:

Figure 5.2 shows an electron microscope photography of the Twaron-PA6 commingled yarn. The fiber diameters are obtained measuring them directly from the longitudinal fiber images as shown in the figure. The Twaron fiber diameter is 15 +/- 1.2 µm. The polyamide 6 fibers diameter is 55 +/- 5.4 µm.

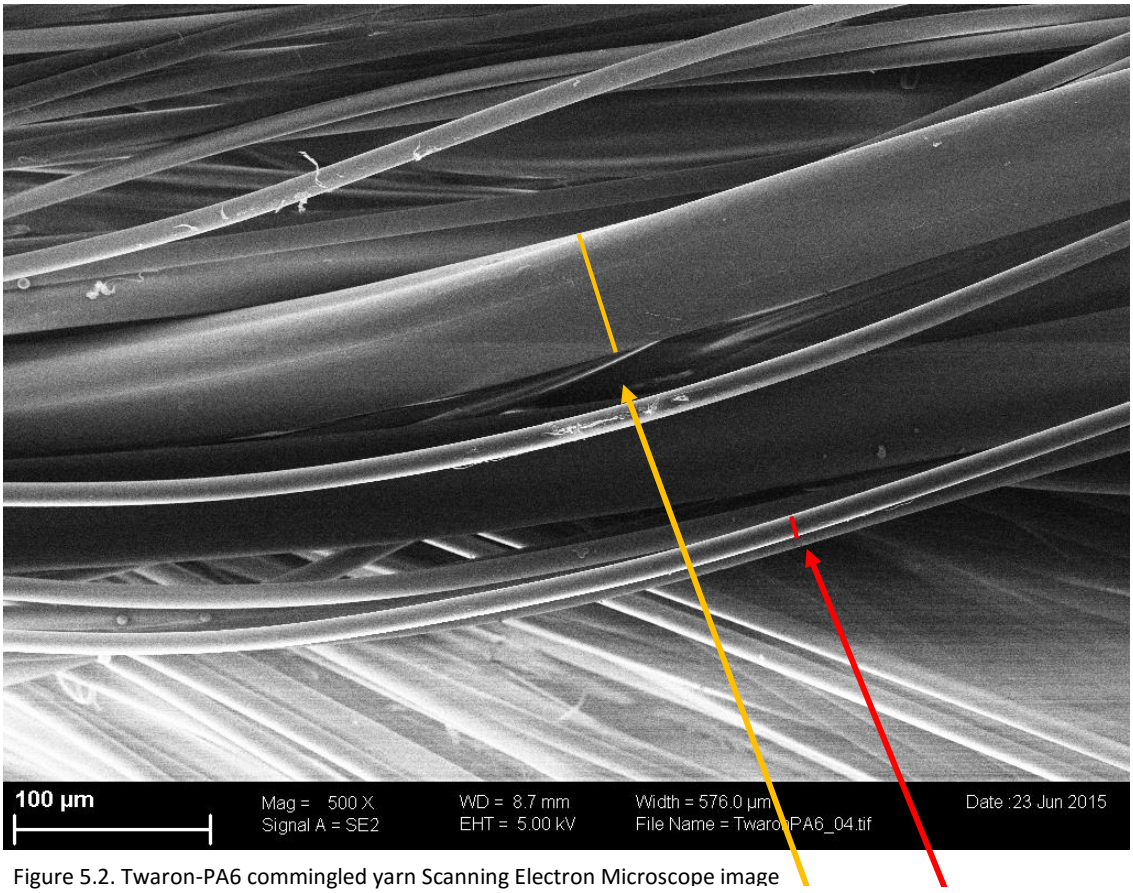

Figure 5.2. Twaron-PA6 commingled yarn Scanning Electron Microscope image

Figure 5.3 shows the PA6 and Twaron fiber distribution in a yarn tow. As observable the commingling degree for the Twaron-PA6 material is far from perfect. Most of the thermoplastic material is concentrated on the central part of the yarn while in the extremes there is nearly no presence of the PA6 fibers.

The reinforcing Twaron fibers have a round section while the PA6 fibers has a more triangular section to ease the intimate material surface contact during the impregnation.

A polished cross section of the intermediate material Twaron-PA6 was prepared and photographed with a standard microscope with 20 times magnification in order to have a more accurate view of the fiber commingling degree.

Figure 5.4 shows once again that the commingling degree is not perfect. The thermoplastic material is again concentrated in the center of the fiber tow while in the corners there is a clear predominance of the Twaron reinforcing fiber.

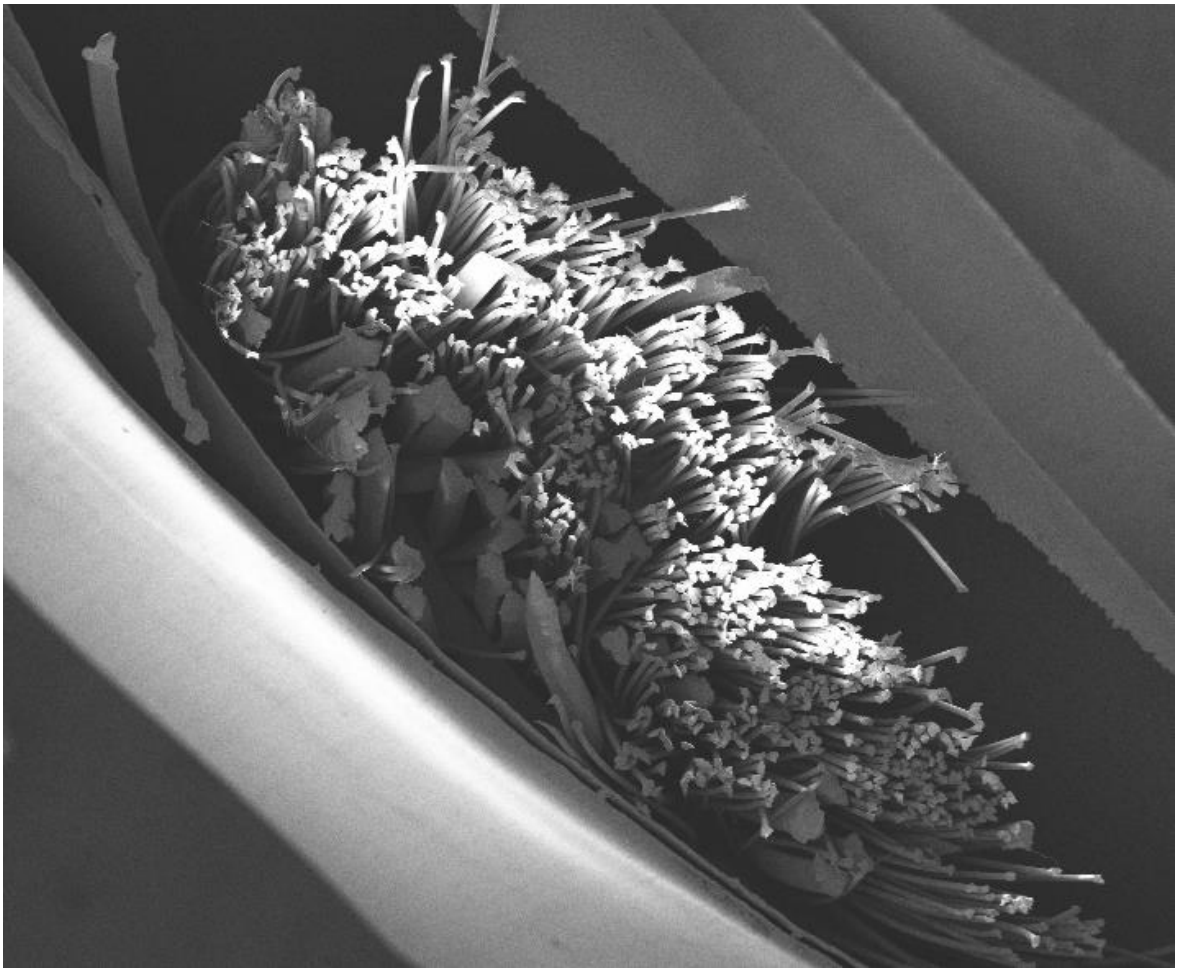

Figure 5.3. SEM image Twaron – PA6 commingled yarn cross section

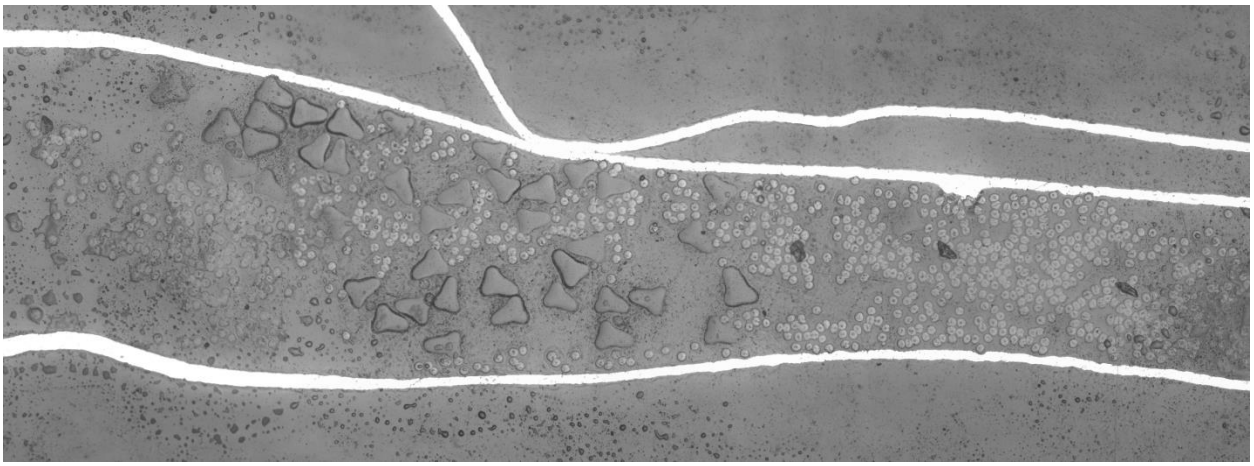

Figure 5.4. Polished cross section of Twaron-PA6 commingled yarn. Commingling degree and fiber volume content evaluation.

5.3.3 Thermal properties

Figure 5.5 shows the 3 equal cycles applied during the differential scanning calorimetry analyse to the Twaron-PA6. Figure 5.6 shows the heat flow-time evolution during the 3 cycles. It displays the melting behaviour of the thermoplastic material polyamide 6. The matrix transition begins approximately at 206°C degrees and ends at 226°C. The glass transition is starting around 50°C were the curve Heat flow-temperature presents an inflexion point sign that the thermoplastic is becoming leathery [52].

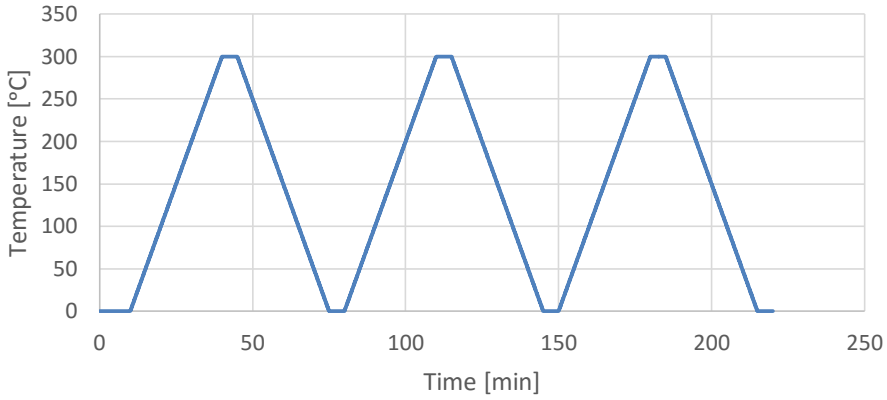

Figure 5.5. Differential scanning calorimetry cycle. Heating rate 20°C/min

The large decrease between 0°C and 5°C is caused for instabilities related to the change from isothermal to isogradient measurements. In the opposite way the large increase between 295°C and 300°C is due to the change from isogradient to isothermal measurements.

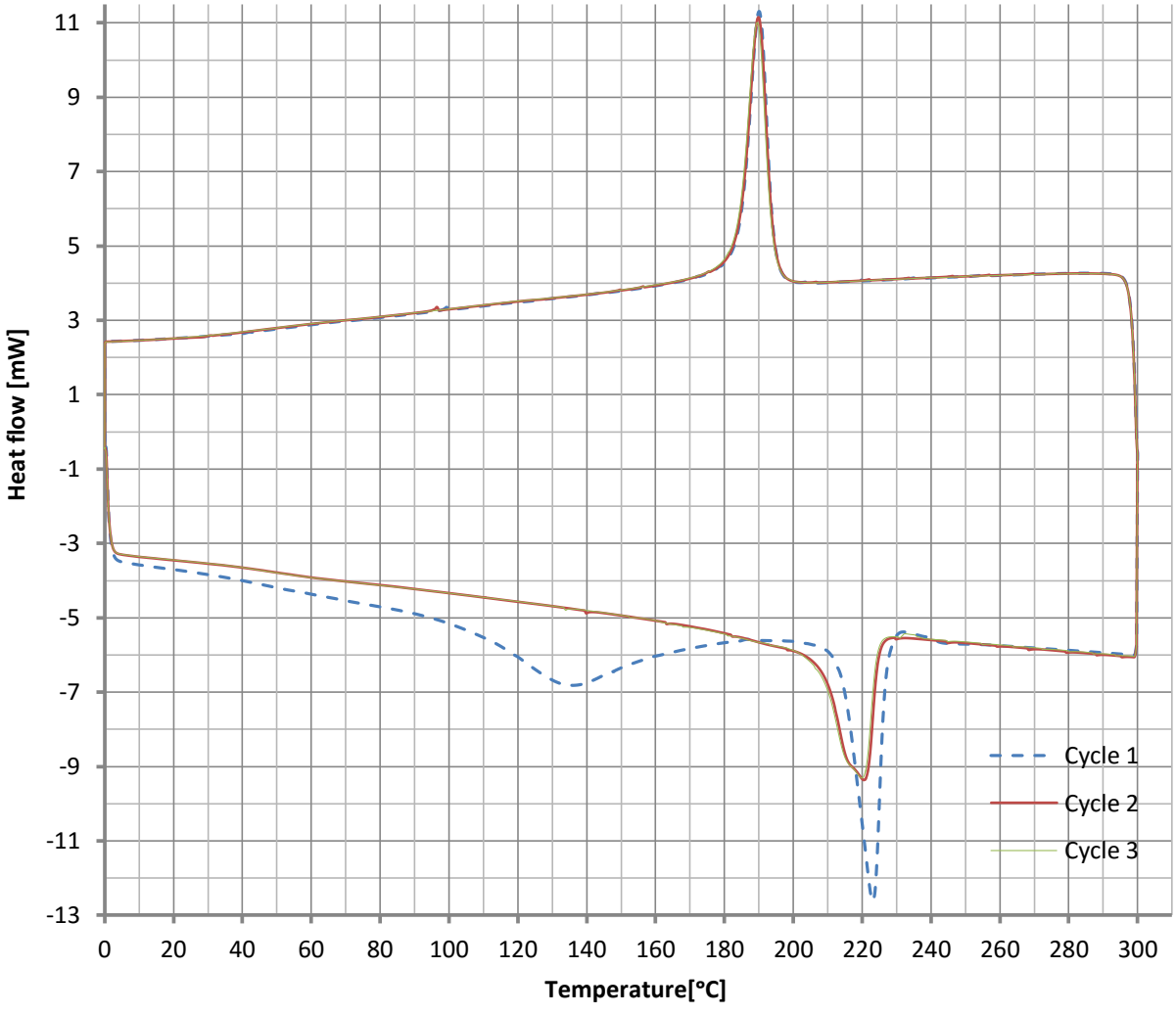

Figure 5.6. Differential scanning calorimeter measurements of reinforced Polyamide 6

It is observable that the material has a different behaviour during the first cycle than during the other 2. This is probably due to and additional component in the commingled yarn, such a Sizing. This material is usually added by the manufacturer company to improve the interface compatibility between the thermoplastic material and the reinforcing fiber. The sizing melting transition begins at approximately 100°C and ends at 180°C. The sizing is being completely degraded during the first cycle therefore there is no presence of it in the rest of cycles.

On the SEM images is clearly observable the presence of the additional component in Figure 5.7.

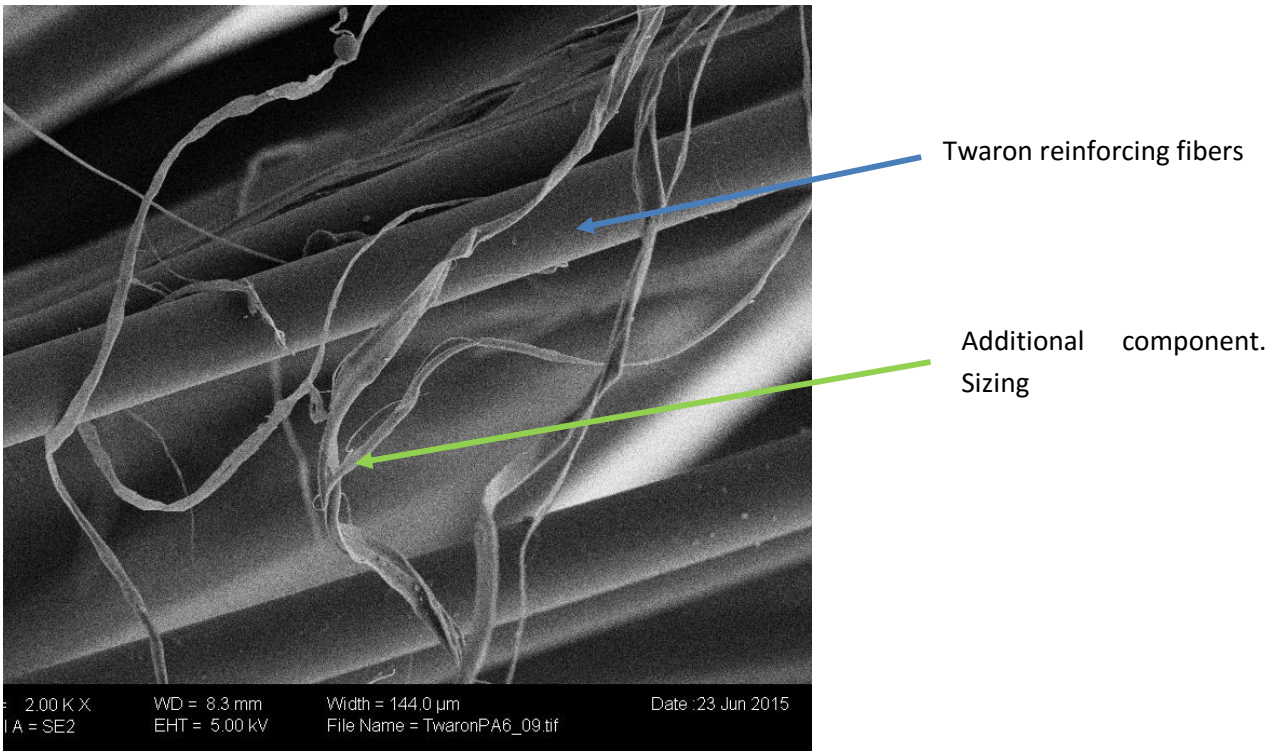

Figure 5.7. SEM image of Twaron-PA6 commingled yarn.

5.3.4 Polymer Degradation and fiber weight %

Figure 5.8 plots the thermogravimetric analysis measurement of the PA6-Twaron reinforced fiber.

The polyamide degradation temperature begins approximately at 320°C. The Twaron degradation temperature begins at 500°C. Therefore the temperature of the yarn must be under 300°C during the filament winding process.

The fiber weight % is calculated by the relation between the mass volume fraction before and after the thermoplastic polymer degradation as explained in methods [38].

Five samples has been tested in the Thermogravimetric analyse for the selected material. The fiber average weight content and standard deviation are calculated:

Fiber weight content% = 68.55 +/- 0.55%

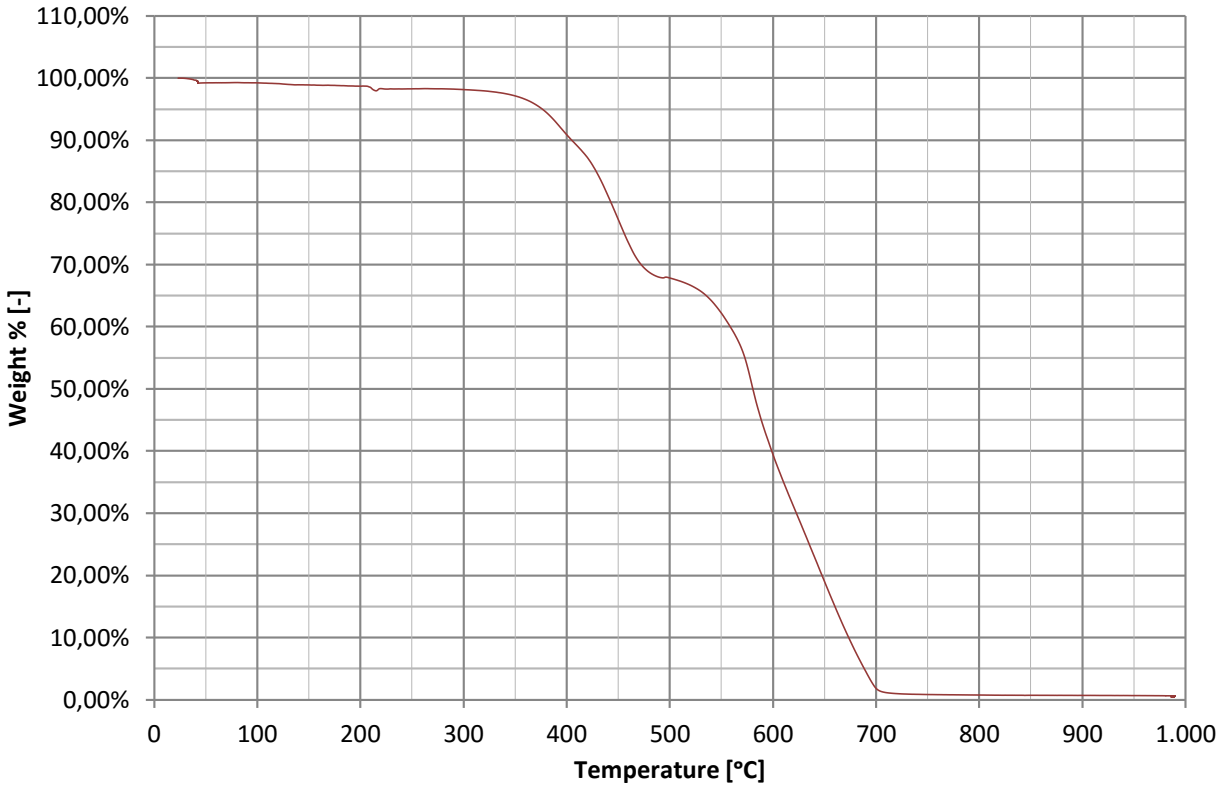

Figure 5.8.Thermogravimetric analyze measurement of Twaron-PA6 at 1000ºC

Is necessary to say that as the Twaron degradation temperature is near to the PA6 degradation temperature, it is possible that both material are being degrade during a time interval and the fiber weight % would be overestimated. To solve that problem the fiber volume % will be calculated separately for the selected material in section 5.4.5.1.

5.3.5 Fiber volume content

The fiber volume content of the 4 different materials has been determined using the matrix and reinforcement fibers theoretical densities and the fiber weight %. Following the next expression:

$$Fiber\ volume\ \% = Fiber\ Weight\% * \frac{Composite\ density}{Fiber\ density} \tag{3.2}$$

The composite material density is calculated as follow:

$$Composite\ density = \left(\frac{Fiber\ weight\%}{Fiber\ density} + \frac{(1-Fiber\ weight\%)}{Matrix\ density}\right)^{-1} \tag{3.3}$$

The theoretical density of Twaron is 1.44 g/cm^3 and the polyamide 6 is 1.13 g/cm^3 [34, 48]. The fiber volume content of the Twaron-PA6 is approximately 63% and the composite density is 1.32g/cm^3.

5.3.5.1 Fiber volume content calculated through area and number of fibers

In order to obtain a more accurate volume content, a second method is used to calculate this parameter for the selected material (Twaron-PA6).

First the fiber areas of each material are measured using an image processing and analysis program (Imagej) of the SEM pictures, as shown on Figure 5.9. Seven measurement are taken for PA6 and ten measurements for Twaron. Second the number of reinforcing fibers and matrix fibers is counted, on the

SEM picture (Figure 5.2) and in the polished cross section pictures (Figure 5.4). Third the volume fraction is calculated using the equation 3.4:

$$Fib.volume\ \% = \frac{Reinf.fiber\ area * nºreinf.fibers}{Reinf.fiber\ area * nºreinf\ fibers + Matrix\ fiber\ area * nºmatrix\ fibers} \quad (3.4)$$

Table 5.3 shows the results of both the SEM picture and the polished cross section methods.

Table 5.3. Fiber volume content calculated with the average areas and number of fibers method

Test	Parameter		Value	Fiber volume content
	Area Twaron fiber	[µm^2]	170.47	
	Area PA6	[µm^2]	2415.84	
SEM picture				
1	Twaron fiber nº	-	730	61.68%
	PA6 fiber nº	-	32	
Polished cross section image				
2	Twaron fiber nº	-	957	62.22%
	PA6 fiber nº	-	41	
3	Twaron fiber nº	-	857	59.43%
	PA6 fiber nº	-	42	

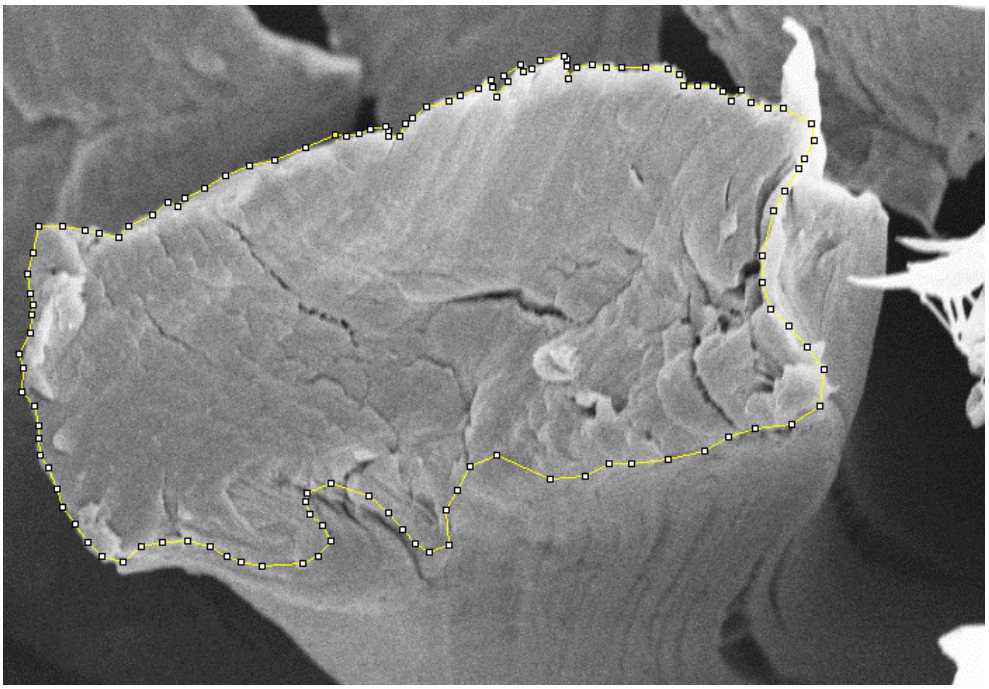

Figure 5.9. Twaron fiber Area measurement method example.

Finally Table 5.4 shows a comparison between the 3 different methods used to calculate the fiber volume %,

Table 5.4. Comparison of fiber volume content calculated with TGA method, SEM image method and polished cross section method.

Method	Volume %	Weight%
TGA	63.09%	68.65%
SEM image	61.68%	67.23%
Polished cross section image	60.83%	66.43%

The fiber volume % is around 60% in the three methods. However the fiber volume content used for the further calculations is 60.83% calculated with the polished cross section method.

Chapter 6

Experimental investigation of automated filament winding for in-situ consolidation of commingled yarns

In this section the automated filament winding process for in-situ consolidation is experimentally investigated. The process parameters are classified and analysed. Different samples are wound for different parameters settings in order to determine the influence of them in the quality of the final part. To determine the quality of the final part the specimens are mechanically characterized. Later the void content is analysed to double check the mechanical results.

A final cylinder is wound with the best parameter combination obtained and compared with a reference part manufactured by compression molding. Finally several cylinder of different dimensions are wound to study the parameter physical properties evolution when changing the dimension.

6.1 Designed part

The designed part for the experimental parameter investigation is an open cylinder. The open cylinder is an axially symmetric simple geometry. The cylinders are wound with hoop winding. Using a hoop winding pattern an individual layer is wound for each winding angle. Each specimen is wound with 8 layers maintaining constant the winding angle [29]. The nominal piece length is 25mm. The nominal inner diameter of the parts is 65mm. The geometry and winding paths selection minimize the process difficulty being able to focus in depth on the process parameters.

Figure 6.1. Experimental investigationpart geometry

6.2 Filament winding parameters description

Filament winding process for in-situ consolidation offers a promising option as a composite manufacturing process. This process allows to manufacture parts with the fiber orientation controlled, leading to optimal mechanical properties, and over large components sizes. Moreover the online consolidation able to completely automatize the process giving the possibility to decrease the product cost for large series.
Thermoplastic matrices composites are attracting the interest of the industries thanks to their processability properties, which enable part corrections and the recyclability behaviour compatible with the environment concerns [18]. Despite the high material potential, the complexity of the thermoplastics processing limits drastically its use. During the process the material have to obtain the fully consolidation in a very short time interval. That lets to the necessity of an accurate parameter configuration.
According to previous experimental investigations the process parameters that influences remarkably in the mechanical properties of the final parts are the process temperature, the feed rate, the compaction force, fiber tension and the preheating temperature [21, 25, and 27].

The filament winding machine parameters are classified in 4 different groups depending on the main influence of each one over the final part.

1. System functionality: Are the parameters that directly affect on the process coordination. The parameters included in this group are the winding angle and the distance between the mandrel and the delivery head.
2. Heat transfer: Include the parameters that influence in the amount of heat a section of the yarn receive during the process. The parameters included in this group are the feed rate and heat gun temperature.
3. Consolidation: Include the parameters that directly influence in the material consolidation. . The parameters included in this group are the compaction force and fiber tension.
4. Pre-consolidation: Include the parameters that influence in the material consolidation before arrive to the nip point. The parameter included in this group is the preheating temperature.

The parameters of group 1 has been fixed and maintained constant during all the experimental investigation.

6.2.1 System functionality parameters

During the filament winding process, using hoop winding the mandrel rotation and the carriage travel are controlled and coordinated by the CNC. The carriage moves the determined distance for each mandrel complete rotation making the yarn lay down over the mandrel in the desired winding angle. As the yarn is not a solid element there is always a delay time between the carriage movement and the yarn laying down over the mandrel. The parameters included in this group affects directly on the delay time between the carriage movement and the yarn reaction on the laying down pattern. The control of that parameters is vital in order to avoid the discrepancies between the programed fiber path and this in the final part.

Figure 6.2. shows a basic layout of the hoop winding process of a basic two axis filament winding machine. The mandrel rotation and the carriage parallel linear travel.

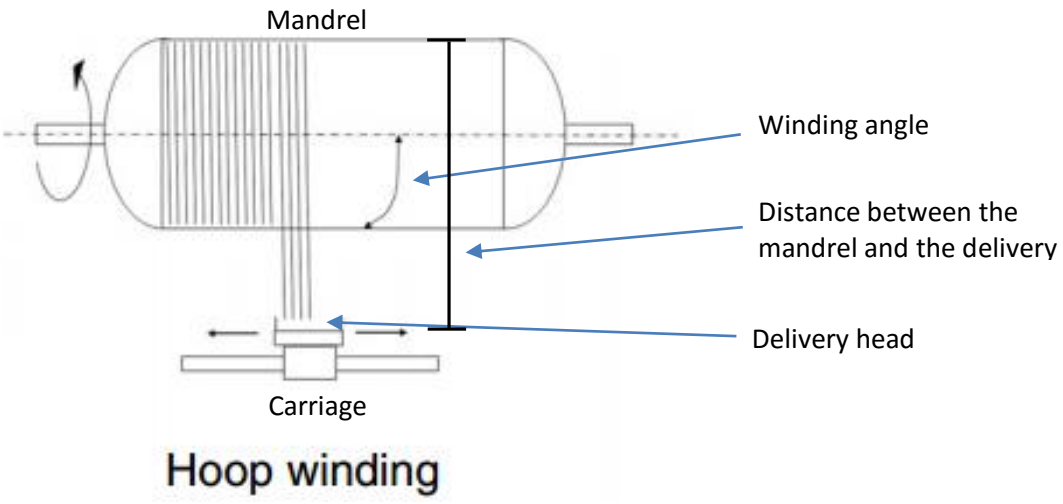

Figure 6.2. Hoop winding layout. Image property of PMCs, Woodhead Publishing.

1. Winding angle

   Is defined as the angle compressed between the winding path and the mandrel rotation axis. The fiber orientation is defined with the winding path. In general terms in hoop winding the winding angle establish the speed relation between the mandrel rotation and the carriage linear travel. So with the winding angle the CNC program calculates the advance of the carriage for each mandrel rotation. The winding angle depends directly of the mandrel and fiber diameters. As the mandrel diameter is always known the winding angle basically depends on the fiber diameter set. If the diameter set in the control program is smaller than the real fiber diameter, the carriage calculated movement will be slower than the yarn winding over the mandrel. This will cause the yarn path going out of the desired trajectory and losing the consolidation area (compaction roller), causing the process failure. On the other hand if the yarn diameter introduced is smaller than the real fiber diameter the carriage movement will be too fast and the layers will not be uniform. There will be gaps between the yarns of every complete revolution, as shown in Figure 6.3.
   The winding angle is fixed during all the experimental investigation to 89.66°.

2. Distance between the mandrel and the delivery head

   Is defined as the distance between the delivery or payout head and the first contact point of the yarn to the mandrel. The distance between the mandrel and the delivery head is represented in Figure 6.2. This parameter affects to the delay time between the carriage (payout head is the last contact point between the carriage and the yarn) movement and the yarn movement over the mandrel.
   This distance should be as small as possible. A big distance will reduce the dimensional accuracy, producing final parts with the not desired fiber orientation or an incorrect length. The distance has been fix to 50mm during all the parameter investigation.

Figure 6.3. Hoop winding example with programed winding angle higher than the necessary.

6.2.2 Heat transfer parameters

The parameters that influence on the amount of heat that the yarn is receiving on the nip point are the heating temperature and the feed rate. The combination of the two of them will determine the temperature evolution of the fiber on the nip point.

3. Heat gun temperature
   As the air flow of the heat gun is fixed and not variable for the instrument. The heat flow focused on the nip point is only dependable on the heating gun air temperature. The heat gun position is fixed during all the parameters study in order to not vary the heat flow the yarn receives. Distance between the mandrel surface and the heat gun nozzle = 30mm, heat gun angle respect the horizontal = 35°.
   The heat gun reference temperature is the maximum temperature on the centre of the heat gun nozzle. This temperature is varied between 350°C and 460°C for the parameters study.
4. Feed rate
   The linear speed of the yarn during the winding process. This parameter affects the time a section of the yarn is exposed to heat flow.
   The feed rate is set with the CNC and is varied between 5mm/s to a 100mm/s during the parameter study.

6.2.3 Consolidation parameters

Include the parameters that influence on the consolidation force.

5. Compaction force
   Applies the consolidation pressure directly on the nip point, in a defined area. The consolidation force is varied between 38N and 190N. The maximum value of the consolidation force is limited by the mandrel maximum weight. The manufacturer of the filament winding machine indicates that the mandrel cannot handle loads over 250N including the mandrel weight.

6. Fiber tension
   Winding the yarn over the mandrel under tension applies a consolidation pressure on the yarn over the mandrel because of the created tangential forces, consolidation forces are built up within

the cylinders in radial direction. The consolidation pressure is not concentrated on the nip point but is distributed over the stressed area as shown in Figure 6.4 [29]. This pressure helps to create a better consolidation on the bottom layers.
However a high fiber tension can cause that the pressure created force the penetration of the fibers into the lower layer breaking the uniformity of the structure. Furthermore it can make the thermoplastic material flow away and create direct contact between the reinforcing fibers [27]. Cirino and Pipes investigate the residual stress that the fiber tension induce on the final part [8].

The fiber tension is necessary for guiding the tow (process functionality), this must be constant during the process in order to achieve constant winding conditions. Inhomogeneous conditions might result in inhomogeneous residual stress in the final part [29, 39].
However as much higher the tension in the fiber is higher will be the fiber damage on the contact points between the fibers and the guiding elements that direct the fiber path toward the mandrel [39].
The fiber tension during the experimental process is limited by the piece extraction difficulty. As much higher is the fiber tension more difficult is the extraction. The maximum tension that able to extract the piece with a solid mandrel without angle of extraction is 13N.

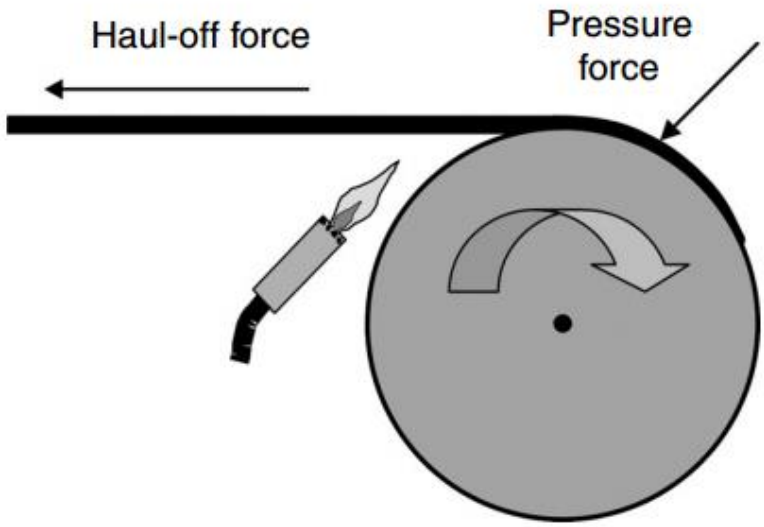

Figure 6.4. Fiber tension as consolidation pressure. Image property PMCs Woodhead Publishing.

6.2.4 Preconsolidation parameters

The preheating temperature system apply the heat by convection and radiation over the fiber before arriving at the nip point. The heat transferred is a function of the feed rate. The surface of the yarn is heated up and the melting temperature of the polymer is reached on the surface. Then the heat is transported to the yarn centre.

During the test experiments even when the preheating is at the maximum capacity (Cylinder temperature 400°C) the temperature of the yarn at the moment it arrives at the nip point is nearly the ambient temperature. Therefore in the CMAS Lab filament winding machine the preheating is not rising the temperature on the yarn before to arrive to the nip point, it is only applying a preconsolidation on the yarn. It is observable that the melting temperature is reached on the surface of the fiber tow at the maximum tested preheating power on the exit of the preheating. By heating the yarn combined with the

fiber tension a first impregnation and consolidation is produced on the yarn. The heat distribution from the yarn surface to the centre of the section is not homogeneous, because the inhomogeneous material and the air trapped on the yarn [27].

The preheating system is referenced measuring the temperature at the exit of the preheater with a thermocouple type k. The preheating yarn temperature at the exit of the preheating is varied between 40ºC and 180ºC. The temperatures obtained with the pyrometer are probably underestimated. The lack of mass on the fiber may prevent the correct measurement of the thermocouple on the yarn. When the temperature measure was 180ºC was observable the yarn had reached the melting temperature for a feed rate of 10mm/s. Increasing the power over 180ºC (yarn exit temperature), the yarn degradation was also observed.

6.2.5 Parameters summary

Table 6.1. divides the fixed process parameters and the studied parameters of the filament winding process. The work range of each parameter is also shown.

Table 6.1. Filament winding parameters. Summary

Fixed parameters				Studied parameters			
Group	Main effect	Parameter	Fixed Value	Group	Main effect	Parameter	Range
1	Process functionality	Winding angle	89.66°	1	Heat transfer	Heating temperature	350-460 °C
2	Process functionality	Distance between mandrel and yarn head	50mm			Feed rate	5-100 mm/s
3	Heat flow	Heat gun position	Dist to mandrel = 30mm Angle=35°	2	Consolidation	Compaction force	38-190 N
						Fiber tension	2-13 N
4	Magnitude received	Compaction device position	Radial	3	Pre-consolidation	Preheating system	40-180 °C

6.3 Test experiments

The study of the process parameters for this thesis has been divided in 4 different experiments:

1) Temperature – feed rate parameter window, 2) Compaction force, 3) Fiber tension and 4) Preheating temperature. They are explained in this section.

As mentioned below the winding angle heat gun position, the compaction device position and the distance between the mandrel and the payout head are fixed during all the experimental investigation.

By fixing the winding angle and the part length the specimen weight remains also fixed.

The weight of the tested specimens is $7.00 \pm 0.10g$.

6.3.1 Experiment 1. Temperature feed-rate parameter window

The first step in the process parameters study is to find the optimum work area in the parameter window between the heat gun temperature and the feed rate.

For experiment 1, 31 cylinders are manufactured varying the feed rate and heat gun temperature across the study range. Figure 6.5 plot the manufactured samples for the different parameter combination.

The different set position has been studied for the heat gun temperature: 350°C, 400°C, 430°C, 460°C. The minimum feed rate considered is 5 mm/s and the maximum 100 mm/s.

The feed rate set values have been varied in function of the visual aspect of the piece. The last tested sample for each temperature point has been set when the specimen is definitely non-consolidated.

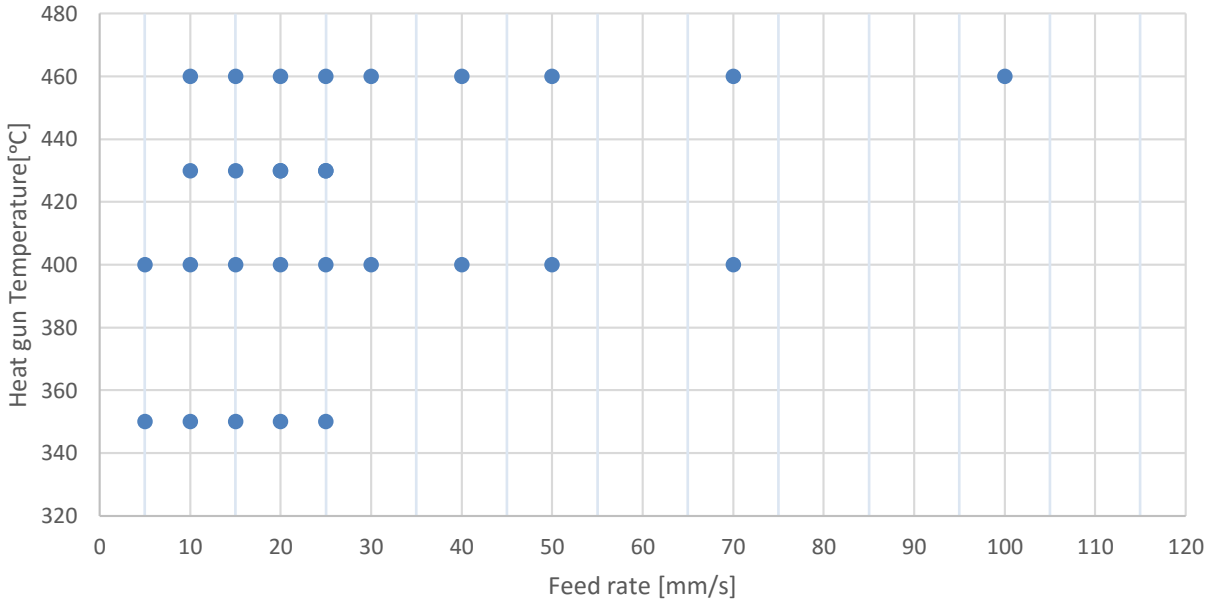

Figure 6.5. Specimen parameter configutaion of experiment 1. Processing window Heat gun temperature- Feed rate

The rest of the parameters are maintained fix during all the sample manufacturing. Table 6.2 show the fixed values of the remaining parameters during the experiment.

Table 6.2. Fixed parameters during heat gun temperature – feed rate experiment

Parameter	Unit	Value
Compaction force	N	38
Fiber tension	N	4.6
Preheating temp	°C	Off

6.3.2 Experiment 2. Compaction force.

To study the effect of the compaction force over the mechanical properties 10 cylinders are manufactured (two cylinders for each parameter combination) increasing the compaction force along the work range. Table 6.3 show the parameters configuration during the experiment.

Table 6.3. Process parameters for compaction force experiment

	Sample	C01	C02	C03	C04	C05
Compaction force	N	38	57	96	134	192
Fiber tension	N	4.6	4.6	4.6	4.6	4.6
Heating gun temp Max	°C	426	426	426	426	426
Preheating temp	°C	0	0	0	0	0
Feed rate	mm/s	20	20	20	20	20

6.3.3 Experiment 3. Fiber tension.

To study the effect of the fiber tension over the specimens 5 additional cylinders are manufactured increasing this parameter along the work range. Table 6.4 show the parameters configuration during the experiment.

Table 6.4. Process parameters for fiber tension experiment

	Sample	F01	F02	F03	F04	F05
Compaction force	N	38	38	38	38	38
Fiber tension	bar	1	1,5	2	2,5	3
Fiber tension	N	2.0	4.6	7.3	10.0	12.7
Heating gun temp Max	°C	426	426	426	426	426
Preheating temp	°C	0	0	0	0	0
Feed rate	mm/s	20	20	20	20	20

6.3.4 Experiment 4. Preheating system.

To study the effect of the preheating system over the specimens 4 additional cylinders are manufactured increasing this parameter along the work range. Table 6.5 show the parameters configuration during the experiment.

Table 6.5. Process parameters for preheating system experiment

	Sample	PT01	PT02	PT03	PT04
Compaction force	N	38	38	38	38
Fiber tension	N	4.6	4.6	4.6	4.6
Heating gun temp Max	°C	424	424	424	424
Heating gun temp AVG	°C	415	415	415	415
Yarn temperature exit preheat	°C	25	40	70	180
Feed rate	mm/s	20	20	20	20

6.3.5 Reference

To normalize the manufactured cylinders measured parameters a reference is manufactured.
In other investigations; A. Maffezzoli compare the pipes of Polypropylene-GF with a dry wound pipe followed by vacuum bagging and cured in an oven [13]. Rosselli compare his test rings from AM7/APC2 with a post processed ring in autoclave (T=460ºC, Pressure=0.6Mpa, Time=20 minutes) [45]. Mantel, manufacture a reference with compression molding process [31].

The reference is finally manufactured using the compression molding process. Table 6.6 show the process parameters for the reference manufacturing.
The references has not the same geometry as the cylinder wound, it is completely flat as shown in Figure 6.6.
An attempt to manufacture the reference with filament winding and later post processed the wound cylinder in autoclave was test. It was not possible due to the available materials for the vacuum bag could not hold the high temperature processing requisites of the thermoplastic material.

Table 6.6. Process parameters of reference manufacturing with compression molding.

Number of layers	-	8
Process temperature	ºC	240
Pressure	kN	50
Pressure time	min	30

Figure 6.6. Reference manufactured with compression molding

6.4 Mechanical characterization

The cylinders wound for the different experiments has been mechanically characterized to quantify and compare the quality of the manufactured specimens.

There are several methods to quantify the mechanical properties of the specimens. Based on different layout tests and testing apparatus the methods quantify the laminate properties of the specimens in one of the three shear modes. In other studies Lauke and Friedrich test their ring of GF-PA12 powder impregnated fiber specimens using the axial beam flexure test and double cantilever [27]. Maffezzoli evaluate the laminate properties of his ring specimens of GF-PP commingled yarn by performing a flexural analyse cutting the specimens in fiber direction and 90° direction [13]. Lauke, Bechert and Schneider study de interlaminar shear stress on curved composite samples with a specific shear device [26].

In this work the samples has been characterized by two different methods. Cylinder radial compression and short beam strength test.

6.4.1 Methods

The two different methods used to characterize the mechanical properties of the cylinders are described in this section. Both test are measured with the Zwick 1474, an international mechanical testing machine for testing samples belonging to the CMAS Lab.

1. Non-destructive test: Cylinder radial compression

   All the cylinders are tested with a non-destructive test, cylinder radial compression, to obtain a tentative idea of the parts mechanical properties. Standards describing the test procedure are not available, but the cylinders were tested by this method due to the advantage that it presents. The cylinders are no damaged during the testing and it is a quick test.

   Figure 6.7. shows the radial compression test layout. The cylinder is positioned between the two plates and compressed 1.5 mm in radial direction. The scatter compression force – z axis deformation is obtain for each cylinder. The spring constant [N/mm] (slope of the curve) is the measured parameter of this test. The spring constant represents a big part of the modulus of elasticity but depends on the specimen dimensions. The thickness variation on the cylinders can influence on this parameter.
   The compression velocity of the Z axis during the test is 2mm/s.

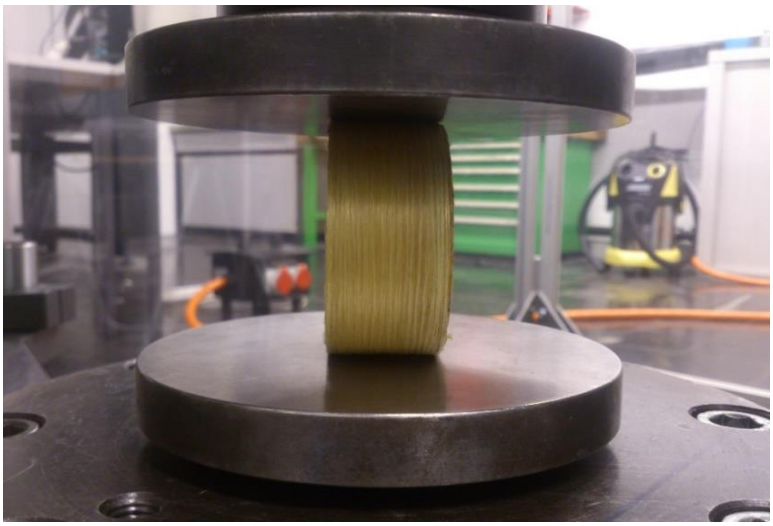

Figure 6.7. Nondestructive test. Cylinder radial compression.

2. Destructive test. Short-beam strength.

   A second mechanical test is applied to the specimens to determine que quality of the cylinders, the short beam strength test. The interlaminar shear stress of the specimens will be determined. The cylinders are cut with a circular diamond saw with water refrigeration. Figure 6.8 and Figure 6.9 show the specimen sample dimensions and the test apparatus. Five samples of each specimen are tested in order to obtain the Short-Beam Strength average, standard deviation and coefficient of variation. The test method is described on the standard ATSM-D2344-89 [3].
   The modulus of elasticity is also calculated as explained in ATSM D790 [4] for the samples tested with this method. It is necessary to comment that is not recommended to analyse the Emodulus in short specimens [4], but the parameter is analysed to observe if it develops the same trends as that of the shear short beam strength.

Not all the cylinders are tested using the short beam strength test due to the amount of time that requires to prepare and test the specimen samples. The cylinders tested are the ones that represent the optimal working area of the cylinder radial compression test results. For the experiment 1, 18 specimens are tested over the 31 manufactured. For the experiment 2 compaction force 5 specimens are tested. All the cylinders of experiment 3 and 4 are tested with this method.

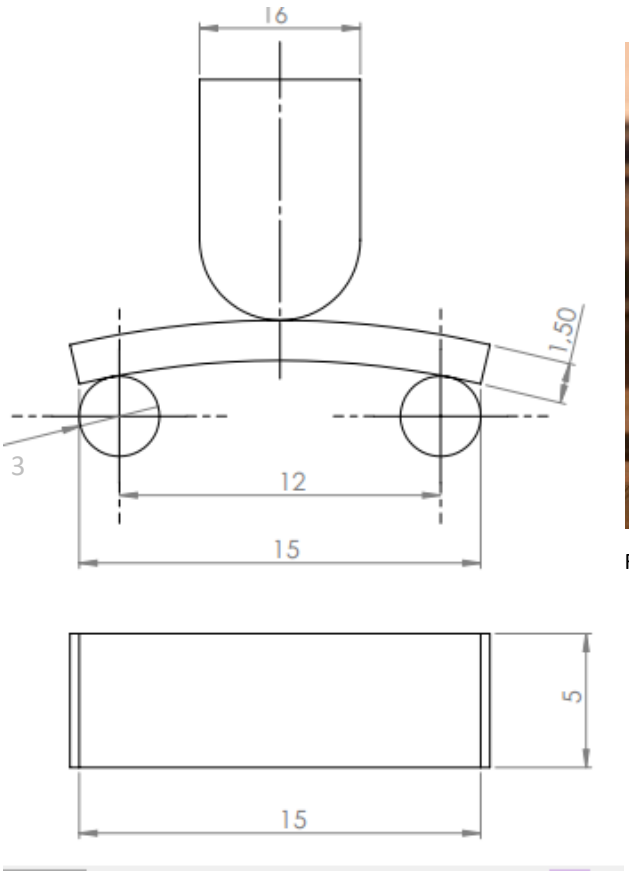

Figure 6.8. Short beam strength test bench apparatus

Figure 6.9.Short beam strength test bench apparatus and sample dimensions

6.4.2 Discussion of the different failure mode in function of the specimen consolidation

During the short beam strength test was observed a difference on the failure modes of the tested samples specimens depending on the specimen degree of consolidation. The degree of consolidation is qualified in function of the mechanical results.

While testing the specimens with higher short beam strength and Emodulus constants was visually identified that the samples were failing by interlaminar shear. On the other hand the specimens with a lower mechanical constants had a more plastic behavior, in this case the sample presented an inelastic deformation failure. Figure 6.11 shows a graphic representation of the two observed failure modes.

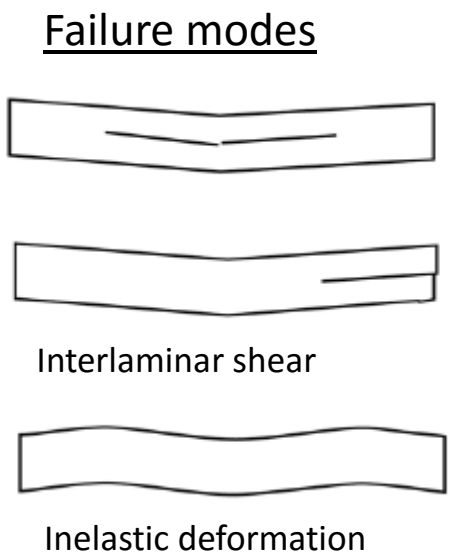

Figure 6.11. Different failure modes on the short beam strength test. Image property of ASTM international.

Figure 6.10. Inelastic deformation failure sample of a non-consolidated specimen.

Figure 6.12 and Figure 6.13 plot the standard force applied over the sample in function of the sample deformation for two different specimens during the short beam strength test. The specimen 1 of

Figure 6.12 is manufactured with a feed rate of 50 mm/s, the specimen 2 of Figure 6.13 was manufactured with a feed rate of 50 mm/s. The rest of the process conditions are maintained fix for both specimens. The specimen 2 that has a higher consolidation degree is failing by interlaminar shear while specimen 1 is not breaking, is failing by inelastic deformation. Then the composite material behaves more plastic when the consolidation decreases.

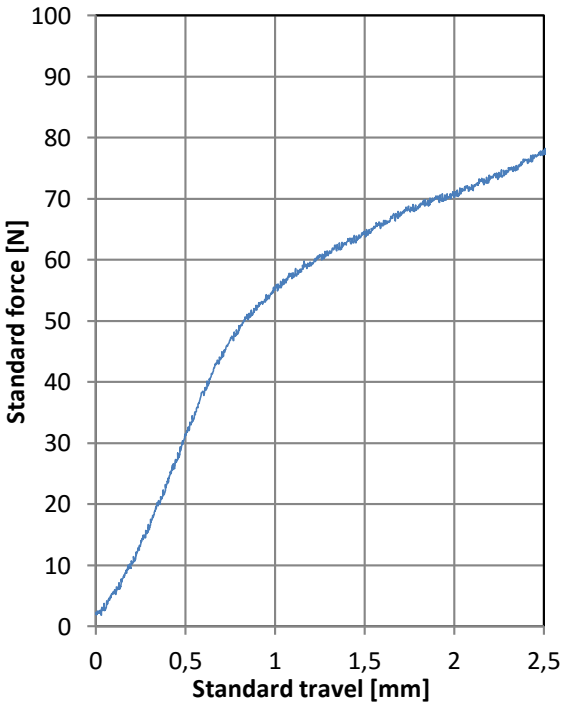

Figure 6.12. Difference on failure mode Short beam strength test. Specimen 2. Process temperature 460ºC, feed rate =50mm/s.

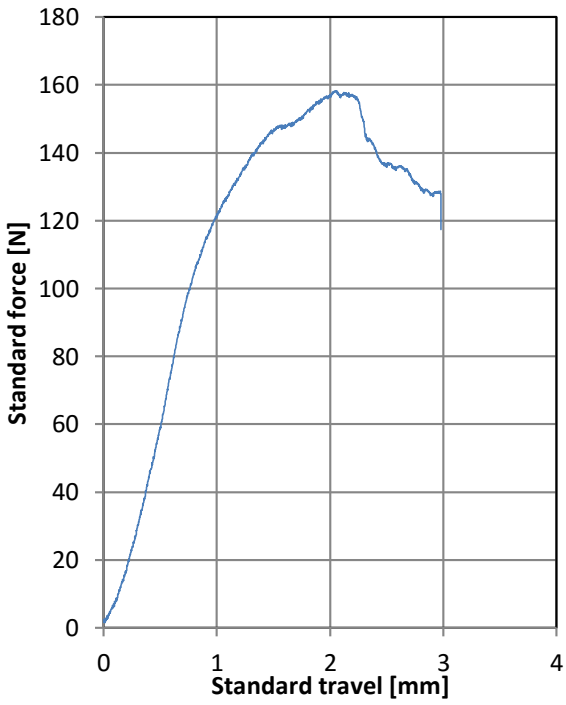

Figure 6.13. Difference on failure mode. Short beam strength test. Specimen 1. Process temperature 460ºC, feed rate =10mm/s.

6.4.3 Experimental results. Experiment 1. Feed rate-heat gun temperature window

This sections collects the experimental results obtained on the experiment 1, feed rate - heat gun temperature window for the two mechanical analyse.

6.4.3.1 Radial compression test results

Figure 6.14 plots the spring constant variation in function of the feed rate for the different heat gun nozzle temperatures.

Figure 6.15 plots the spring constant variation in function of heat gun nozzle temperature for the different process feed rates.

The spring constant value increases when the work temperature increase and the process feed rate is lower. Then, is possible to obtain an equal value of the spring rate for higher process feed rates by increasing the work temperatures. The process velocity then is highly dependent on the quality of the main heat source.

A surface is fit using the collected data points covering all the parameters range to visualize the optimum working area of the parameter window. Figure 6.16 and Figure 6.17 plot the generated surface.

The radial compression cylinder test results indicates that the optimum work area is positioned around 410ºC and 440ºC degrees and a feed rate interval between 5mm/s and 30mm/s.

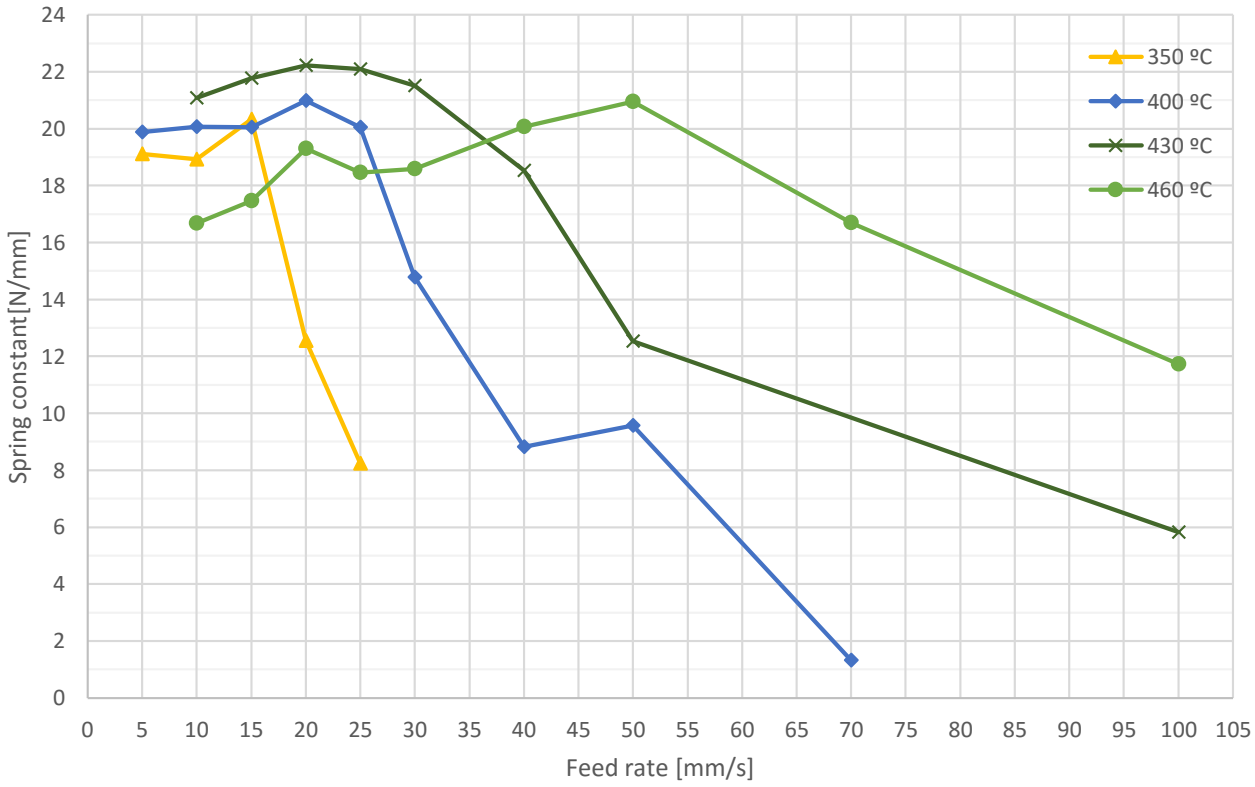

Figure 6.14. Spring constant variation in function of the process feed rate for different heat gun nozzle temperature.

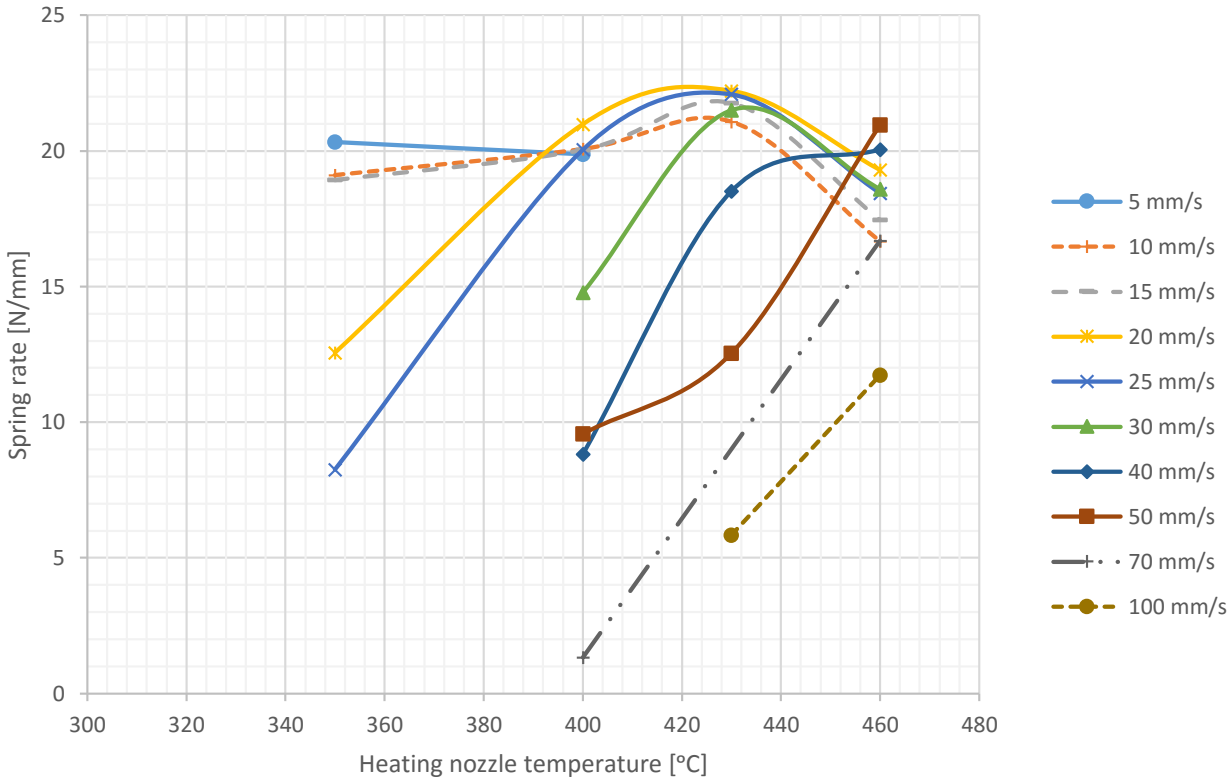

Figure 6.15. Spring constant variation in function of the heat gun nozzle temperature for different process feed rate

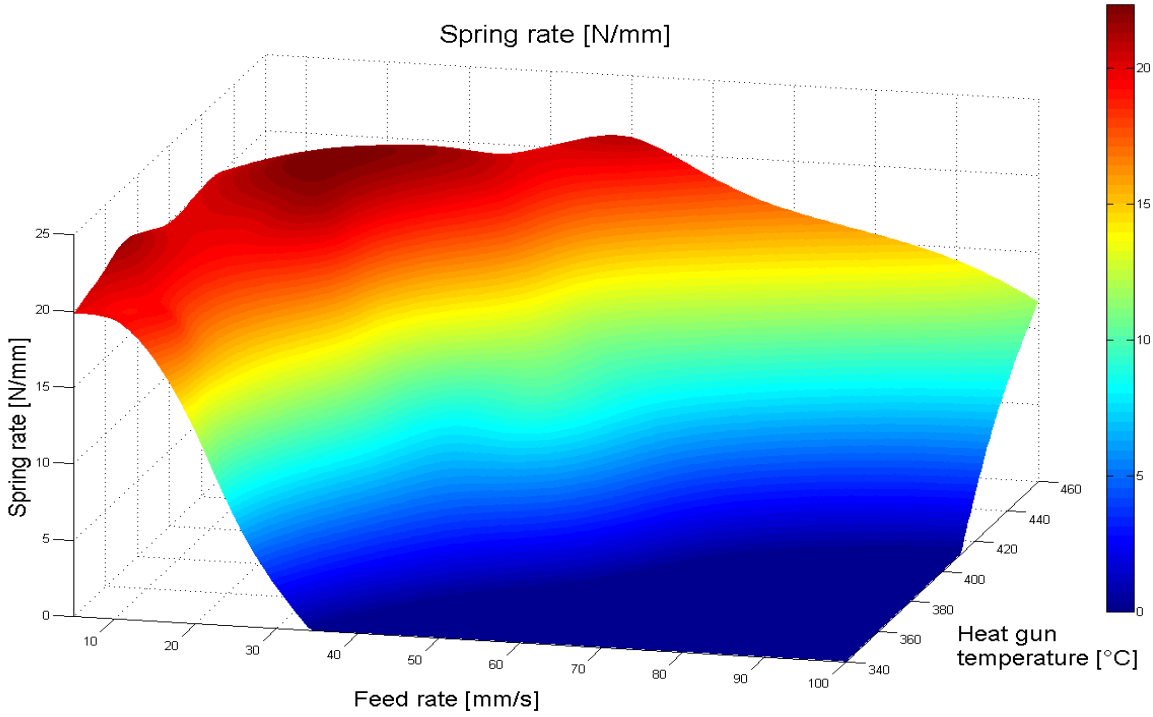

Figure 6.16. Spring constant – feed rate – heat gun temperature fit surface results. 1

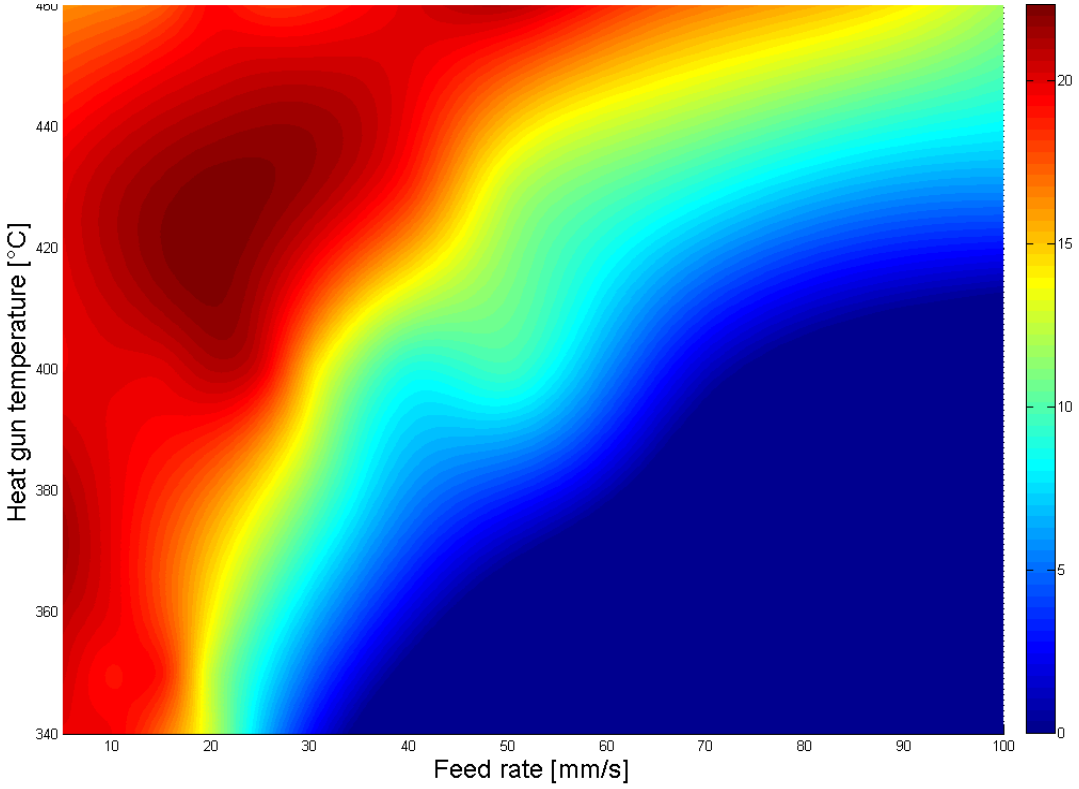

Figure 6.17. Spring constant – feed rate – heat gun temperature fit surface results. 2

6.4.3.2 Discussion of the thickness and length variation along the parameter window

During the experiment analyse it is observed that varying the parameter window the specimen thickness and length dimension also vary.

Figure 6.18 plots the thickness variation for the different heat gun temperature – feed rate parameter combination. It is observable that the specimen thickness decrease by increasing the temperature and reducing the feed rate. The consolidation force and fiber tension remains constant during all the experiment 1.

This thickness variation may be due to a lower viscosity on the thermoplastic polymer when a higher temperature is reached. The thermoplastic matrix impregnates the fibers easily and as the consolidation forces are maintained constant, the result is a more consolidated part when the viscosity of the polymer is minor.

A length variation on the cylindes is also observed along the parameter window of experiment 1. Figure 6.19 plots the length variation for the feed rate – heat gun temperature window. The cylinders length increase when the heat gun temperature increase and the feed rate decrease.

As the weight of the samples is the same for all the specimens, if the piece thickness is reduced the excess material tent to expand in length. So the more consolidated the material is longer is the final specimen, as observable in Figure 6.19.

That also indicates that the process parameters will have to be adjust for each temperature – feed rate point in order to obtain the desired final part dimensions.

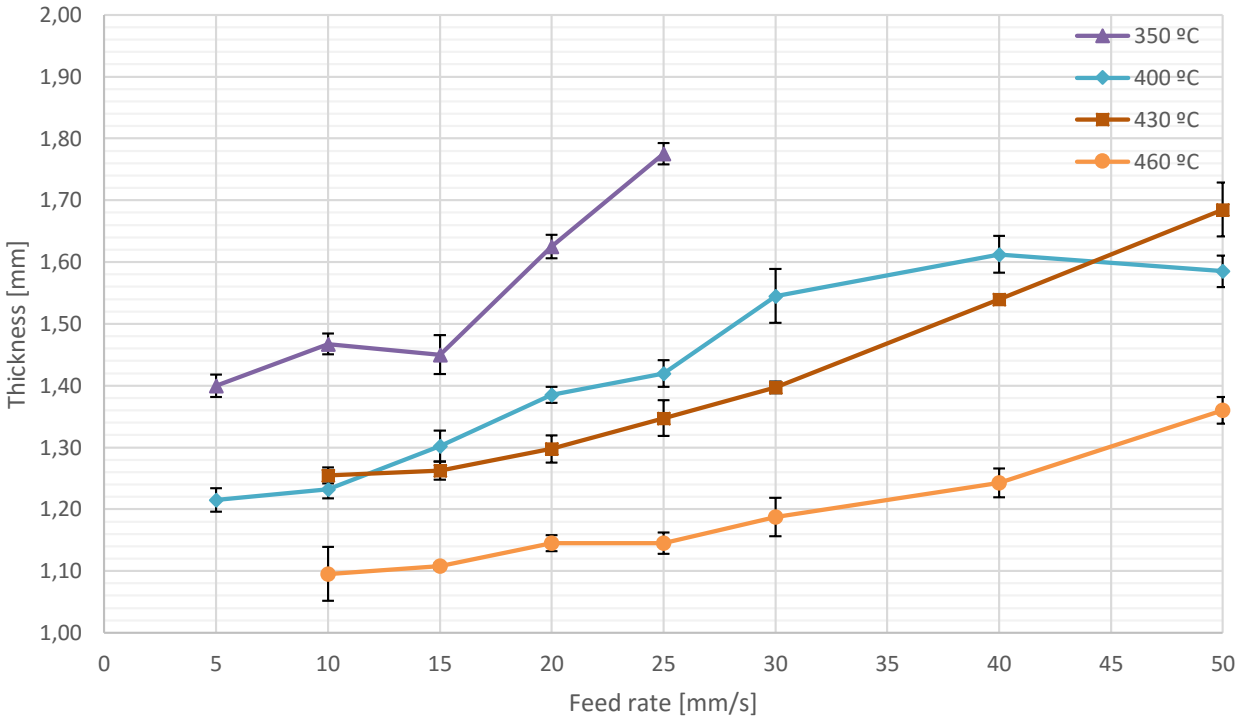

Figure 6.18. Thickness variation for the feed rate- Heat gun temperature processing window

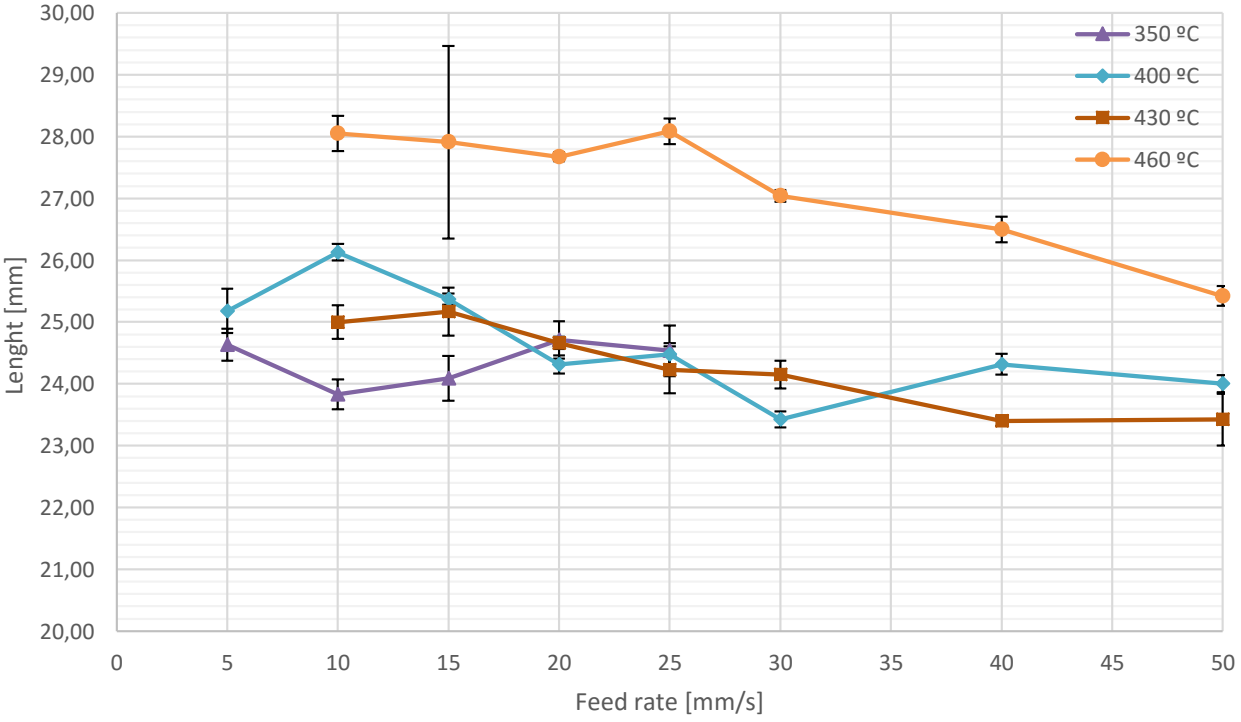

Figure 6.19. Length variation for the feed rate- Heat gun temperature processing window

6.4.3.3 Short beam shear strength test results

As the cylinder thickness and length is varied with the temperature and feed rate, the radial compression test results are considerably affected by the inertia variation caused by differences in thickness on the cylinders section. The optimal area specimens are tested with the second method, to correct that trend variation.

Figure 6.20 and Figure 6.21 plot the short-beam strength and Emodulus values variation along the feed rate for the 4 different analysed temperature values.

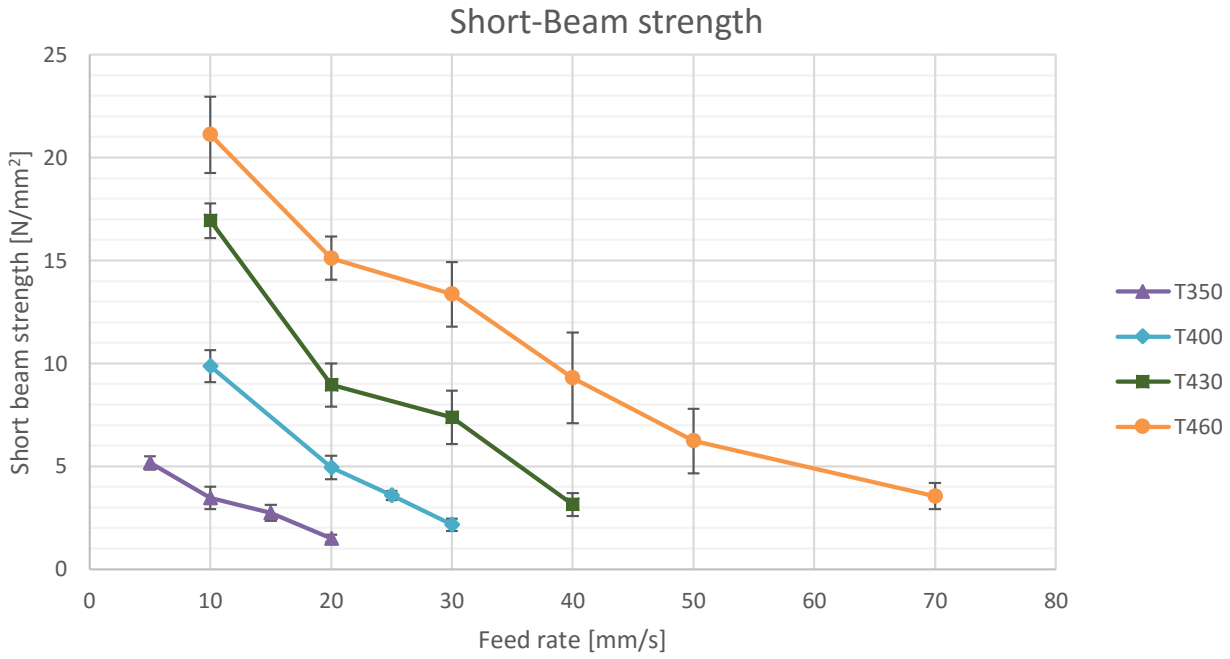

Figure 6.20. Short beam strength variation in function of the process feed rate for different temperatures.

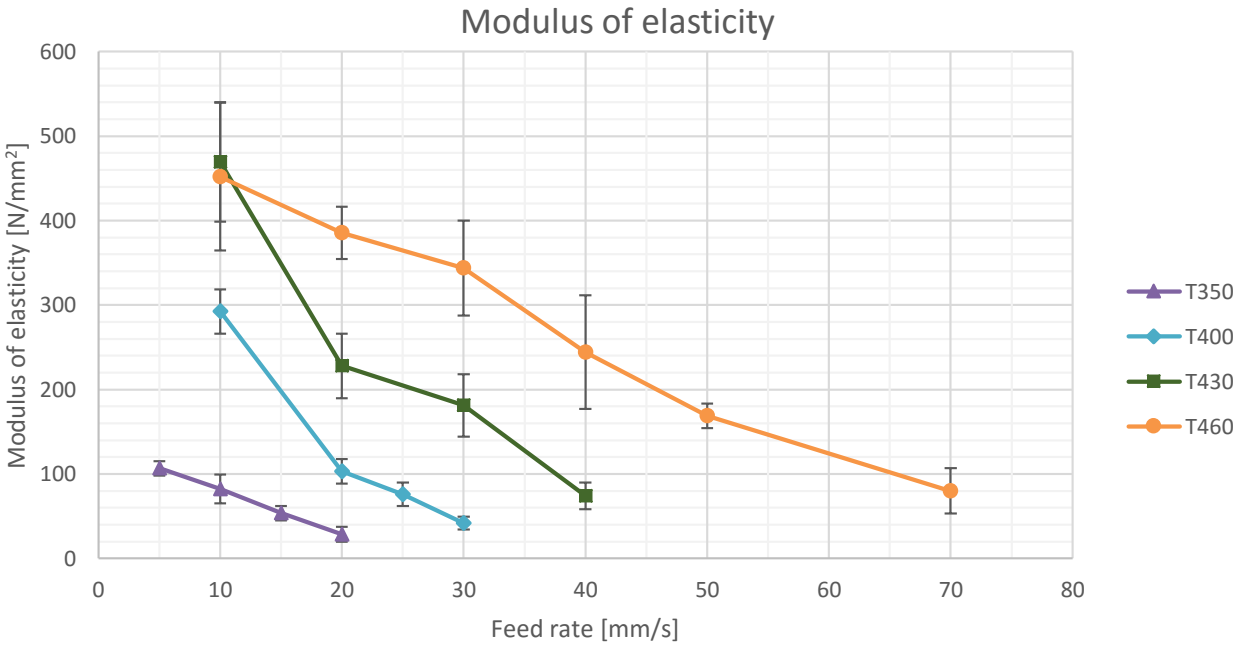

Figure 6.21. Emodulus variation in function of the process feed rate for different temperatures.

The thickness variation interferes in the trend in the radial compression test results. Is observable than the short beam strength is increasing when increasing the heat gun temperature and reducing the feed rate. The fitted surface (Figure 6.16) is corrected with the short beam test results. Figure 6.22. shows the corrected fitted surface for the short beam strength values.

The optimum working area is moved to the corner of the working area of the parameter window heat gun temperature – feed rate. So in accordance with other investigations [9, 21, 27, 50], by increasing the source temperature and reducing the feed rate the mechanical properties increases.

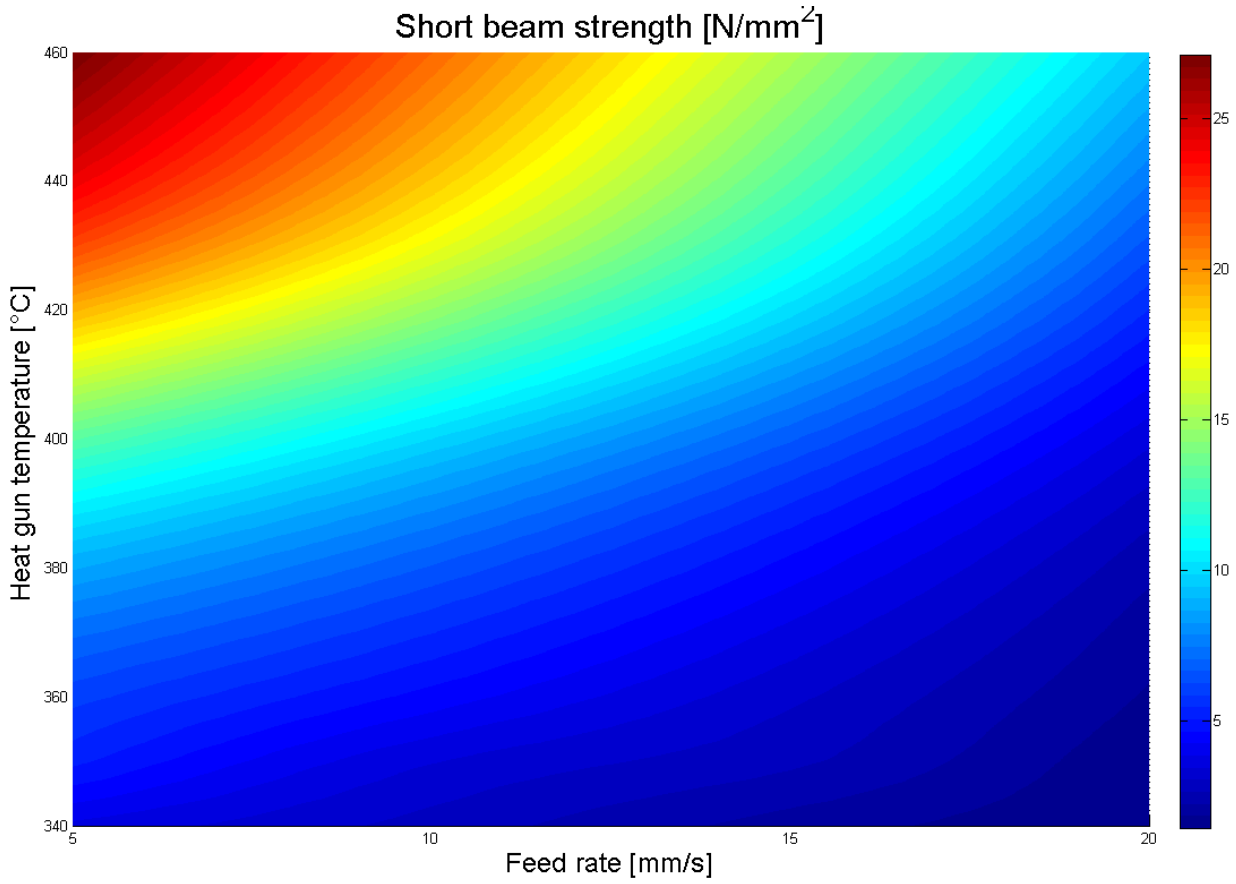

Figure 6.22. Short beam strength fit surface in function of the heat gun temperature and the feed rate. Surface created from 18 data points.

6.4.3.4 Discussion of the mechanical properties evolution with the specimen partial degradation

During the experiment one is observed that the specimens that presents the best mechanical characteristics (short beam strength, Emodulus) presents a darker tonality than the less consolidated cylinders. This specimens presents a superficial degradation in the thermoplastic fibers on the surface. There is also no appreciable degradation observed in the polished cross section microscope pictures of the specimens, Figure 6.23. Figure 6.24 show the cylinders color variation for the feed rate – main heat source temperature parameter window.

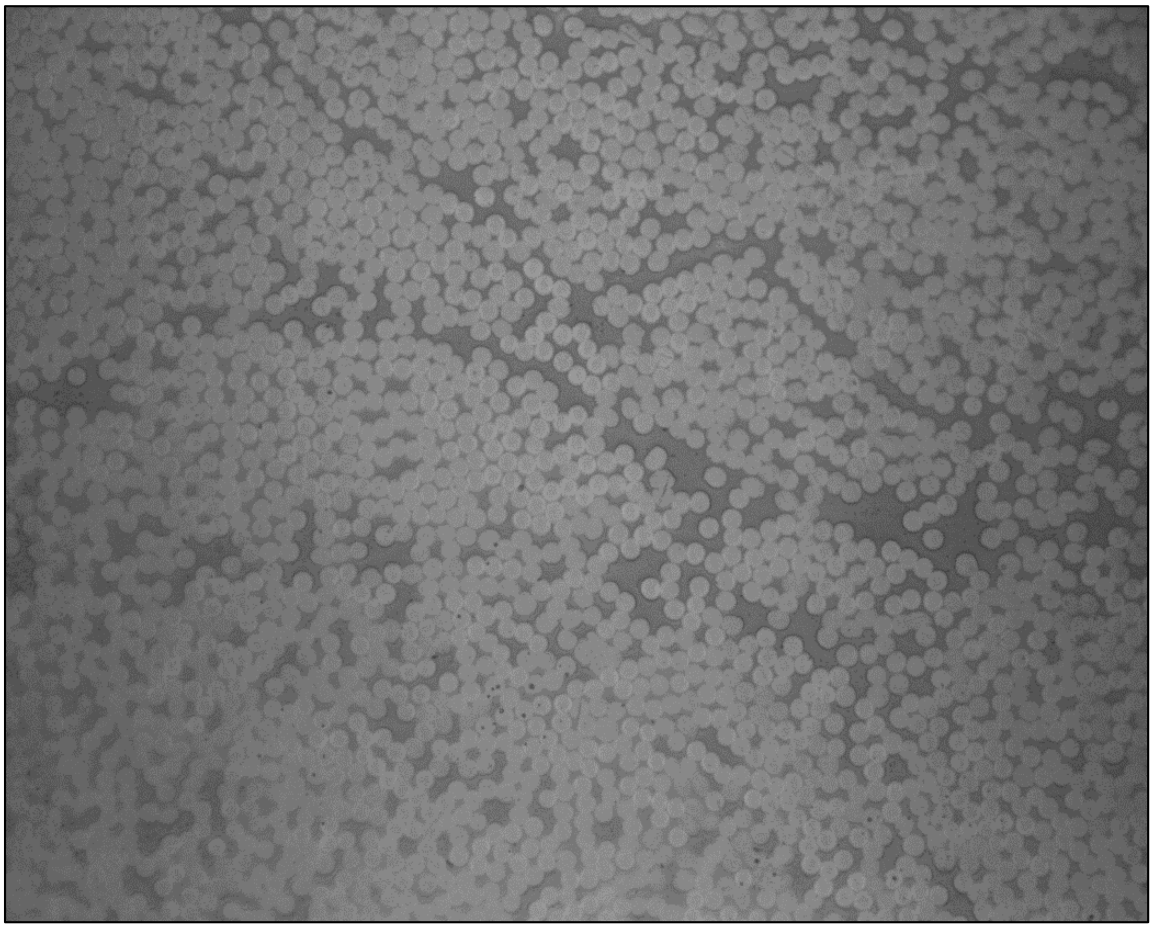

Figure 6.23. Microscope image of polished cross section of a specimen with some superficial oxidation.

Figure 6.6 show the reference manufactured with compression molding. The reference also presents that degradation on the zones near to the lateral ends (the ones exposed to the atmosphere) and presents a clear yellow color in the central part, the part that is isolated of the atmosphere by the working plastic bag.

To study the degradation behaviour of the Twaron-PA6 comingled yarn at the working process temperature. Two samples are tested with a thermogravimetric analyse tester. One under an oxidative atmosphere and the other in a non-oxidative atmosphere.

The samples are summited to 230ºC during 8 hours. Figure 6.25 and Figure 6.26 plots the weight % evolution of the material in function of the time and the sample temperature in function of the time under an oxidant and non-oxidant atmosphere repetitively.

The weight loss in Figure 6.25 and Figure 6.26 on the samples weight at the temperature of 100 °C approximately is due to the water sample evaporation.

The results show that the PA6 is starting to degrade in the oxidant atmosphere after 50 minutes of the beginning of the temperature exposition. This degradation is not occurring in the case of the non-oxidant atmosphere results. During the filament winding process the degradation is occurring in a shorter period of time. It has not been proved if the time and amount of material being degrade depends on the material heat rate. Under a greater temperature the material oxidation would start in a shorter time interval. During the experiments in the thermogravimetric analyse the heat rate is 40°C/min, but in the filament winding process is much higher. If a region is subjected to such a high temperature/time gradient is possible to over-heat some regions reducing the time interval the material bear the heat before the oxidation. The two samples are photographed with a microscope to identify the material degraded and the zones it is degraded. Figure 6.27 and Figure 6.28 show the microscope images of the sample under oxidative conditions. As the section was not flat the quality of the images is not perfect, but still to confirm that the degradation is occurring in the thermoplastic material.

The material is not heated up over the degradation temperature for any of the temperature points. So the superficial oxidative reactions may be occurring for a too long exposition period of the polymeric matrix to the heat [29].

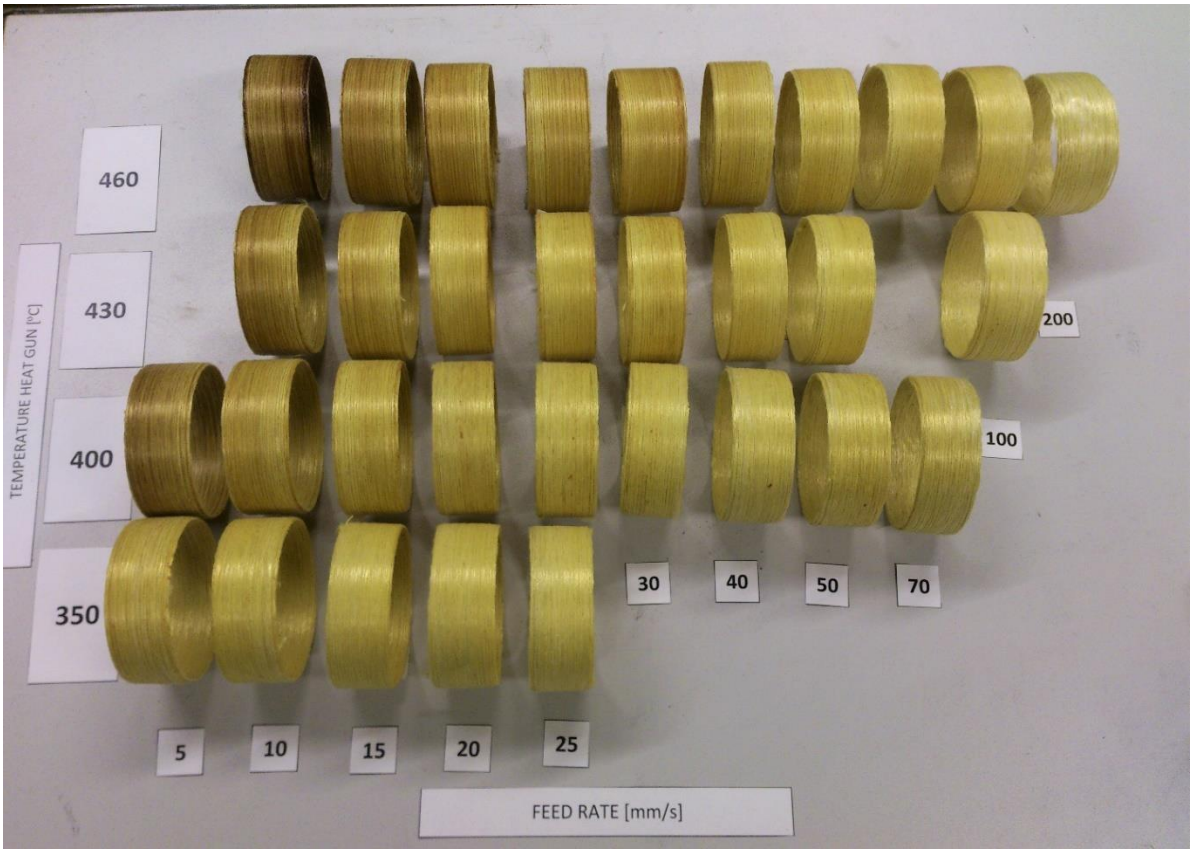

Figure 6.24. Cylinders tonality variation with the mechanical properties improvement

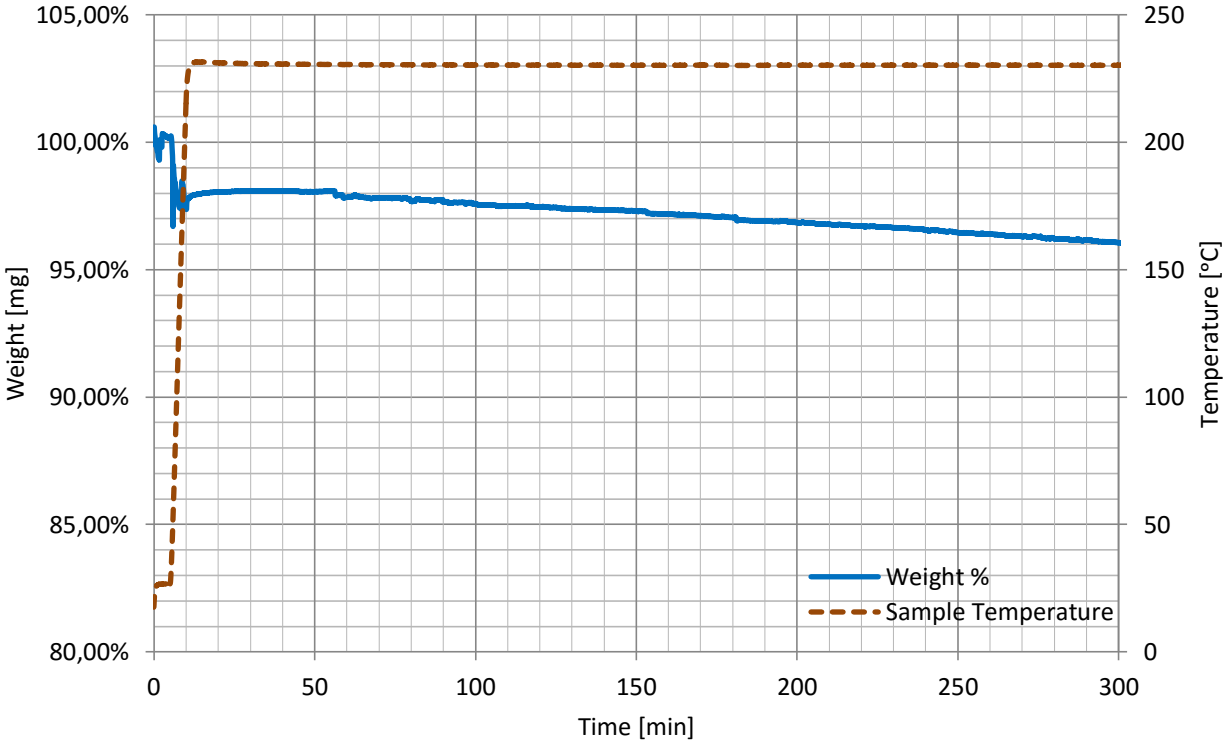

Figure 6.25. Thermogravimetric analyze measurements of commingled yarn Twaron PA6 under an Oxidant atmosphere.

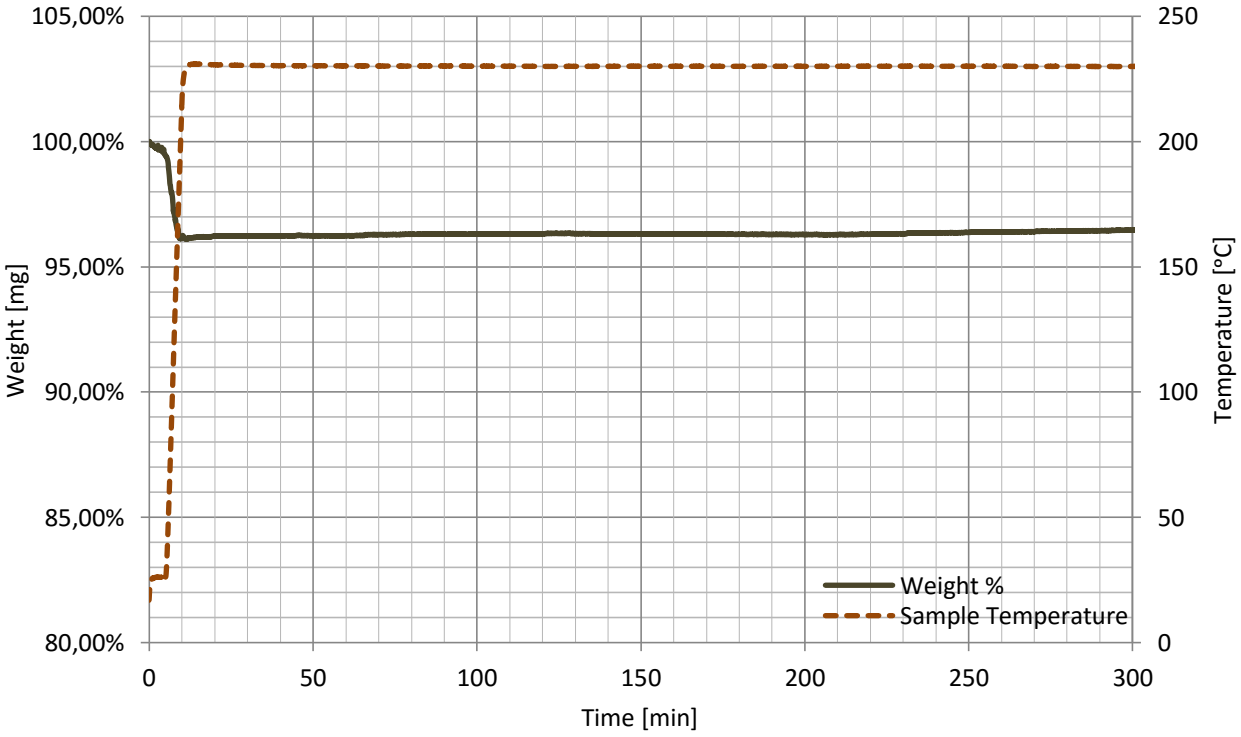

Figure 6.26. Thermogravimetric analyze measurements of commingled yarn Twaron PA6 under non-Oxidant atmosphere.

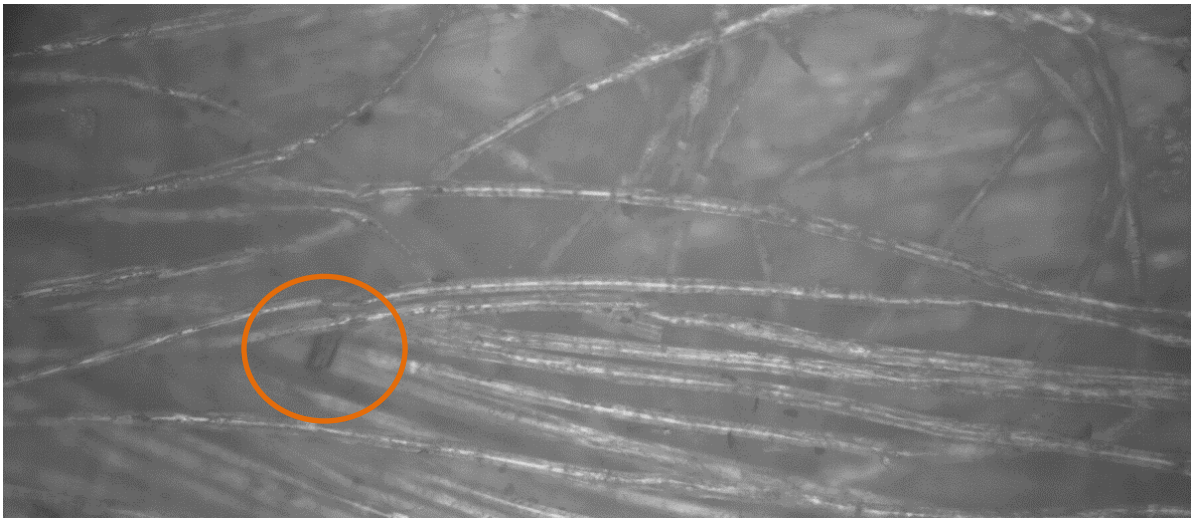

Figure 6.27. Microscope image of Twaron-PA6 summited to TGA in an oxidant atmosphere during 8 hours. 1.

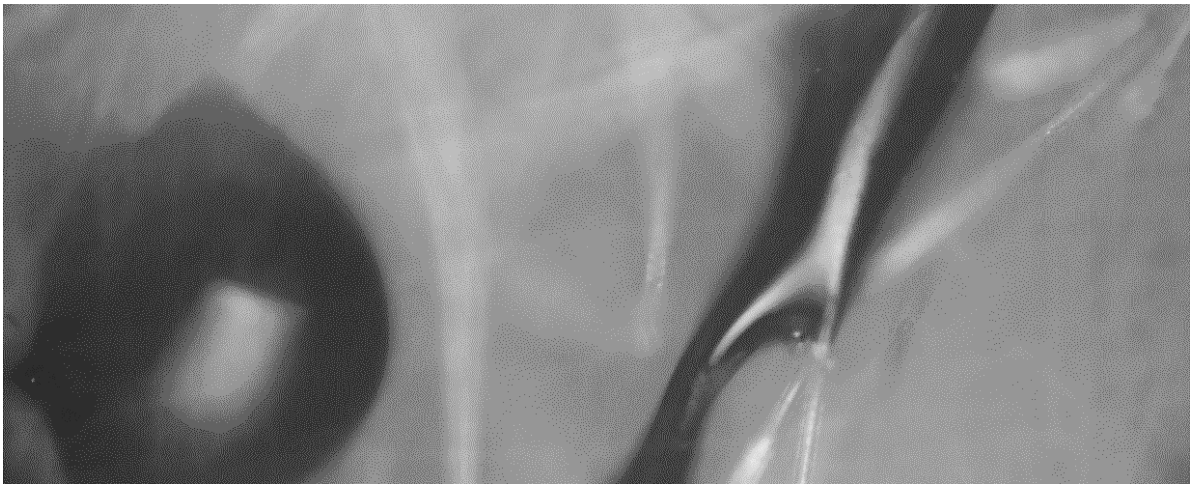

Figure 6.28. Microscope image of Twaron-PA6 summited to TGA in an oxidant atmosphere during 8 hours. 2.

6.4.4 Experimental results. Experiment 2. Compaction force

This sections collects the experimental results obtained on experiment 2, compaction force evolution. The results of the radial compression test are not considered due to the variation on the spring rate is smaller than in the experiment one results (one or two units) and the test error is too big what makes impossible to define a real trend.

6.4.4.1 Short beam shear strength test results

The 5 cylinders of experiment 2 are tested using the shear short beam strength method. The short beam strength and Emodulus is measured five times for each specimen, average and standard deviation are calculated.

Figure 6.29 and Figure 6.30 plot the short beam strength and modulus of elasticity evolution for the different compaction force inputs.

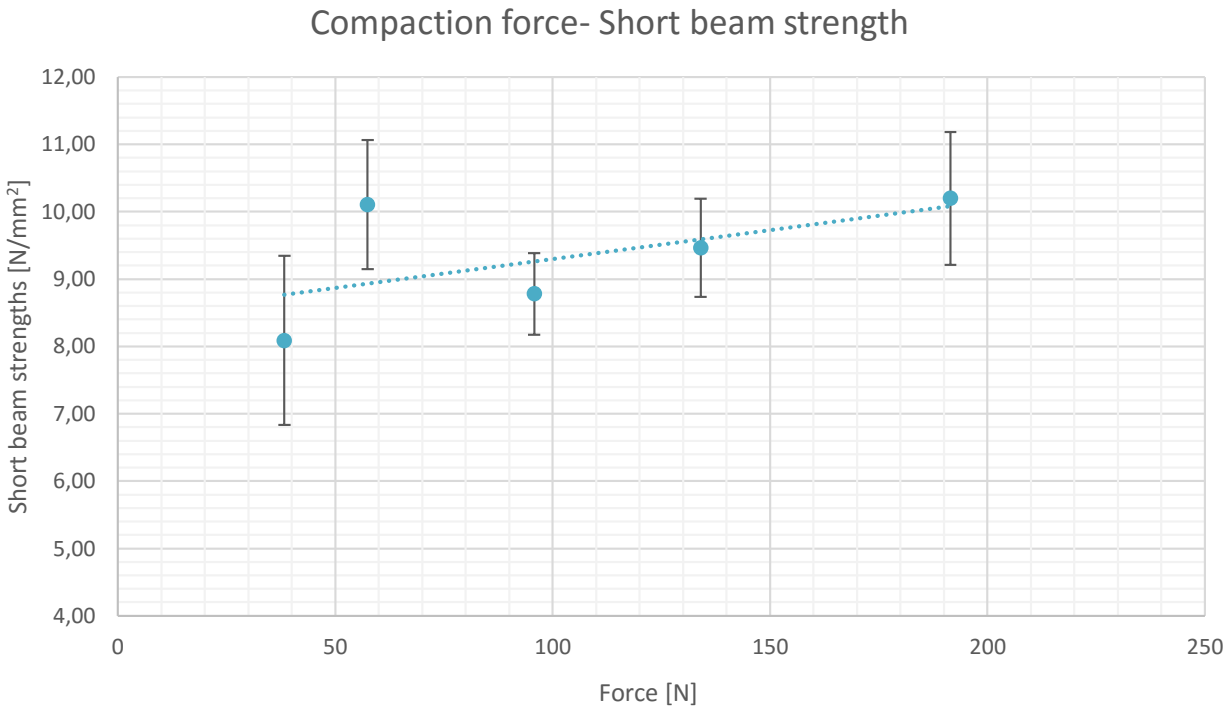

Figure 6.29. Short beam strength variation in function of the compaction force.

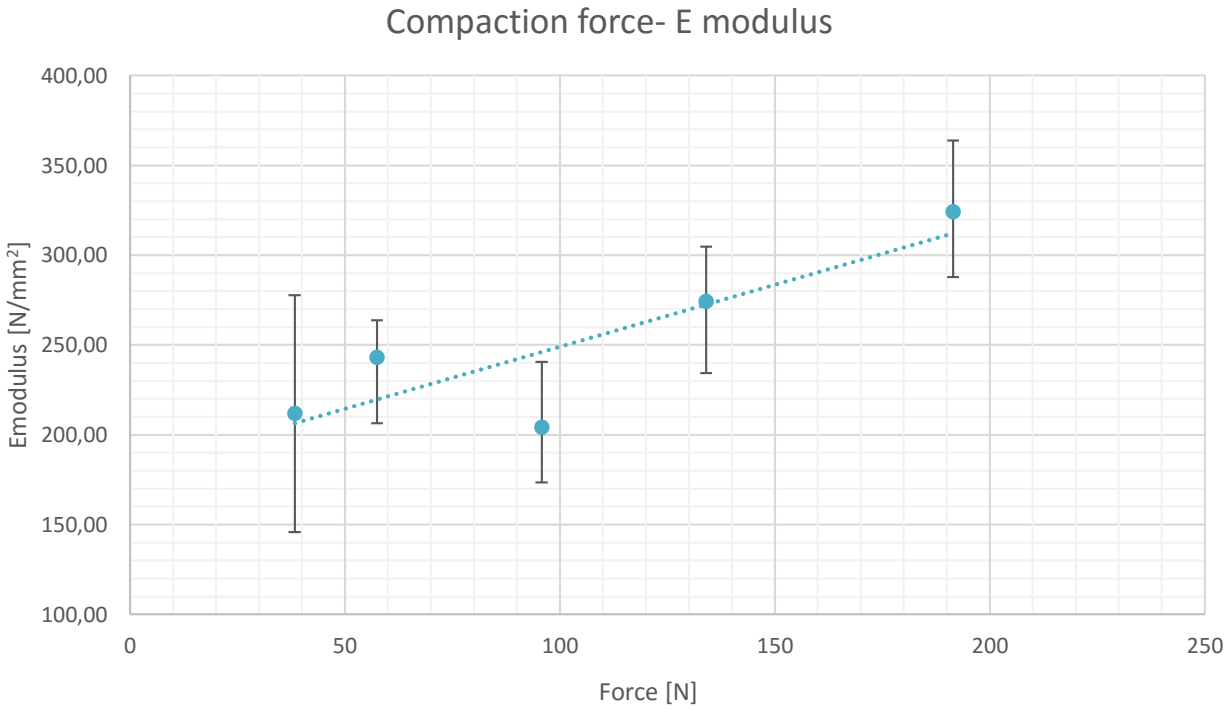

Figure 6.30. Emodulus variation in function of the compaction force.

The results show that increasing the compaction force the short beam strength and Emodulus also increase, in accordance with literature [9].

Other investigation [28] point that the shear strength does not always increase with increasing the compaction force. It is natural to think that there is always a limit to the maximum possible compaction of a part. In the actual investigation the limit has been not reached for the heat gun temperature of 430°C and feed rate 20mm/s (results above). If the consolidation limit is achieved with the compaction force the material will flow to the ends as happens during the experiment 1 with the longer cylinders (results point 6.4.2.2). Also once the limits is reached the short beam strength should not increase.

6.4.5 Experimental results. Experiment 3. Fiber tension

This sections collects the experimental results obtained on experiment 3, fiber tension. The results of the radial compression test are not considered due to the variation on the spring rate is smaller than in the experiment one results (one or two units) and the test error is too big what makes impossible to define a real trend.

6.4.5.1 Short beam shear strength test results

The 6 cylinders (there is two specimens for the fiber tension 4.6N point, average given) of experiment 3 are tested using the shear short beam strength method. The short beam strength and Emodulus is measured five times for each specimen, average and standard deviation are calculated.

Figure 6.31 and Figure 6.32 plot the short beam strength and modulus of elasticity evolution for the different compaction force inputs.

The mechanical properties of the specimens increase when increasing the fiber tension. This results has to be carefully interpreted due to the fiber tension can introduce internal stresses in the cylinders and affect to the interlaminar shear measurements [50]. Again to work with a fiber tension greater than 12 N difficulties the piece extraction.

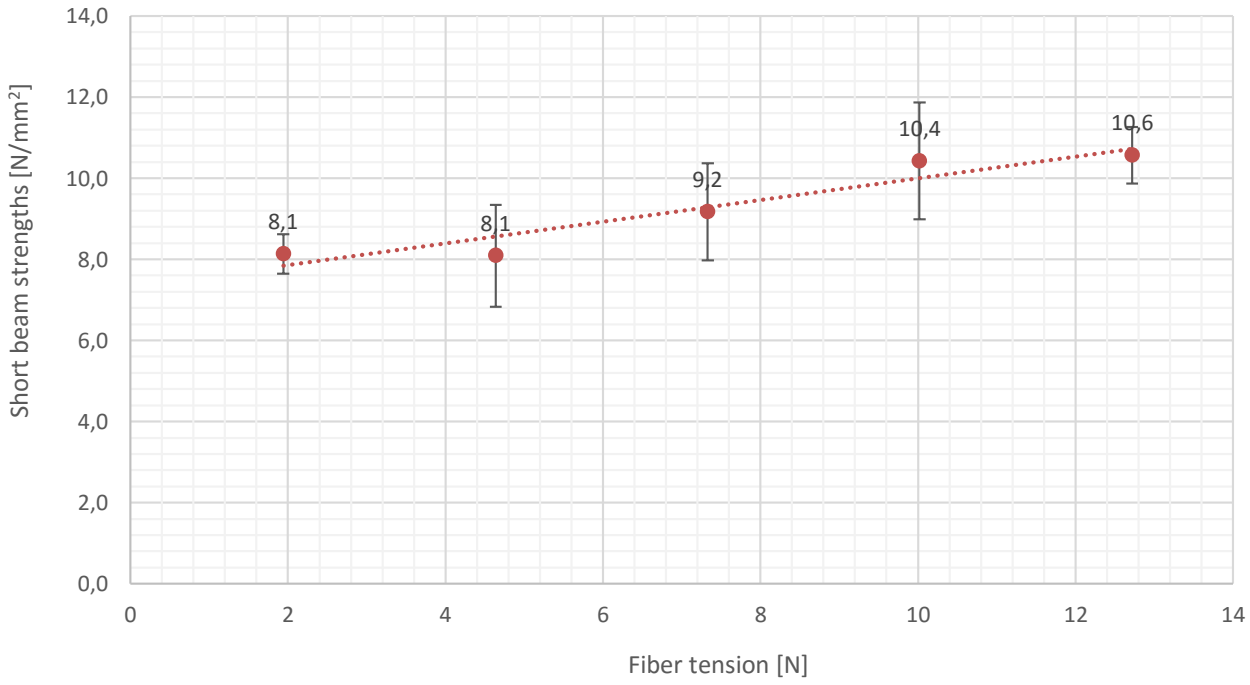

Figure 6.31. Short beam strength variation in function of the fiber tension

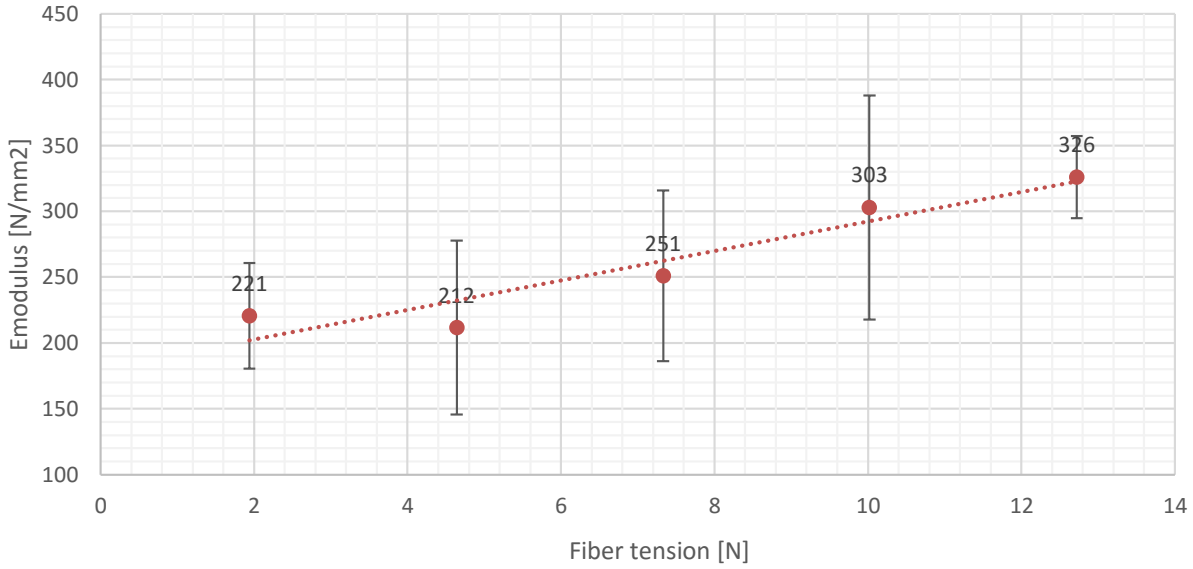

Figure 6.32. Emodulus variation in function of the fiber tension

6.4.6 Experimental results. Experiment 4. Preheating system

This sections collects the experimental results obtained on experiment 4, preheating system. The results of the radial compression test are not considered due to the variation on the spring rate is smaller than in the experiment one results and the test error is too big what makes impossible to define a real trend.

6.4.6.1 Short beam shear strength test results

The 4 cylinders of experiment 4 are tested using the shear short beam strength method. The short beam strength and Emodulus is measured five times for each specimen, average and standard deviation are calculated.

Figure 6.33 and Figure 6.34 plot the short beam strength and modulus of elasticity evolution for the different preheating temperatures.

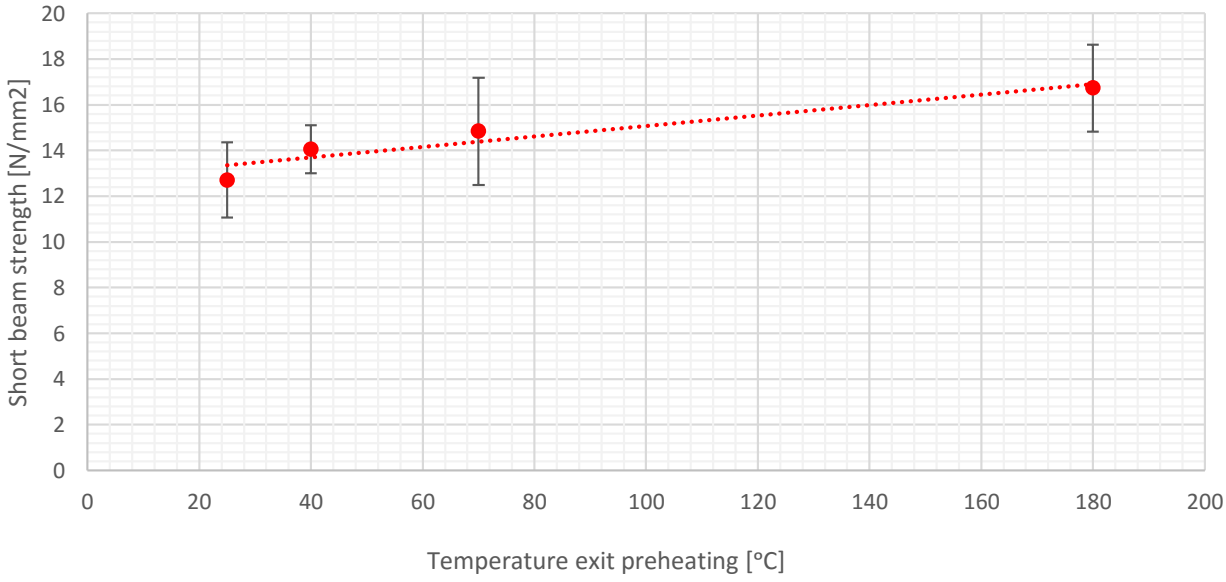

Figure 6.33. Short beam strength variation in function of the yarn temperature at the exit of the preheating system.

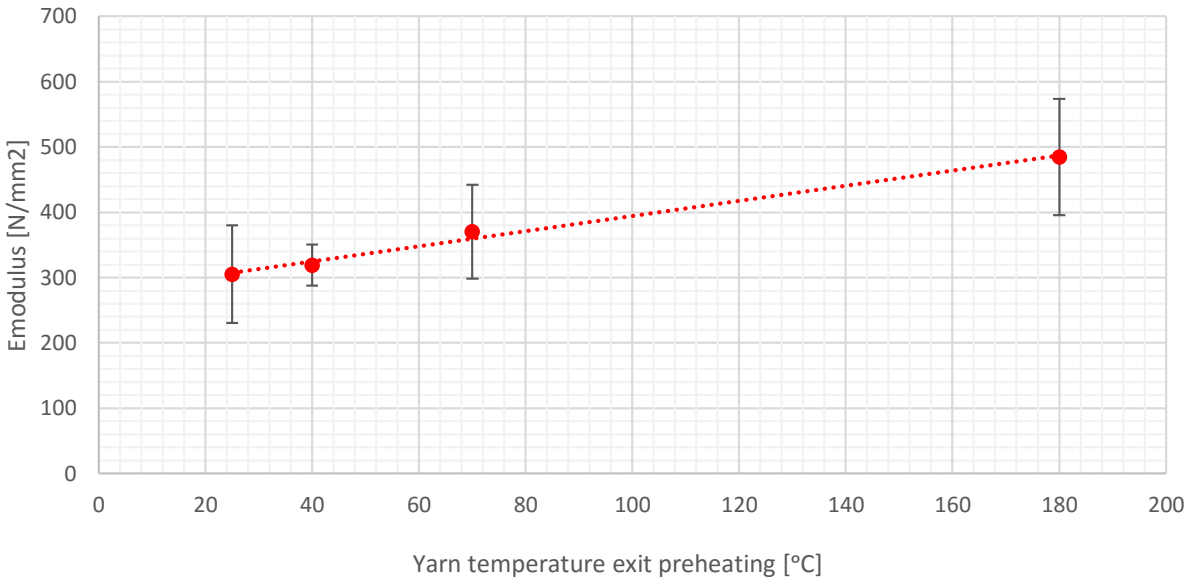

Figure 6.34. Emodulus variation in function of the yarn temperature at the exit of the preheating system.

By increasing the temperature at the exit of the preheating the short beam strength and the E modulus also increase. For an exit temperature higher than 180°C the thermoplastic material begins to be degraded. Results in accordance with literature [50].

B. Lauke and K. Friedrich discuss the effect of the preheating system in filament winding [27]. The filament winding machine layout used in their experiments includes a heated mandrel. They conclude that the influence of the preheating system decreases when the temperature on the mandrel is increased. The heat on the mandrel region is enough to melt the incoming tow and consequently the preheating is not as influent on the final quality of the product. However they also determine that the influence of the preheating system for low mandrel temperatures is significant on the consolidation quality.

It is possible that having an auto heated mandrel the pre-consolidation of the yarn occurring on the preheating is moved to the mandrel function. In the present work the mandrel is not heated for a controlled temperature so the influence of the preheating system is remarkable as shown in the results. Moreover the inner quality surface is greatly better compared than those produced without the use of the preheating system.

Probably the temperature on the yarn is higher than the values obtained with the thermocouple, the small mass of the yarn interferes with the thermocouple measurements. For this reason, the values of the preheating exit temperature are considered orientative.

6.5 Void content % characterization

The void content of the specimens is characterized and compared in order to obtain a second estimation of the quality of the cylinders.

6.5.1 Methods

Two different methods has been used to determine the fiber void content %.

1. Relation between specimen's density and theoretical density at 0% volume content

   An alternative method of the density calculation by Archimedes method, described in ASTM D792 [5, 28], is used in this thesis in order to avoid the water absorption of the cylinders.

   All the manufactured specimens has been measured with a calliper, resolution 0.01 mm. For each specimen the volume is calculated by measuring the following dimensions:

   - Inner diameter, 1 measurement to stablish the reference
   - Thickness, 4 measurements
   - Cylinder length, 4 measurements

   The specimens are weight in a scale with a resolution of 0.0001g and the density is calculated.

   The density of the specimens is calculated as follow:

$$Calculated\ density = \frac{Mass}{\pi/4(d_{out}^2 - d_{in}^2) * Length} \tag{6.1}$$

   The theoretical density of the composite yarn at 0% volume content is obtained using the calculated fiber volume % in chapter '4 Material characterization', and the theoretical densities of the Twaron and Polyamide 6 as shown in equation 1.

$$Theoretical\ yarn\ \rho = Reinforcing\ fiber\ \rho * V\% + Matrix\ fiber\ \rho * (1 - V\%) \tag{6.2}$$

   Finally the void content % of each specimen is obtained with the relation of the equation 6.2.

$$Void\ \% = \frac{Calculated\ density}{Theoretical\ composite\ density} \tag{6.3}$$

   The calculation of the standard deviation of the Void content % by the relation between specimen's density and theoretical density at 0% volume content is explained in APPENDIX D.

   Method one does not measure accurately the thickness variation along the cylinder length. Moreover the outer and inner surfaces of the open cylinders are not completely flat, so measuring the thickness with the calliper is including as void % the empty zones between the inner and outer surfaces and the calliper. A variation of 0.05 mm on the thickness of the specimens cause a void% variation of 3%. However the trends obtained with this method are correct, as the measured error inevitably committed is systematic and affect to all the samples. As a systematic error is possible to correct it.

2. Polished cross section image analyse

   The cross section of the cylinder specimens is photographed and analysed to quantify the void volume % as follow:

Twelve specimens are analysed with this method. For each specimen analysed 2 different samples are cut in order to obtain different sections on the same specimen.
Sample preparation: The cut specimens are placed in a mold and fix with a holder. Later, the mold is filled with a thermoset resin (Specifix resin). Once the resin harden the samples are grind and polished in five different steps. Figure 6.35 shows an example of the polished cross section samples. Each sample includes 5 slices.

Figure 6.35. Polished cross section samples image.

The polished cross sections are photographed with a microscope under 20 times magnification. The pictures are digitalized with an image processing and analyse program, image j. Once the picture is digitalized the void content is determined using the expressions 6.4 and 6.5. Five pictures of each sample section are analysed, a total of 10 pictures for specimen. The void content % and total pixel number of every image is annotated.

$$Void\ content\ \% = \frac{N_{void}}{N_{total}} \qquad \text{for every picture} \qquad (6.4)$$

$$Void\ content\ \%\ total = \frac{\sum Void\ content\% * N_{total}}{\sum Ntotal} \qquad (6.5)$$

Where N is the total number of pixels.

An example of the polished cross section analyse is shown in Figure 6.36.

Xiaowen Yuan compares the accuracy of the methods calculating the void % using densities relation and using image analyze [28], showing the error of the last one is minor. Therefore the second method able to obtain a good void % representative data.

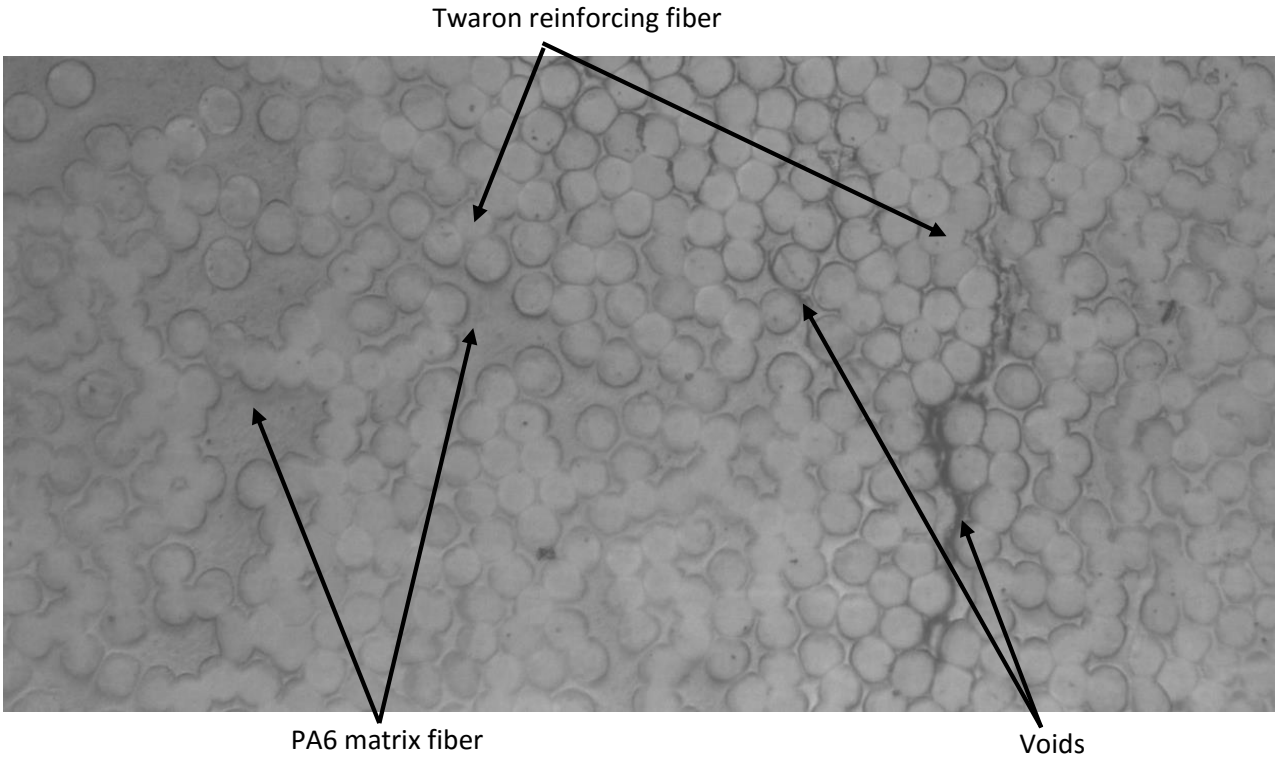

Figure 6.36. Polished cross section of Twaron-PA6 commingled yarn manufactured cylinder.

6.5.2 Experimental void content results

The results of the void content % analyse are shown in this section.

6.5.2.1 Method 1 results correction using the results calculated in method two.

Due to the high time spend to obtain the void content % of a specimen using method 2, was impossible to calculate the void % for all them. Therefore the void content % is calculated for 12 specimen using method two. The results of the 12 specimens have been used to apply a correction in the method one and that way obtain the void content % for all the desired specimens.

Figure 6.37. plots the scatter diagram of the specimen's void % calculated with method 1 and the void % calculated with method 2. A linear regression is adjusted between the two void % quantification methods. This regression is applied to the data points obtained by method one. The coefficient of correlation of the adjustment is 0.92.

The results of both methods are presented together, the corrected method 1 results and the method two results. The maximum error on the correction between the two void % calculation methods is 0.34% void.

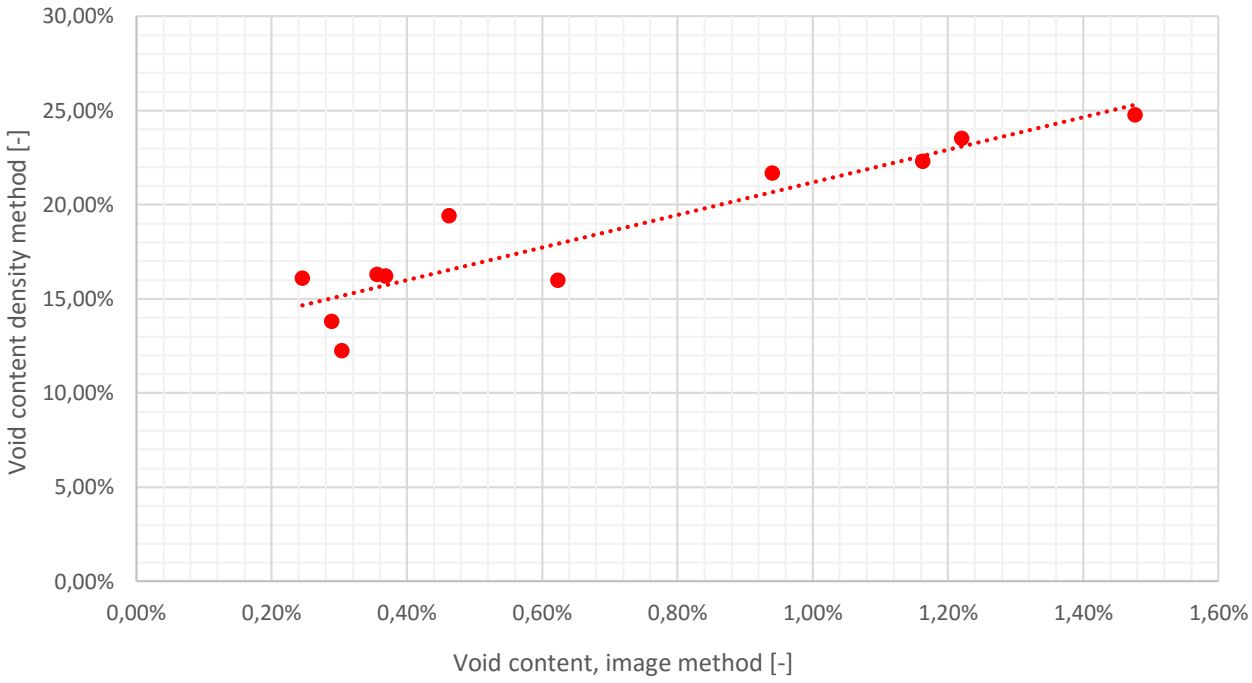

Figure 6.37. Void content % calculated by method 1 in function of the Void % calculated by method 2.

6.5.2.2 *Heat gun temperature – Process feed rate results*

The void content of the 31 cylinders manufactured in the experiment 1 is plot in Figure 6.38.

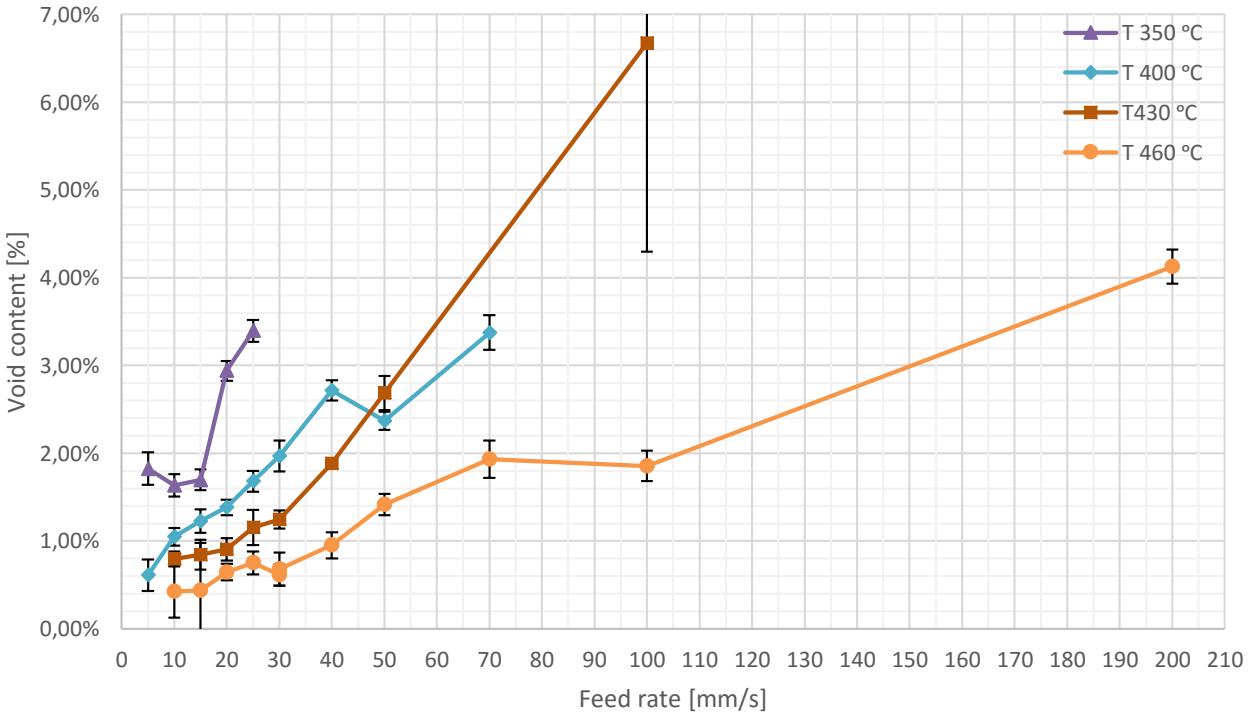

Figure 6.38. Method 1 corrected results. Void content % in function of the heat gun temperature – feed rate processing window.

The method 1 corrected results show that the void content % decrease when the feed rate decrease and the process temperature on the nip point increases. The trends shown in Figure 6.38 match with the

mechanical results, the open cylinders with best mechanical characteristics are the ones that presents a lower void content %.

The error increases when the cylinders are less consolidated. The variation of the thickness across the length is higher in this cylinders. For example the cylinder processed at 100mm/s feed rate and 430°C heat gun temperature is easily breakable by hand and possess one of the more instable results.

Figure 6.39. plots the comparison between the void % obtained by method one once this is corrected and the void obtained by method two.

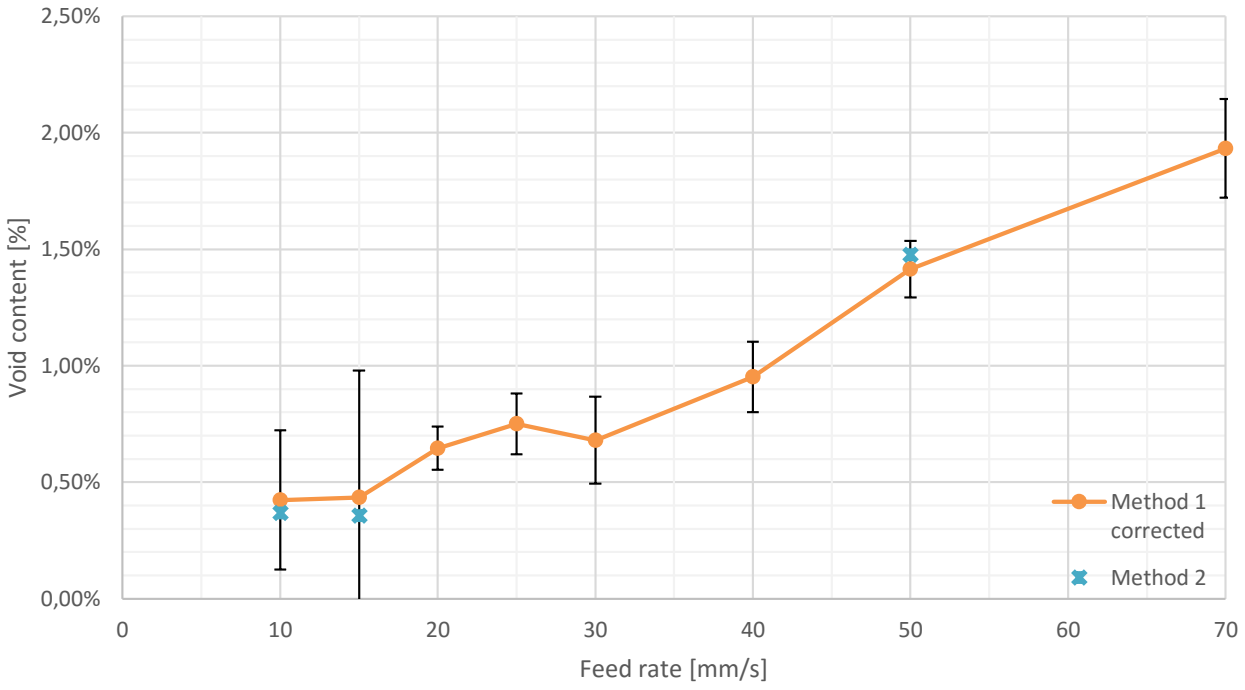

Figure 6.39. Comparison between method one corrected results and method 2 void % results. Experiment 1. Process temperature T=460°C.

6.5.2.3 Compaction force results

Figure 6.40 shows the void content % results of the corrected method 1 for the two manufactured cylinder series. The 2 void % results calculated using the method two are also included.

The void content % behaviour decrease when the compaction force increase. The results show that the cylinders with a lower volume content are the ones that presents better mechanical properties.

Again the compaction force is not reaching the limit of the piece compaction, the void content keep decreasing until the last value. It was not possible to increase more the compaction force. The force applied by the compaction device is transmitted to the mandrel supports that has a weight limit of 250N including the mandrel weight.

It would be possible to increase the temperature and observe the effect of the compaction force for higher temperatures. Probably the effect of the force decrease until reach a top limit. As in the filament winding the material is not restricted by the laterals when the piece reach or is near to reach the compaction limit this will expand for the laterals. This is proven in the section 6.4.2.2 (page 65) when the specimens under the same compaction force increase his length when the temperature increases (viscosity decrease).

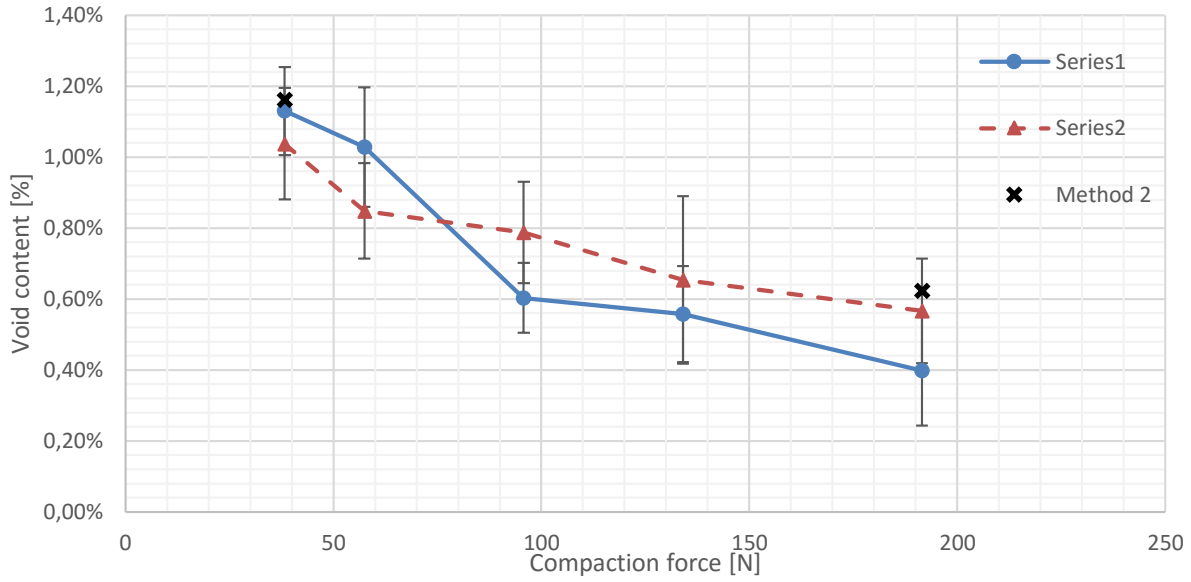

Figure 6.40. Void content % in function of the compaction force. Serie 1 and Serie 2 calculated with method 1 and method 2.

6.5.2.4 *Fiber tension results*

Figure 6.41. shows the void content % results of the corrected method 1 for the manufactured cylinders. The 3 void % results calculated using the method two are also included.

A clear reduction on the void% of the specimens when increasing the fiber tension using method one is not observable. However the results calculated by method two show a decreasement in the void content % when increasing the fiber tension in accordance with the mechanical results.

The lack of information obtained by method one may be due to a smaller influence on the fiber tension over the consolidation on the cylinder than with the rest of parameters. Also the cylinder wound with a fiber tension greater than 1.5 bar (4.6N) could have been damaged in the extraction procedure. Because as much the fiber tension increases, more difficult is the extraction of the specimens. It is then not recommended to increase the fiber tension, the consolidation obtained does not compensate the created disadvantages.

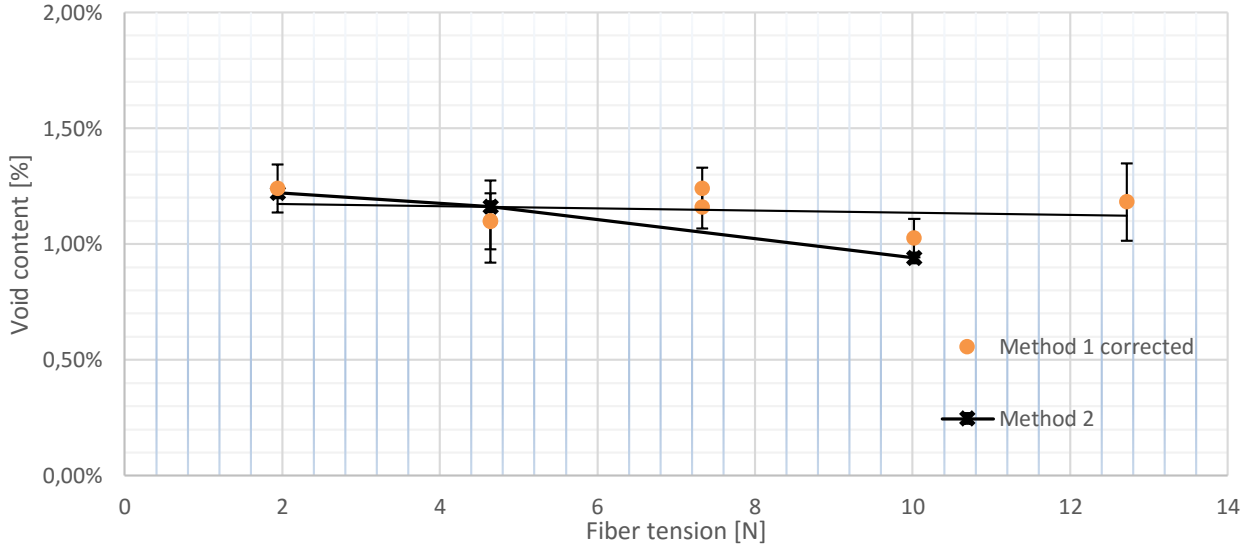

Figure 6.41. Void content % in function of the fiber tension parameter calculated with method 1 corrected and method 2.

6.5.2.5 Preheating system results

Figure 6.42. shows the void content % results of the corrected method 1 for the manufactured cylinders. The 2 void % results calculated using the method two are also included.

The void content % decrease when the preheating temperature increase. The results show that the cylinders with a lower void content are the ones that presents better mechanical properties.

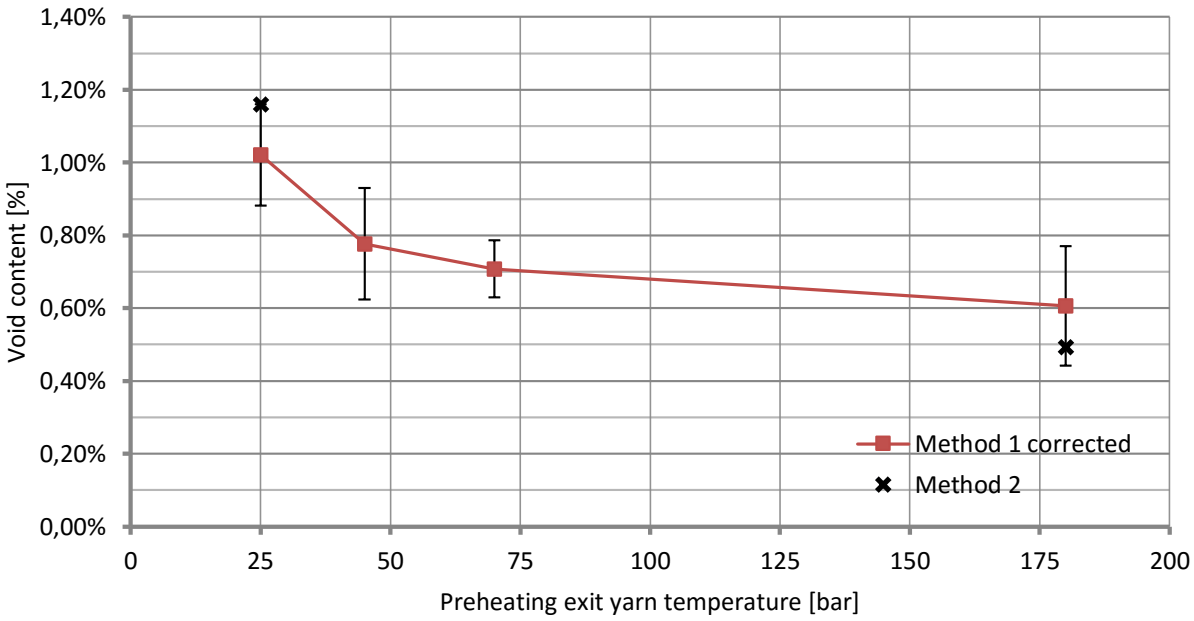

Figure 6.42. Void content % in function of the preheating exit yarn temperature. Method one corrected and method 2

6.6 Mechanical analyze results and void content results comparison

The short beam strength test results are compared with the void content % calculation. The correlation between the two measurements is studied.

Figure 6.43 plots the scatter diagram of the short beam strength results as a function of the void % calculated with method 1. The cylinders analyzed with the short beam strength method are compared with the results of the void content calculated by method 1 and later corrected with exception of:

- The 3 compared fiber tension cylinders. Void content obtained by method two is directly compared.
- Final cylinder, thick and long: The void content used in the scatter diagram are the calculated by method 2. Cylinders explained in section 6.7.1, page 84.

The results show a clear negative correlation. The coefficient of correlation is 0.9347. Then the results of the mechanical analyze has been successfully double checked with the void content results. The mechanical analyze and the void content % are good indicators of the quality of the final part consolidation degree.

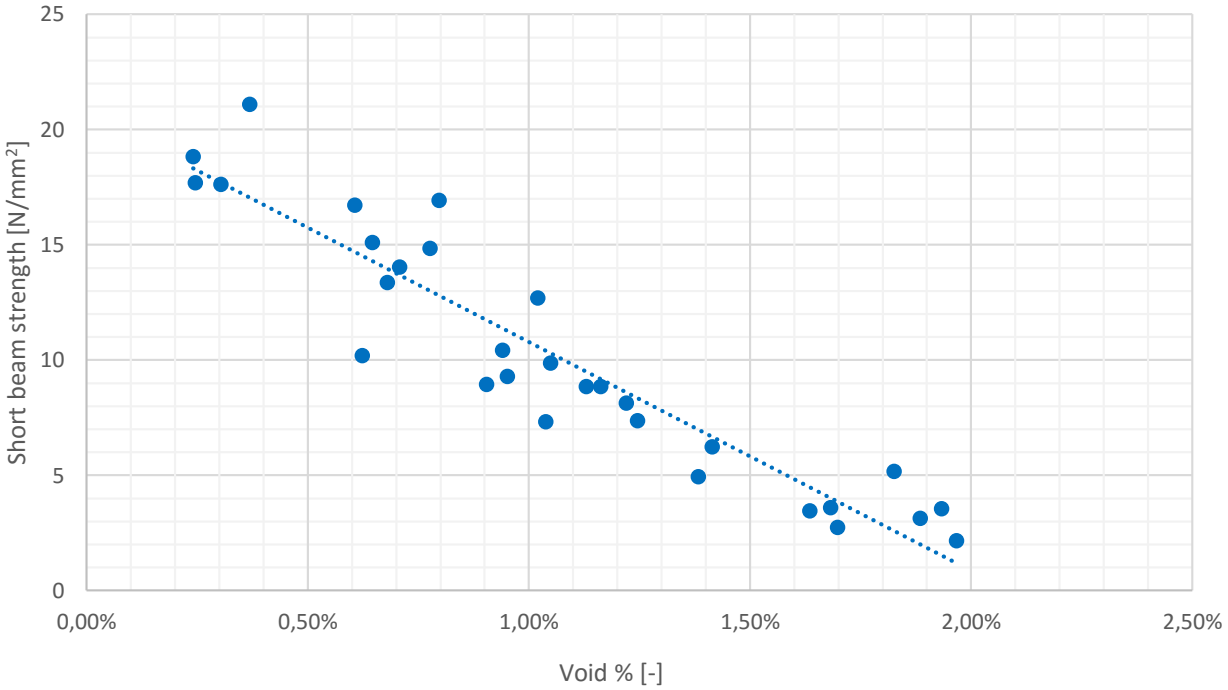

Figure 6.43. Scatter diagram between void content and short beam strength experimental results.

6.7 Final cylinder and dimension results extrapolation. Reference comparison.

6.7.1 Final cylinder

A final cylinder is wound using the parameters as shown in Table 6.7. First the heat gun temperature and feed rate parameter window is adjusted to a point in the optimum area but not the maximum (maximum temperature 460ºC) to avoid the possible degradation observed in the previous specimens. The compaction force is set up to the maximum value as the top compaction has been not observed during the experiments. The fiber tension is maintained to the standard value used to manufacture the rest of cylinders in order to ease the piece extraction and avoid the fiber damage as much as possible. Finally the preheating system is set up to 330 degrees, when surpassing this value some fiber degradation is observed.

The final cylinder is mechanically characterized with method 2, short beam strength test, and the void content is analyzed using the polished cross section analyze method.

Table 6.7. Final cylinder processing parameters

	Sample	FIN01
Compaction force	N	192
Fiber tension	N	8
Heating gun temp Max	ºC	450
Heating gun temp AVG	ºC	435
Preheating temp Max	ºC	314
Preheating temp Min	ºC	334,9
Preheating temp AVG	ºC	320
Yarn temperature exit	ºC	117
Feed rate	mm/s	10

6.7.2 Dimension extrapolation

To experimentally demonstrate if the experimental results obtained in this thesis can be extrapolated for other cylinder dimensions two more cylinders are wound, one longer and one thicker than the final cylinder.

Both cylinders are wound with the same parameter configuration as the final cylinder (Table 6.7). The first cylinder, labeled as THICK is wound with 16 layers during the process, the double than the normal specimens. The second cylinder, labeled as LONG, is wound with a length of 50 mm, double than the normal specimens.

The final cylinder are mechanically characterized with method 2, short beam strength test, and the void content is analyzed using the polished cross section analyze method.

6.7.3 Reference comparison

The final cylinder, the THICK cylinder and the LONG cylinder are compared with the reference manufactured by compression molding.

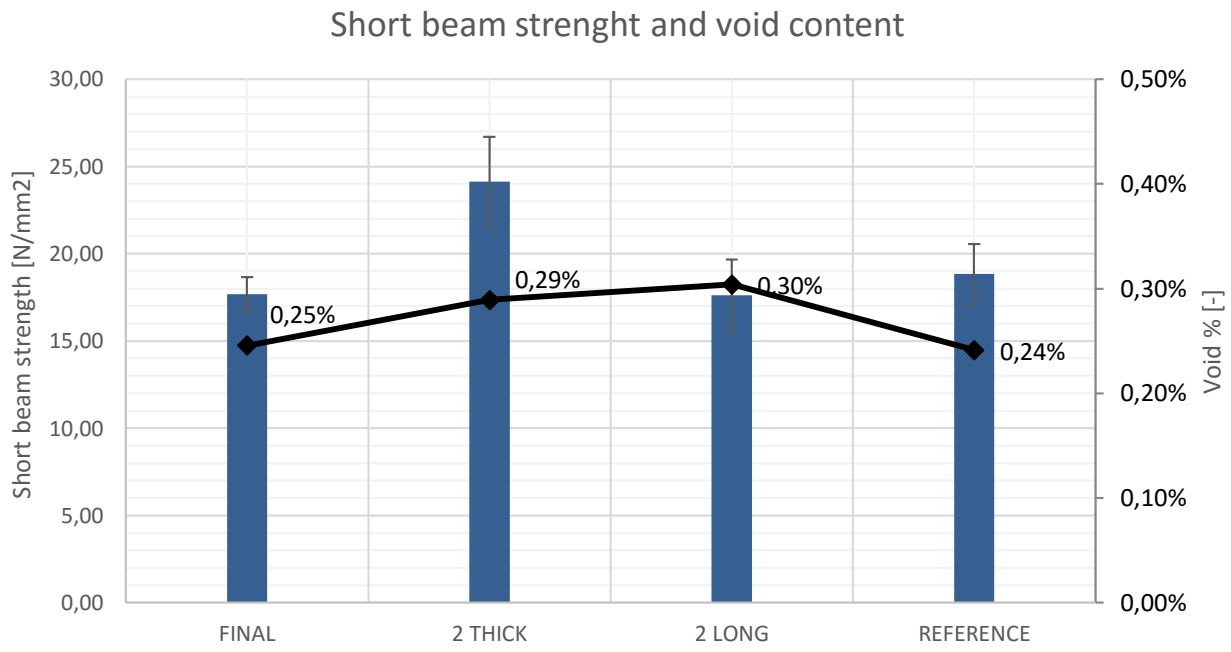

Figure 6.44. Final cylinder, THICK, LONG and reference comparison

Figure 6.44 shows the comparison of the short beam strength and the void % (method 2 calculated) of the 4 specimens. As shown in Figure 6.44 the final cylinder short beam strength is comparable with the reference, the short beam strength of the final cylinder is the 94% of the reference. The void % is nearly equal to the reference with 0.01% void variation.

The LONG cylinder presents a mechanical short beam strength equal to the final cylinder, and 94% of the reference. The void content % is nearly equal at 0.30%, representing 0.05% variation. There is no visual difference observed in the microscope photographs of the polished cross section between both cylinders.

The THICK cylinder presents a higher short beam strength, may be due to the thickness variation. The standard ASTM D2344 describe that the specimens should have the same dimension proportions in order to be properly compared.

However the void content is 0.29%, 0.04% variation with the final cylinder. There is no visual difference observed in the microscope photography of the polished cross section between both cylinders.

So the dimension of the parts manufactured with the filament winding machine can be varied without a noticeable variation on the quality of the final part.

The final part is comparable with the reference manufactured in compression molding with a 94% of the short beam strength value and a difference in void content of 0.01%.

For manufacture longer cylinders the need of heated mandrel in necessary in order to maintain the temperature of the areas when these are far from the heat source.

Figure 6.45 show the 3 compared cylinders. The quality of the inner surface is appreciably better than the one of the other specimens.

Figure 6.45. Final cylinder, Long and thick. Filament winding of Twaron-PA6 commingled yarn

6.8 Discussion on the polished polymer cross section in function on the degree of the cylinder consolidation

The polished cross section of the different samples studied has been investigated. The influence of the process parameters in the final part quality is clearly observable.

Figure 6.46. shows the polished cross section of the specimen labelled T07, process parameters:

- Nozzle heat gun Temperature = 460°C, Feed rate = 50mm/s
- Compaction force = 40N , Fiber tension = 8N
- Preheating temperature = No preheating

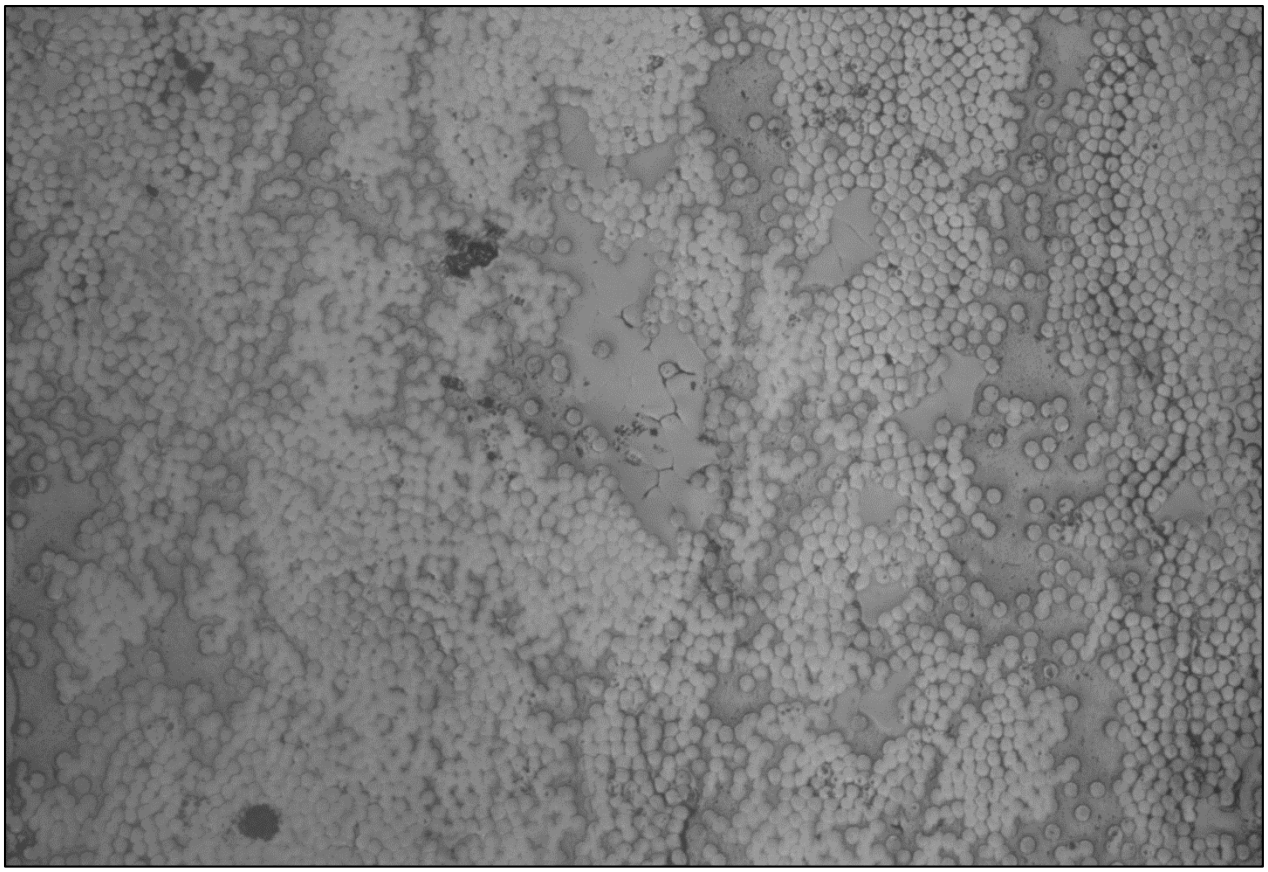

Figure 6.46. Polished cross section image of specimen T07. Twaron – PA6. Process parameters T= 460ºC, Feed rate=50mm/s, Comp. Force=40N, Fb. tension=1.5N, Preheat T= none

It is appreciable that the thermoplastic material has not completely reached the melting temperature in all the cylinder section. The consolidation force has been unable to distribute the thermoplastic and impregnate all the fibers. As a result there is reinforcing fiber areas without contact of the thermoplastic matrix. The lack of thermoplastic generates voids on the interface between the reinforcing fiber and the thermoplastic. It is possible to observe some voids in the thermoplastic parts between the fibers, again the viscosity of the thermoplastic was too high during the consolidation. That would be solved increasing the process temperature or reducing the feed rate. The wrong process configuration results in a low mechanical behaviour and high void % content. The short beam strength of the T07 specimen is 6.22N/mm^2.

Figure 6.47. shows the polished cross section of the specimen labelled FIN, process parameters:

- Nozzle heat gun Temperature = 450ºC, Feed rate = 10mm/s
- Compaction force = 190N , Fiber tension = 8N
- Preheating temperature = 120ºC

Even when the process temperature is lower the exposition time of the specimen FIN is five times the T07 exposition. As a result is observable that the thermoplastic material has properly impregnated the reinforcing fibers and the consolidation force was sufficient. It is still possible to observe the different fiber tows in Figure 6.47. The distribution of the fibers around the material section is not perfectly uniform. That may be solved by increasing the consolidation force. The section shown in Figure 6.47 belongs at any rate to the cylinder wound with the best parameter configuration. The interlaminar shear stress of the FIN specimen is much greater being 17.69N/mm^2.

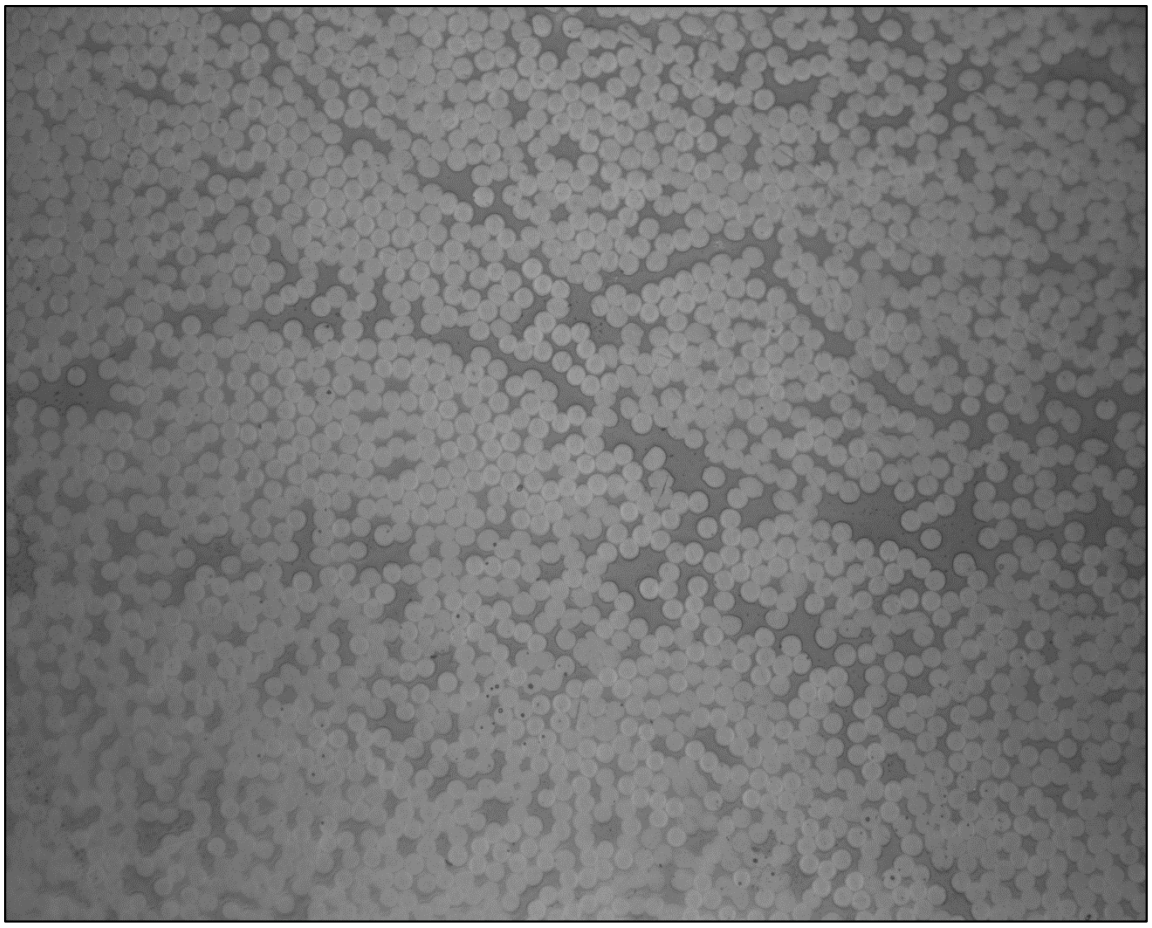

Figure 6.47. Polished cross section image of specimen TH01. Process parameters: Heat gun temperature = 450ºC, Feed rate=10mm/s, Comp. force=190N, Fb. tension=8N, Preheat T=120ºC

6.9 Discussion of the yarn temperature evolution during filament winding

During the filament winding process the temperature of the yarn was measured with a non-contact sensor, a digital pyrometer. The area of the pyrometer measurements depends on the distance between the pyrometer and the measured point. At the minimum distance, the pyrometer measuring area is 5 mm, what made impossible to properly measure the temperature on the yarn before the nip point due to the yarn diameter is approximately 1mm. So, the pyrometer was set right after the nip point, pointing the cylinder being wound. It is fix in a distance of 15 mm to the mandrel surface in radial direction and in an angle of 60º from the top plane.

The pyrometer is maintained in a fix point to always collect the temperature of the same point of the cylinder and that way observe the temperature variation when the heat source is over the measured point and the moment the heat source is far from the measured point while winding the cylinder.

Figure 6.48. plots the temperature evolution detected by the pyrometer in the centre of the cylinder length during the filament winding process of the specimen T01. Heat gun temperature 460°C, feed rate 10 mm/s. The temperature of every layer during the winding process is increasing. As the temperature is not measured on the nip point (the temperature of the compaction device would interfere on the measurements) this results may show a temperature inferior to the consolidation temperature. Anyway, Figure 6.48 show that the degradation temperature of the thermoplastic material is not reached for the higher source temperature and slower feed rate.

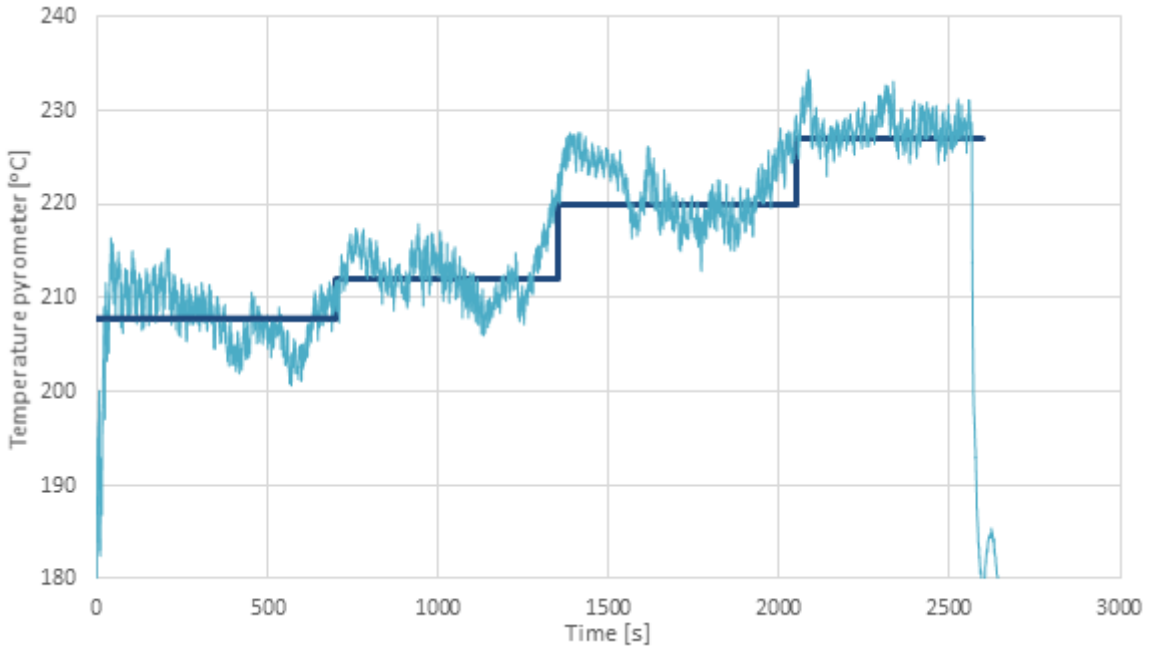

Figure 6.48. Temperature evolution of pyrometer measurements during the filament winding process. Heat gun temperature 460°C, feed rate = 10mm/s

To demonstrate that the temperature evolution is maintained stable and equal during the experiments. The results of the experiment 2, consolidation force with the temperature and feed rate constant are plot in function of the process time. Figure 6.49 plots the results of the pyrometer measurements.

It is also observable that the compaction force do not generate temperature variations on the manufacturing process.

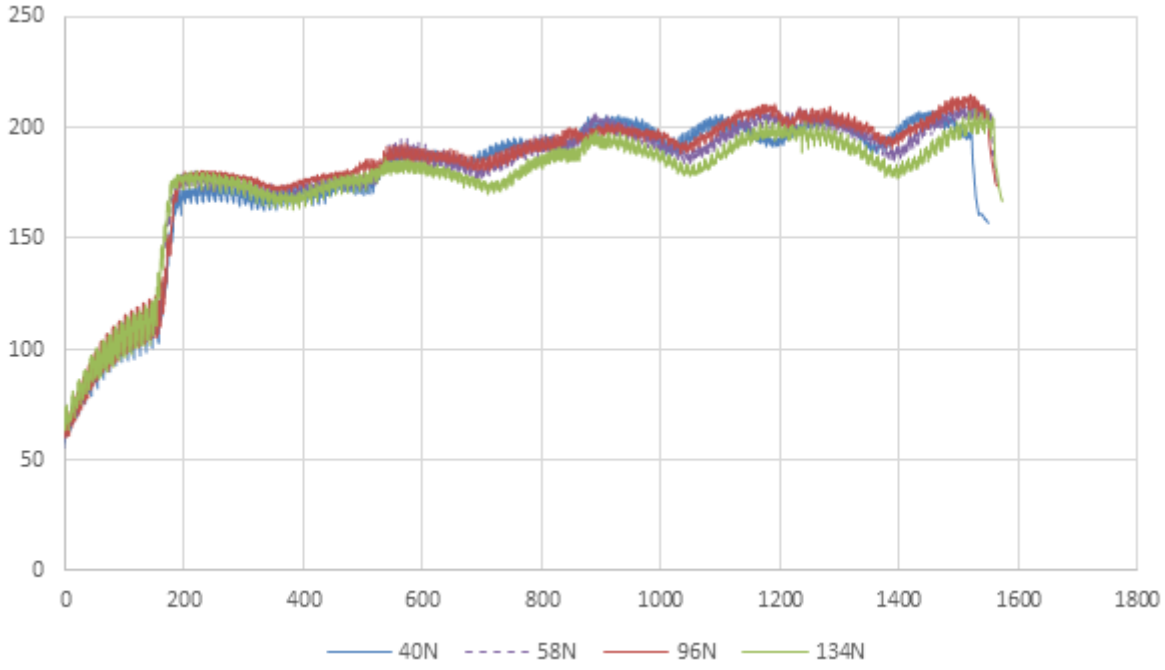

Figure 6.49. Temperature pyrometer measurements on the material surface for the different process compaction force. Heat gun temperature 430°C, feed rate = 20mm/s.

Figure 6.50. plots the pyrometer measurements for the different heat gun temperatures and a feed rate of 10mm/s. The temperature values obtained with the pyrometer show a temperature inferior than the yarn temperature on the nip point but are valid to show the trend between de different heat gun temperatures.

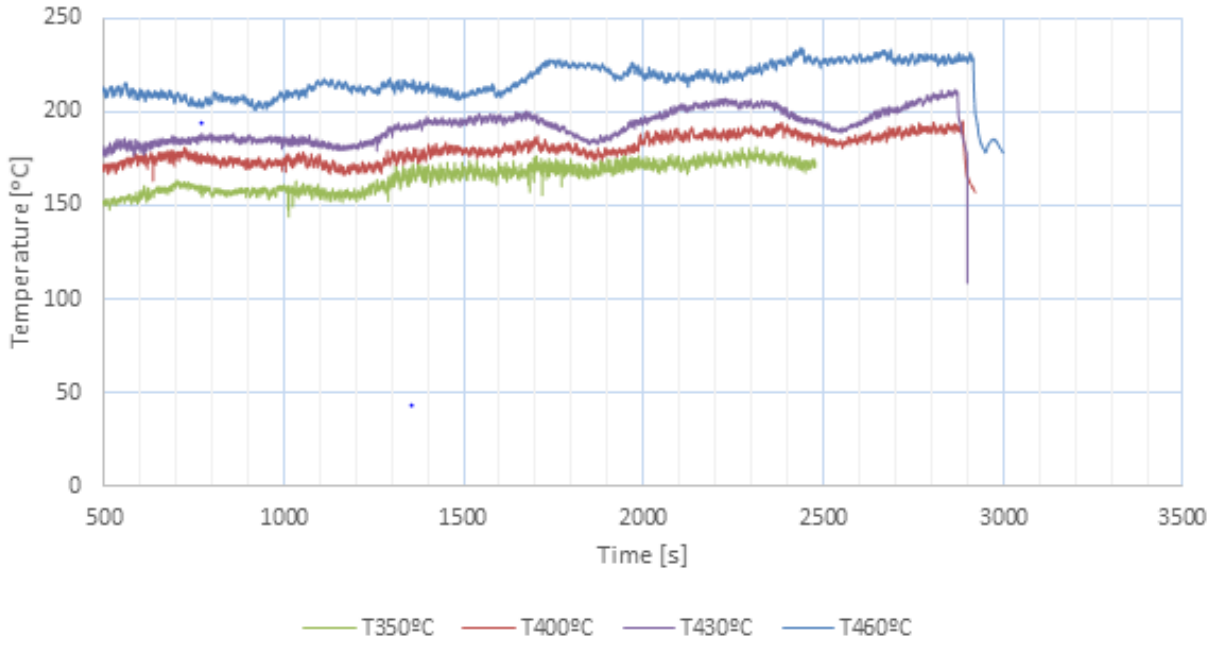

Figure 6.50. Pyrometer measurements in function of the process time for the different process heat gun temperatures.

6.10 Parameter influence results conclusion

The results of the parameter investigation confirms that all the studied parameters affect in the consolidation quality of the final specimens; heat source temperature, feed rate, compaction force, fiber tension and preheating temperature have an influence on the mechanical properties and obn the void content of the produced parts.

By increasing the heat source temperature and reducing the feed rate the consolidation in the final part increases. The feed rate or winding speed is a decisive economical factor for the evaluation of this process technique. For that reason the feed rate has been investigated for several velocities. However the results indicate that with the actual heat source is not possible to obtain the best quality parts for a feed rate greater than 10 mm/s. Further investigation should be done increasing the heat source power and the feed rate to observe if the mechanical properties and void % are maintained for different parameter combinations.

Increasing the compaction force increase the consolidation quality of the specimens. The magnitude of the force can be reduced if the temperature is increased. Another experiment should be carried out to increase the temperature and observe the effect of the compaction force for higher temperatures. Probably the effect of the force decrease until reach a top limit. As in the filament winding the material is not restricted by the ends when the piece reach or is near to reach the compaction limit this will expand for ends. It is proved that specimens under the same compaction force increase his length when the temperature increases (viscosity decrease).

Increasing the fiber tension the quality of the final part also increases. However it generates disadvantages such as the piece extraction difficulty, the fiber damage in the guiding elements and the penetration of the upper yarn in the top layers. For these reasons in this work the best specimen has been wound with just the necessary fiber tension for guiding the yarn and not the maximum.

By increasing the preheating temperature the quality of the final part also increases, without arrive to the degradation of the material. The preheating system is tested in a layout without a temperature controlled mandrel.

This experimental work shows the best cylinder is wound with the 94% of the short beam strength of a reference manufactured with compression molding and 96% of the void content.

The parameters obtained can be extrapolated to a different parts dimensions, at least for double dimension variation.

Chapter 7

Conclusions and outlook

7.1 Conclusions

The aim of this work has been to restore functionality of the filament winding system and to adapt it to manufacturing thermoplastic materials as well as to study the effect of the process parameter on the consolidation degree of the final specimens defining the optimal processing window for the process with Twaron-PA6 commingled yarn.

The machine has been successfully restored and is capable to process fibre bundles, such as commingled yarns. The set up is appropriate and the machine functionality is correct. The winding system is capable of manufacturing cylinders with 94% of short beam strength value of a reference fabricated with compression molding. The difference in void volume % between that cylinder and the reference is 0.01%.

From the experimental investigation the following conclusion can be drawn:

The following investigated process parameters affect on the consolidation degree of the final specimen: Heat source temperature, feed rate, compaction force, fiber tension, preheating temperature. The optimum specimens are obtained for high process temperatures of the main heat source and the preheating source, slow feed rates, high compaction force and fiber tension, inside the range elements studied in this work.

With the main heating source installed the best results are obtained for a feed rate of 10 mm/s. Improving the heat sources will lead on the improvement of the process speed. The mechanical properties of the specimens are highly sensitive to the process speed. An increase of the process speed over 10 mm/s leads to a decrease of the approximately 25% of the short beam strength value. The optimal area in the main source temperature – feed rate processing window is located on the upper limit of the main heat source temperature and slow feed rate. The heat power needs to be increased in order to increase the process speed and with it the process productivity.

The temperature measurements taken with the pyrometer just after the nip, have shown that the temperature is lower than the melting temperature of the PA6 thermoplastic. However in the analysed cross sections is shown that the thermoplastic material has completely molten at least for the higher temperatures. Therefore the melting temperature of the commingled yarn is reached before the nip point. It is also observed that the substrate temperature continuously varies during the process.

The specimen dimensions variation has not produced a short beam strength value variation or a void content % variation on the specimens. Thus the dimension variation of the specimens does not have a significant effect on the specimen's consolidation when maintaining constant the process parameters. Conversely for longer specimens a heated mandrel may be needed, in order to maintain the surface temperature on the areas that become far of the heat source and imitate the process conditions.

A superficial degradation has been detected on the specimens that exhibit best mechanical properties and lower void content %. It is identified that the degradation is due to a partial oxidation of the thermoplastic material. The pyrometer measurements show that the degradation temperature of the PA6 has not been reached in all the experimental investigation. Therefore the superficial oxidation may be caused for a too long exposure time of the thermoplastic material to the process heat flow.

7.2 Outlook

The main drawback of the thermoplastic filament winding process is the reduced process speed due to the online consolidation and hence the long process cycles. In order to make the automated filament winding process more attractive, the cycle times needs to be reduced. The reduction of the cycle times can be achieved by improving the heat source power. Further investigations needs to be done studying the effects of increase considerably the heat power and the process speed on the final parts.

However, the temperature increment will also introduce a higher degradation risk which will require to know the temperature on the incoming yarn and substrate to avoid that phenomena. The necessity of a consolidation model for the filament winding process with commingled yarns is then one of the necessary steps. Some simulations have already reproduced the thermal behaviour of the cylinder during the process in automated tape winding. Further investigations can adapt those simulations to the commingled yarn materials.

This investigation test the variation of the processing parameters when being extrapolated to different dimensions. However for longer specimens would be recommended the installation of a heated mandrel in order to maintain the substrate temperature of the cylinder sections when they are not exposed to the heat source. Further investigations are needed to study the influence of the different geometries on the set parameters. To manufacture different geometries the compaction device needs to be modified to be able to maintain the pressure level and area in all the surface geometry.

During the experimental investigation the thermoplastic adheres to the compaction roller. To reduce the mentioned adhesion a releaser XTENT 818 was applied to the compaction roller of stainless steel. However this was just half effective. The adhesion of the material kept occurring, even when the amount of material was reduced. Also, the amount of material adhesion increases when the compaction force is increased. The replacement of the stainless steel roller for other one made of TEFLON for example may be a solution to reduce this material adhesion, as well as install a heat cooling system to maintain the temperature of the compaction roller under control avoiding the adhesion.

Part 3

Appendix

APPENDIX A.

CMAS Lab filament winding system information

A.1 Technical data. Winding machine WW2-0600-01450

Mandrel axis data. AXIS C		
Axis height above the ground:	1000	[mm]
Max winding diameter:	600	[mm]
Max clamping length:	1050	[mm]
Max mandrel weight:	25	[kg]
Max mandrel inertia	1.4	[$kgmm^2$]
Mandrel speed max	185	[min^{-1}]
Mandrel speed max jogging mode	92.5	[min^{-1}]
Mandrel position accuracy	0.04	[°C]
Carriage axis data. Axis Z		
Max winding length:	850	[mm]
Carriage speed max:		
Program (without machine cover):	300	[mm/s]
Program (with machine cover):	750	[mm/s]
Jogging mode:	150	[mm/s]
Position accuracy	0.05	[mm]
General data		
Control	Siemens 840D	
NCU_Type (SW-Stand):	571.3 (06.03.19)	
MMC-Type (SW-Stand):	PCU 20 (06.03.29)	
Power consumption	3x400 V, 50Hz, 32A	
Compressed air connection (Tension control):	6	[bar]

Machine functional data is included in this page. More specific data about the axis motors included in CD. Documentation provided by Waltritsch & Wachter gmbh.

A.2 Spring dimensioning

This section explain the spring dimensioned method used for the compaction device spring selection.

To be able to easily control the applied force, the type of spring selected is a helical coil spring working in compression. This type of spring has a linear behavior between the spring longitudinal length compression and the applied force. Moreover the force and spring deformation act in the same action line [41] what ease the design.

The important parameters and dimension for the calculation of a helical coil spring are:

- The maximum and minimum spring loads (F_i,F_S) N
- The maximum and minimum deformation values ($\delta i, \delta s$) mm
- The spring constant (K) N/mm
- The elastic potential energy (E_{pe}) Nmm
- Torsion resistance (W_t) mm^3
- The wire diameter (d) mm
- The spring diameter (D) mm
- The free length (L_0) mm
- The spring diameter (D) mm
- The number of coils (N) -
- Shear stress (τ) MPa
- Stiffness modulus (G) MPa
- The tension correction factor (q) -

Figure APPENDIX A.1 show the graphic illustration of the spring parameters.

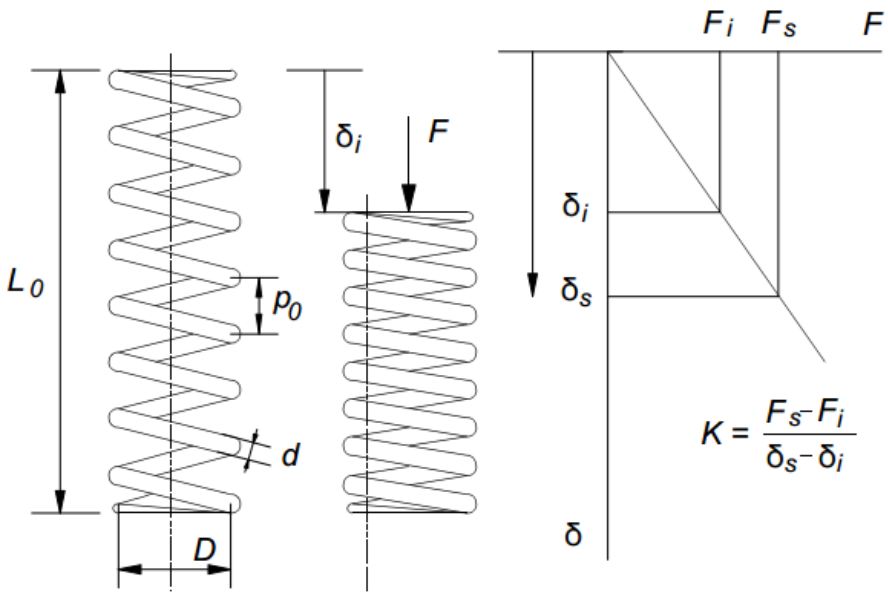

Figure APPENDIX A.1. Helical coil spring working in compression. Image property of Edicions UPC.

The material in a helical spring is working in torsion as shown in Figure APPENDIX A.2 so the spring dimensions are dimensioned for the shear failure of the material. The equations presented are not developed from the main root. The development of all the equation is shown in 'Disseny i Càlcul de Molles', (Design and Calculation of Springs) [41]. The calculation procedure followed for the book is the one included in DIN 2089-T1 and DIN 2089-T2 [10, 11].

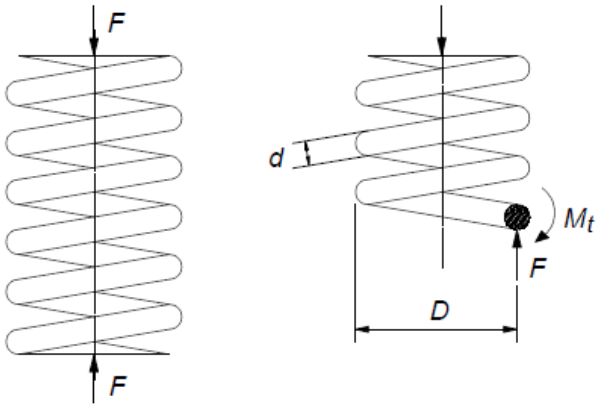

Figure APPENDIX A.2. Compression helical spring stress. Image property of Edicions UPC

Fixing the desired work force range (50N-300N) and the possible spring length variation the spring constant is calculated with the following expression:

$$\Delta F = k\Delta x \qquad \text{(APPENDIX A.1)}$$

Then for different spring and wire diameters, the number of coils N is calculated with the relation:

$$k = \frac{F}{\delta} = \frac{d^4}{8D^3N}G \qquad \text{(APPENDIX A.2)}$$

The process shown with equation 1, 2 is an iterative process to obtain the desired spring geometry with the desired load behavior that fit with the available nominal dimensions on the market.

Once the desired dimension are set the material shear stress is calculated using the equation APPENDIX A.3. As the spring of the compaction device is working under static conditions the failure criteria is that the shear stress suffered for the material is minor that the maximum shear stress.

$$\tau = \frac{F8qD}{\pi d^3} \qquad \text{(APPENDIX A.3)}$$

Where q is the tension correction factor. The correction factor is 1 when the spring works in compression [41].

Finally the buckling on the spring is checked graphically from Figure APPENDIX A.3. Dependig on the join base spring joins the bucking correction parameter U is selected

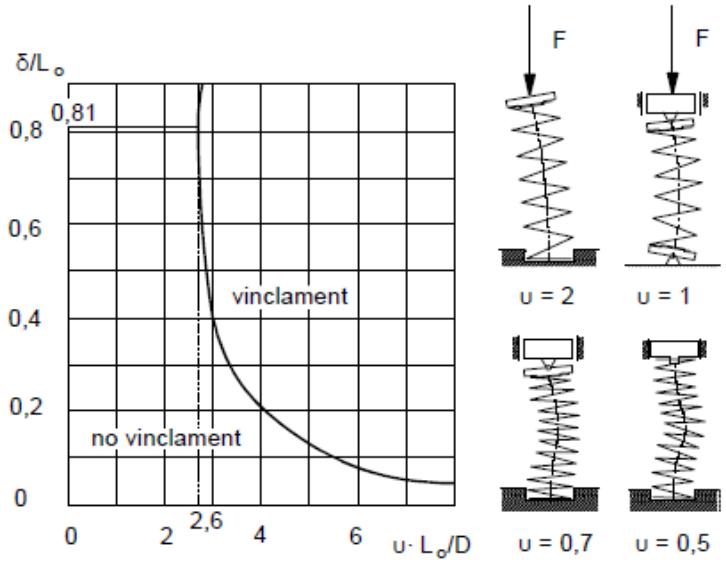

Figure APPENDIX A.3. Buckling spring control.

Where δ is the maximum spring deformation.

The spring selected belongs to the company Durovis.

Codice 66/4/3

Materiale	1.1200 classe C
d = diametro del filo mm	3.20
D = diametro medio mm	32.00
Dd = diametro albero massimo mm	27.80
Dh = diametro foro minimo, in mm	36.80
Lo = lunghezza libera mm	135.00
R = costante, in N/mm	3.83
n = numero spire attive +2=nt	8.50
Ln = lunghezza minima mm	40.40
sn = flessione a carico Fn mm	94.60
Fn = carico massimo a Ln N	354.863

APPENDIX A.3. Material list implemented systems

Item nº	Stck.	Denomination	Article	Dimensions	Material	DIN	ISO	Comment
FIBER INLET SYSTEM. 01								
001	1	Deflection pulley plasma coated			X5CrNi189	1,4301		
002	2	Pulley Bearing			-			
003	1	Pulley holder			X5CrNi189			ETH D-PHYS shop
004	1	Pulley support	20006.13	80x40x8	Anticorodal-110 hart AlSi1MgMn			ETH D-PHYS shop
005	2	Fixation plate, pulley system connections	20068.4	20x4x35	RSt37-2 steel, killed steel iron			ETH D-PHYS shop
006	2	Centring plate	32315	90x50x5	Anticorodal-110 hart AlSi1MgMn			ETH D-PHYS shop
007	2	Pole	C02-1-02-02/,,,		AlMgSiO,5			Fa: Kanya
008	1	Bridge	C02-1-02-02/300		AlMgSiO,5			Fa: Kanya
009	2	End cap. c40-10	C40-10(-G)		AlMgSiO,5			Fa: Kanya
010	2	Standard connection Kayla C20-20-a	C20-10(-I/-P)					Fa: Kanya
011	2	Standard connection Kayla C20-20-b	C20-10(-I/-P)					Fa: Kanya
012	1	Axe. Socket shoulder screw M5x20. Class 12,9	31-520-5 20	M5x20X9,75	Steel class 12,9		7379	EMILE MAURYN
013	2	Hexagonal socket countersunk head screw		M8x20	Steel class 8,8		10642	EMILE MAURYN
014	8	Hexagonal socket countersunk head screw		M6X20	Steel class 8,8		10642	EMILE MAURYN
015	1	Nut M5		M8x4	Steel class 8,8		934	EMILE MAURYN
FIBER PAYOUT SYSTEM. 02								
021	1	Fiber eye holder		L120X80X10x160	AlMgSiO,5	1771		KANYA
022	1	Outer Roll holder			AlMgSiO, 5	1799		
023	1	Inner Roll holder			AlMgSiO, 5	1799		
024	1	Outer roll axis		15x57	X5Cr5Ni189	1,4301		
025	1	Outer Pulley		50x33	X5Cr5Ni189	1,4301		
026	1	Inner roll axis		15x57	X5Cr5Ni189	1,4301		
027	1	Inner pulley		50X33	X5Cr5Ni189	1,4301		
028	1	Yarn eye		Rd. 50x35	X5Cr5Ni189	1,4301		ETH D-PHYS shop
029								
030								
031								
032								
033	2	Socket head screw		M8x20	Stainless steel	912		
034	4	Socket head screw		M6X20		933		
035	2	Socket head screw M6X16				933		
036	4	Washer	B6,4, verzinkt	M6		125		
037	4	Shims		12X18X1		988		
038	16	Shims		12X18X0,1		988		
039	4	Circlip		A 12X1		471		
040	1	Wave mother KM6		M30X1,5		981		Fa.SKF
041	4	Pulley ball bearing	12x24x26 - 61901-C3					Fa. SKF

APPENDIX A.3. Material list implemented systems

Item nº	Stck.	Denomination	Article	Dimensions	Material	DIN	ISO	Comment
042	2	Screw taps	M6					Fa. Norelem
043	2	Dichtung						Fa. Festo
044	1	Carriage profile						Fa. Item
		MAIN HEATING SYSTEM. 03						
050	1	Heat air gun. CMAS Lab						
051	1	Precision articulated arm #4300-40	1.430	Radius act. 390mm	-	-		Fa. FISSO
052	1	Clamp KT· ST M8	5.160					Fa. FISSO
053	1	Clamping base 30sz, M8	5.204					Fa. FISSO
		MANDREL. 04						
055	1	Pipe stainless steel	20056.35	65x61x1010	Stainless steel X5CrNi18 10			ETH D-PHYS shop
		COMPACTION DEVICE. STRUCTURE. 05						
061	4	Tube 1. D30	803020 1 750	-	St 37-2			RK ROSE+KRIEGER
062	2	Tube 2. D30	803020 1 700	-	St 37-2			RK ROSE+KRIEGER
063	1	Tube 3. D30	803020 1 400		St 37-2			RK ROSE+KRIEGER
065	4	Base clamp FS-VA 30	13300000390					RK ROSE+KRIEGER
066	6	Cross clamp KVA-30	103000003900					RK ROSE+KRIEGER
067	1	Flange Clamp FK-VA 30	12300000390					RK ROSE+KRIEGER
068	4	Compaction structure bed	20068.11	80x10x105	St 37-2			ETH D-PHYS shop
070	4	Hexagonal socket screw M6x30 or 25	-				4017	ETH D-PHYS shop
071	4	Hexagon nuts M6				934		ETH D-PHYS shop
072	4	Washer M6				1587		ETH D-PHYS shop
075	16	Hexagonal head screw M6x20					4017	ETH D-PHYS shop
076	16	Washer M6				934		ETH D-PHYS shop
077	16	Nut M6				1587		ETH D-PHYS shop
078	8	Hexagonal head screw M10x					4017	ETH D-PHYS shop
079	8	Washer M10				934		ETH D-PHYS shop
080	8	Nut M10				1587		ETH D-PHYS shop
		COMPACTION DEVICE. 06						
081	1	Base 1	20077.8	40*40*136	Steel (St37-2 K)			ETH D-PHYS shop
082	1	Base 2	20068.11	80*10*78	Steel (St37-2 K)			ETH D-PHYS shop

APPENDIX A.3. Material list implemented systems

Item nº	Stck.	Denomination	Article	Dimensions	Material	DIN	ISO	Comment
083	1	Load part 1	20068.12	80x30x156	RSt37-2 steel, killed steel iron			ETH D-PHYS shop
084	1	Load part 2	20077.9	50x50x26	Steel (St37-2 K)			ETH D-PHYS shop
085	2	Load part 3	20068.9	50x8x66	RSt37-2 steel, killed steel iron			ETH D-PHYS shop
087	2	Linear bushings standard	R0600 020 00					
088	2	Guide			Calibrated steel	Request inquiry		
089	1	Shaft 2			Calibrated steel			
090	4	Elastic ring D32	20,244,21					ETH D-PHYS shop
091	2	Elastic ring D20	20,244,13					ETH D-PHYS shop
095	1	Spring	66/4/3					Durovis
096		Lock nut KM4, M20x1, nut				981		
097		Adjustable piece	20071.15	50x10x50	CuZn38Pb2			ETH D-PHYS shop
105	1	Roller shaft	20232.91	10x70	Stainless steel h8			
106	1	Elastic ring D6	20244.3		Spring steel black	417		ETH D-PHYS shop
107	2	Ball bearings	20268.11					ETH D-PHYS shop
108	1	Compaction roller	20034.16	30x40	Stainless steel h8			
109	1	Distance part	20035.14	30x40	Steel St37-2 K blank, drawn			ETH D-PHYS shop
110	1	Nut M4						
111	1	Washer M4						
PREHEATING SYSTEM. 07								
120	1	Preheating support 1						
121	1	Preheating support 2						
122	1	Preheating support 3						
125	4	L angle						CMAS Lab

APPENDIX A.3. Material list implemented systems

Item nº	Stck.	Denomination	Article	Dimensions	Material	DIN	ISO	Comment
126	2	Resistance heating element						
129	8	Cylindrical head screw M6X10						
130	8	Hexagonal nut M6						
132	8	Cylindrical head screw M4X10						
133	8	Hexagonal nut M4						
STRUCTURE POWER CONTROL PREHEATING. 08								
136	1	Variable regulator	x10207					United automation
137	1	Heatsink	20006.9	130X140X3 mm				ETH D-PHYS shop
138	2	Leg	-		Aluminium			CMAS Lab
140		Cylindrical head screw M6X10						ETH D-PHYS shop
141		Hexagonal nut M6						ETH D-PHYS shop

APPENDIX A.4. Machine systems drawings

This section includes the drawings of the designed systems for the CMAS Lab filament winding machine.

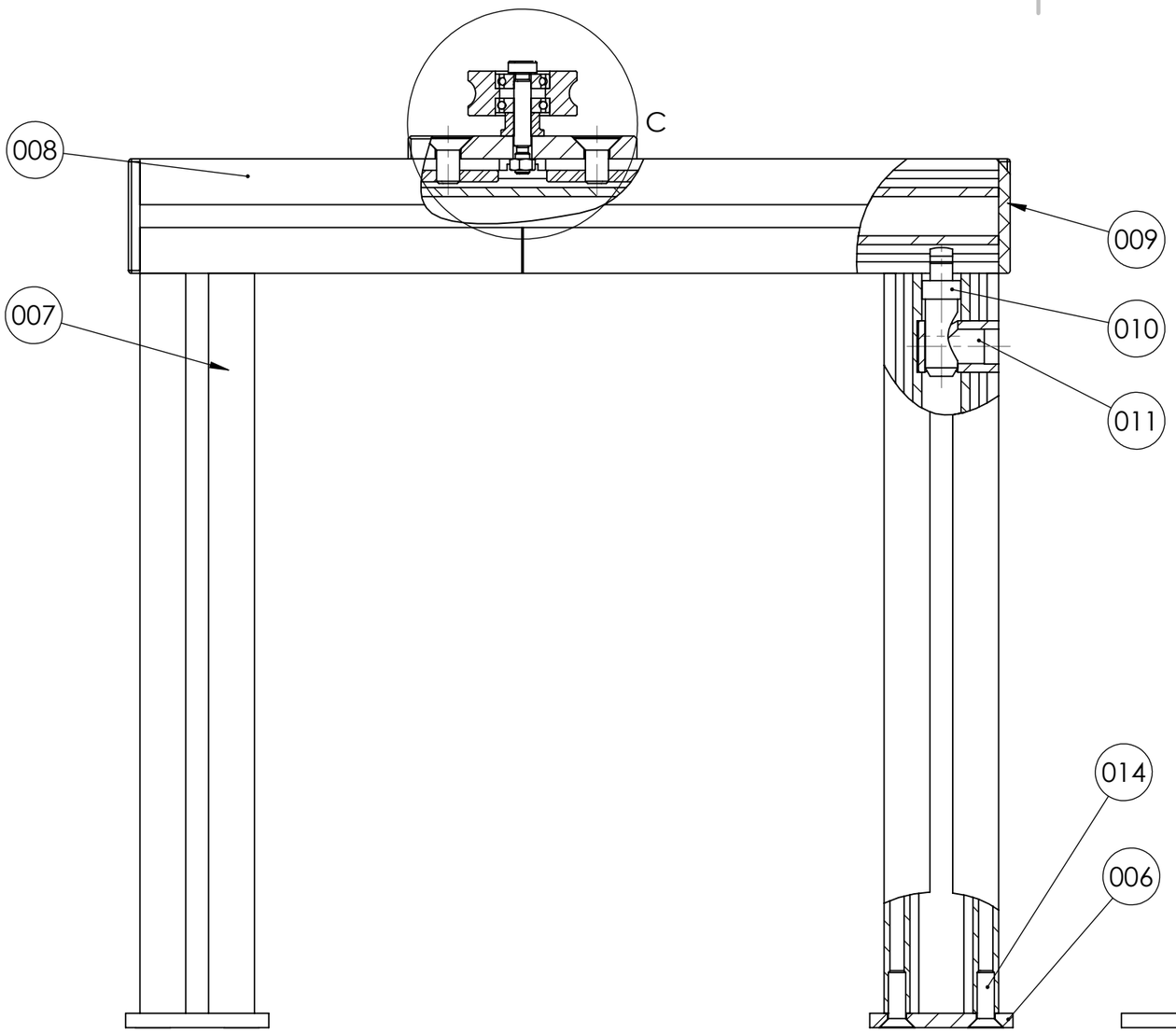

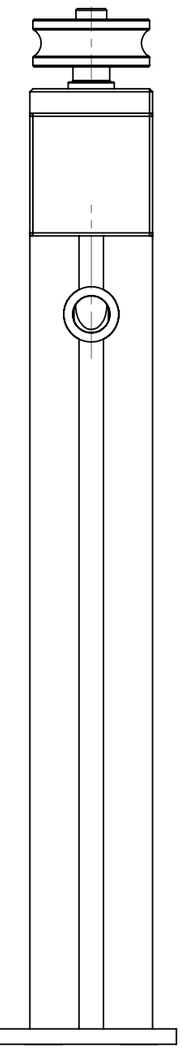

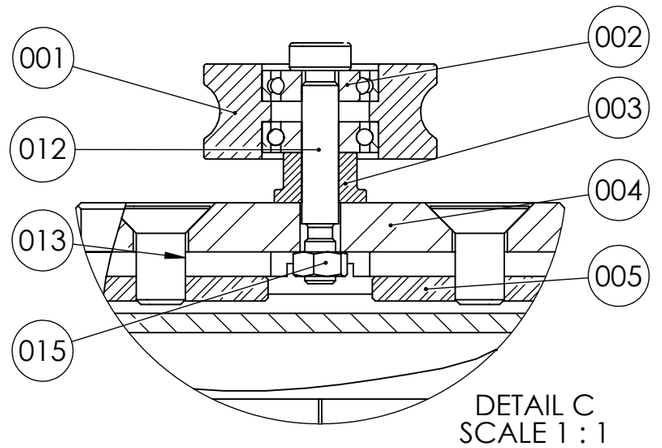

DETAIL C
SCALE 1 : 1

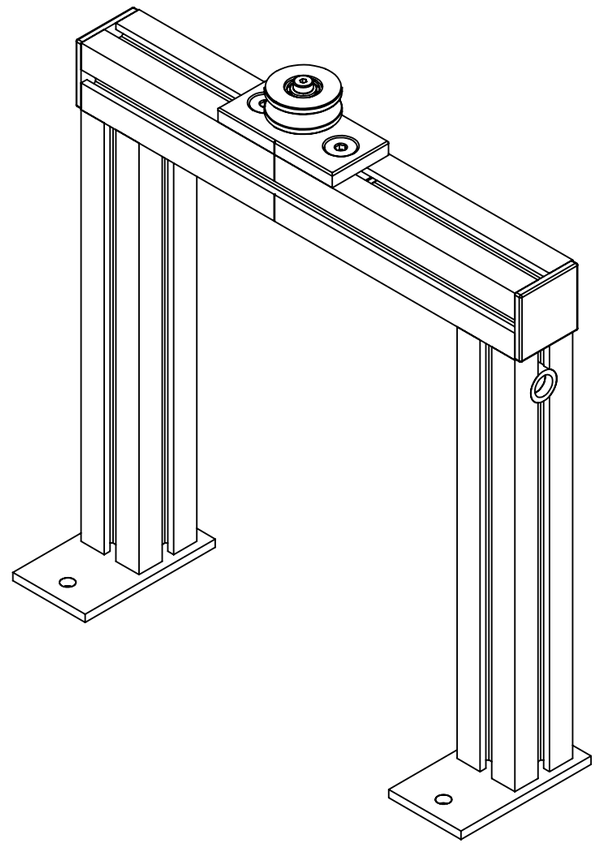

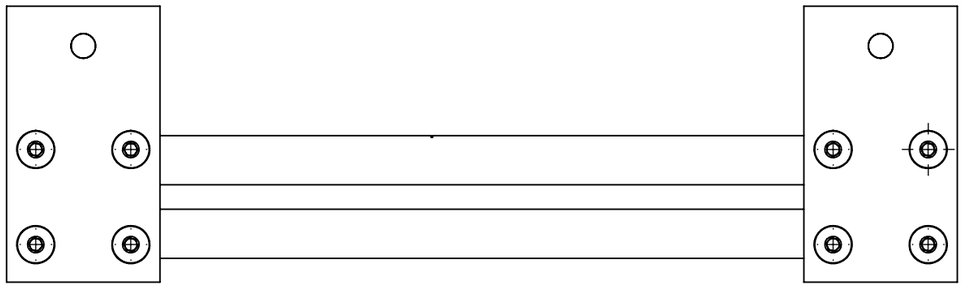

UNLESS OTHERWISE SPECIFIED: DIMENSIONS ARE IN MILLIMETERS SURFACE FINISH: TOLERANCES: LINEAR: ANGULAR:		FINISH:				DEBURR AND BREAK SHARP EDGES	DO NOT SCALE DRAWING	REVISION
							LABORATORY OF COMPOSITE MATERIALS AND ADAPTIVE STRUCTURES ETH Zürich	
	NAME	SIGNATURE	DATE				TITLE: Fiber inlet system	
DRAWN	J. Molina Blanco							
CHK'D	Heinrich Thomas							
APPV'D								
MFG								
Q.A				MATERIAL:			DWG NO. 01	A3
				WEIGHT:			SCALE: 1:2	SHEET 1 OF 1

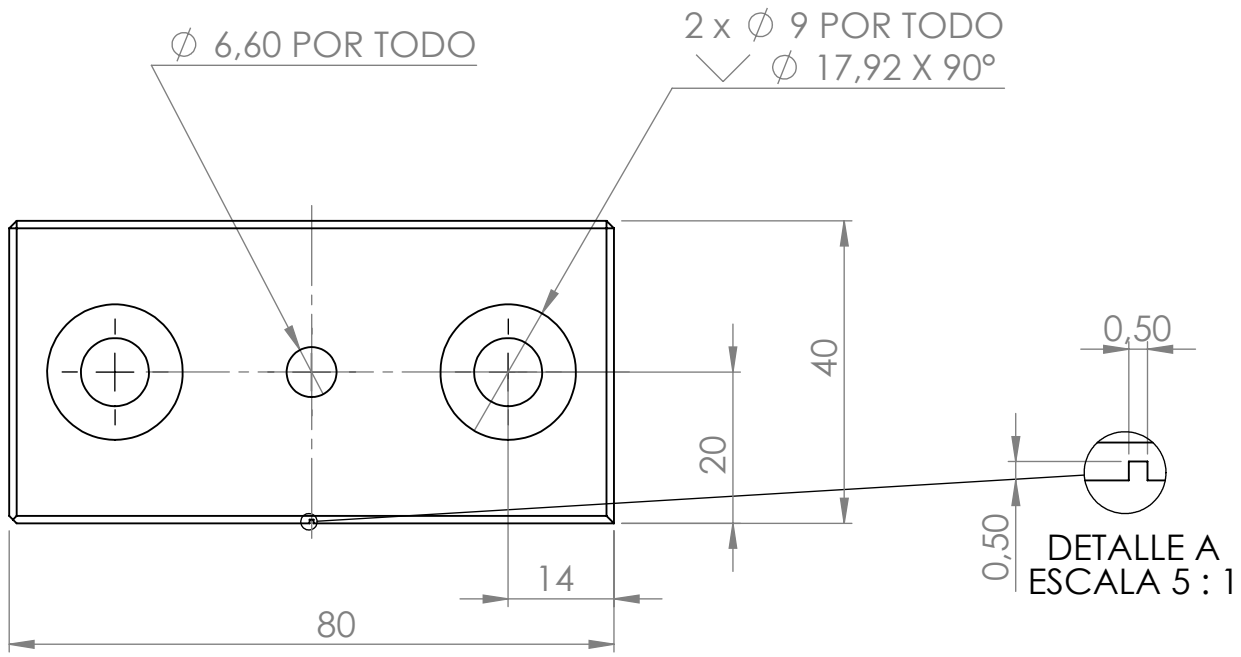

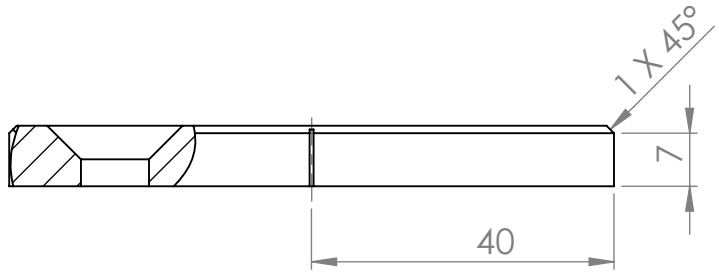

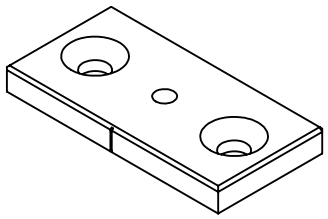

-UNLESS OTHERWISE SPECIFIED: DIMENSIONS ARE IN MILLIMETERS -SURFACE FINISH: - -General tolerance for linear and angular dimensions without individual tolerance indication ISO 2768-m	FINISH: -	DEBUR AND BREAK SHARP EDGES	DO NOT SCALE DRAWING	REVISION
			LABORATORY OF COMPOSITE MATERIALS AND ADAPTIVE STRUCTURES — ETH Zürich	
	NAME	SIGNATURE	DATE	TITLE: PULLEY SUPPORT
DRAWN	J. Molina Blanco			
CHK'D	Heinrich Thomas			
APPV'D				
MFG			MATERIAL: Al	DWG NO. 004 — A4
Q.A				
			WEIGHT:	SCALE: 1:1 — SHEET 1 OF 1

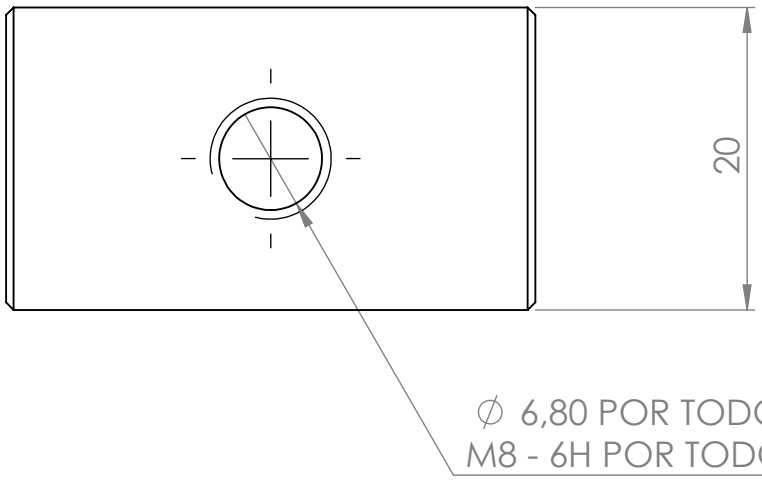

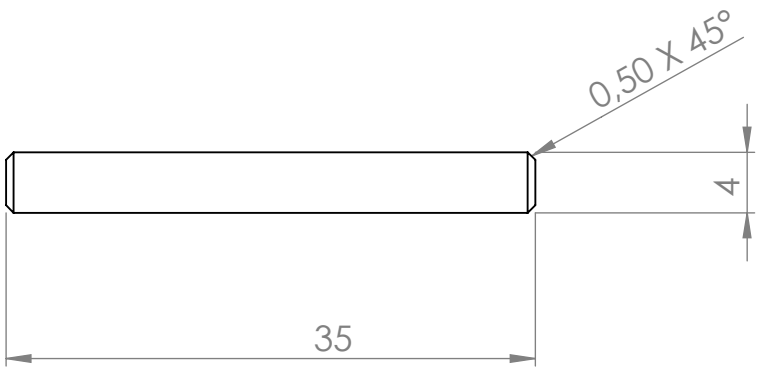

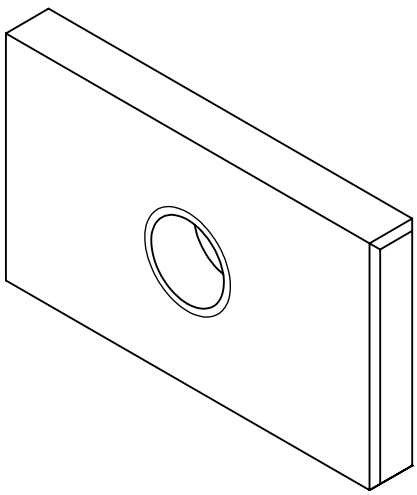

-UNLESS OTHERWISE SPECIFIED: DIMENSIONS ARE IN MILLIMETERS -SURFACE FINISH: - -General tolerance for linear and angular dimensions without individual tolerance indication ISO 2768-m	FINISH: -	DEBUR AND BREAK SHARP EDGES	DO NOT SCALE DRAWING	REVISION
			LABORATORY OF COMPOSITE MATERIALS AND ADAPTIVE STRUCTURES — ETH Zürich	
	NAME	SIGNATURE	DATE	
DRAWN	J. Molina Blanco			
CHK'D	Heinrich Thomas			
APPV'D				
MFG			MATERIAL: RSt 37-2 steel	DWG NO. 005 — A4
Q.A				
			WEIGHT:	SCALE: 1:1 — SHEET 1 OF 1

TITLE:

FIXATION PLATE

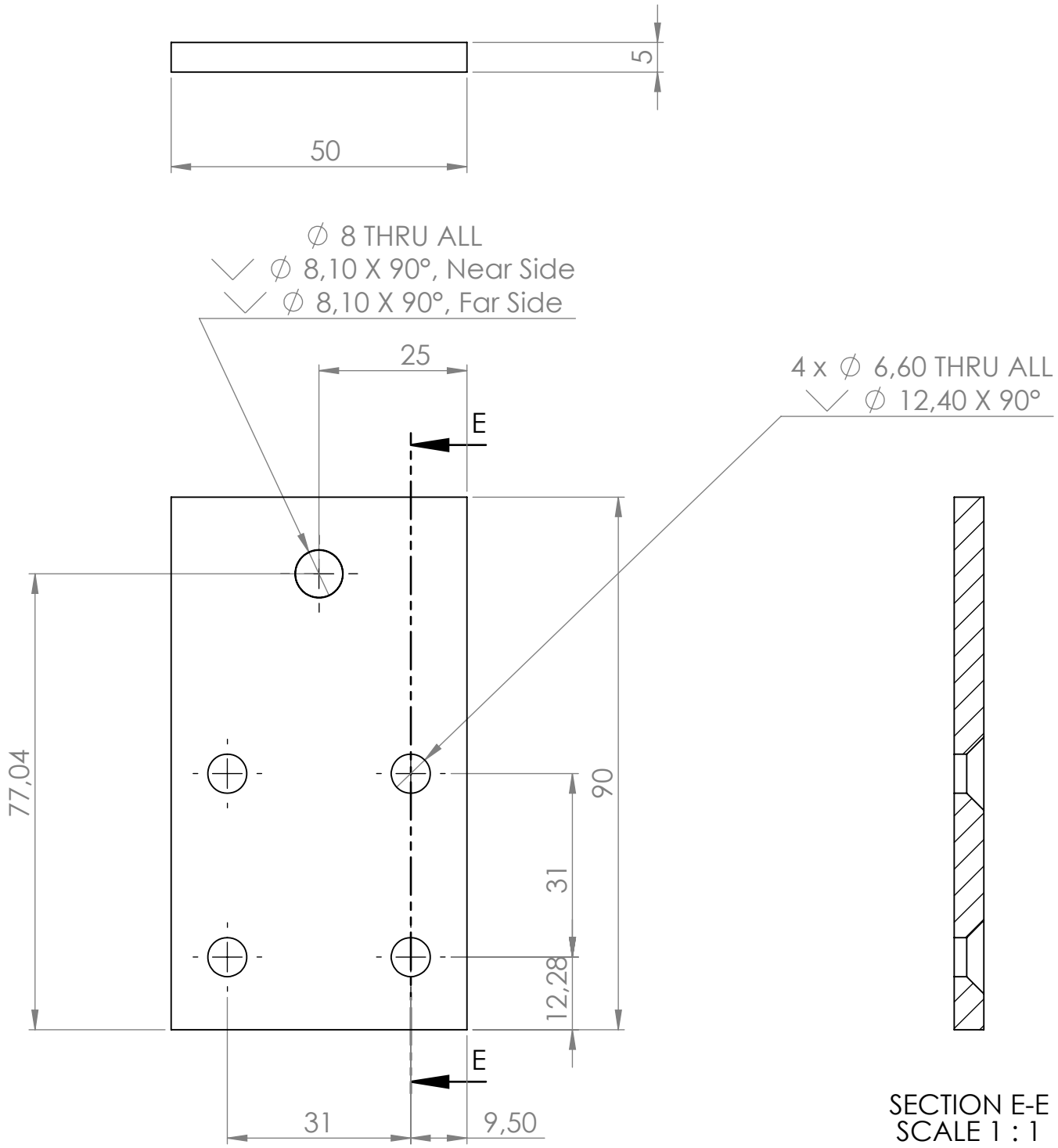

-UNLESS OTHERWISE SPECIFIED: DIMENSIONS ARE IN MILLIMETERS -SURFACE FINISH: - -General tolerance for linear and angular dimensions without individual tolerance indication ISO 2768-m	FINISH: -	DEBUR AND BREAK SHARP EDGES	DO NOT SCALE DRAWING	REVISION
			LABORATORY OF COMPOSITE MATERIALS AND ADAPTIVE STRUCTURES — ETH Zürich	
	NAME	SIGNATURE	DATE	TITLE: CENTRING PLATE
DRAWN	J. Molina Blanco			
CHK'D	Heinrich Thomas			
APPV'D				
MFG			MATERIAL: Anticorodal-110 hard AlSi1MgMn	DWG NO. 006 — A4
Q.A				
			WEIGHT:	SCALE: 1: 1 — SHEET 1 OF 1

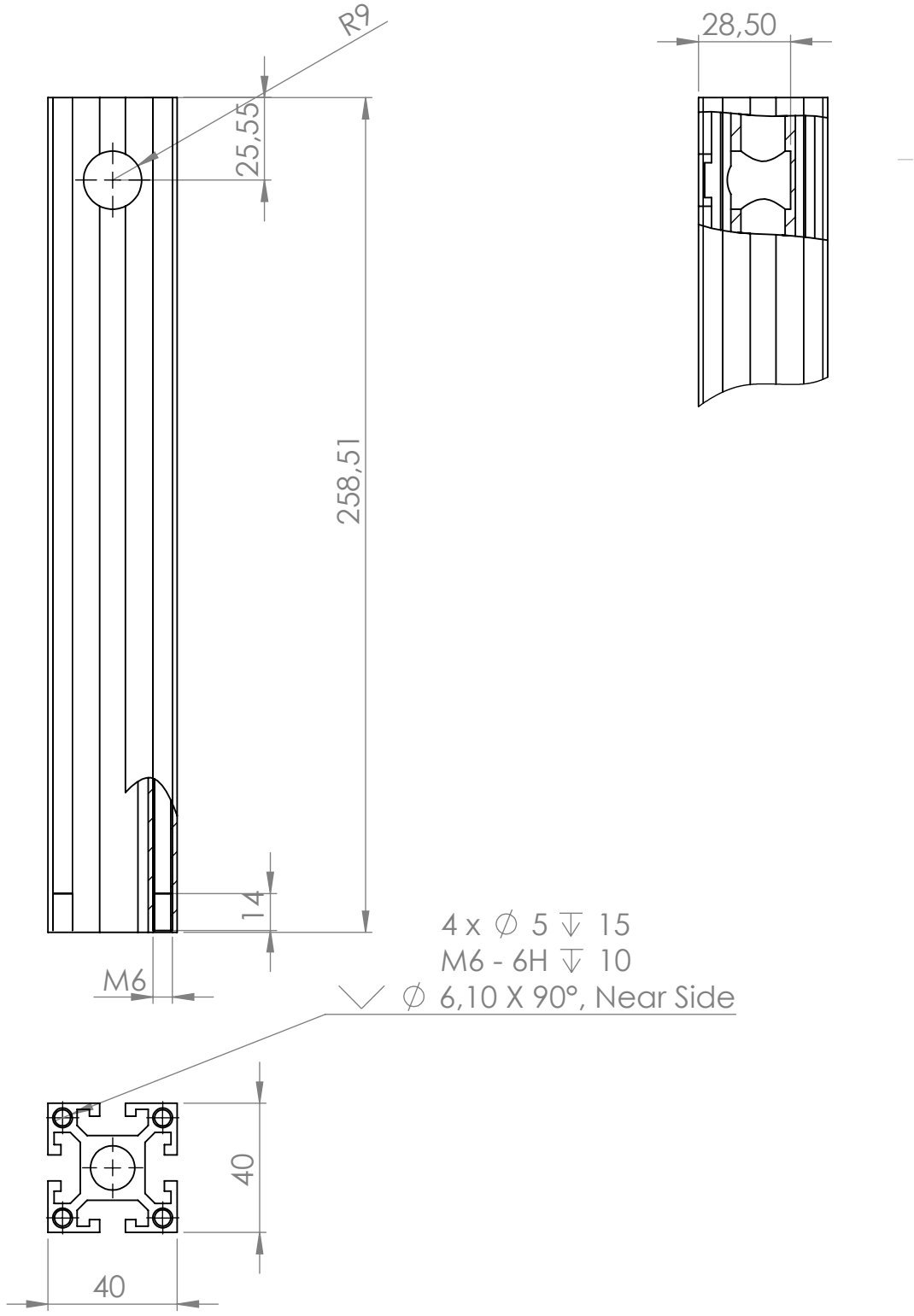

-UNLESS OTHERWISE SPECIFIED: DIMENSIONS ARE IN MILLIMETERS -SURFACE FINISH: - -General tolerance for linear and angular dimensions without individual tolerance indication ISO 2768-m	FINISH: -	DEBUR AND BREAK SHARP EDGES	DO NOT SCALE DRAWING	REVISION
			LABORATORY OF COMPOSITE MATERIALS AND ADAPTIVE STRUCTURES — ETH Zürich	
	NAME	SIGNATURE	DATE	TITLE: POLE
DRAWN	J. Molina Blanco			
CHK'D	Heinrich Thomas			
APPV'D				
MFG			Al	DWG NO. 007 — A4
Q.A				
			WEIGHT:	SCALE: 1:2 — SHEET 1 OF 1

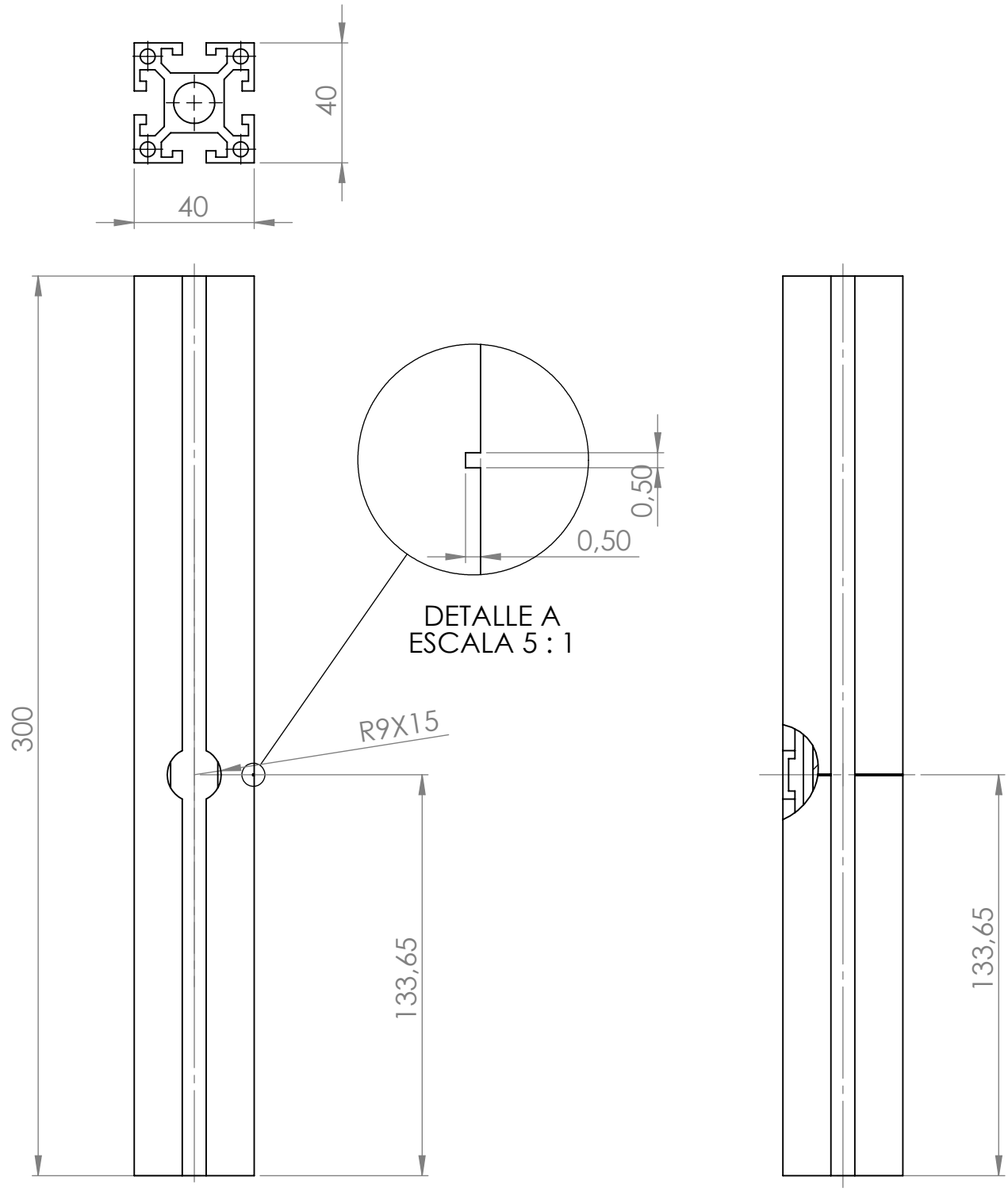

-UNLESS OTHERWISE SPECIFIED: DIMENSIONS ARE IN MILLIMETERS -SURFACE FINISH: - -General tolerance for linear and angular dimensions without individual tolerance indication ISO 2768-m	FINISH: -	DEBUR AND BREAK SHARP EDGES	DO NOT SCALE DRAWING	REVISION
			LABORATORY OF COMPOSITE MATERIALS AND ADAPTIVE STRUCTURES — ETH Zürich	
	NAME	SIGNATURE	DATE	
DRAWN	J. Molina Blanco			
CHK'D	Heinrich Thomas			
APPV'D				
MFG			MATERIAL: Al	
Q.A				
			WEIGHT:	SCALE: 1:2

TITLE:

BRIDGE

DWG NO. 008

A4

SHEET 1 OF 1

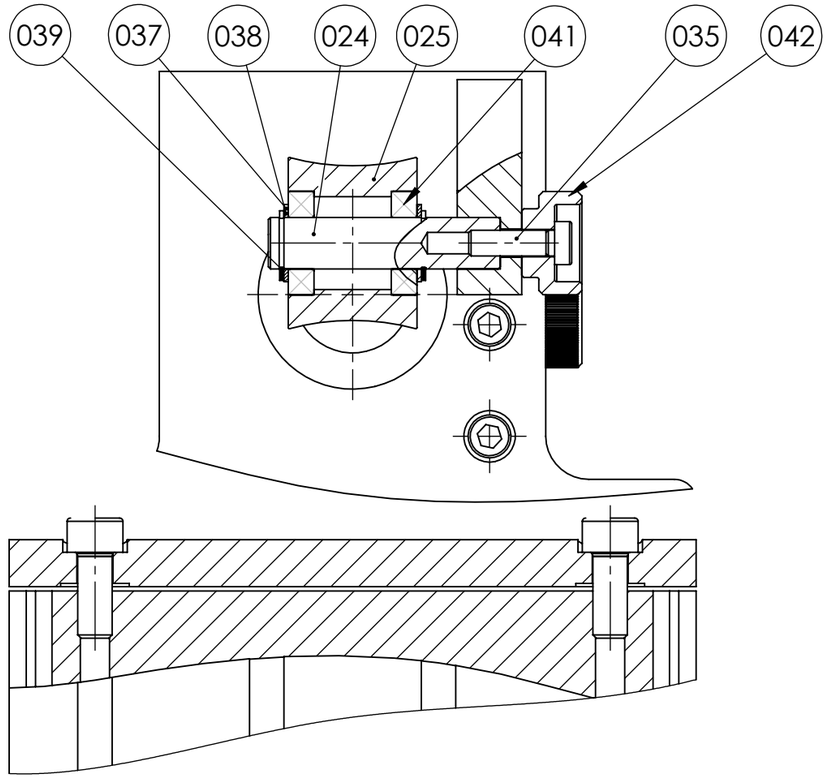

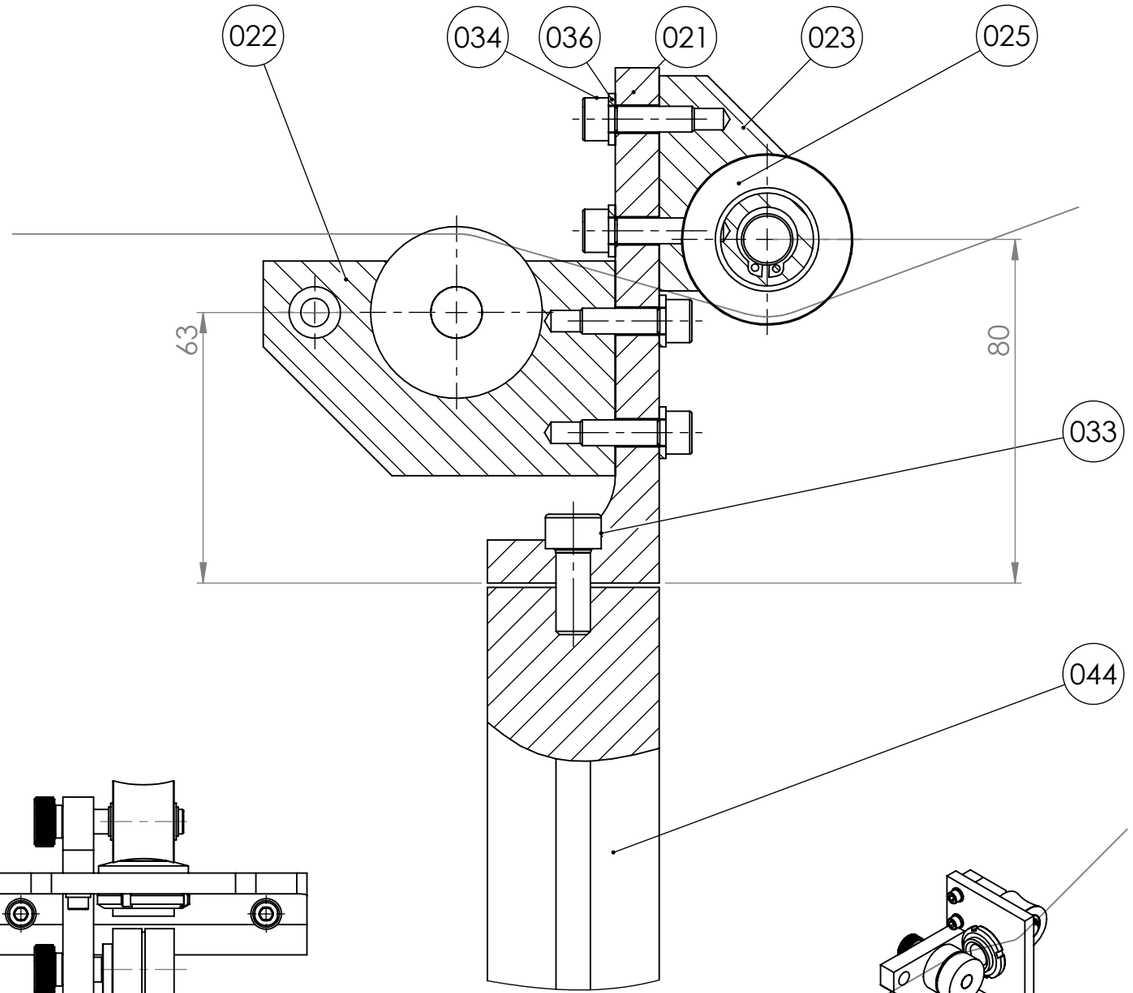

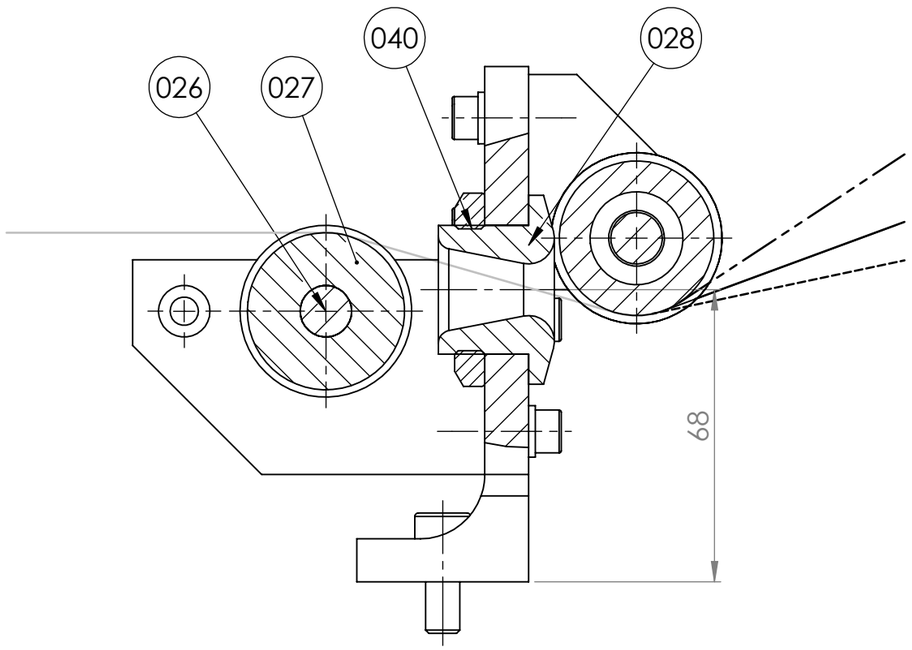

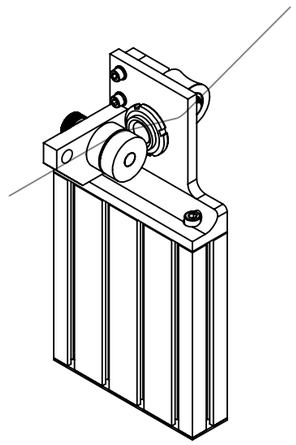

UNLESS OTHERWISE SPECIFIED: DIMENSIONS ARE IN MILLIMETERS SURFACE FINISH: TOLERANCES: LINEAR: ANGULAR:	FINISH:				DEBURR AND BREAK SHARP EDGES	DO NOT SCALE DRAWING	REVISION
						LABORATORY OF COMPOSITE MATERIALS AND ADAPTIVE STRUCTURES — ETH Zürich	
	NAME	SIGNATURE	DATE			TITLE:	
DRAWN	J. Molina Blanco					FIBER PAYOUT SYSTEM	
CHK'D	Heinrich Thomas						
APPV'D							
MFG							
Q.A				MATERIAL:		DWG NO. 02	A3
				WEIGHT:		SCALE: -	SHEET 1 OF 1

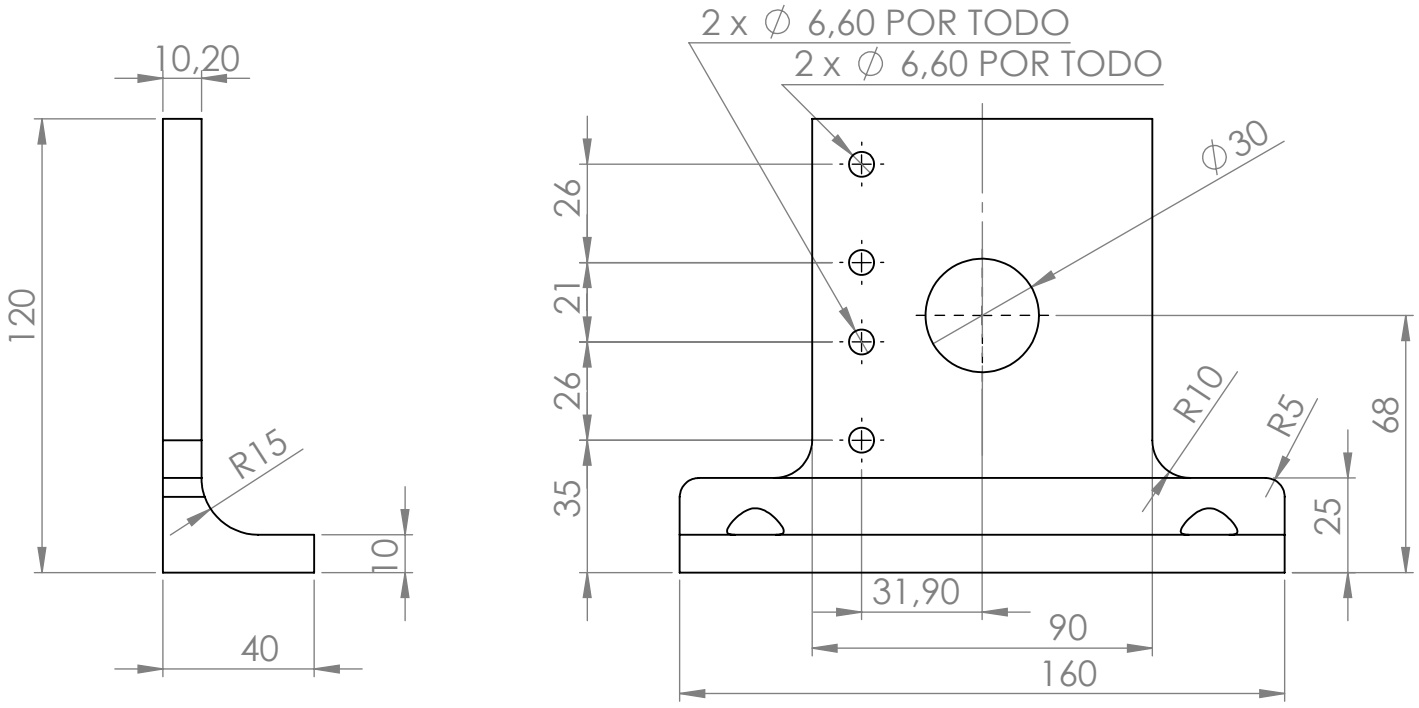

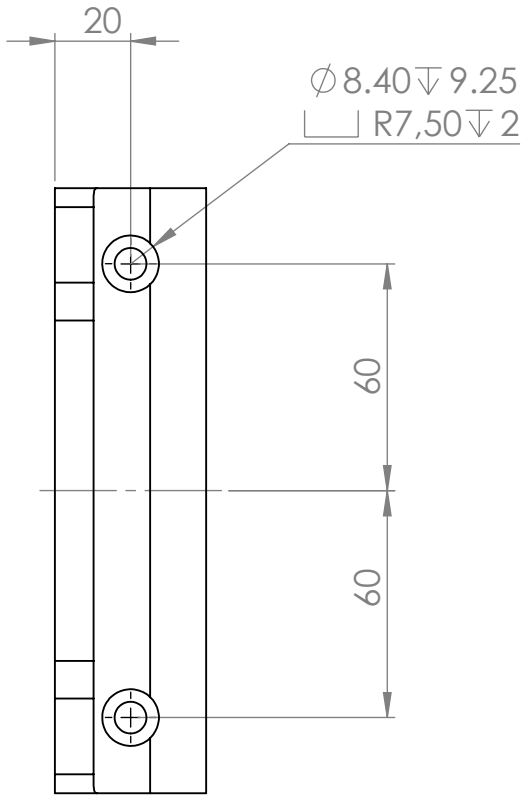

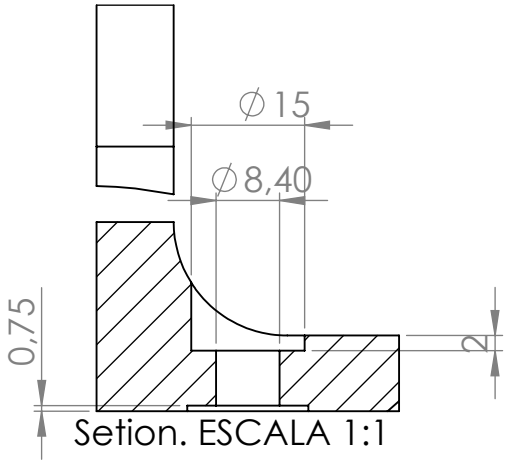

Setion. ESCALA 1:1

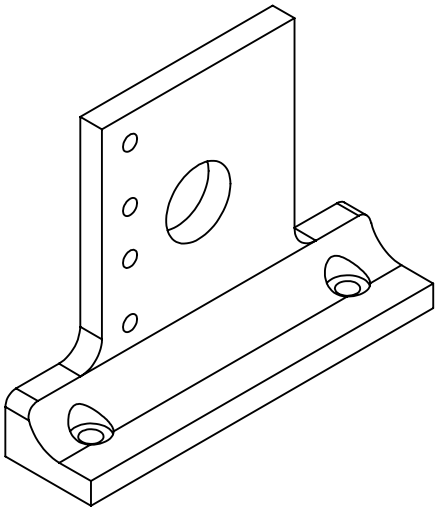

Screwed to carriage holes of filament winding

-UNLESS OTHERWISE SPECIFIED: DIMENSIONS ARE IN MILLIMETERS -SURFACE FINISH: - -General tolerance for linear and angular dimensions without individual tolerance indication ISO 2768-m	FINISH: -	DEBUR AND BREAK SHARP EDGES	DO NOT SCALE DRAWING	REVISION
			LABORATORY OF COMPOSITE MATERIALS AND ADAPTIVE STRUCTURES — ETH Zürich	
	NAME	SIGNATURE	DATE	TITLE: FIBER EYE HOLDER
DRAWN	J. Molina Blanco			
CHK'D	Heinrich Thomas			
APPV'D				
MFG			MATERIAL: AlMgSiO	DWG NO. 021 — A4
Q.A				
			WEIGHT:	SCALE: 1:2 — SHEET 1 OF 1

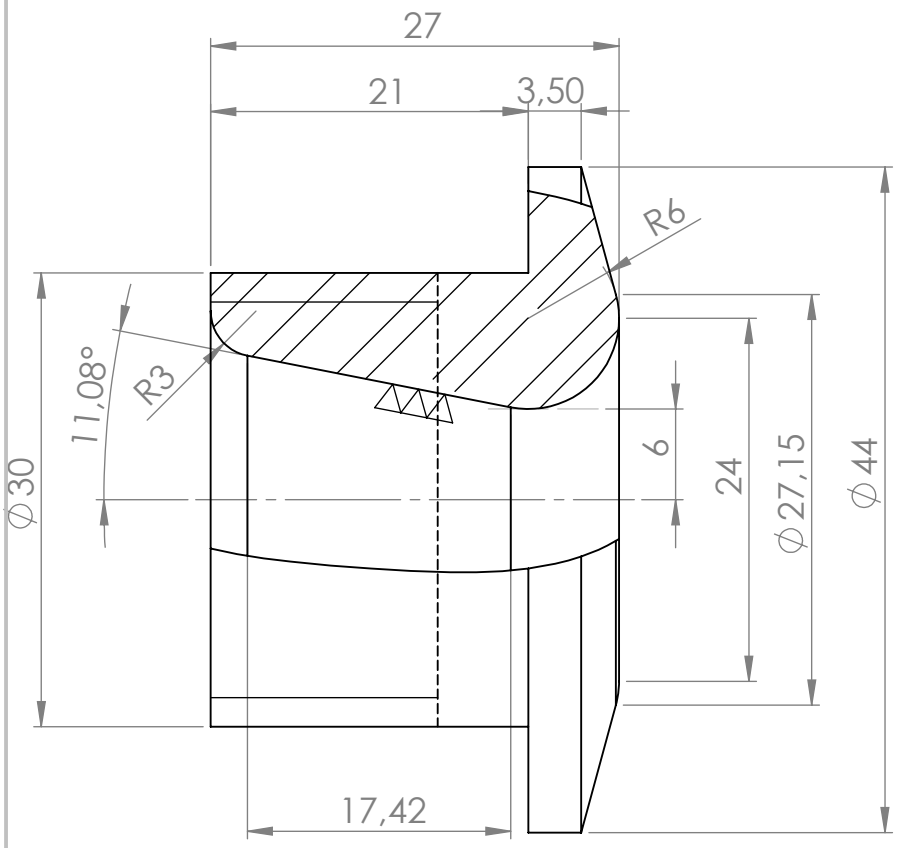

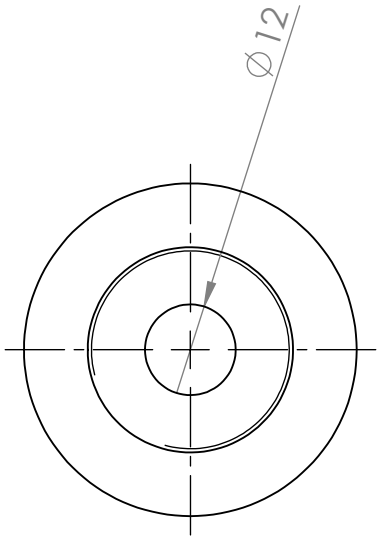

Scale 1:1

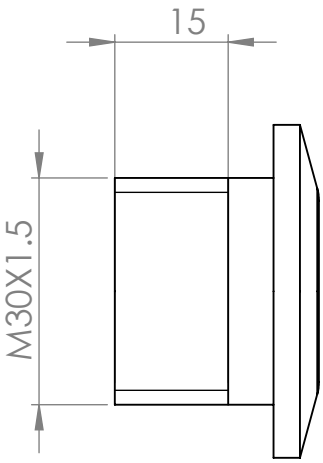

Scale 1:1

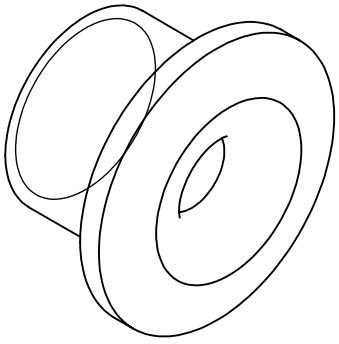

-UNLESS OTHERWISE SPECIFIED: DIMENSIONS ARE IN MILLIMETERS -SURFACE FINISH: - -General tolerance for linear and angular dimensions without individual tolerance indication ISO 2768-m	FINISH: -	DEBUR AND BREAK SHARP EDGES	DO NOT SCALE DRAWING	REVISION
			LABORATORY OF COMPOSITE MATERIALS AND ADAPTIVE STRUCTURES	ETH Zürich
	NAME	SIGNATURE	DATE	TITLE: YARN EYE
DRAWN	J. Molina Blanco			
CHK'D	Heinrich Thomas			
APPV'D				
MFG			MATERIAL: Stainless steel	DWG NO. 028
Q.A				A4
			WEIGHT:	SCALE: 2:1
				SHEET 1 OF 1

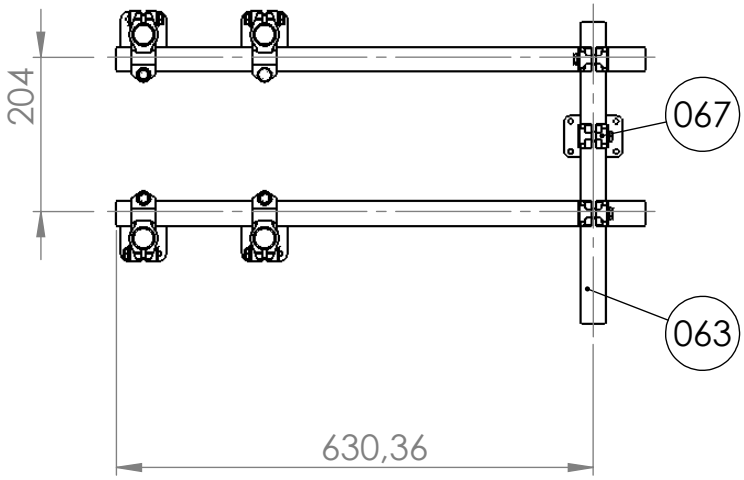

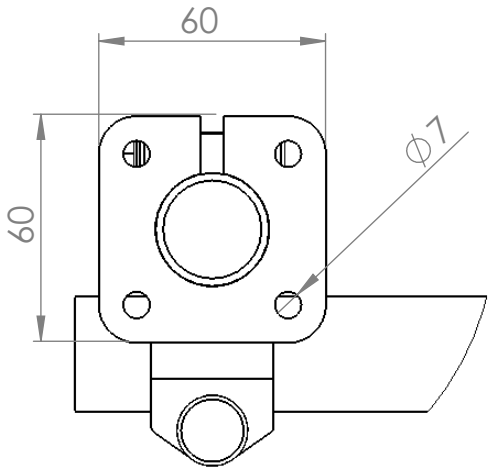

DETAIL A
SCALE 1 : 2

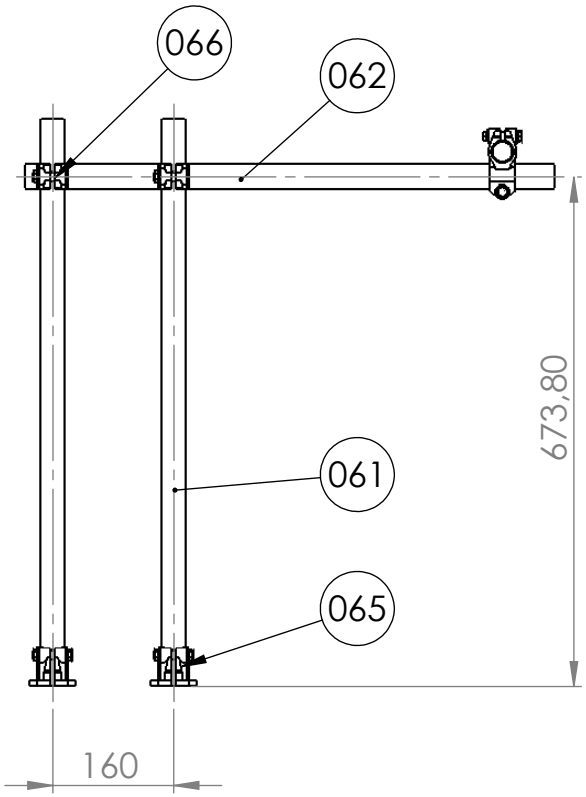

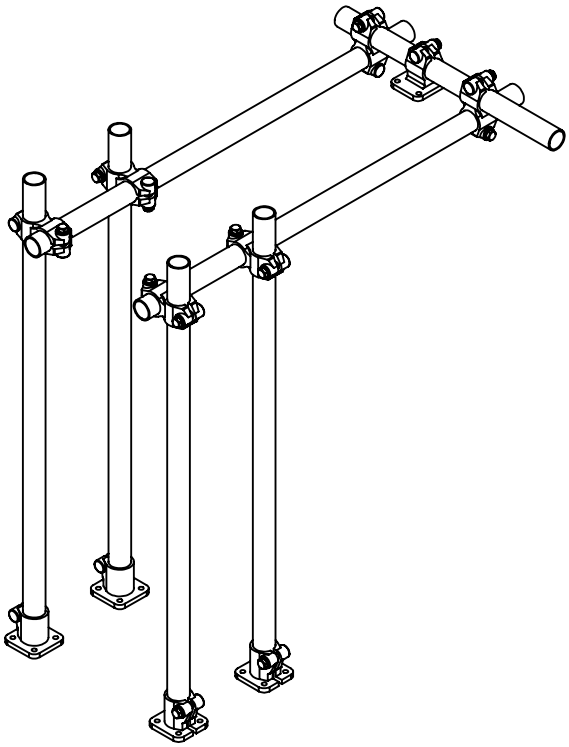

-UNLESS OTHERWISE SPECIFIED: DIMENSIONS ARE IN MILLIMETERS -SURFACE FINISH: - -General tolerance for linear and angular dimensions without individual tolerance indication ISO 2768-m	FINISH: -	DEBUR AND BREAK SHARP EDGES	DO NOT SCALE DRAWING	REVISION
			LABORATORY OF COMPOSITE MATERIALS AND ADAPTIVE STRUCTURES	ETH Zürich

	NAME	SIGNATURE	DATE
DRAWN	J. Molina Blanco		
CHK'D	Heinrich Thomas		
APPV'D			
MFG			
Q.A			

TITLE:

COMPACTION DEVICE STRUCTURE

DWG NO. **05**		A4
WEIGHT:	SCALE: 1:2	SHEET 1 OF 1

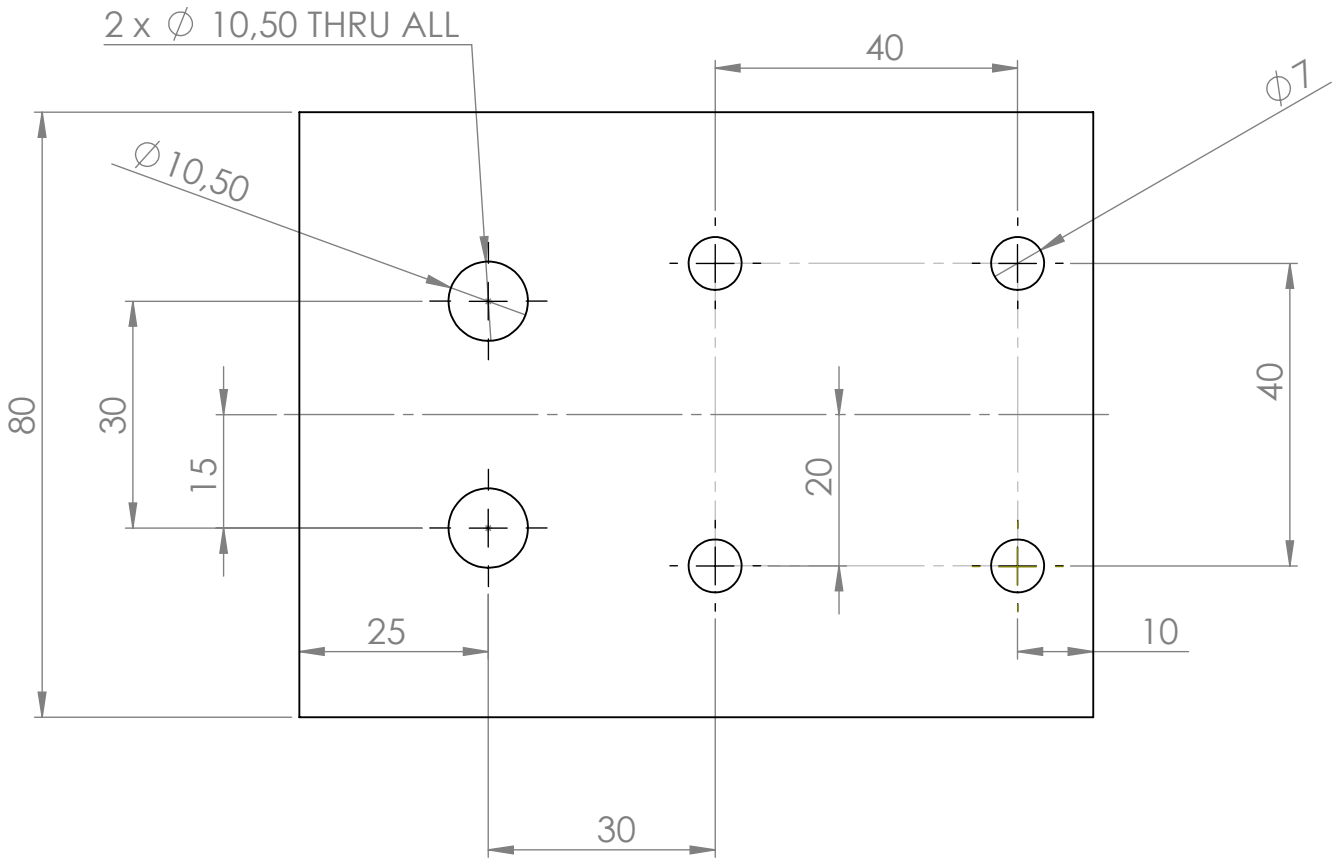

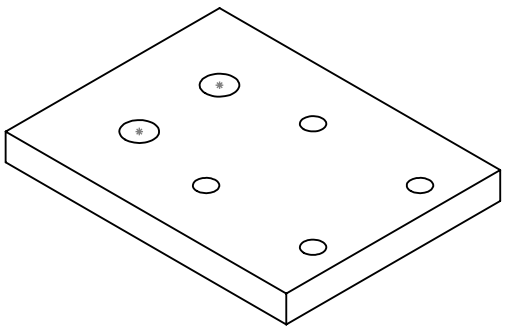

-UNLESS OTHERWISE SPECIFIED: DIMENSIONS ARE IN MILLIMETERS -SURFACE FINISH: - -General tolerance for linear and angular dimensions without individual tolerance indication ISO 2768-m	FINISH: -		DEBUR AND BREAK SHARP EDGES	DO NOT SCALE DRAWING / REVISION
				LABORATORY OF COMPOSITE MATERIALS AND ADAPTIVE STRUCTURES — ETH Zürich
	NAME	SIGNATURE	DATE	TITLE: COMPACTION STRUCTURE BED
DRAWN	J. Molina Blanco			
CHK'D	Heinrich Thomas			
APPV'D				
MFG			St 37-2	DWG NO. 068 — A4
Q.A				
			WEIGHT:	SCALE: 1:1 — SHEET 1 OF 1

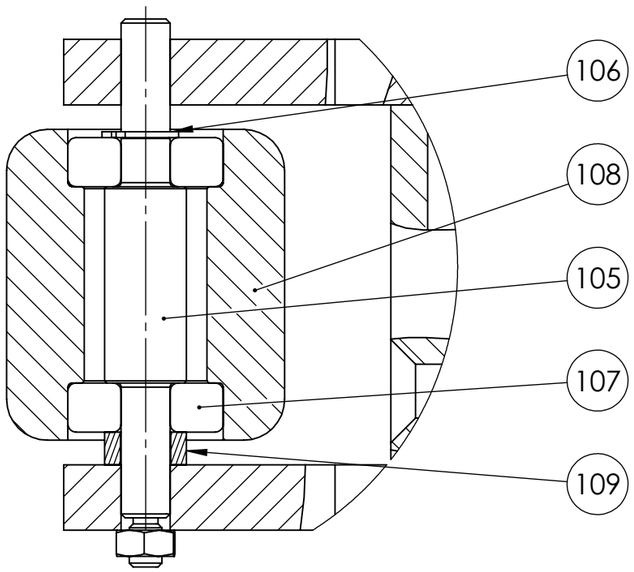

DETAIL A
SCALE 2 : 1.5

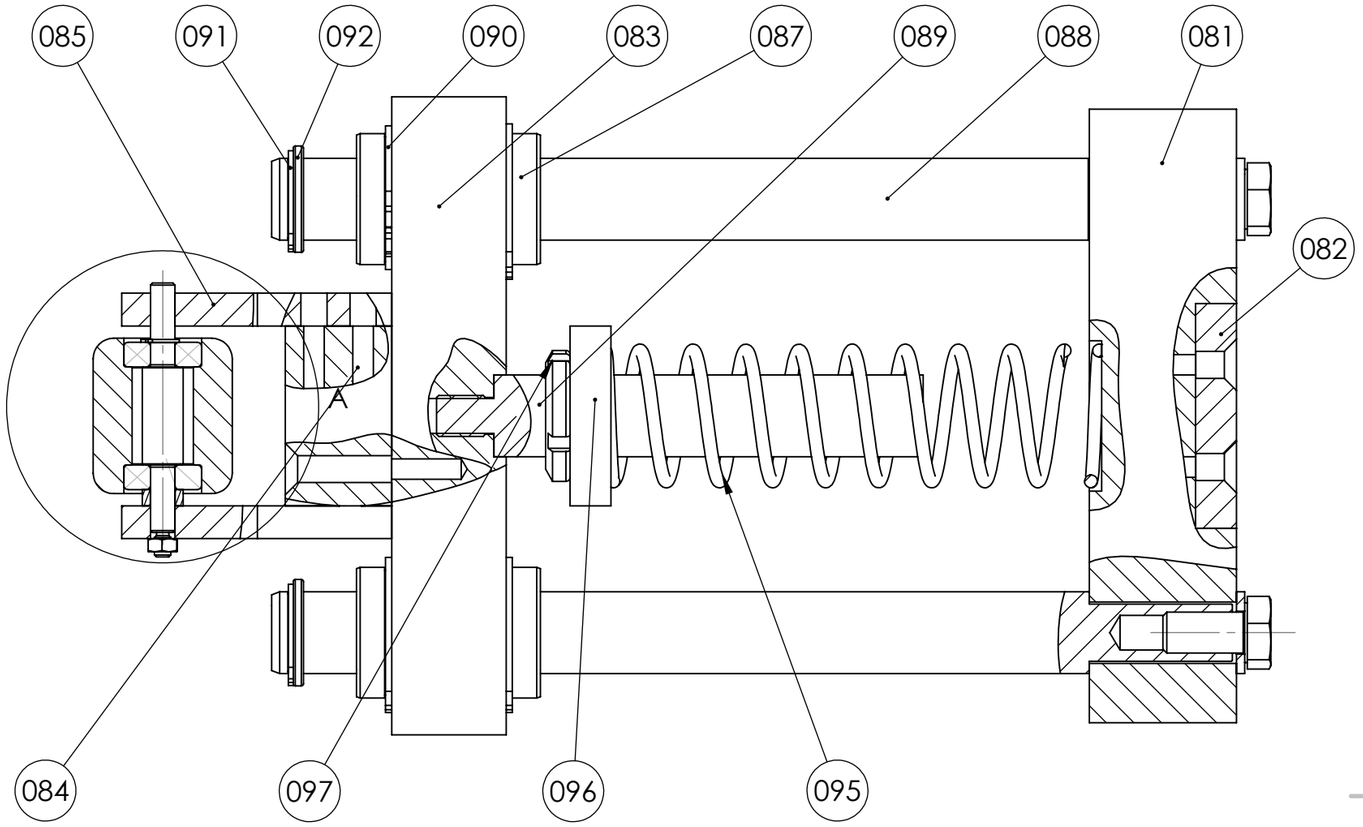

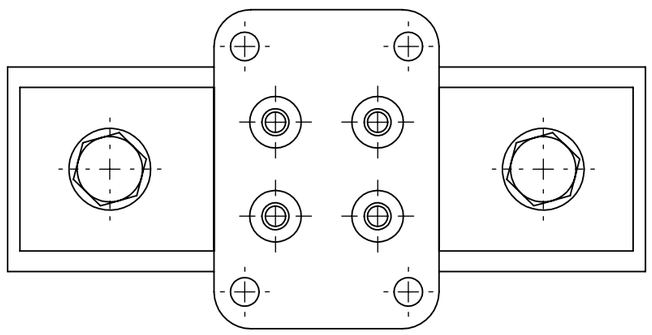

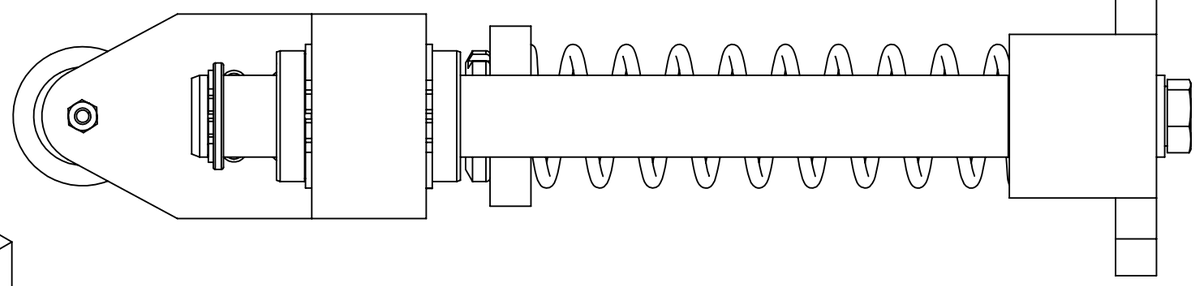

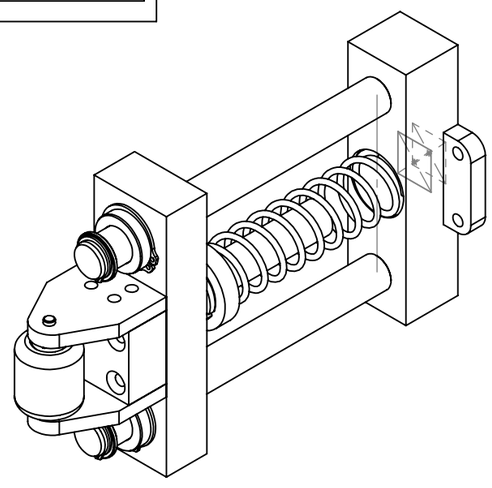

UNLESS OTHERWISE SPECIFIED: DIMENSIONS ARE IN MILLIMETERS SURFACE FINISH: TOLERANCES: LINEAR: ANGULAR:		FINISH:				DEBURR AND BREAK SHARP EDGES	DO NOT SCALE DRAWING	REVISION
							LABORATORY OF COMPOSITE MATERIALS AND ADAPTIVE STRUCTURES — ETH Zürich	
	NAME	SIGNATURE	DATE				TITLE:	
DRAWN	J. Molina Blanco						COMPACTION DEVICE	
CHK'D	Heinrich Thomas							
APPV'D								
MFG								
Q.A				MATERIAL:			DWG NO. 06	A3
				WEIGHT:			SCALE:1:1	SHEET 1 OF 1

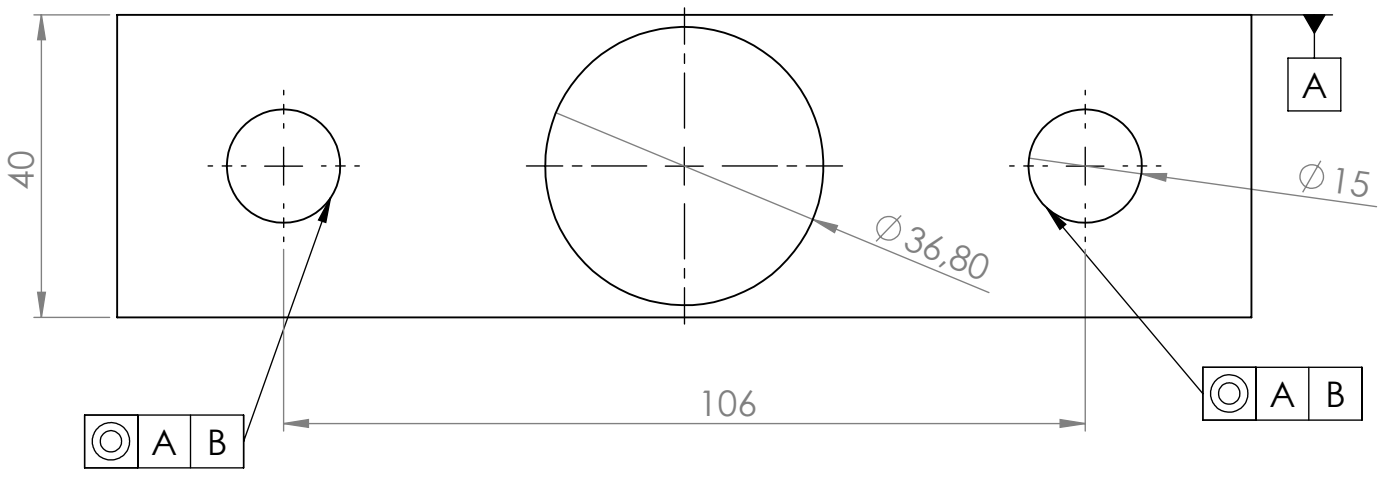

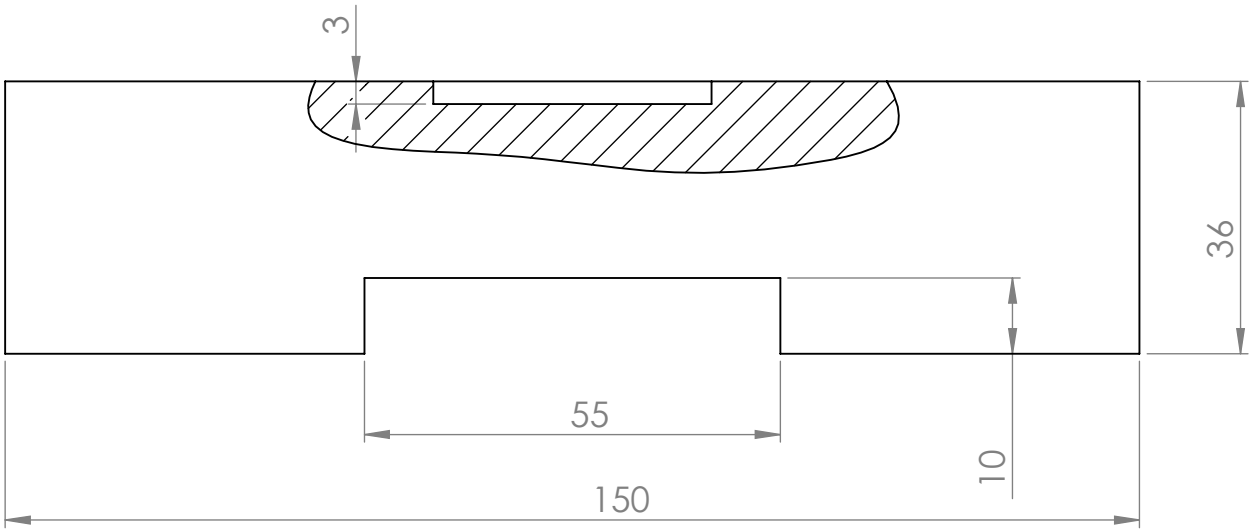

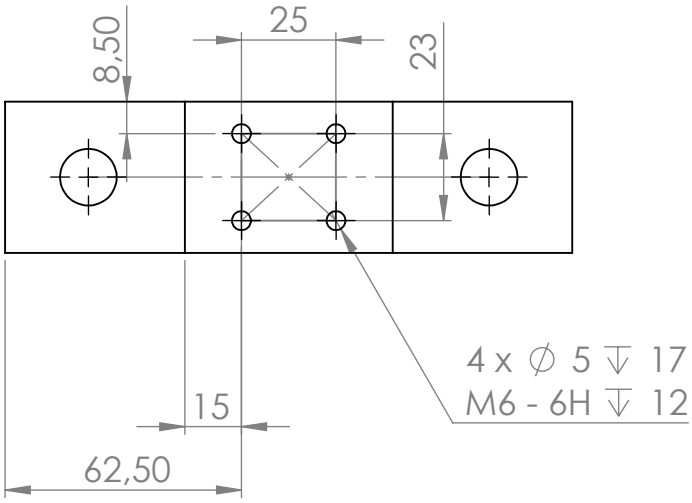

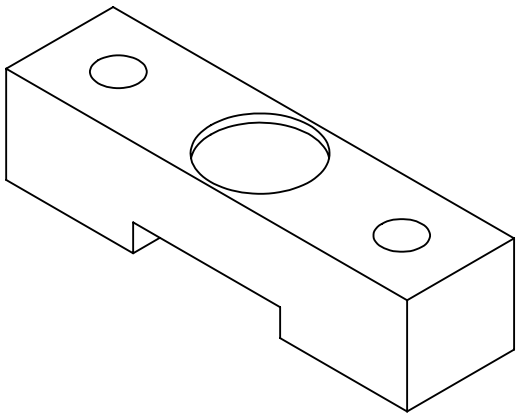

-UNLESS OTHERWISE SPECIFIED: DIMENSIONS ARE IN MILLIMETERS -SURFACE FINISH: - -General tolerance for linear and angular dimensions without individual tolerance indication ISO 2768-m	FINISH: -	DEBUR AND BREAK SHARP EDGES	DO NOT SCALE DRAWING	REVISION
			LABORATORY OF COMPOSITE MATERIALS AND ADAPTIVE STRUCTURES ETH Zürich	
	NAME	SIGNATURE	DATE	TITLE: BASE 1
DRAWN	J. Molina Blanco			
CHK'D	Heinrich Thomas			
APPV'D				
MFG			St 37	DWG NO. 081 A4
Q.A				
			WEIGHT:	SCALE: 1:1 SHEET 1 OF 1

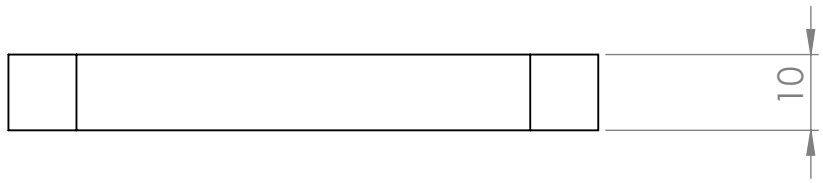

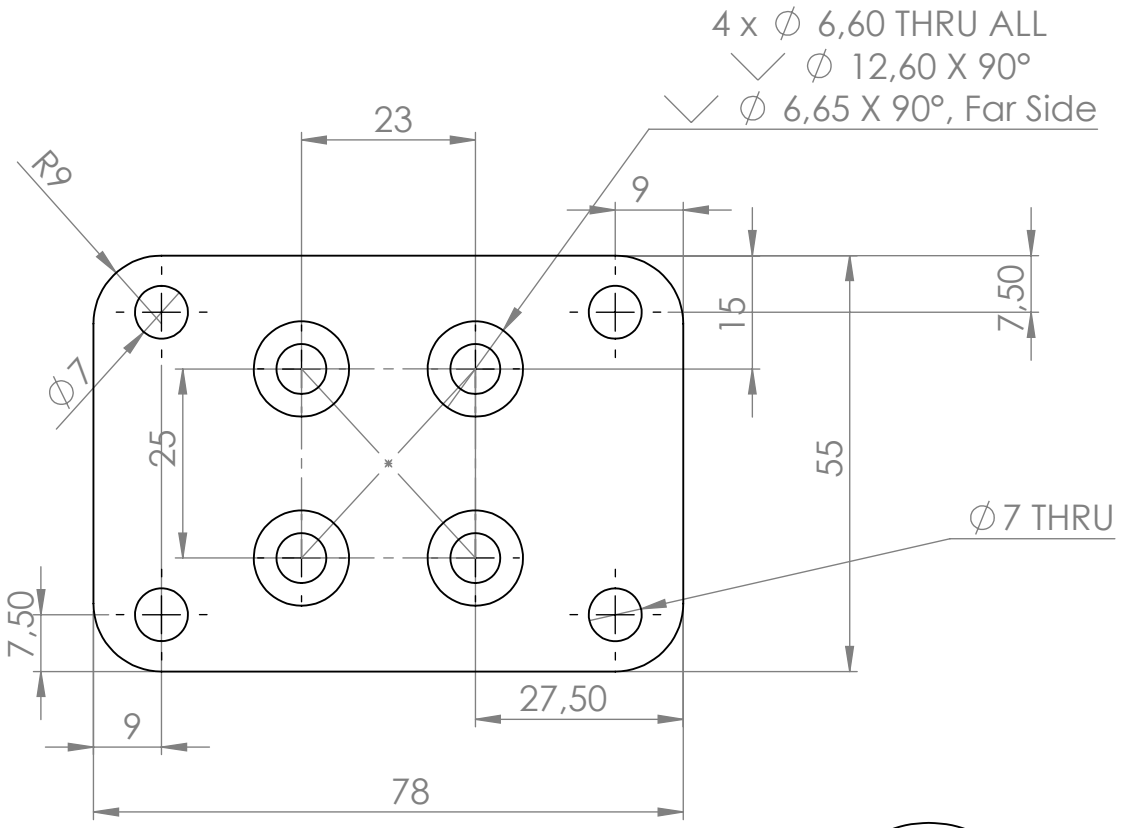

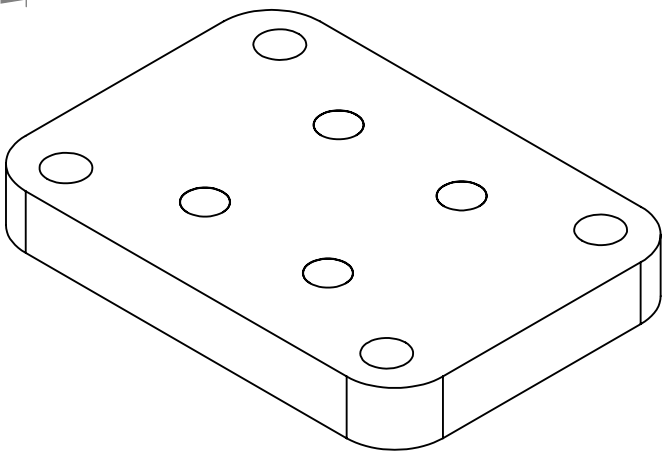

-UNLESS OTHERWISE SPECIFIED: DIMENSIONS ARE IN MILLIMETERS -SURFACE FINISH: - -General tolerance for linear and angular dimensions without individual tolerance indication ISO 2768-m	FINISH: -	DEBUR AND BREAK SHARP EDGES	DO NOT SCALE DRAWING	REVISION
			LABORATORY OF COMPOSITE MATERIALS AND ADAPTIVE STRUCTURES ETH Zürich	
	NAME	SIGNATURE	DATE	TITLE: BASE 2
DRAWN	J. Molina Blanco			
CHK'D	Heinrich Thomas			
APPV'D				
MFG			St 37	DWG NO. 082 A4
Q.A				
			WEIGHT:	SCALE: 1:1 SHEET 1 OF 1

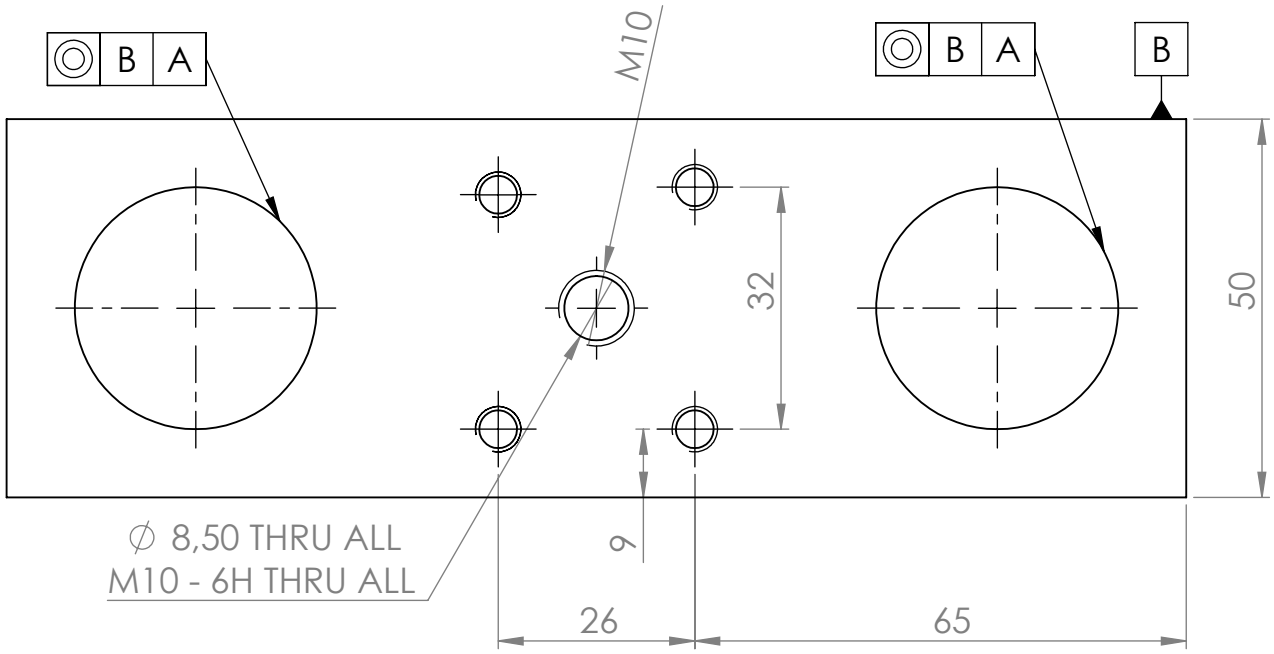

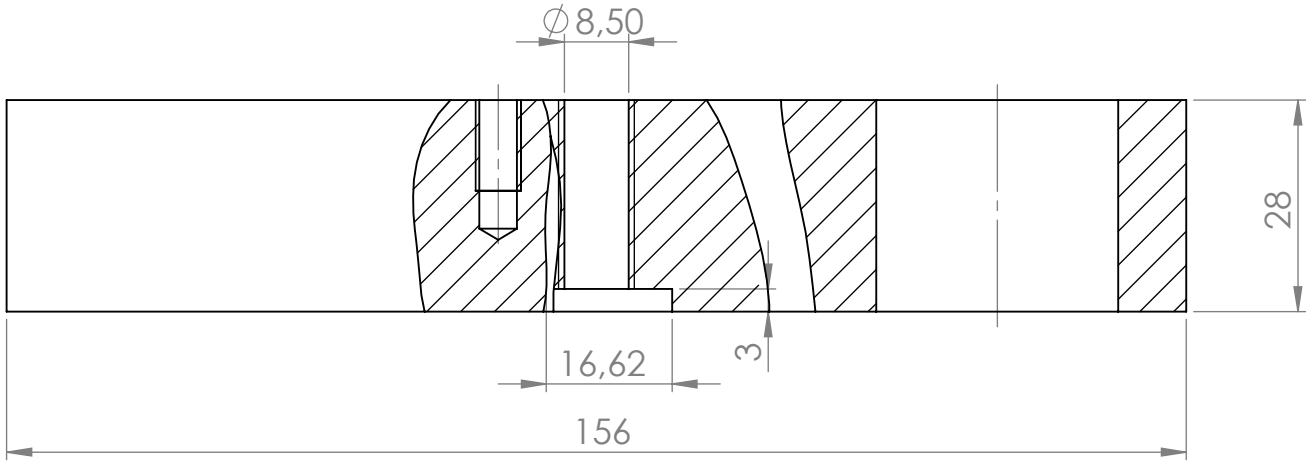

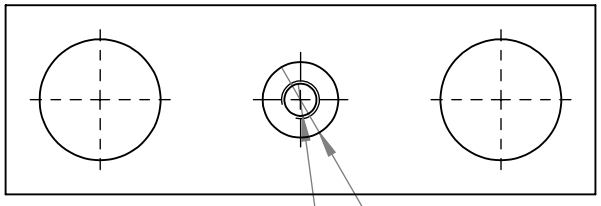

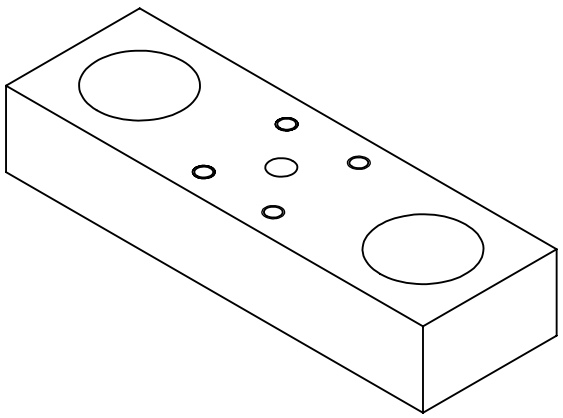

-UNLESS OTHERWISE SPECIFIED: DIMENSIONS ARE IN MILLIMETERS -SURFACE FINISH: - -General tolerance for linear and angular dimensions without individual tolerance indication ISO 2768-m	FINISH: -	DEBUR AND BREAK SHARP EDGES	DO NOT SCALE DRAWING	REVISION
			LABORATORY OF COMPOSITE MATERIALS AND ADAPTIVE STRUCTURES — ETH Zürich	
	NAME	SIGNATURE	DATE	TITLE: LOAD PART 1
DRAWN	J. Molina Blanco			
CHK'D	Heinrich Thomas			
APPV'D				
MFG			MATERIAL: St37 steel	DWG NO. 083 — A4
Q.A				
			WEIGHT:	SCALE: 1:1 — SHEET 1 OF 1

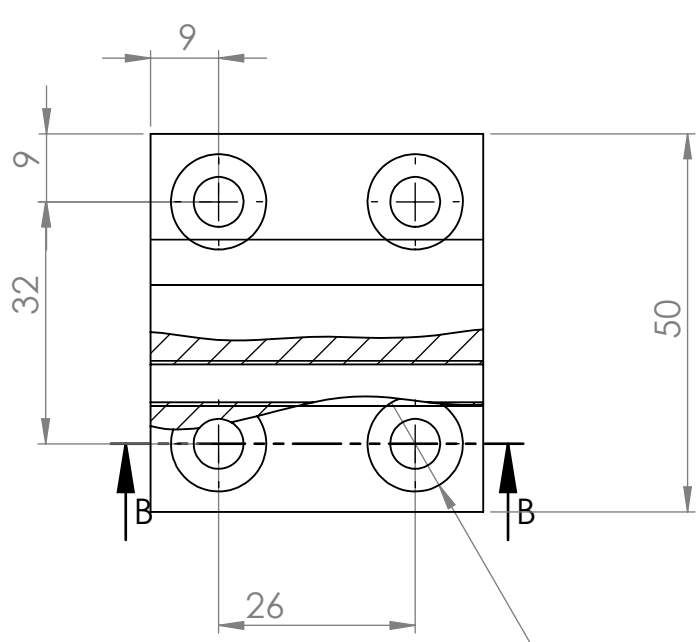

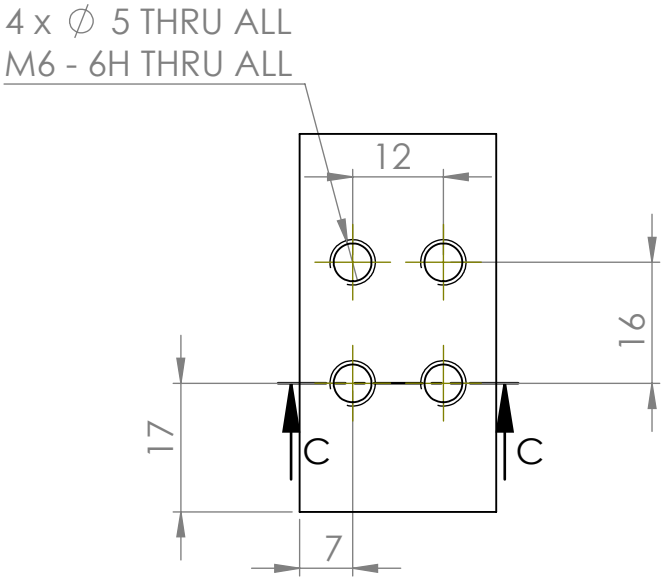

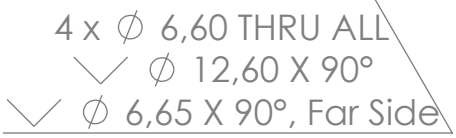

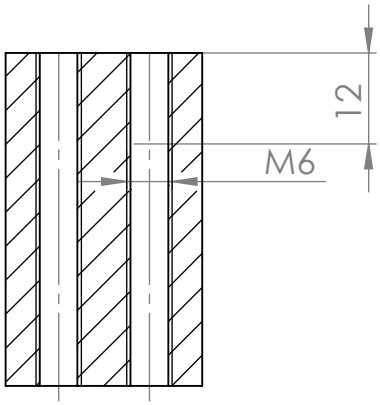

SECCIÓN C-C

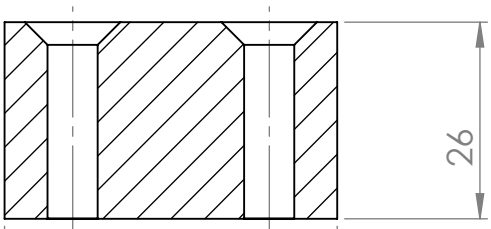

SECCIÓN B-B

44

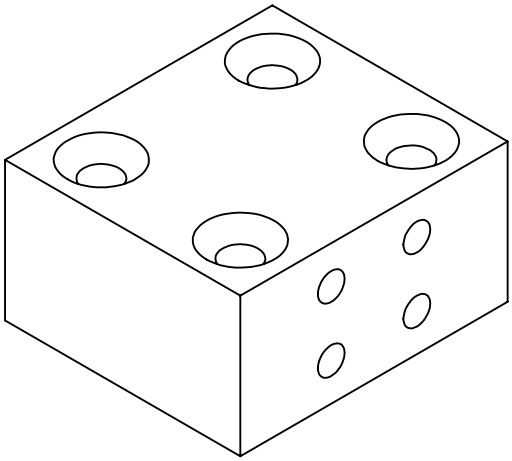

-UNLESS OTHERWISE SPECIFIED: DIMENSIONS ARE IN MILLIMETERS -SURFACE FINISH: - -General tolerance for linear and angular dimensions without individual tolerance indication ISO 2768-m	FINISH: -	DEBUR AND BREAK SHARP EDGES	DO NOT SCALE DRAWING	REVISION
			LABORATORY OF COMPOSITE MATERIALS AND ADAPTIVE STRUCTURES — ETH Zürich	
	NAME	SIGNATURE	DATE	TITLE: LOAD PART 2
DRAWN	J. Molina Blanco			
CHK'D	Heinrich Thomas			
APPV'D				
MFG			St37	DWG NO. 084 — A4
Q.A				
			WEIGHT:	SCALE: 1:1 — SHEET 1 OF 1

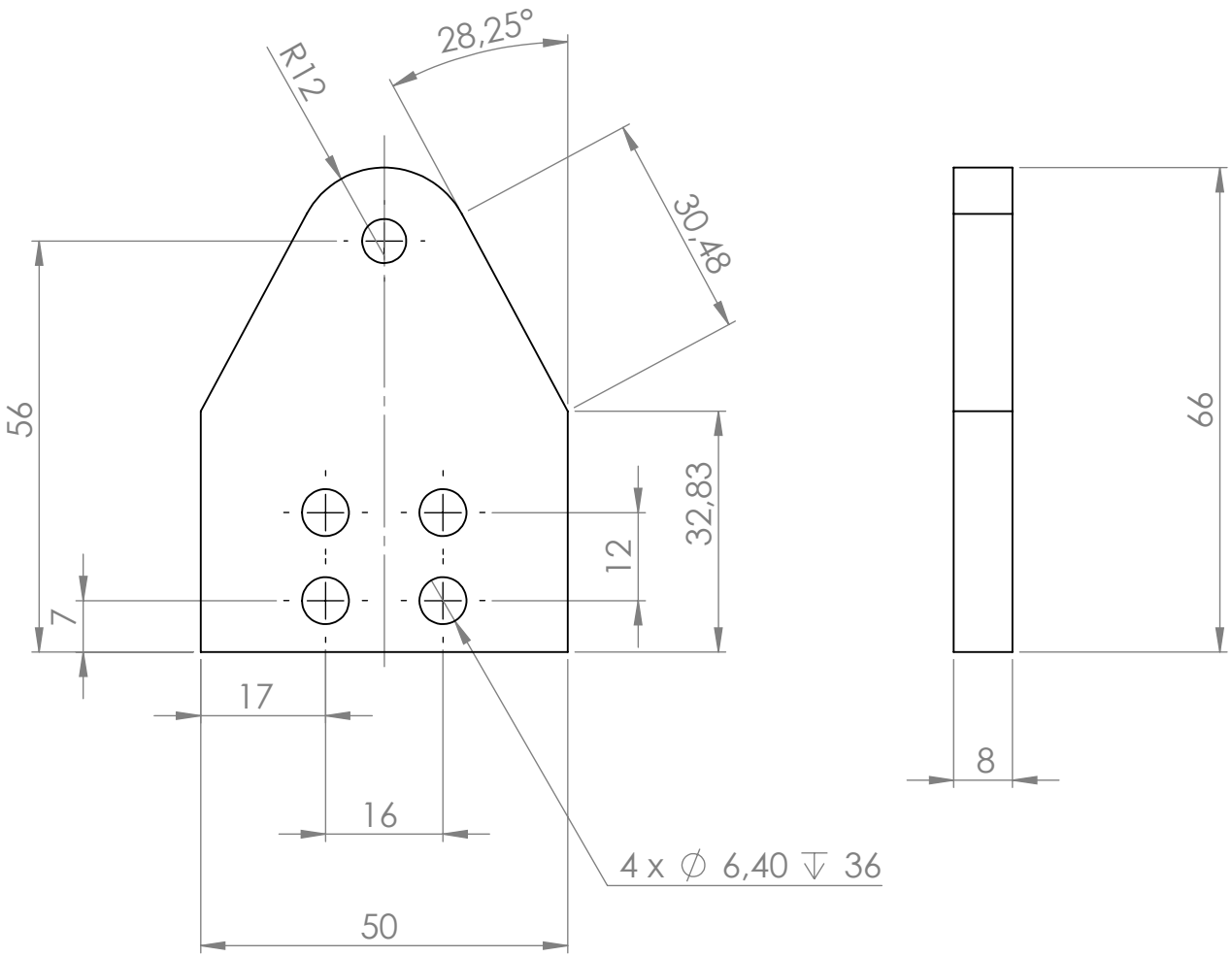

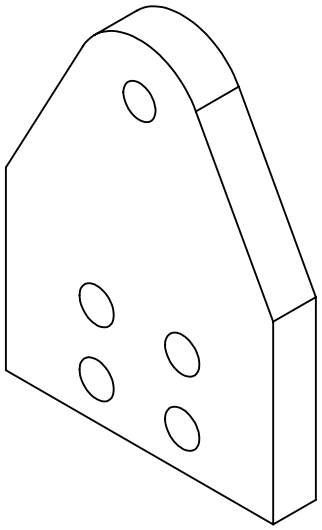

-UNLESS OTHERWISE SPECIFIED: DIMENSIONS ARE IN MILLIMETERS -SURFACE FINISH: - -General tolerance for linear and angular dimensions without individual tolerance indication ISO 2768-m	FINISH: -	DEBUR AND BREAK SHARP EDGES	DO NOT SCALE DRAWING	REVISION
			LABORATORY OF COMPOSITE MATERIALS AND ADAPTIVE STRUCTURES — ETH Zürich	
	NAME	SIGNATURE	DATE	
DRAWN	J. Molina Blanco			
CHK'D	Heinrich Thomas			
APPV'D				
MFG				
Q.A				
			WEIGHT:	SCALE: 1:1

TITLE:

LOAD PART 3

St 37

DWG NO. 085

A4

SHEET 1 OF 1

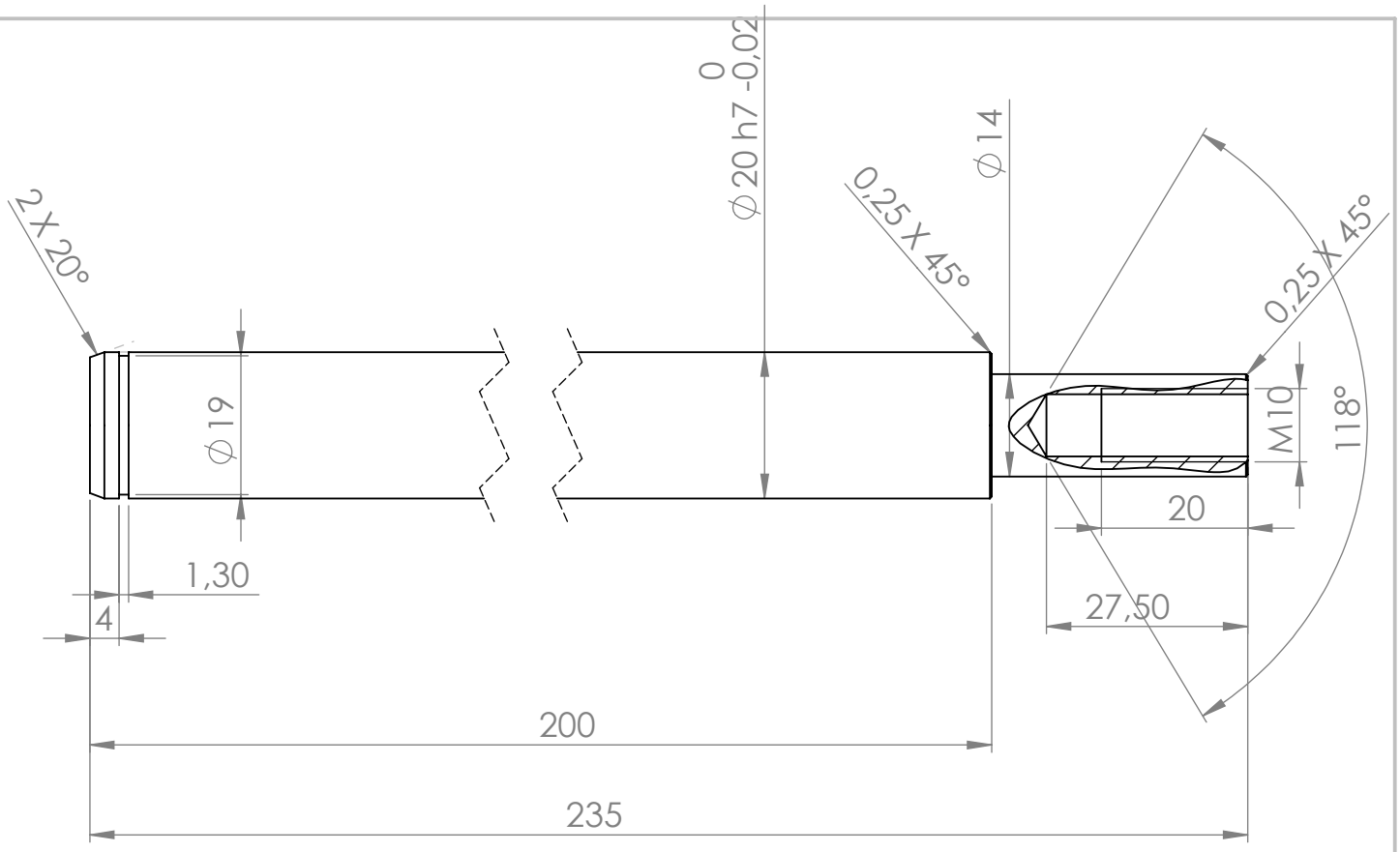

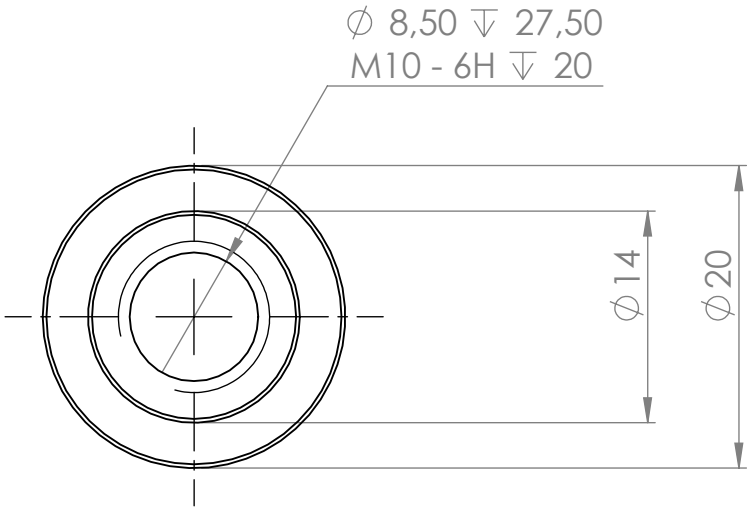

-UNLESS OTHERWISE SPECIFIED: DIMENSIONS ARE IN MILLIMETERS -SURFACE FINISH: - -General tolerance for linear and angular dimensions without individual tolerance indication ISO 2768-m	FINISH: -	DEBUR AND BREAK SHARP EDGES	DO NOT SCALE DRAWING	REVISION
			LABORATORY OF COMPOSITE MATERIALS AND ADAPTIVE STRUCTURES — ETH Zürich	
	NAME	SIGNATURE	DATE	TITLE: GUIDE
DRAWN	J. Molina Blanco			
CHK'D	Heinrich Thomas			
APPV'D				
MFG			Calibrated steel	DWG NO. 088 — A4
Q.A				
			WEIGHT:	SCALE: 1:1 — SHEET 1 OF 1

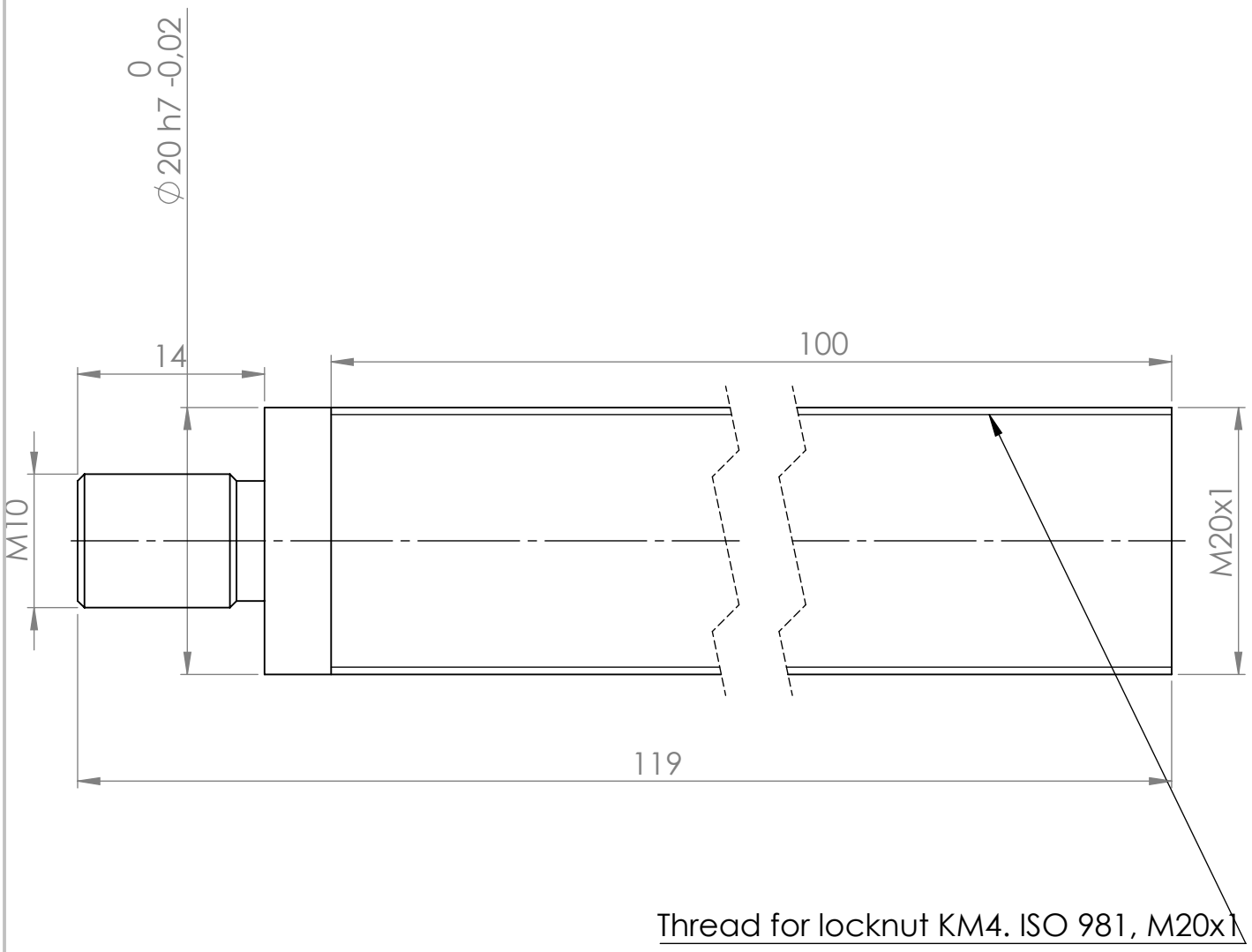

-UNLESS OTHERWISE SPECIFIED: DIMENSIONS ARE IN MILLIMETERS -SURFACE FINISH: - -General tolerance for linear and angular dimensions without individual tolerance indication ISO 2768-m	FINISH: -	DEBUR AND BREAK SHARP EDGES	DO NOT SCALE DRAWING	REVISION
			LABORATORY OF COMPOSITE MATERIALS AND ADAPTIVE STRUCTURES ETH Zürich	
	NAME	SIGNATURE	DATE	
DRAWN	J. Molina Blanco			
CHK'D	Heinrich Thomas			
APPV'D				
MFG				
Q.A				

TITLE:

SHAFT 2

MATERIAL: Calibrated steel	DWG NO. 089	A4
WEIGHT:	SCALE: 2:1	SHEET 1 OF 1

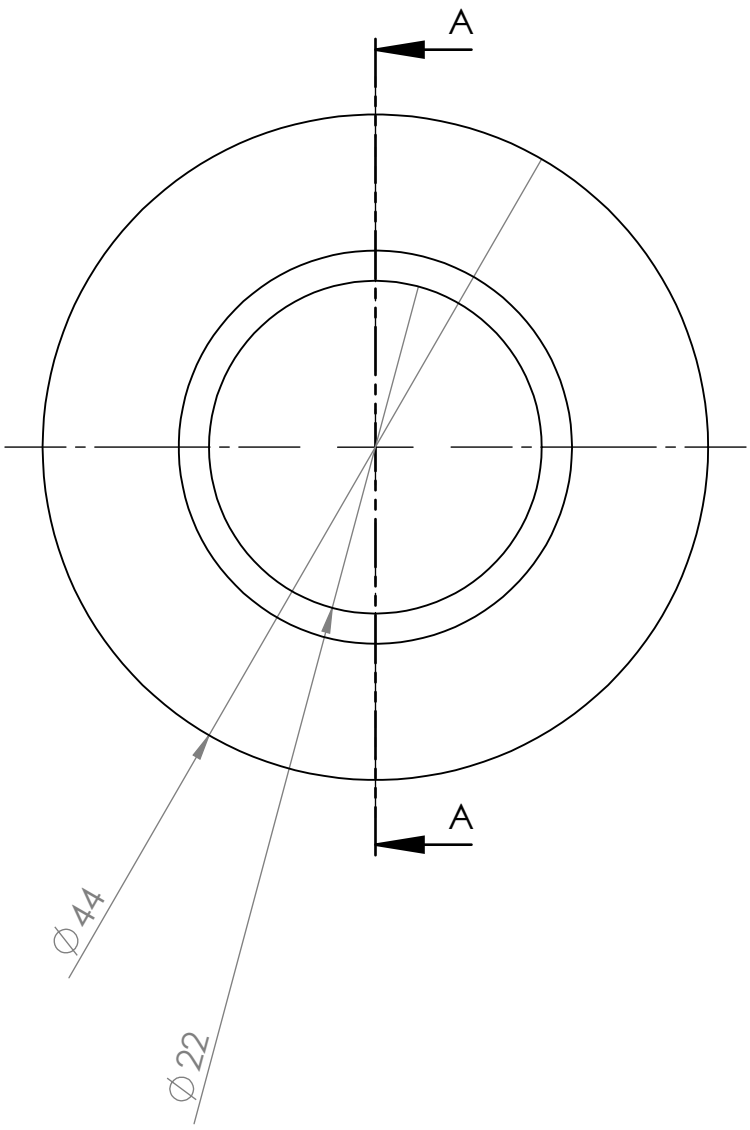

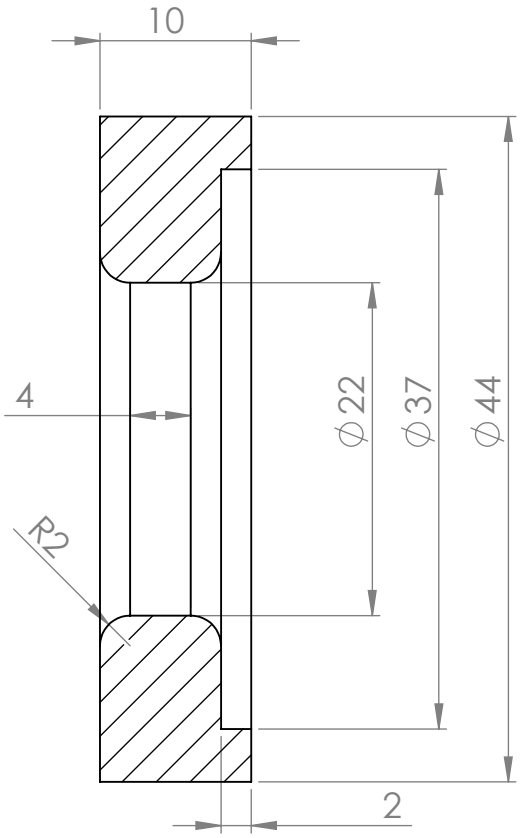

SECCIÓN A-A

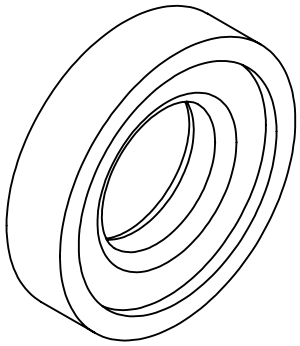

-UNLESS OTHERWISE SPECIFIED: DIMENSIONS ARE IN MILLIMETERS -SURFACE FINISH: - -General tolerance for linear and angular dimensions without individual tolerance indication ISO 2768-m	FINISH: -	DEBUR AND BREAK SHARP EDGES	DO NOT SCALE DRAWING	REVISION
			LABORATORY OF COMPOSITE MATERIALS AND ADAPTIVE STRUCTURES	ETH Zürich
	NAME	SIGNATURE	DATE	TITLE: ADJUSTABLE RING
DRAWN	J. Molina Blanco			
CHK'D	Heinrich Thomas			
APPV'D				
MFG			CuZn38Pb2	DWG NO. 097
Q.A				A4
			WEIGHT:	SCALE: 2:1 SHEET 1 OF 1

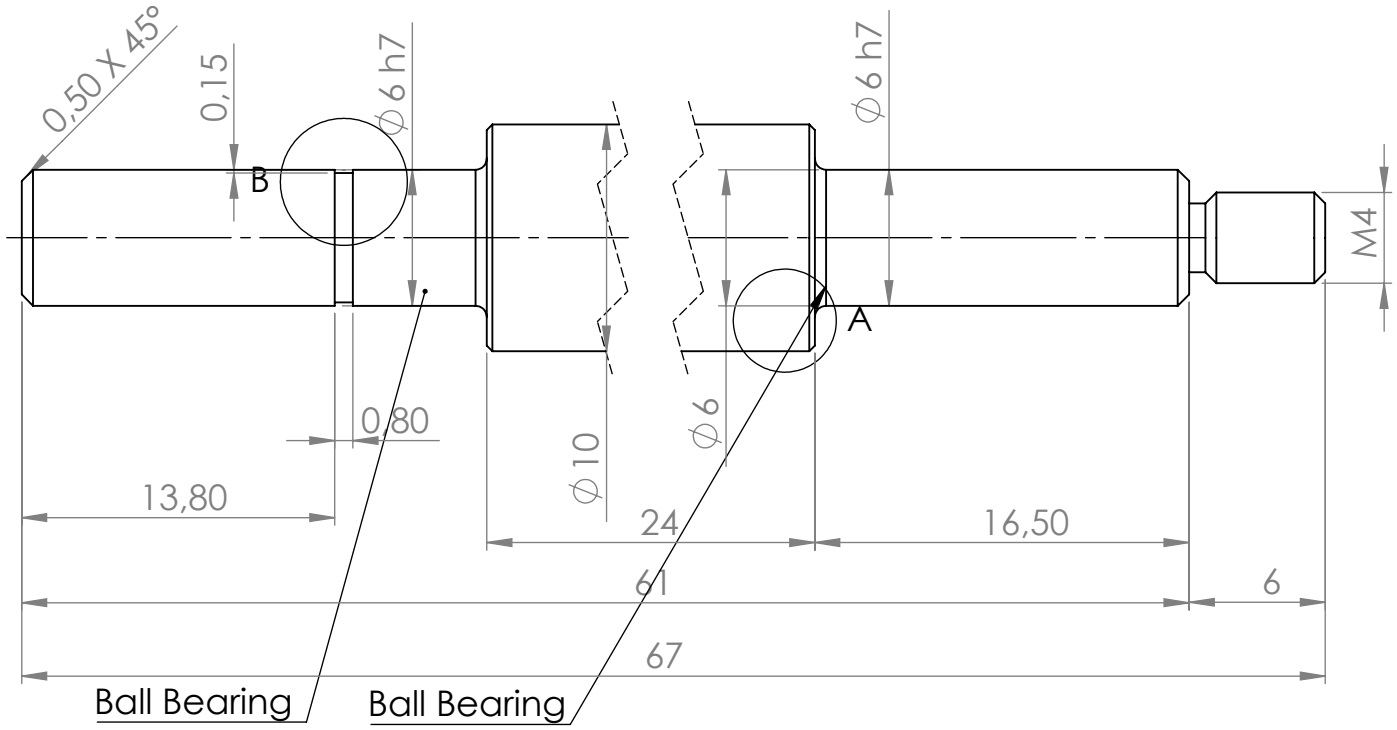

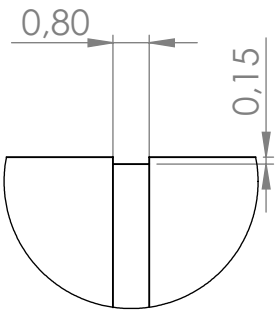

DETAIL B Elastic ring. DIN471
SCALE 6 : 1

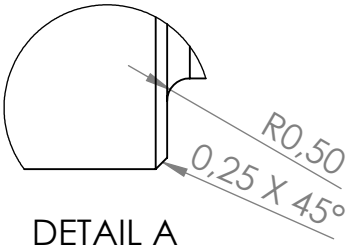

DETAIL A
SCALE 6 : 1

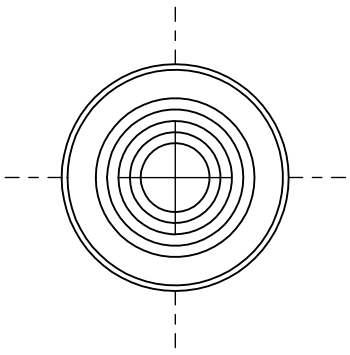

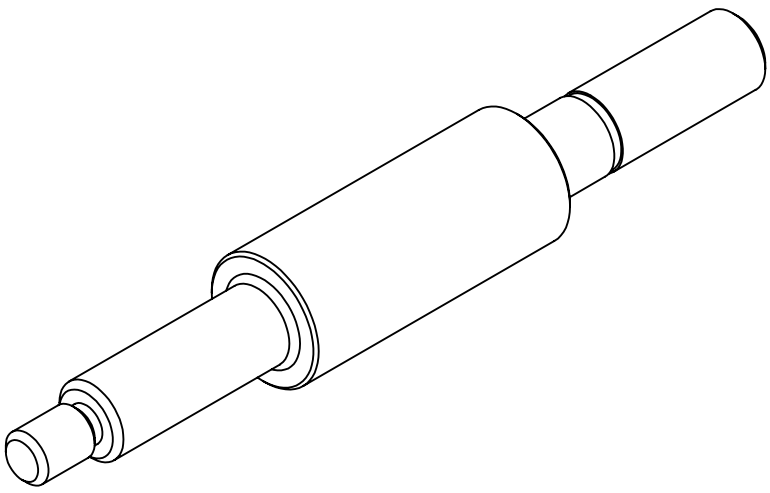

-UNLESS OTHERWISE SPECIFIED: DIMENSIONS ARE IN MILLIMETERS -SURFACE FINISH: - -General tolerance for linear and angular dimensions without individual tolerance indication ISO 2768-m	FINISH: -	DEBUR AND BREAK SHARP EDGES	DO NOT SCALE DRAWING	REVISION
			LABORATORY OF COMPOSITE MATERIALS AND ADAPTIVE STRUCTURES — ETH Zürich	
	NAME	SIGNATURE	DATE	TITLE: ROLLER SHAFT
DRAWN	J. Molina Blanco			
CHK'D	Heinrich Thomas			
APPV'D				
MFG			MATERIAL: Calibrated steel	DWG NO. 105 — A4
Q.A				
			WEIGHT:	SCALE: 3:1 — SHEET 1 OF 1

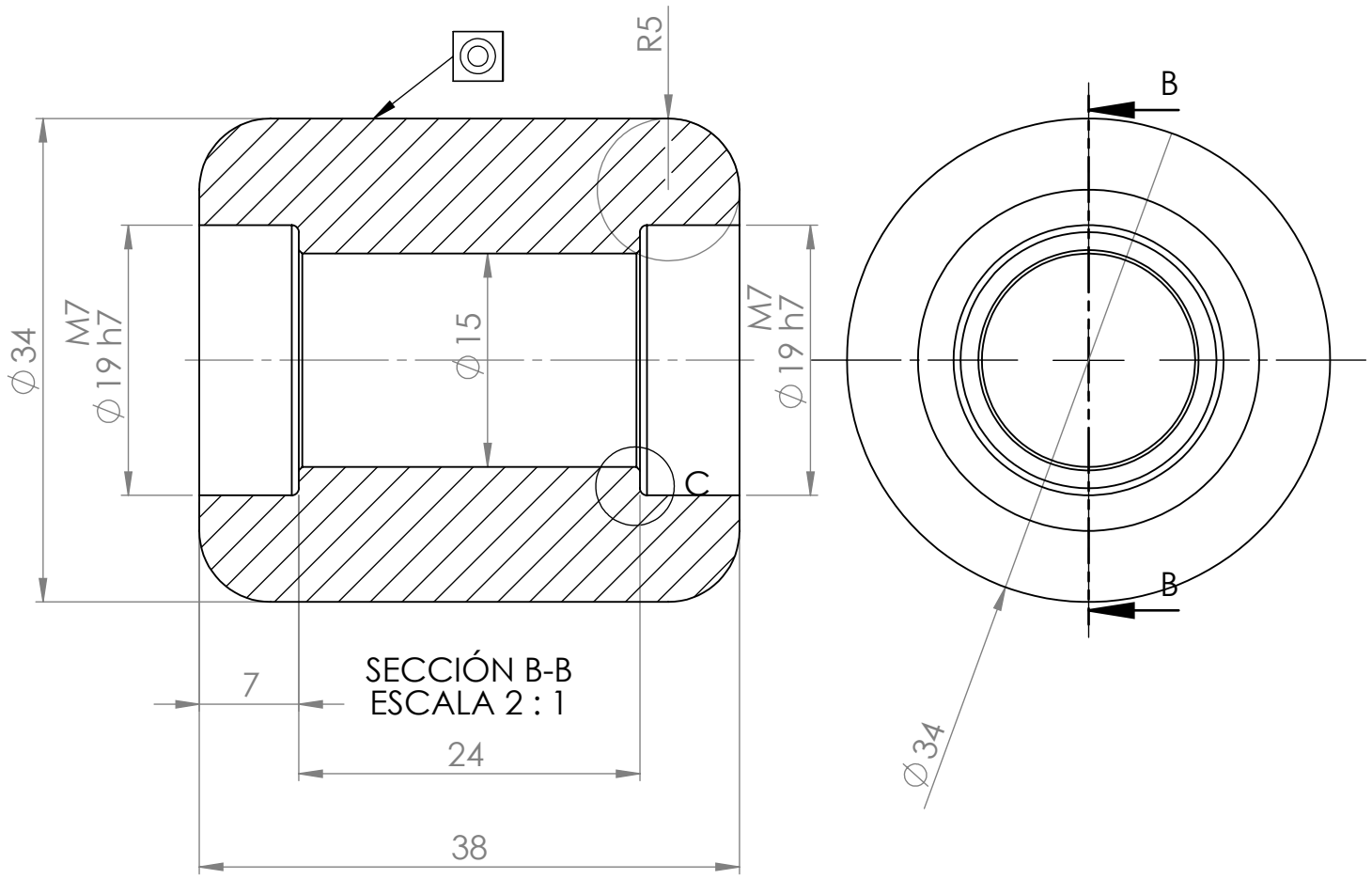

SECCIÓN B-B
ESCALA 2 : 1

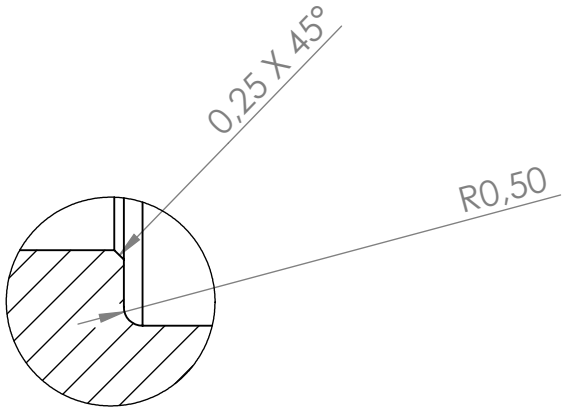

DETAIL C
SCALE 5 : 1

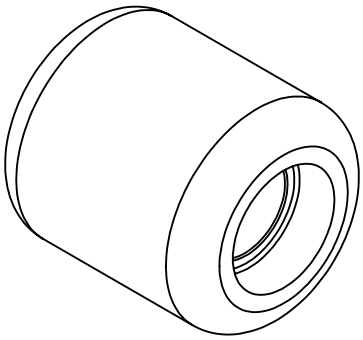

-UNLESS OTHERWISE SPECIFIED: DIMENSIONS ARE IN MILLIMETERS -SURFACE FINISH: - -General tolerance for linear and angular dimensions without individual tolerance indication ISO 2768-m	FINISH: -	DEBUR AND BREAK SHARP EDGES	DO NOT SCALE DRAWING	REVISION
			LABORATORY OF COMPOSITE MATERIALS AND ADAPTIVE STRUCTURES — ETH Zürich	
	NAME	SIGNATURE	DATE	TITLE: COMPACTION ROLLER
DRAWN	J. Molina Blanco			
CHK'D	Heinrich Thomas			
APPV'D				
MFG			MATERIAL: Stainless steel	DWG NO. 108 — A4
Q.A				
			WEIGHT:	SCALE: 1:2 — SHEET 1 OF 1

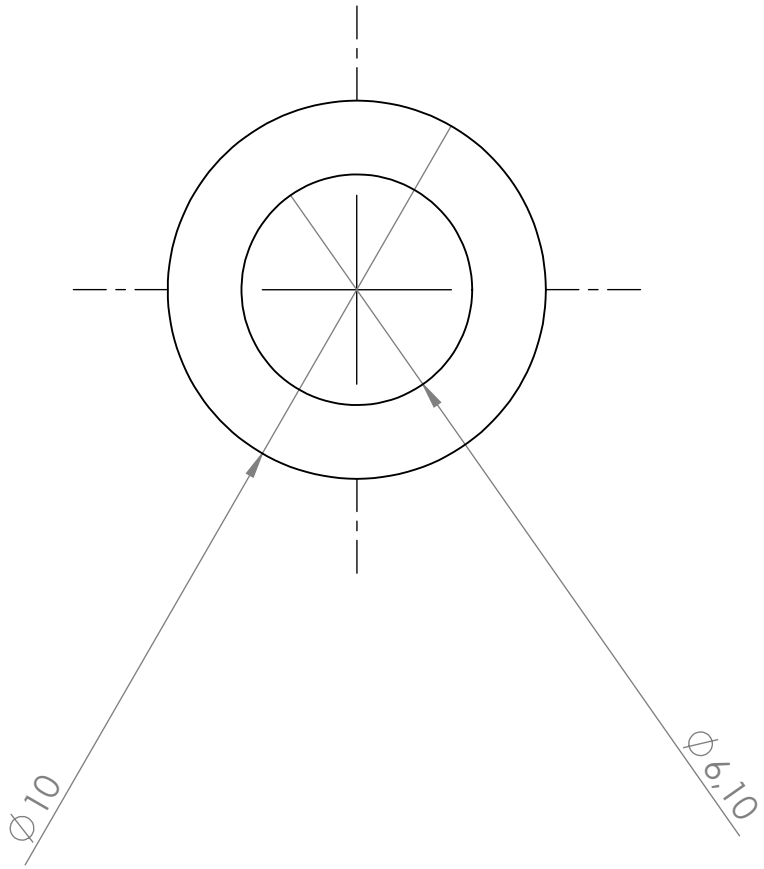

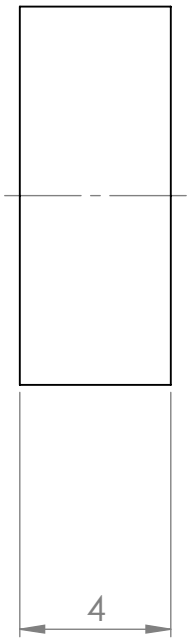

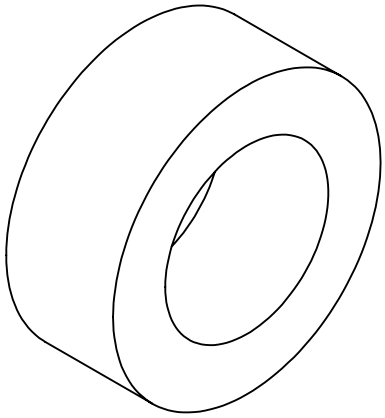

-UNLESS OTHERWISE SPECIFIED: DIMENSIONS ARE IN MILLIMETERS -SURFACE FINISH: - -General tolerance for linear and angular dimensions without individual tolerance indication ISO 2768-m	FINISH: -	DEBUR AND BREAK SHARP EDGES	DO NOT SCALE DRAWING	REVISION
			LABORATORY OF COMPOSITE MATERIALS AND ADAPTIVE STRUCTURES ETH Zürich	
	NAME	SIGNATURE	DATE	
DRAWN	J. Molina Blanco			
CHK'D	Heinrich Thomas			
APPV'D				
MFG			TITLE: DISTANCE PART	
Q.A				
			St 37	DWG NO. 109 A4
			WEIGHT:	SCALE: 5:1 SHEET 1 OF 1

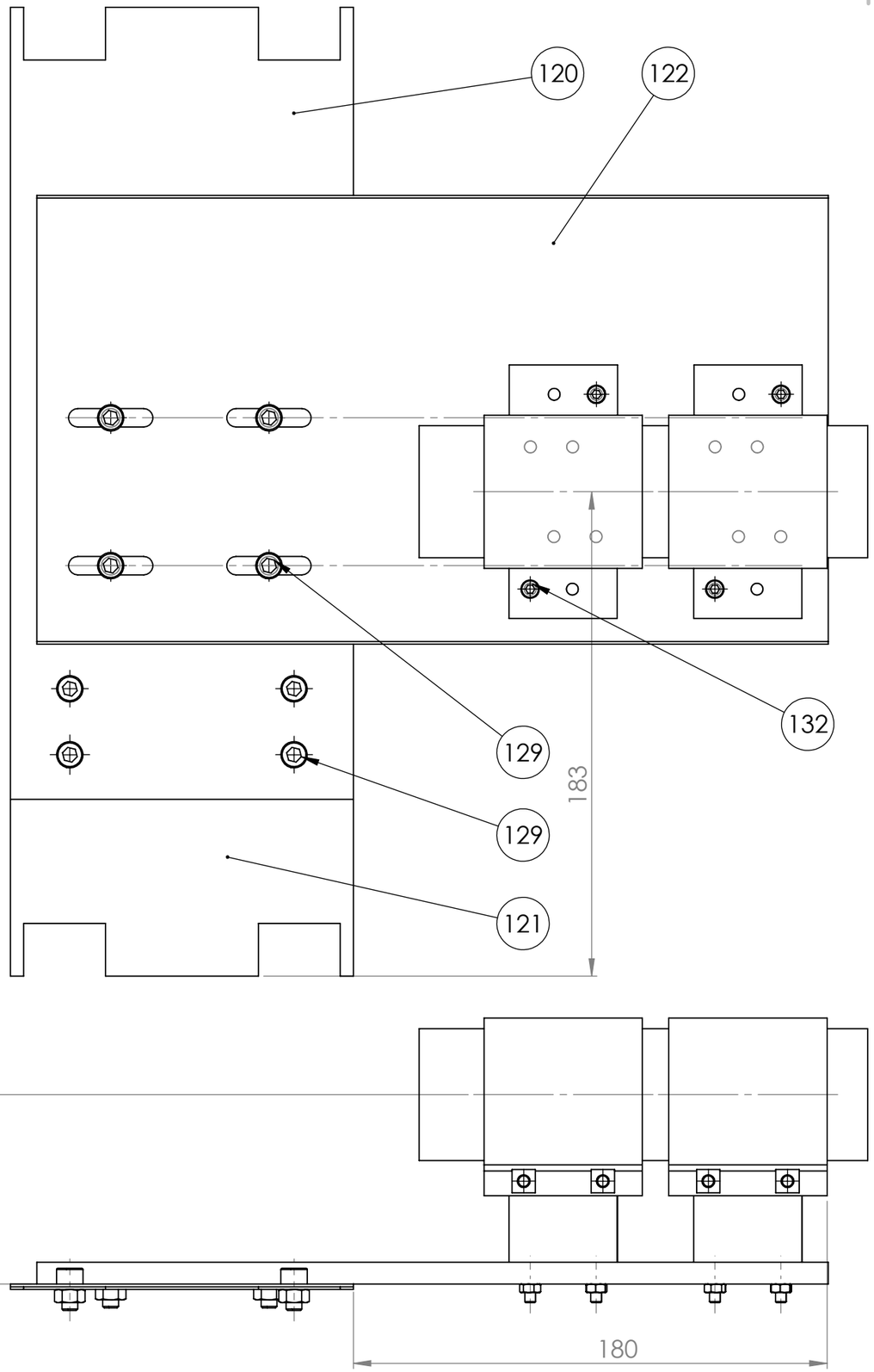

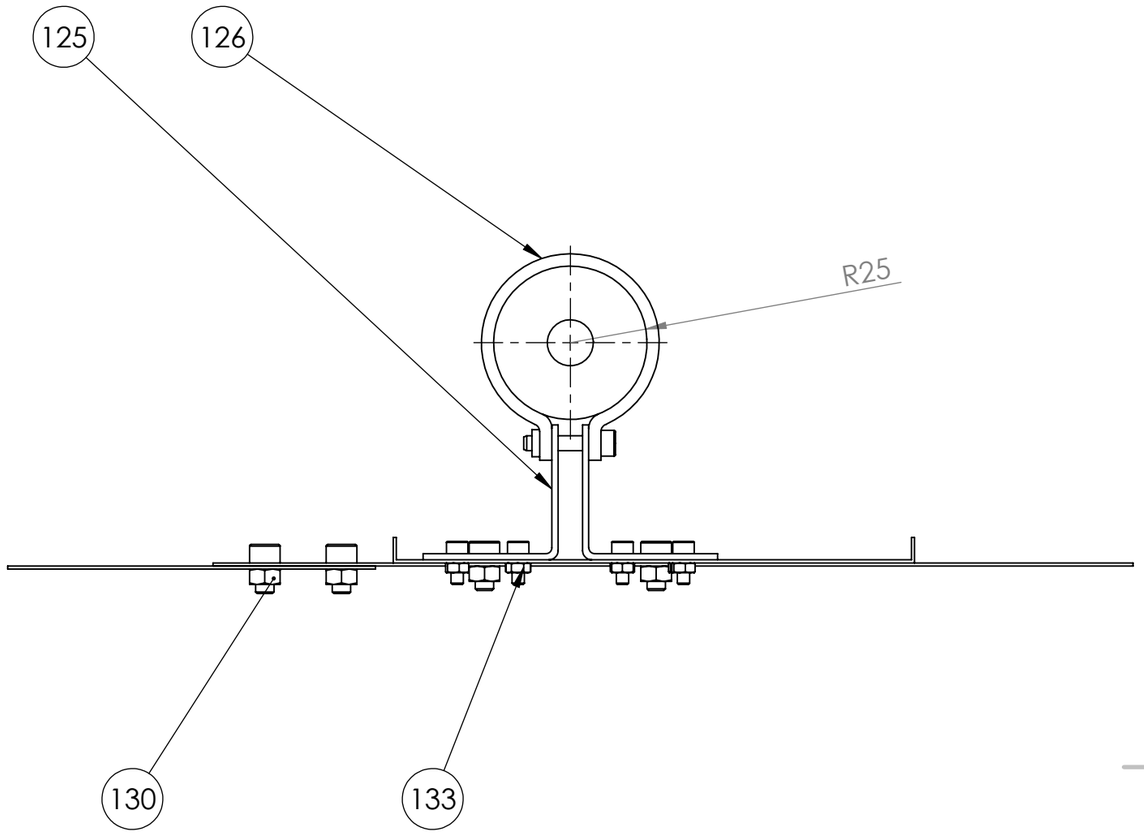

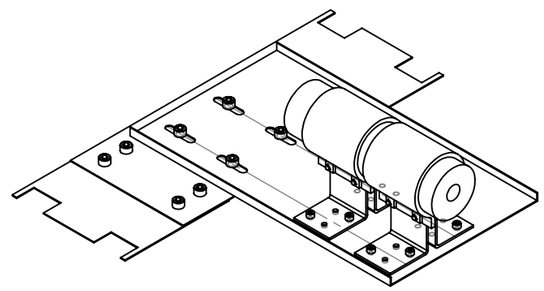

UNLESS OTHERWISE SPECIFIED: DIMENSIONS ARE IN MILLIMETERS SURFACE FINISH: TOLERANCES: LINEAR: ANGULAR:		FINISH:				DEBURR AND BREAK SHARP EDGES	DO NOT SCALE DRAWING / REVISION
							LABORATORY OF COMPOSITE MATERIALS AND ADAPTIVE STRUCTURES — ETH Zürich
	NAME	SIGNATURE	DATE				TITLE:
DRAWN	J. Molina Blanco						PREHEATING SYSTEM
CHK'D	Heinrich Thomas						
APPV'D							
MFG							
Q.A				MATERIAL:			DWG NO. 07 / A3
				WEIGHT:			SCALE:1:1 / SHEET 1 OF 1

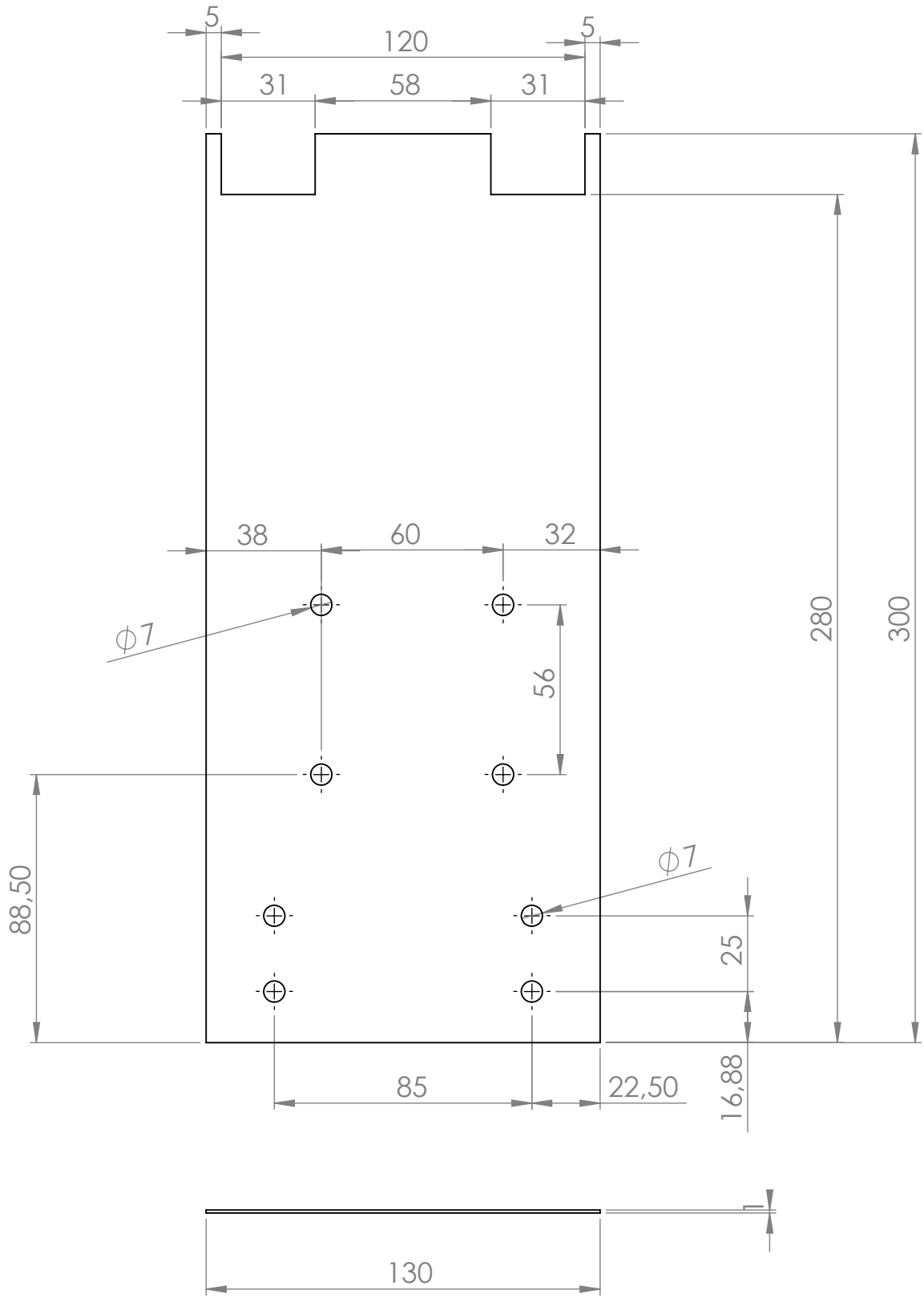

-UNLESS OTHERWISE SPECIFIED: DIMENSIONS ARE IN MILLIMETERS -SURFACE FINISH: - -General tolerance for linear and angular dimensions without individual tolerance indication ISO 2768-m	FINISH: -	DEBUR AND BREAK SHARP EDGES

	NAME	SIGNATURE	DATE
DRAWN	J. Molina Blanco		
CHK'D	Heinrich Thomas		
APPV'D			
MFG			
Q.A			

		St 37	
		WEIGHT:	

DO NOT SCALE DRAWING | REVISION

LABORATORY OF COMPOSITE MATERIALS AND ADAPTIVE STRUCTURES

ETH Zürich

TITLE:

PREHEATING SUPPORT 1

DWG NO. 120

A4

SCALE:1:5 | SHEET 1 OF 1

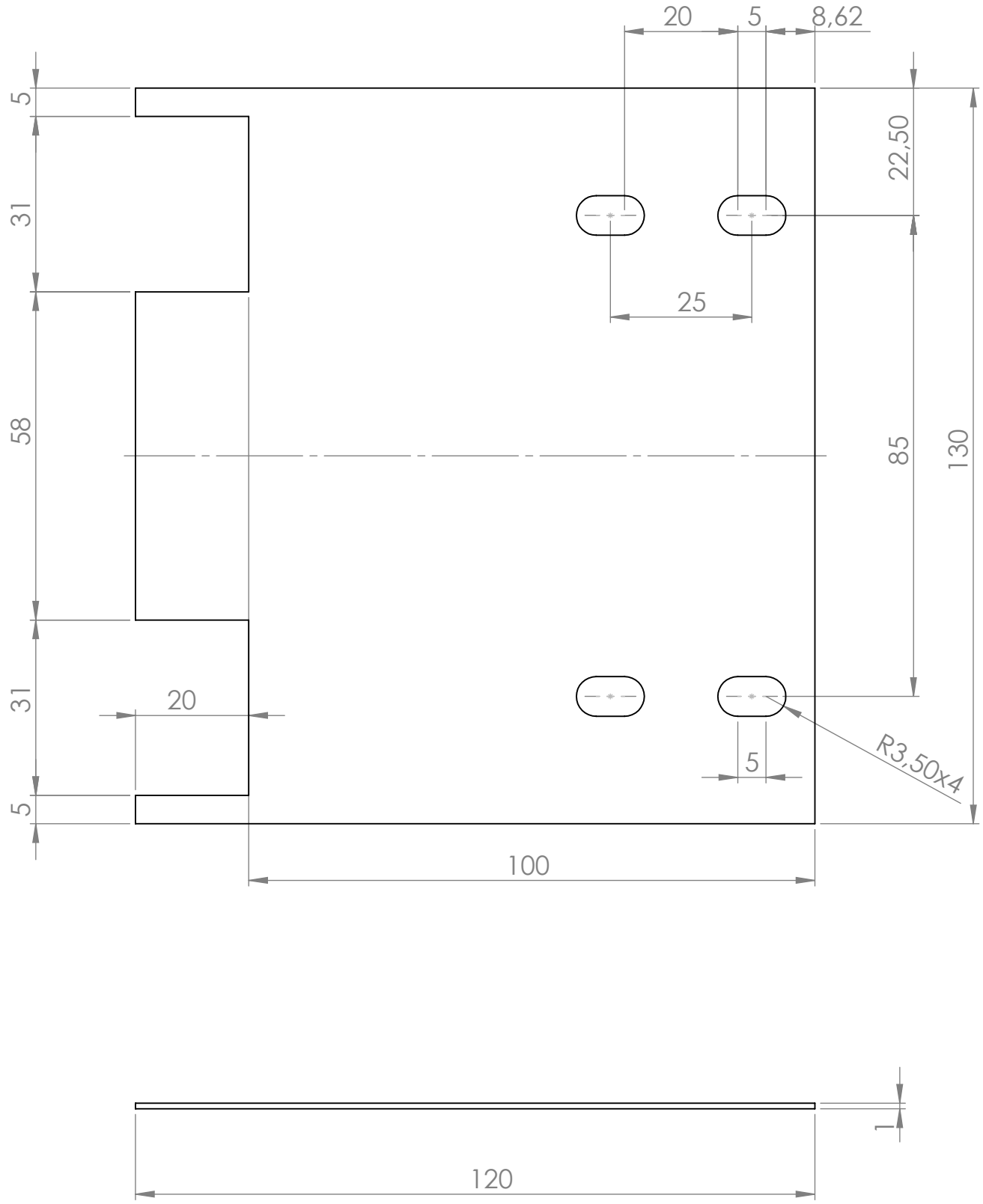

-UNLESS OTHERWISE SPECIFIED: DIMENSIONS ARE IN MILLIMETERS -SURFACE FINISH: - -General tolerance for linear and angular dimensions without individual tolerance indication ISO 2768-m	FINISH: -	DEBUR AND BREAK SHARP EDGES	DO NOT SCALE DRAWING	REVISION
			LABORATORY OF COMPOSITE MATERIALS AND ADAPTIVE STRUCTURES ETH Zürich	

	NAME	SIGNATURE	DATE	
DRAWN	J. Molina Blanco			
CHK'D	Heinrich Thomas			
APPV'D				
MFG				
Q.A				

TITLE: PREHEATING SUPPORT 2			
St 37	DWG NO. 121		A4
WEIGHT:	SCALE: 1:1	SHEET 1 OF 1	

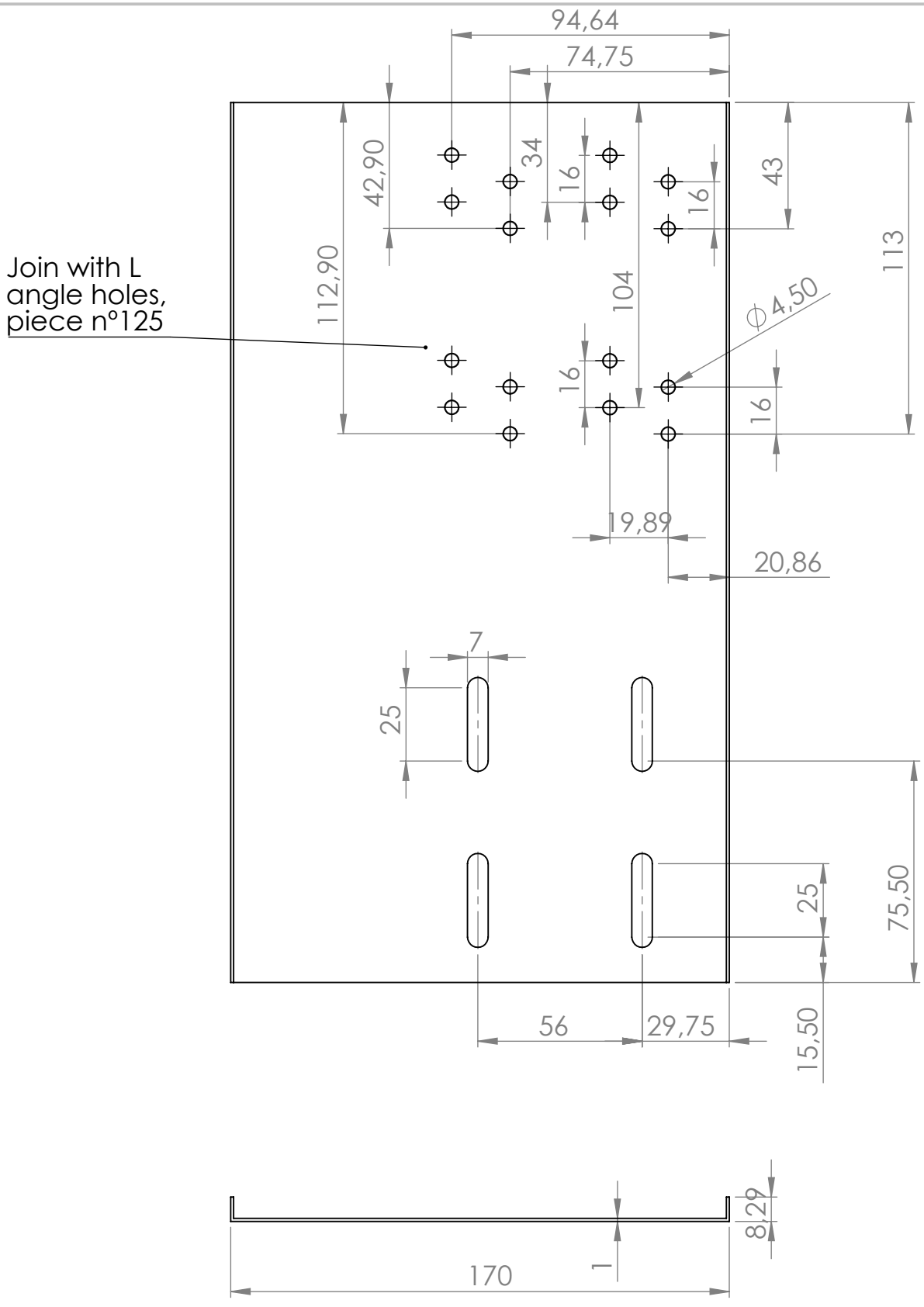

-UNLESS OTHERWISE SPECIFIED: DIMENSIONS ARE IN MILLIMETERS -SURFACE FINISH: - -General tolerance for linear and angular dimensions without individual tolerance indication ISO 2768-m	FINISH: -	DEBUR AND BREAK SHARP EDGES	DO NOT SCALE DRAWING	REVISION
			LABORATORY OF COMPOSITE MATERIALS AND ADAPTIVE STRUCTURES — ETH Zürich	
	NAME	SIGNATURE	DATE	TITLE: PREHEATING SUPPORT 3
DRAWN	J. Molina Blanco			
CHK'D	Heinrich Thomas			
APPV'D				
MFG				
Q.A				
			St 37	DWG NO. 122 — A4
			WEIGHT:	SCALE: 1:2 — SHEET 1 OF 1

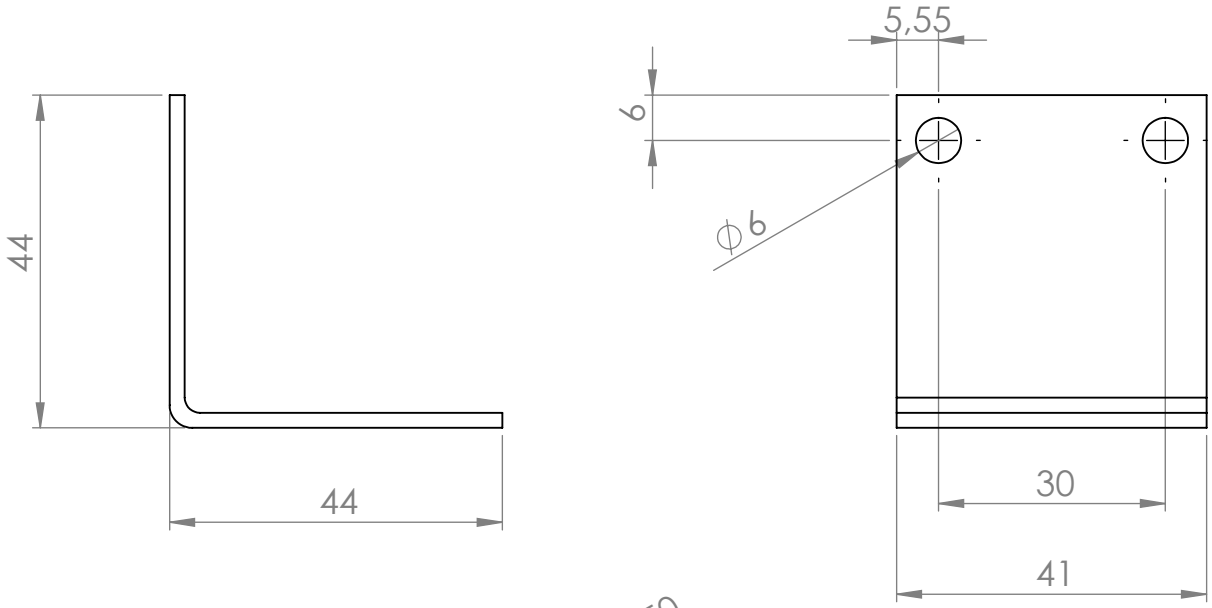

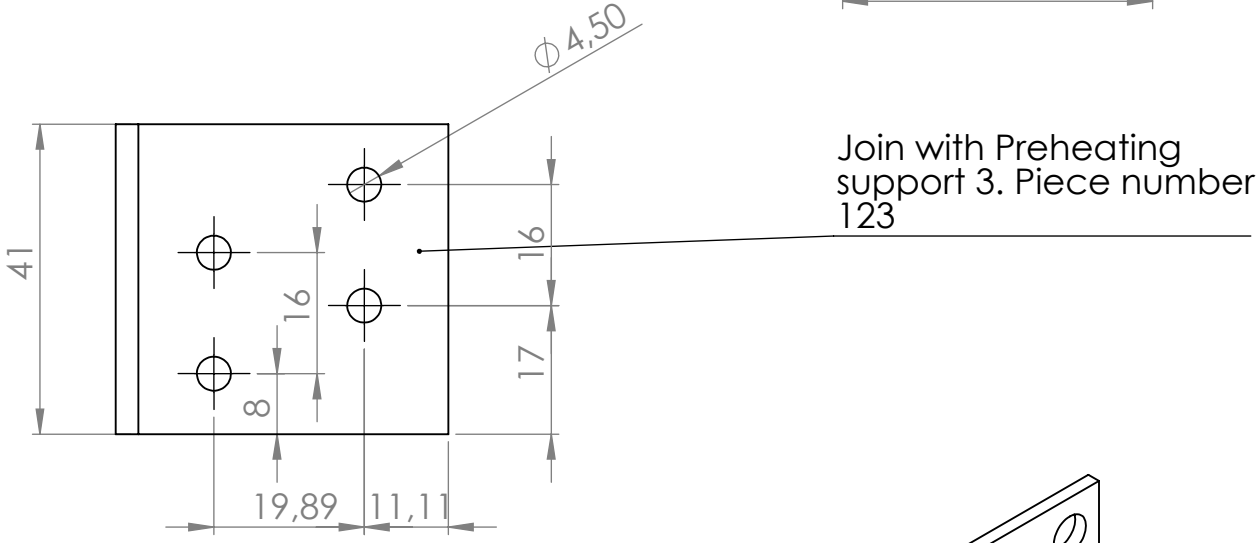

Join with Preheating support 3. Piece number 123

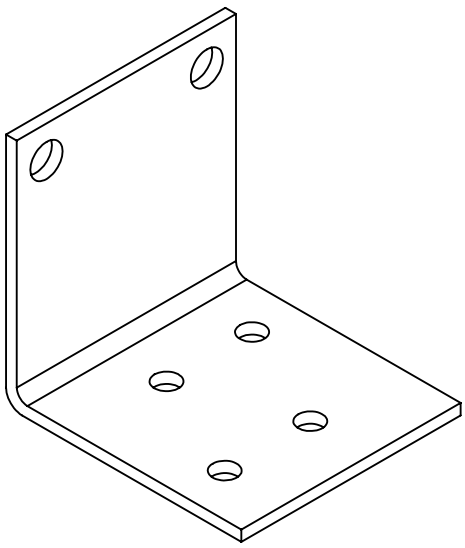

-UNLESS OTHERWISE SPECIFIED: DIMENSIONS ARE IN MILLIMETERS -SURFACE FINISH: - -General tolerance for linear and angular dimensions without individual tolerance indication ISO 2768-m	FINISH: -	DEBUR AND BREAK SHARP EDGES	DO NOT SCALE DRAWING	REVISION
			LABORATORY OF COMPOSITE MATERIALS AND ADAPTIVE STRUCTURES	ETH Zürich
			TITLE: L ANGLE	

	NAME	SIGNATURE	DATE	
DRAWN	J. Molina Blanco			
CHK'D	Heinrich Thomas			
APPV'D				
MFG				
Q.A				
			WEIGHT:	

DWG NO. 125	A4	
SCALE:1:1	SHEET 1 OF 1	

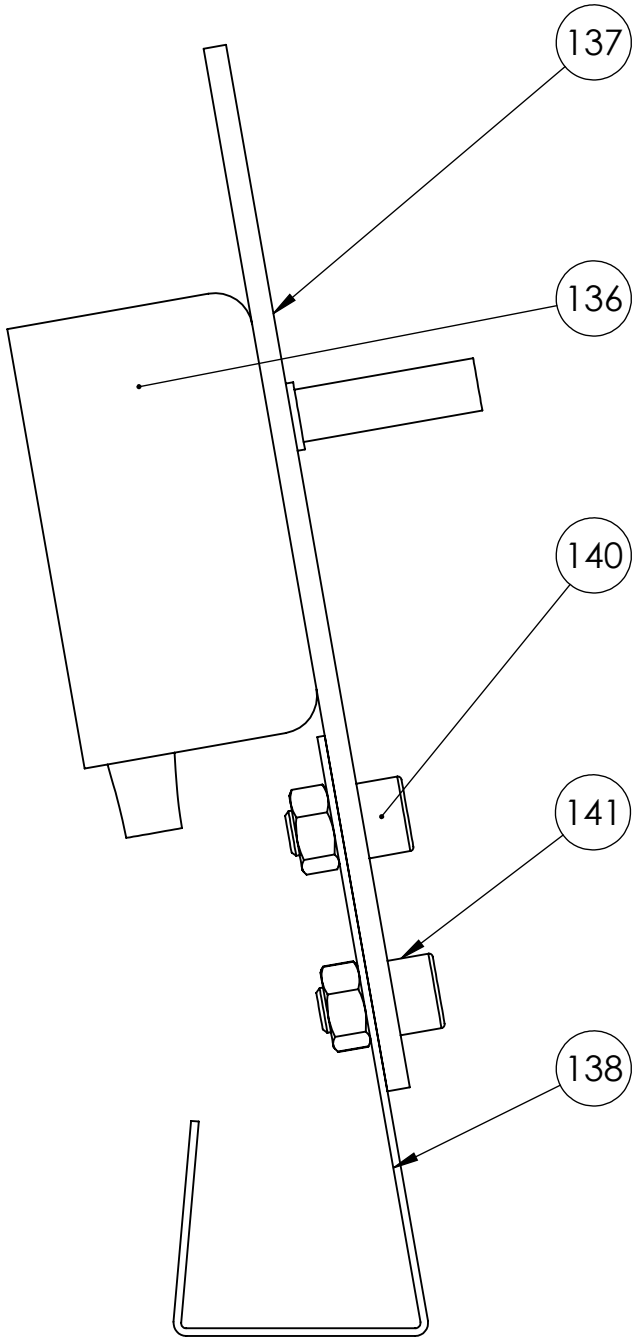

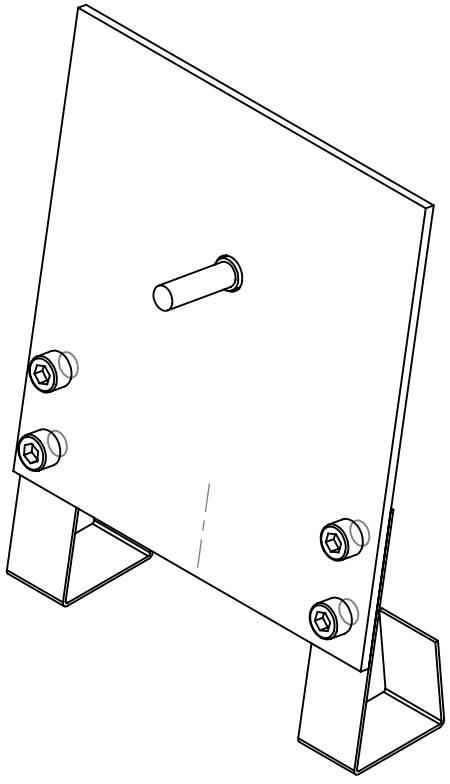

-UNLESS OTHERWISE SPECIFIED: DIMENSIONS ARE IN MILLIMETERS -SURFACE FINISH: - -General tolerance for linear and angular dimensions without individual tolerance indication ISO 2768-m	FINISH: -	DEBUR AND BREAK SHARP EDGES

	NAME	SIGNATURE	DATE
DRAWN	J. Molina Blanco		
CHK'D	Heinrich Thomas		
APPV'D			
MFG			
Q.A			

WEIGHT:

DO NOT SCALE DRAWING | REVISION

LABORATORY OF COMPOSITE MATERIALS AND ADAPTIVE STRUCTURES

ETH Zürich

TITLE:

POWER CONTROL

DWG NO. **08**

A4

SCALE:1:2 | SHEET 1 OF 1

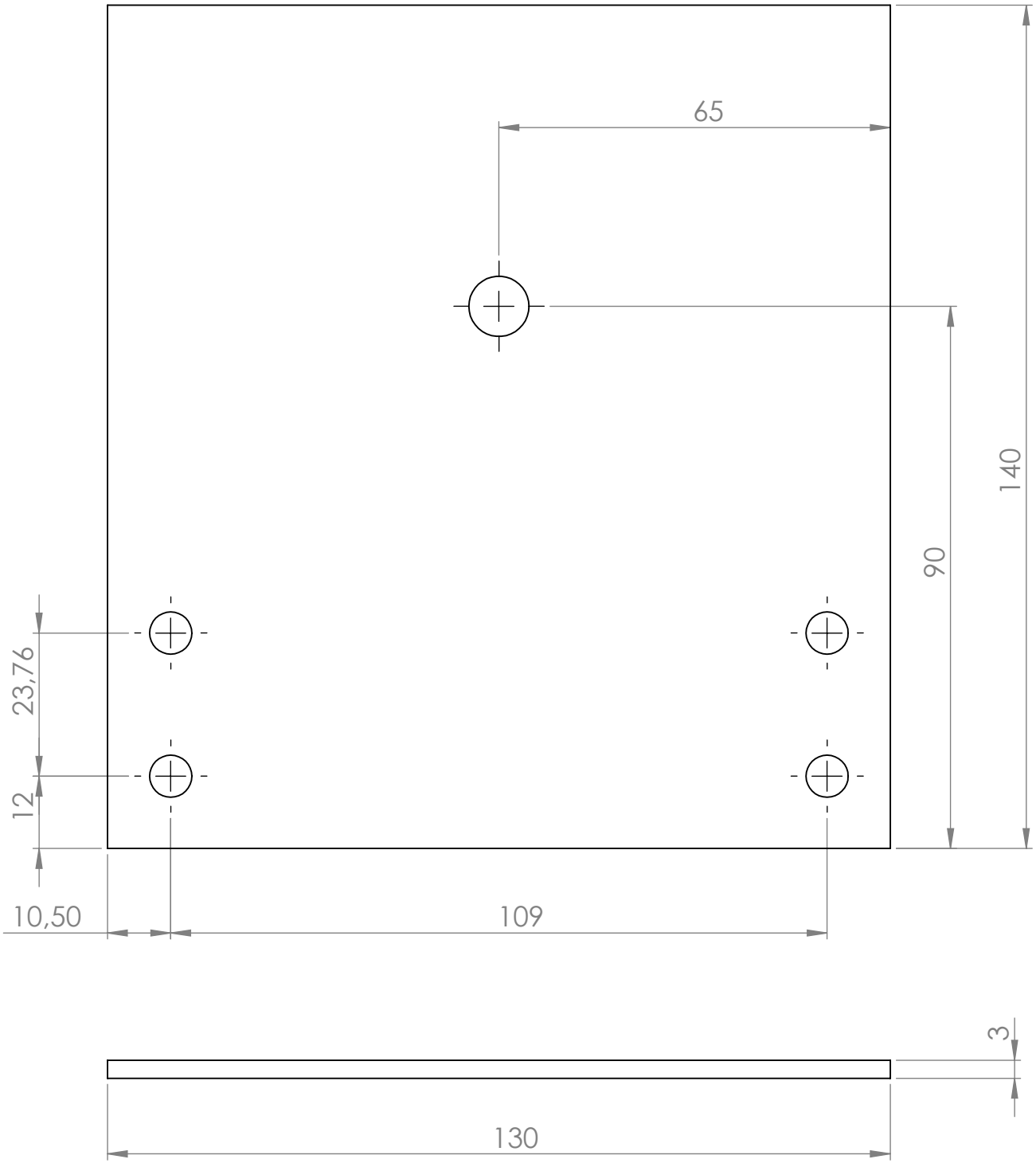

-UNLESS OTHERWISE SPECIFIED: DIMENSIONS ARE IN MILLIMETERS -SURFACE FINISH: - -General tolerance for linear and angular dimensions without individual tolerance indication ISO 2768-m	FINISH: -	DEBUR AND BREAK SHARP EDGES

	NAME	SIGNATURE	DATE
DRAWN	J. Molina Blanco		
CHK'D	Heinrich Thomas		
APPV'D			
MFG			
Q.A			

Al		DO NOT SCALE DRAWING	REVISION
WEIGHT:		SCALE: 1:1	SHEET 1 OF 1

LABORATORY OF COMPOSITE MATERIALS AND ADAPTIVE STRUCTURES

ETH Zürich

TITLE:

HEATSINK

DWG NO. 137

A4

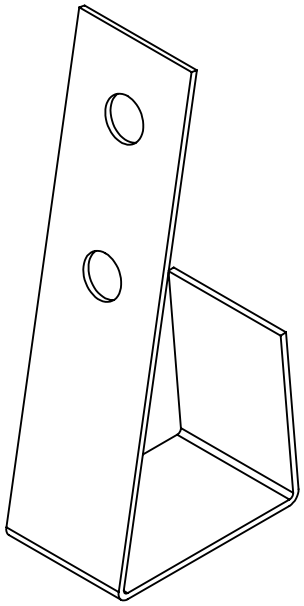

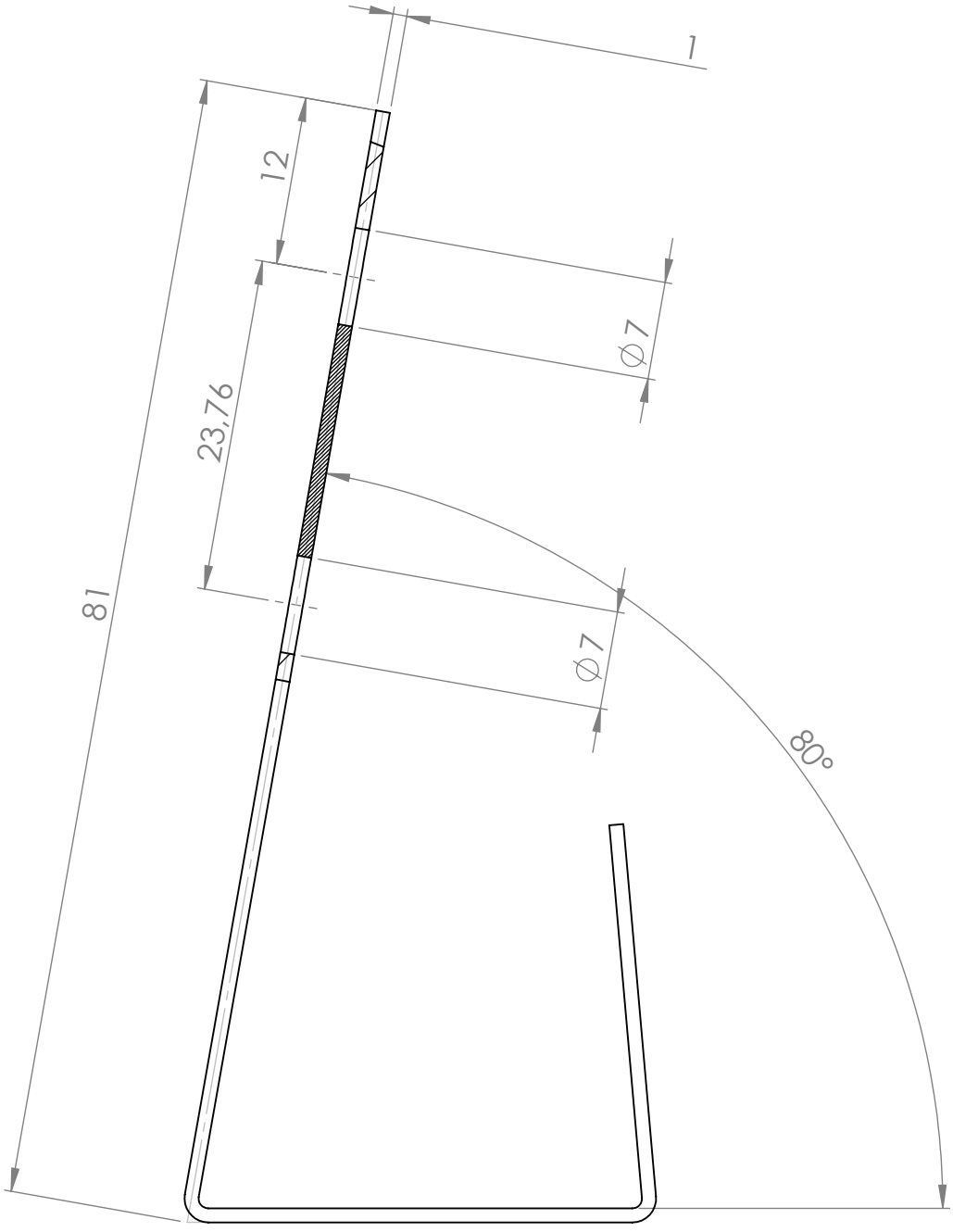

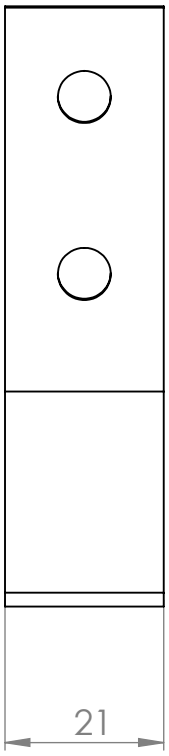

-UNLESS OTHERWISE SPECIFIED: DIMENSIONS ARE IN MILLIMETERS -SURFACE FINISH: - -General tolerance for linear and angular dimensions without individual tolerance indication ISO 2768-m	FINISH: -	DEBUR AND BREAK SHARP EDGES	DO NOT SCALE DRAWING	REVISION
			LABORATORY OF COMPOSITE MATERIALS AND ADAPTIVE STRUCTURES	ETH Zürich
	NAME	SIGNATURE	DATE	
DRAWN	J. Molina Blanco			
CHK'D	Heinrich Thomas			
APPV'D				
MFG			TITLE: VR LEG	
Q.A				
			DWG NO. 138	A4
		WEIGHT: Al	SCALE:1:1	SHEET 1 OF 1

APPENDIX B.

Calibration procedure

B.1 Calibration methods

This section explain the calculations used to calibrate the incorporate machine elements on the CMAS Lab filament winding process.

This is an explanation of the procedure for a static calibration. The calibration procedure is divided in two test in order to obtain all the necessary errors. A random test and a sequential test [12, 32, 35].

B.1.1 Random test

In the random test a random order is applied on the input values over the desired input range to ensure that each application of the input value is independent than the next application. Using the random test the next errors are detected:

- Sensitivity error: Dispersion that presents the curve slope adjusted to the data set.
- Zero shift error: Dispersion presented by the intersection of curve adjusted with the data set and the output axis.
  Both errors are calculated with a confidence interval of 95%.
  Figure APPENDIX B.1 shows a graphic representation of both errors.

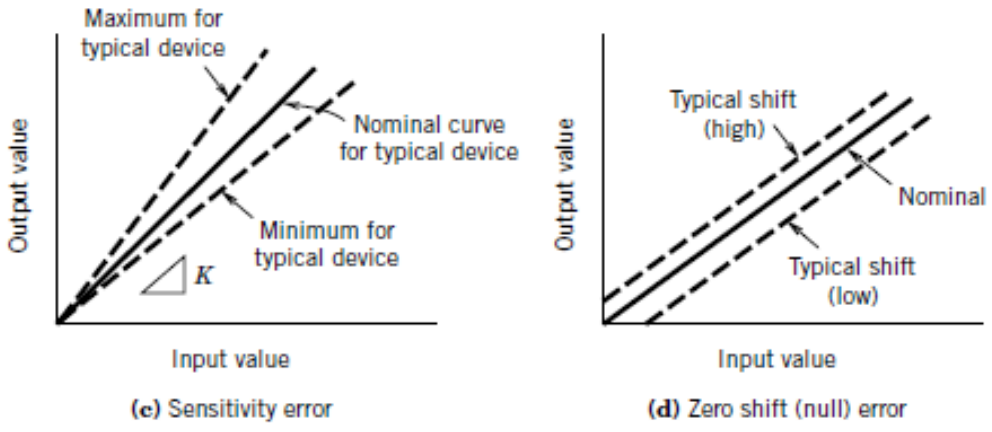

Figure APPENDIX B.1. Graphic representation of sensibility and zero error for linear regression. Image property of Theory and Design for Mechanical measurements. John Wiley & Sons, Inc.

The error are calculated as follow:

Linear adjusted curve $$y = a_0 + a_1 x$$ (APPENDIX B.1)

$$U_k = t_v S_{a1} \quad \text{and} \quad \text{v=N-2}$$ (APPENDIX B.1)

$$U_0 = t_v S_{a0} \quad \text{and} \quad \text{v=N-2}$$ (APPENDIX B.2)

$$S_{a1} = S_{yx}\sqrt{\frac{N}{N\sum x_i{}^2 - (\sum x_i)^2}}$$ (APPENDIX B.3)

$$S_{a0} = S_{yx}\sqrt{\frac{\sum x_i{}^2}{N\sum x_i{}^2 - (\sum x_i)^2}}$$ (APPENDIX B.4)

$$S_{yx} = \sqrt{\frac{\sum y_i{}^2 - a_0\sum y_i + a_1\sum y_i x_i}{N-2}}$$ (APPENDIX B.5)

- Repeatability error: Is the dispersion presented by the measures of a same input value N times. This dispersion has been determine for one point and accepted as the maxim repeatability error. Figure APPENDIX B.2 show a graphic representation of the error.

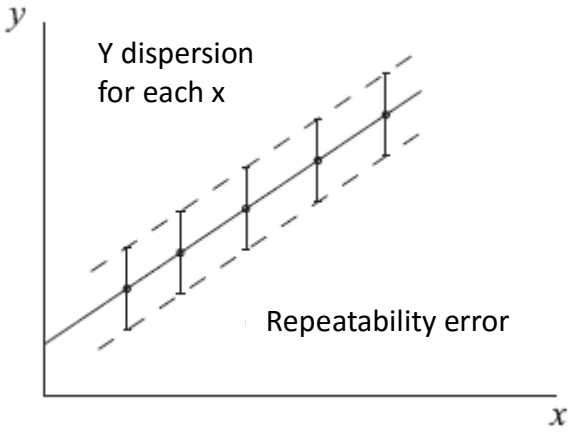

Figure APPENDIX B.2. Graphic representation of repeatability error for linear regression. Image property of UPC, Universitat Politècnica de Catalunya

The repeatability error is estimated with a confidence interval of 95% as follow:

$$U_r = t_v * Ssamples \quad \text{and} \quad \text{v=N-1}$$ (APPENDIX B.6)

B.1.2 Sequential test

During the sequential test a sequential variation is applied in the desired input range. The variation is applied by increasing the input value (upscale) or decreasing the input value (downscale). The sequential test is reliable and useful to identify and quantify the linearity and hysteresis errors.

- Linearity error: Refers to the maximum difference obtained between the data measured and the imaginary line created with the maximum and minimum input values of the desired work range.
- Hysteresis error: Refers to the difference between the data measurements upscale and the data measurements downscale. Are quantified by:

$$U_L = Max(|y_i - (a_0 + a_1 x_i|) \quad \text{(APPENDIX B.7)}$$

$$U_h = Max(|y_{upscale} - y_{downscale}|) \quad \text{(APPENDIX B.8)}$$

Figure APPENDIX B.3 show a graphic representation of both errors.

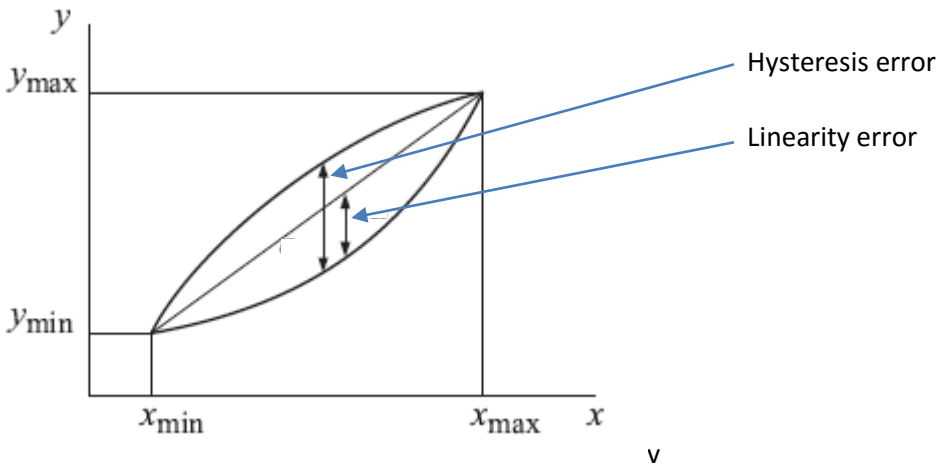

v

Figure APPENDIX B.3. Graphic representation of the linearity and hysteresis errors

B.1.3 APPENDIX B.3. Overall instrument error. Uncertainty

Overall instrument error is made by the combination of all the known errors. It is also called uncertainty of the instrument

$$U_G = \sqrt{\sum U_i^2} \quad \text{(APPENDIX B.9)}$$

The errors are combined quadratically because they are expressed as confidence interval whose are represented by the standard deviation.

APPENDIX B. Fiber Tension System conversion table.

Pressure [bar]	Fiber tension [N]	Error [N]	Pressure [bar]	Fiber tension [N]	Error [N]
1,0	1,94	0,73	3,3	17,78	0,76
1,1	2,48	0,73	3,4	18,32	0,76
1,2	3,02	0,73	3,5	18,86	0,77
1,3	3,56	0,73	3,6	19,39	0,77
1,4	4,10	0,73	3,7	19,93	0,77
1,5	4,64	0,74	3,8	20,47	0,77
1,6	5,18	0,74	3,9	21,01	0,78
1,7	5,71	0,74	4,0	21,55	0,78
1,8	6,25	0,74	4,1	22,09	0,78
1,9	6,79	0,74	4,2	22,63	0,78
2,0	7,33	0,74	4,3	23,17	0,79
2,1	7,87	0,74	4,4	23,70	0,79
2,2	8,41	0,74	4,5	24,24	0,79
2,3	8,95	0,74	4,6	24,78	0,79
2,4	9,49	0,75	4,7	25,32	0,80
2,5	10,02	0,75	4,8	25,86	0,80
2,6	10,56	0,75	4,9	26,40	0,80
2,7	11,10	0,75	5,0	26,94	0,80
2,8	11,64	0,75	5,1	27,47	0,81
2,9	12,18	0,75	5,2	28,01	0,81
3,0	12,72	0,76	5,3	28,55	0,81
3,1	13,26	0,76	5,4	29,09	0,82
3,2	13,80	0,76	5,5	29,63	0,82

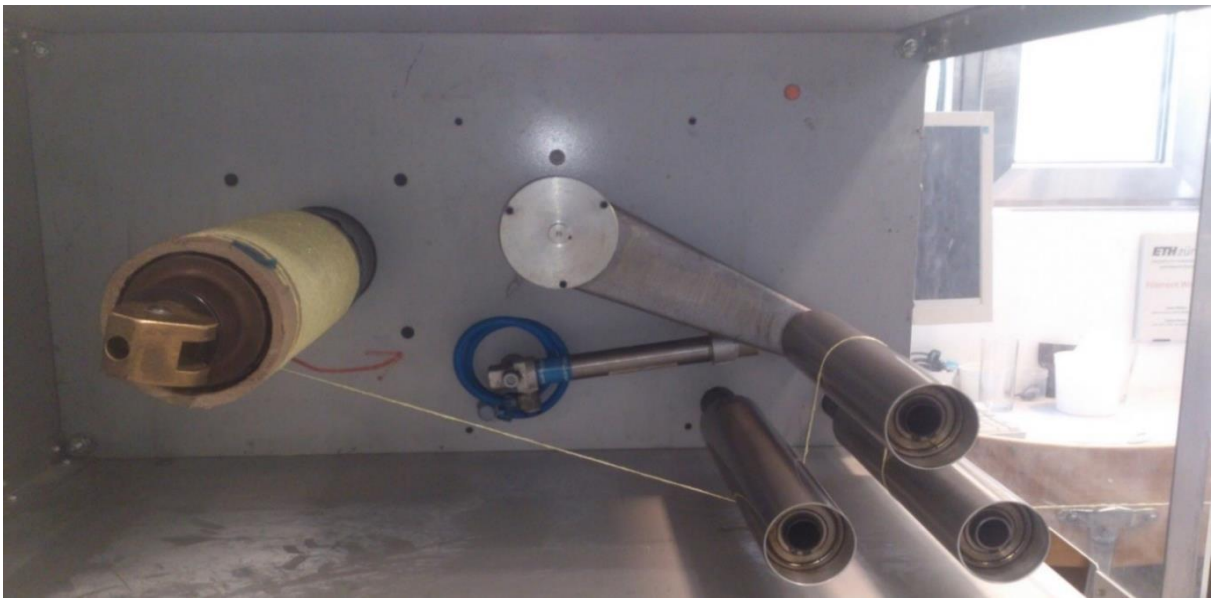

APPENDIX B. Compaction force - spring length conversion table

l[mm]	F[N]	Linear pressure [N/mm]	l[mm]	F[N]	Linear pressure [N/mm]	l[mm]	F[N]	Linear pressure [N/mm]	l[mm]	F[N]	Linear pressure [N/mm]
135	0	0,00	109	99,58	4,15	83	199,16	8,30	57	298,74	12,45
134	3,83	0,16	108	103,41	4,31	82	202,99	8,46	56	302,57	12,61
133	7,66	0,32	107	107,24	4,47	81	206,82	8,62	55	306,4	12,77
132	11,49	0,48	106	111,07	4,63	80	210,65	8,78	54	310,23	12,93
131	15,32	0,64	105	114,9	4,79	79	214,48	8,94	53	314,06	13,09
130	19,15	0,80	104	118,73	4,95	78	218,31	9,10	52	317,89	13,25
129	22,98	0,96	103	122,56	5,11	77	222,14	9,26	51	321,72	13,41
128	26,81	1,12	102	126,39	5,27	76	225,97	9,42	50	325,55	13,56
127	30,64	1,28	101	130,22	5,43	75	229,8	9,58	49	329,38	13,72
126	34,47	1,44	100	134,05	5,59	74	233,63	9,73	48	333,21	13,88
125	38,3	1,60	99	137,88	5,75	73	237,46	9,89	47	337,04	14,04
124	42,13	1,76	98	141,71	5,90	72	241,29	10,05	46	340,87	14,20
123	45,96	1,92	97	145,54	6,06	71	245,12	10,21	45	344,7	14,36
122	49,79	2,07	96	149,37	6,22	70	248,95	10,37	44	348,53	14,52
121	53,62	2,23	95	153,2	6,38	69	252,78	10,53	43	352,36	14,68
120	57,45	2,39	94	157,03	6,54	68	256,61	10,69	42	356,19	14,84
119	61,28	2,55	93	160,86	6,70	67	260,44	10,85	41	360,02	15,00
118	65,11	2,71	92	164,69	6,86	66	264,27	11,01	40	363,85	15,16
117	68,94	2,87	91	168,52	7,02	65	268,1	11,17			
116	72,77	3,03	90	172,35	7,18	64	271,93	11,33			
115	76,6	3,19	89	176,18	7,34	63	275,76	11,49			
114	80,43	3,35	88	180,01	7,50	62	279,59	11,65			
113	84,26	3,51	87	183,84	7,66	61	283,42	11,81			
112	88,09	3,67	86	187,67	7,82	60	287,25	11,97			
111	91,92	3,83	85	191,5	7,98	59	291,08	12,13			
110	95,75	3,99	84	195,33	8,14	58	294,91	12,29			

l: Spring length, To the measured value, add 2 mm (depth not visible of the spring support).

APPENDIX C.

Material characterization data

This section includes the material characterization data of the not selected materials. The analyse method is exactly equal to the methods described in 'Chapter 4. Material characterization' therefore they are not explained in this section. The calculation of the volume fiber % by analysing the polished cross section pictures of the yarns is not carried out for the next 3 materials.

Table APPENDIX C.1. shows the characterized materials.

Table APPENDIX C.1. Non selected characterized intermediate materials

Specimen	Fiber type	Thermoplastic Fiber	Reinforcing fiber
1	Powder impregnated fiber	Unknown	Glass fiber
3	Commingled yarn	Polyamide 6	Carbon Fiber
4	Commingled yarn	Polyether ether ketone	Carbon Fiber

C.1 Material data summary table

Table APPENDIX C.2 summarize the material characterization magnitudes.

Table APPENDIX C.2. Summary material characterized properties table

Sample	Material	Yarn type	Theo. Density [g/cm³]		Fiber weight % [-]	Fiber volume % [-]	Fiber density [g/cm³]
			Matrix	Reinforcement			
1	GF-Unknown	Powder impregnated	-	2,49	65,67%	-	-
2	Twaron-PA6	Commingled yarn	1,12	1,44	66,43%	60,83%	1,31
3	CF-PA6	Commingled yarn	1,12	1,79	61,87%	50,38%	1,46
4	CF-PeeK	Commingled yarn	1,31	1,79	72,02%	65,32%	1,62

Sample	Fiber diameter [µm]				Melting matrix temperature [°C]	Temperature of degradation [°C]	
	Matrix		Reinforcement				
	AVG	Desv	AVG	Desv		Matrix	Reinforcement
1	10,91	+/-4,03	14,40	0,84	214	500	-
2	55,46	+/-5,42	14,73	1,20	220	320	500
3	22,43	+/-1,30	6,98	0,34	220	320	740
4	31,19	+/-3,22	7,07	0,53	342	545	700

C.2 Powder impregnated fiber. Unknown thermoplastic matrix-Glass fiber reinforcement

The first material analysed is a powder impregnated fiber manufactured in the university. There is no information about the materials that compose it. A sample of the fiber is analysed on the Scanning Electron Microscope in order to qualitative estimate the powder distribution and calculate the fiber and powder diameters.

Figure APPENDIX C.1 shows an image of the fiber obtained with the SEM microscope. The powder coated fiber present the thermoplastic material in two forms: powder form distributed between the glass reinforcing fibers and in a shell form covering the fibers, avoiding the powder to go out. The glass fiber and thermoplastic powder diameters are measured using an image processing and analyzing program. 10 measurements are taken of each material diameter.The reinforcing glass fiber diameter is 14.14 +/- 0.84 µm. The powder spheres diameter is 10.91 +/- 4.03 µm.

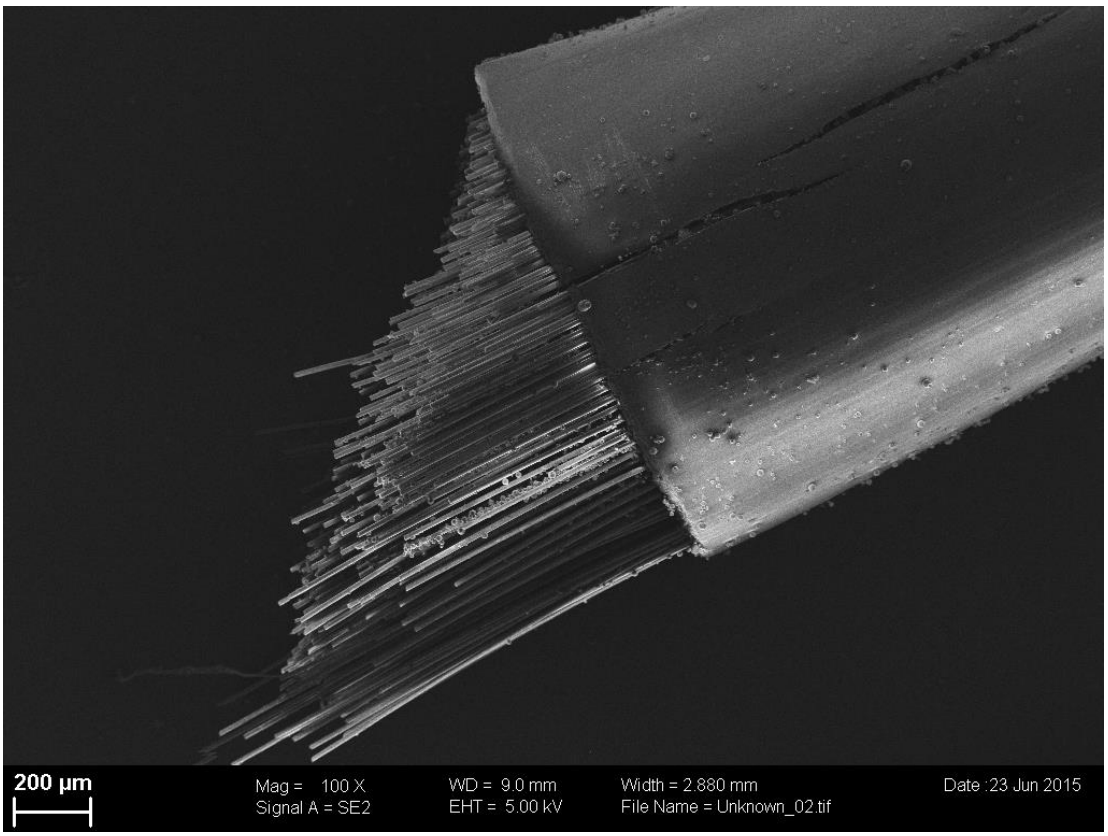

Figure APPENDIX C.1. Powder impregnated yarn, SEM image

The powder is properly distribute around the glass fibers in all the section as shown in Figure APPENDIX C.2. There is a noticeable variation in the thermoplastic powder spheres diameters.

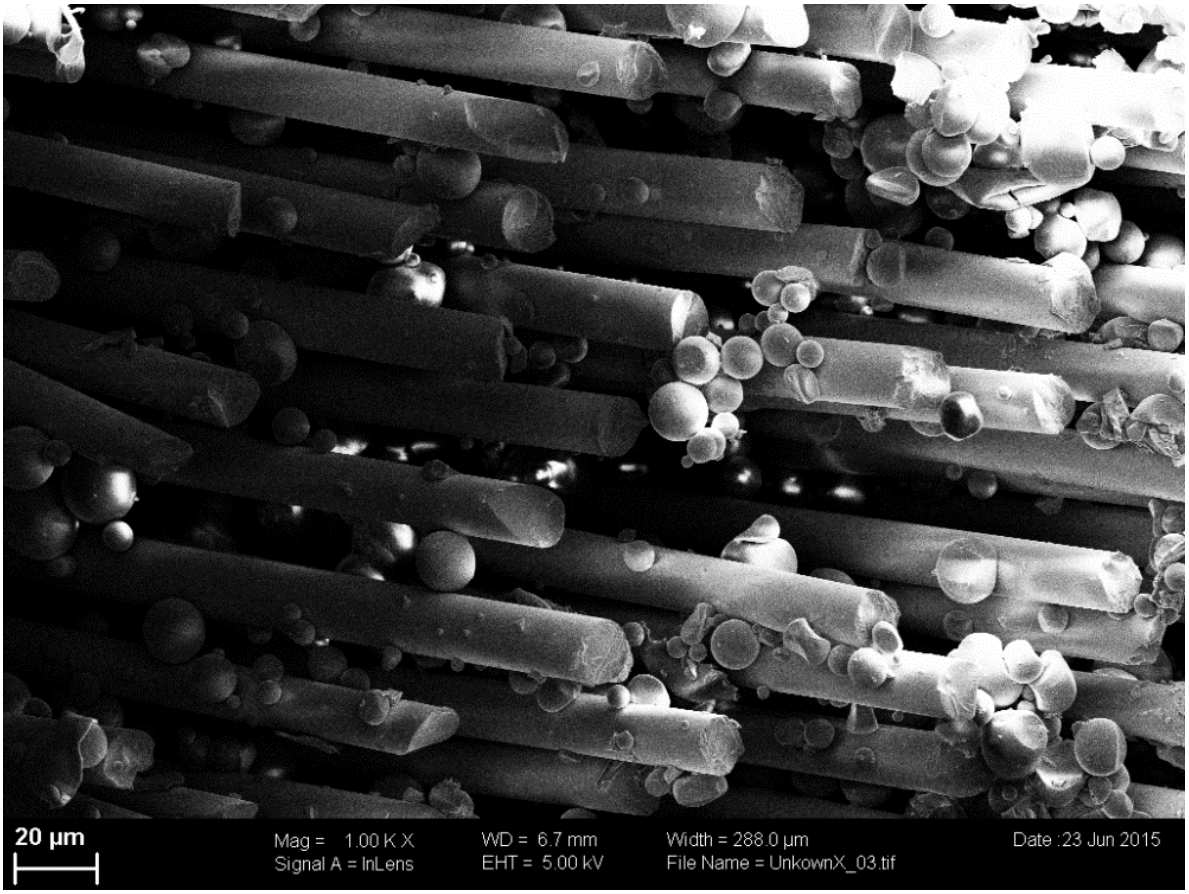

Figure APPENDIX C.2. Powder distribution in the powder impregnated yarn. SEM image

This powder impregnated fibers can present process problems due to the different amount of material in the powder and shell, what makes impossible the uniform heat distribution. Also the presence of the shell limits the fiber volume content making difficult to achieve high fiber volume levels. If the quantity of powder is reduced the distances necessary to achieve for the thermoplastic material during the impregnation will increase. As advantages, there is a large materials combinations available of that preform and as most of the thermoplastics are produced already in powder form the production of the intermediate materials is economical [49].

A thermogravimetric analyse is carried out to obtain the degradation thermoplastic temperature and fiber content of the yarn. Figure APPENDIX C.3 plots the starting temperature of the thermoplastic material approximately at 450ºC. The fiber weight % is approximately 66%.

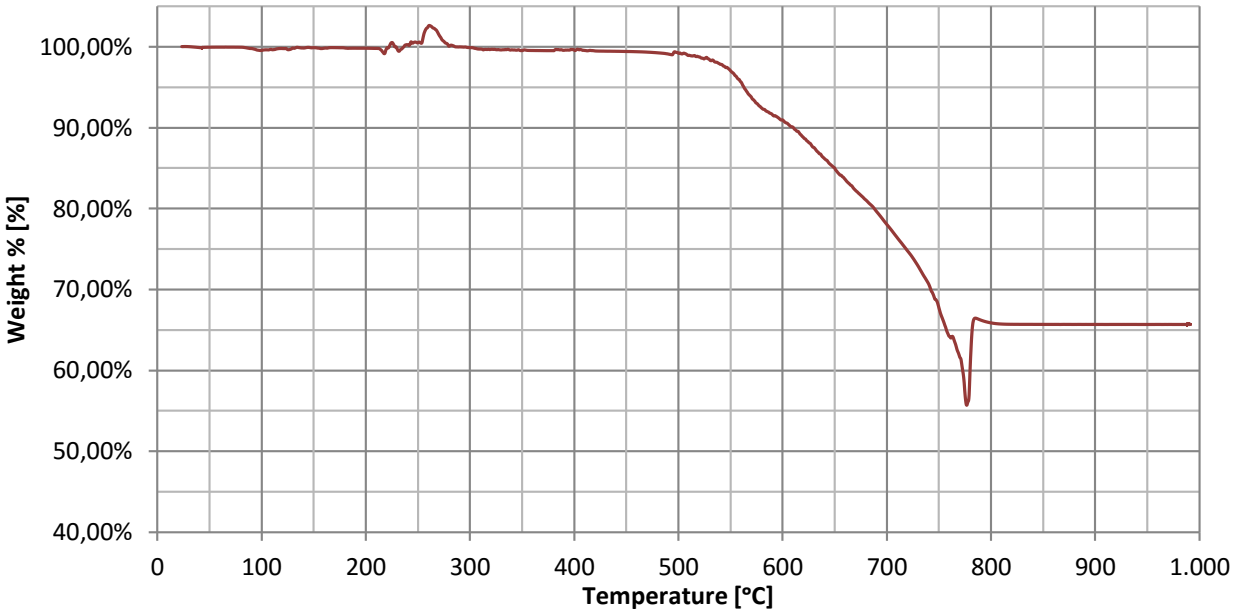

Figure APPENDIX C.3. Thermogravimetric analyze measurements of powder impregnated fiber-Glass reinforcement

In order to obtain the melting temperature of the thermoplastic material a sample is tested in a differential scanning calorimetry instrument. Figure APPENDIX C.4 show the DSC measurements of the CF-PA6 commingled. The melting temperature of the thermoplastic begins at approximately 205 degrees and ends at 215 degrees.

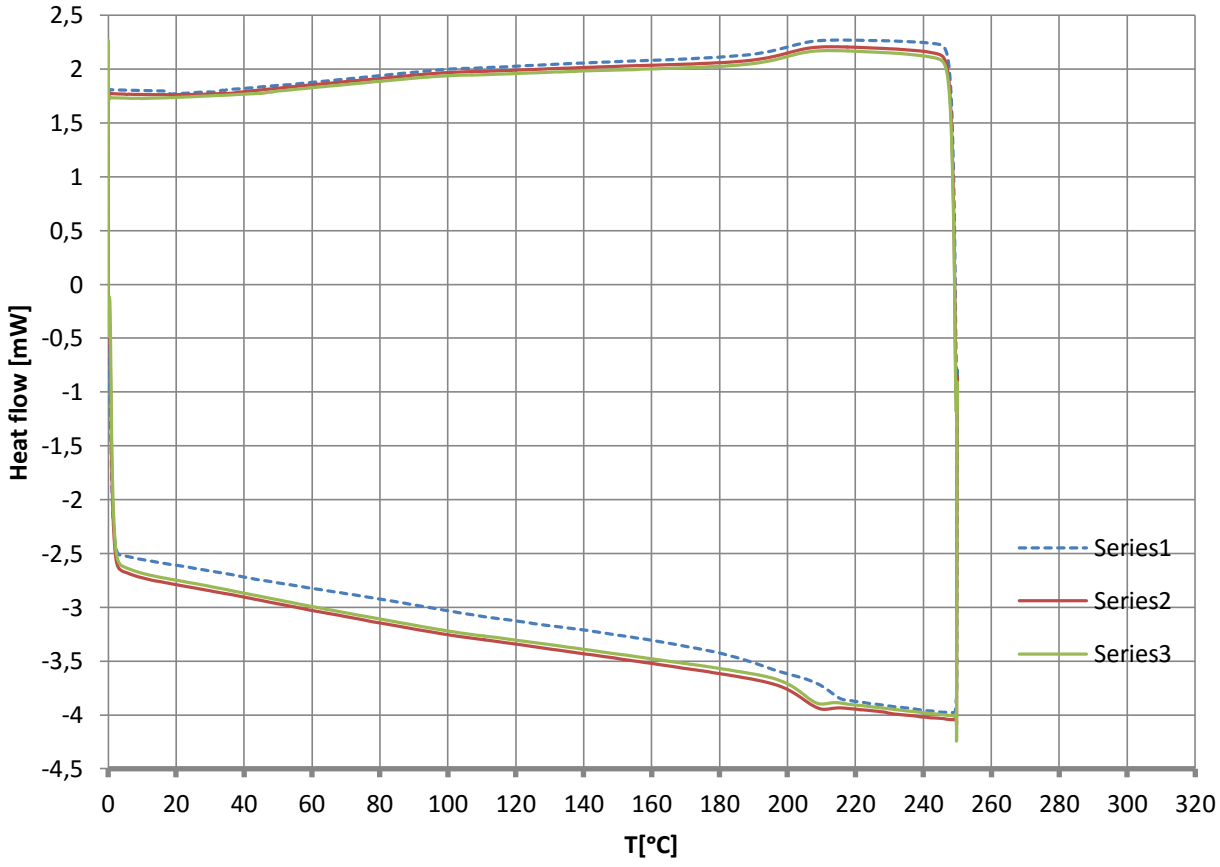

Figure APPENDIX C.4. Differential scanning calorimetry measurement of powder impregnated yarn-glass fiber reinforcement

C.3 Commingled yarn. Polyamide 6 matrix-Carbon reinforcing fiber

The third material analysed is a commingled yarn, Polyamide 6 with Carbon reinforcing fiber. Numerical results shown in Table APPENDIX C.2. This commingled yarn presents the PA6 in fiber form mingled between the reinforcing CF and in an external bundle tying the reinforcing fibers as shown in Figure APPENDIX C.5

Figure APPENDIX C.6 and Figure APPENDIX C.7 show the commingled yarn structure. The carbon fiber diameter is 7.07 +/- 0.53 µm and the PA6 fiber diameter is 22.43 +/- 1.3mm. The fiber volume content is approximately of 50.38%. The commingling degree of the yarn seems correct. The thermoplastic material is evenly distributed all over the yarn section.

Figure APPENDIX C.5. SEM image of CF-PA6 commingled yarn.

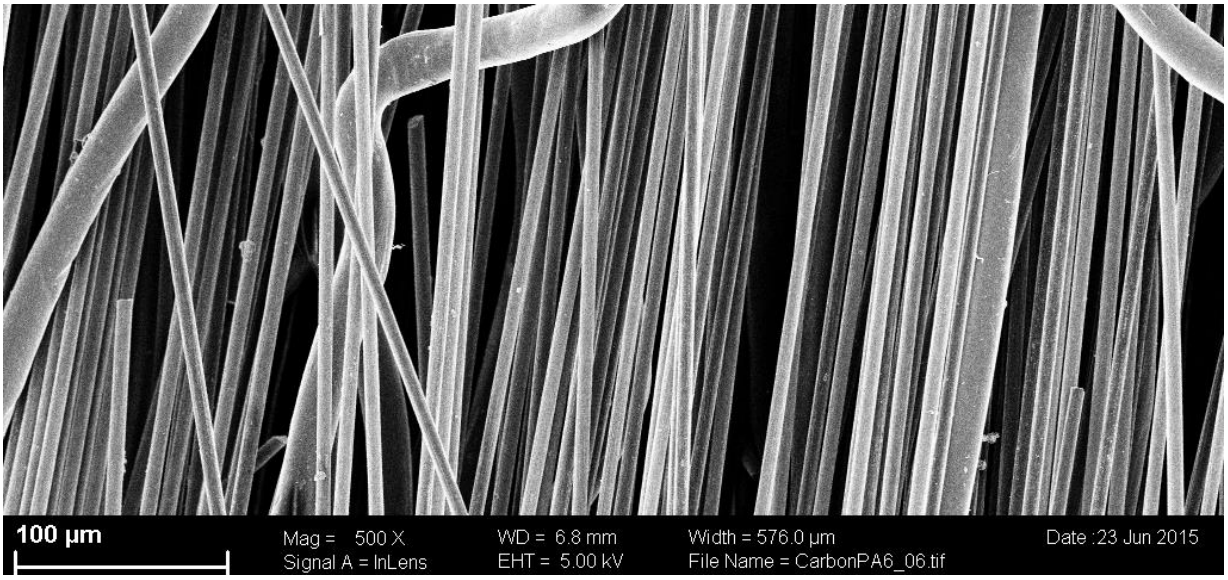

Figure APPENDIX C.6. PA6 carbon reinforcing fiber SEM image

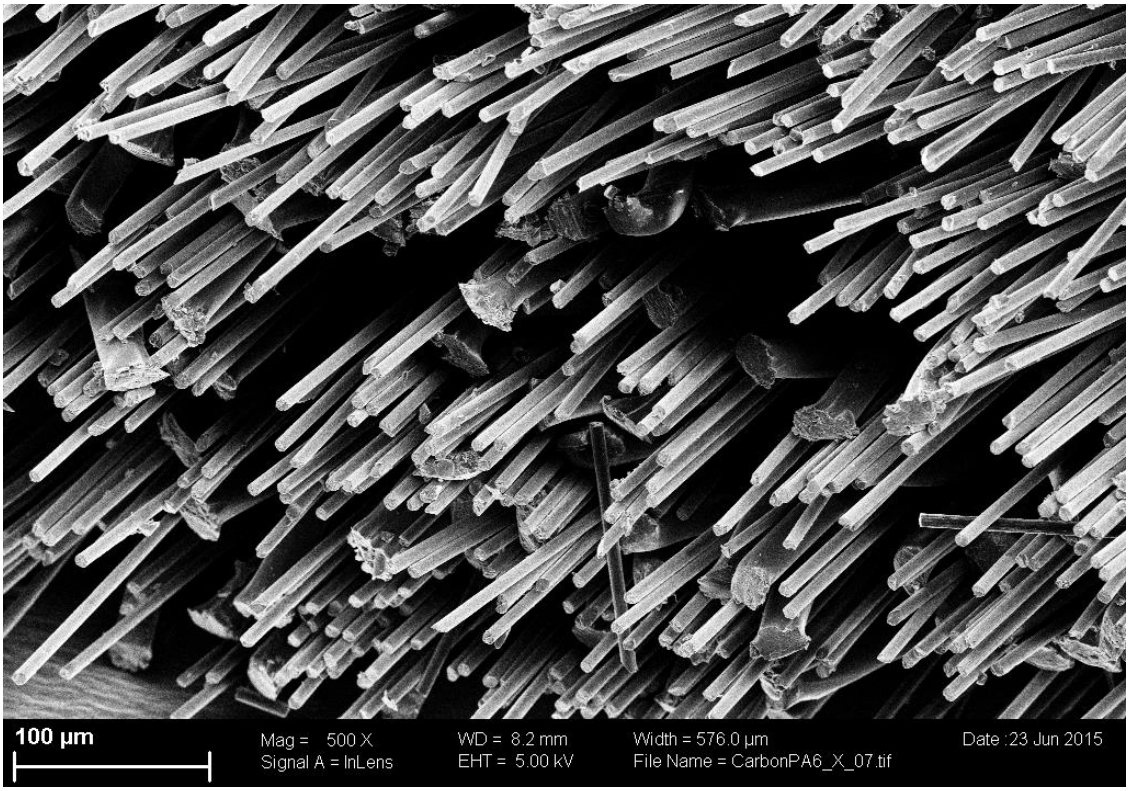

Figure APPENDIX C.7. PA6 carbon-reinforcing fiber SEM cross section.

Figure APPENDIX C.8 shows the TGA analyze of the material. The degradation of the thermoplastic material starts at approximately 300°C and the calculated fiber weight % is approximately 62%.

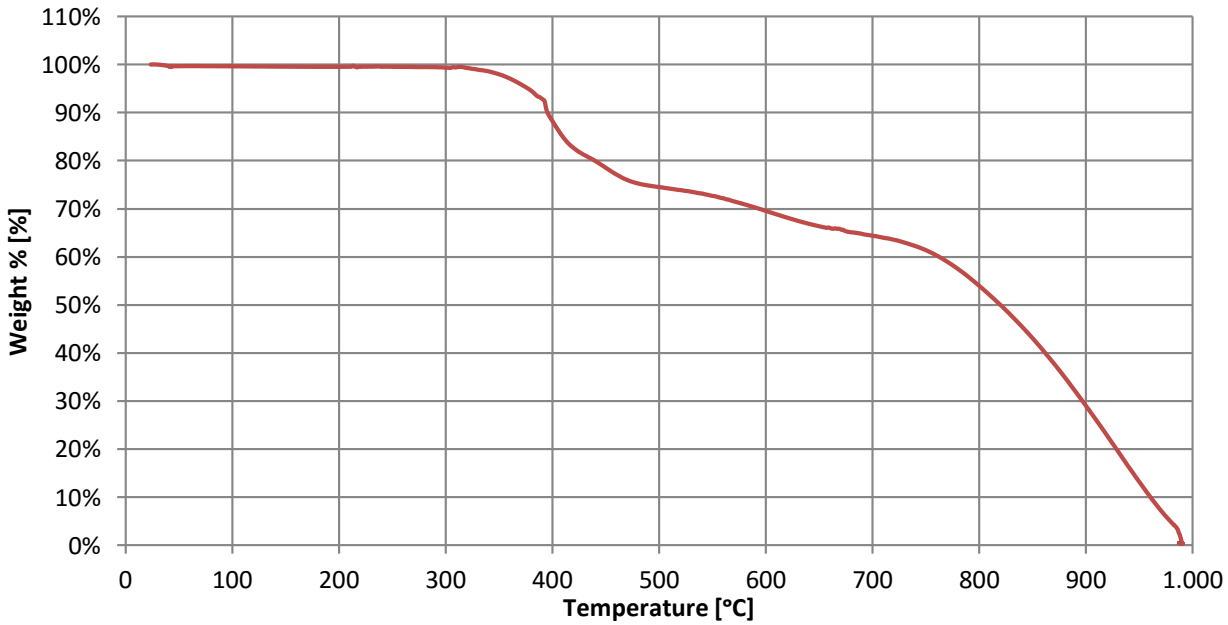

Figure APPENDIX C.8. Thermogravimetric analyze measurements CF-PA6 commingled yarn

Figure APPENDIX C.9 show the DSC measurements of the CF-PA6 commingled yarn. The thermoplastic material starts the melting transition at approximately 200°C and finish at 225°C. Results shown on Table APPENDIX C.2.

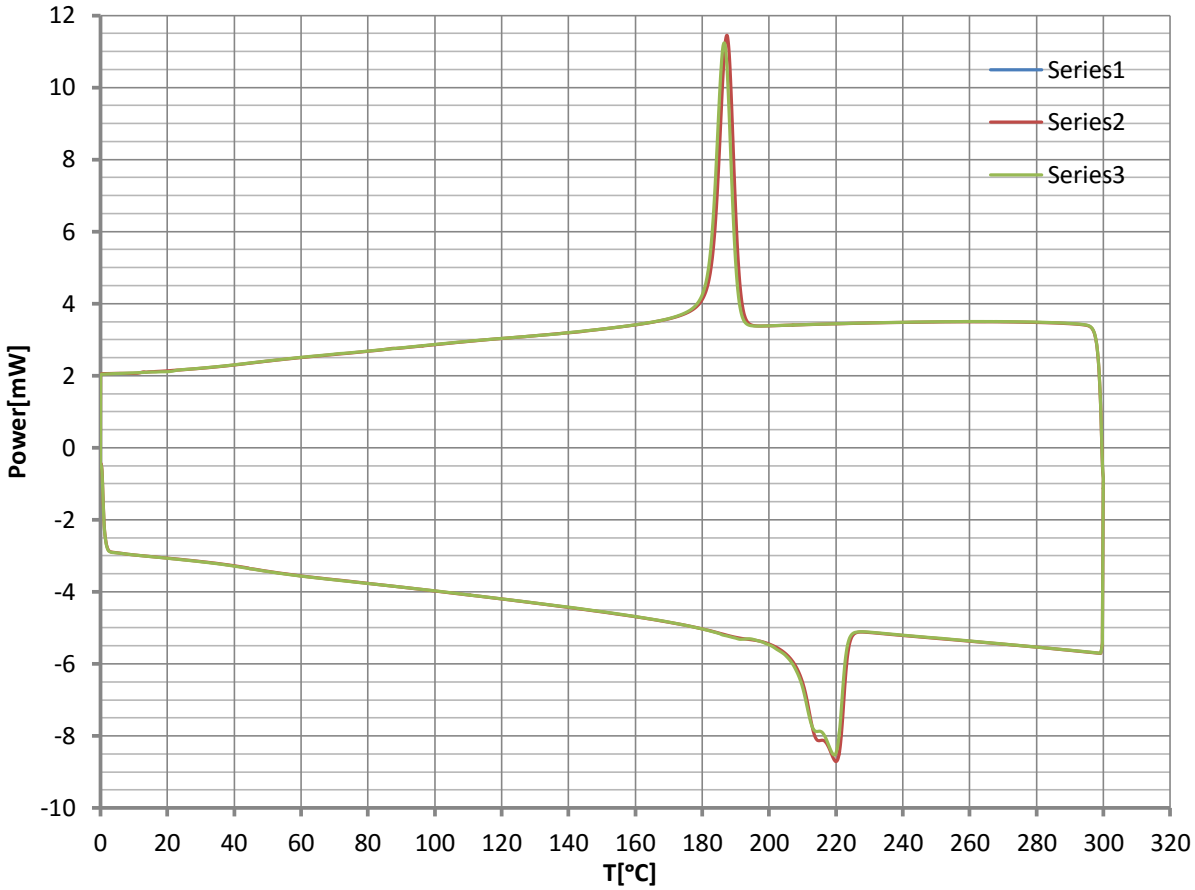

Figure APPENDIX C.9. Differential scanning calorimetry measurements. CF-PA6

C.4 Commingled yarn. Polyether ether ketone matrix-Carbon reinforcing fiber 7

The last analysed materials is a commingled yarn, PEEK thermoplastic matrix and Carbon reinforcing fiber. Figure APPENDIX.C.10, Figure APPENDIX C.11 and Figure APPENDIX C.12 show the commingled yarn structure. The commingling degree is not possible to properly qualify due to the fiber is smashed by the sample holder. But in the figures the thermoplastic material is concentrate on the left end of the yarn while the presence of it on the right is nearly inexistent. The carbon fiber diameter is 7.07 +/- 0.53 µm, and the PEEK dimeter is 31.19 +/-3.22µm. The fiber volume content of the commingled yarn is approximately 65.32%.

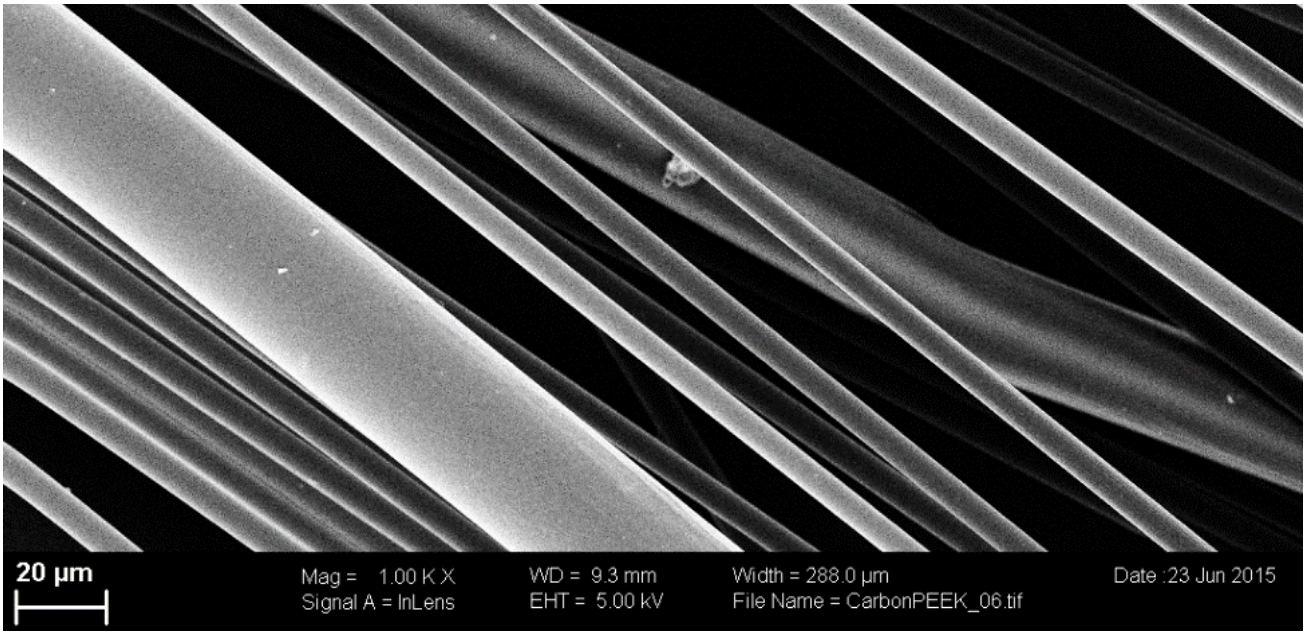

Figure APPENDIX.C.10.SEM image. PEEK-Carbon fiber commingled yarn

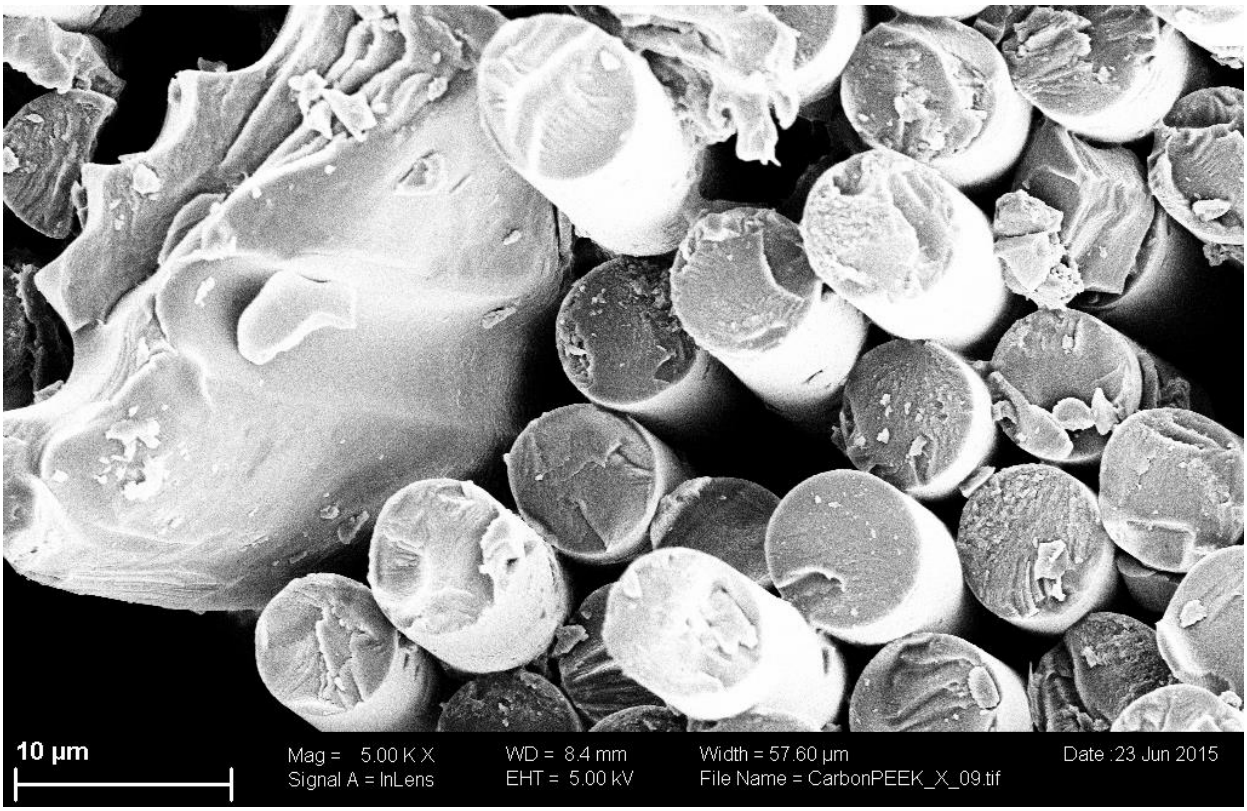

Figure APPENDIX C.11. Carbon fiber –PEEK commingled yarn. Cross section.

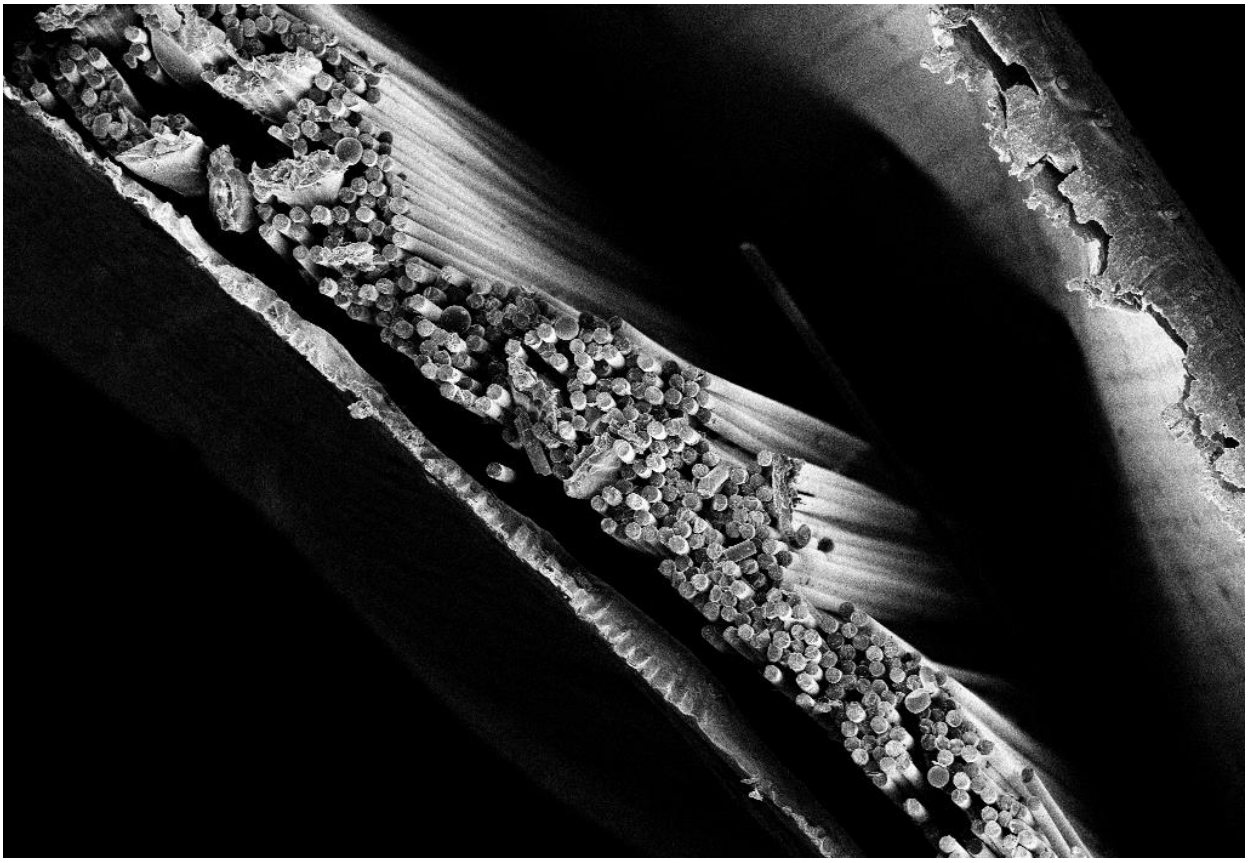

Figure APPENDIX C.12. SEM image, cross section PEEK-Carbon fiber

Figure APPENDIX C.13 shows the TGA measurements on the CF-PEEK commingled yarn. The material starts the degradation at approximately 540 °C. The fiber weight % is 76%. This measurement could be overestimated because both materials mingled have a near degradation temperature, so it is possible for the carbon fiber to start the degradation before the PEEK matrix is completely degraded.

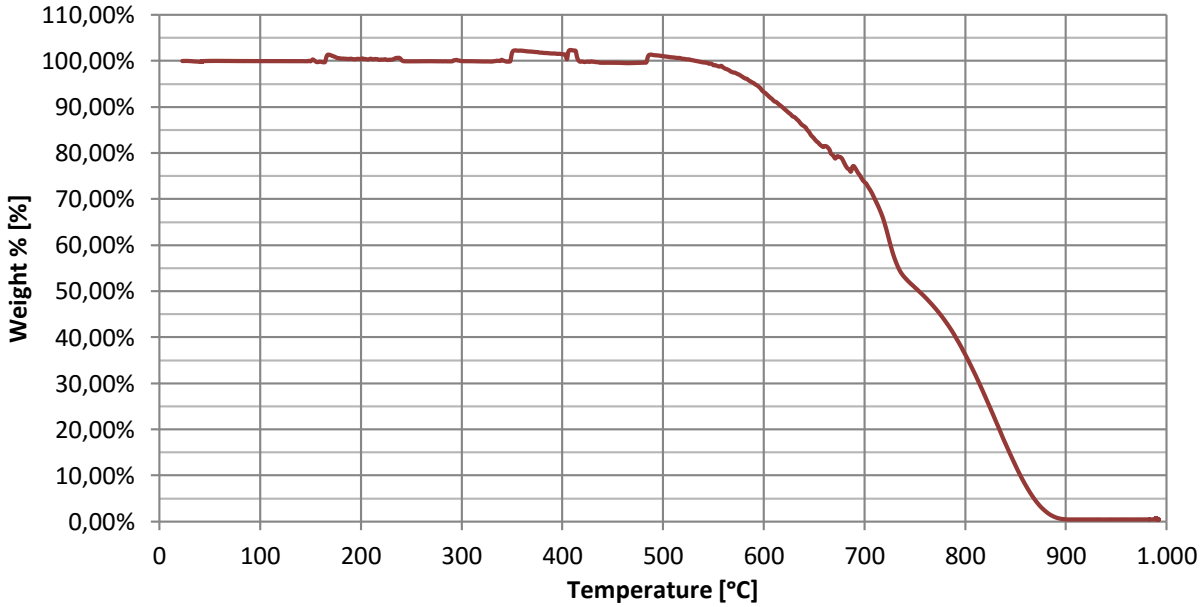

Figure APPENDIX C.13. Thermogravimetric analyze measurements CF-PEEK

Figure APPENDIX C.14 show the DSC measurements of the CF-PEEK commingled yarn. The thermoplastic material starts the melting transition at approximately 320°C and finish at 350°C approximately. Results shown on Table APPENDIX C.2.

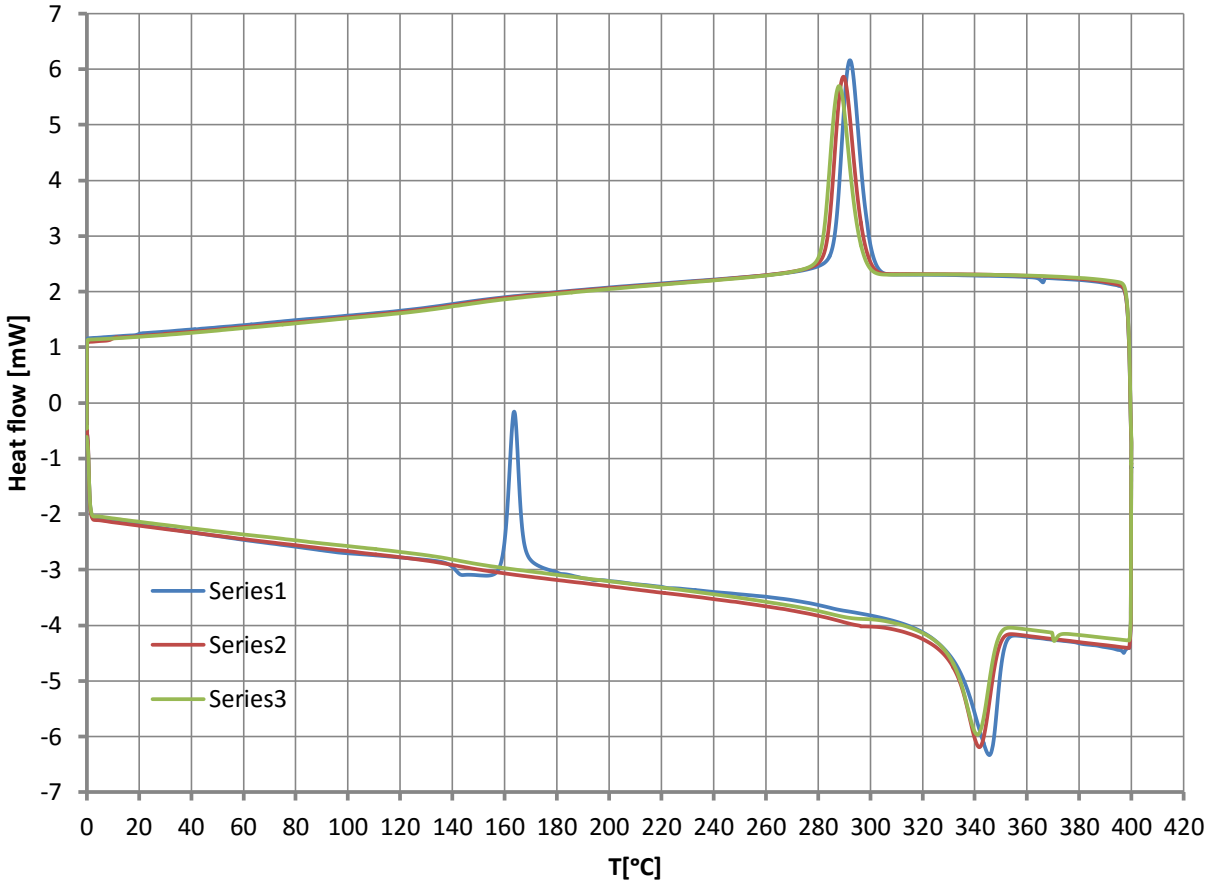

Figure APPENDIX C.14. Differential scanning calorimetry measurements. CF-PEEK commingled yarn.

APPENDIX D.

Void content standard deviation calculation

This section explain the calculations of the standard deviation for the void content obtained by method 1. As explained in section 6.1, first the density of the specimens is calculated, then the void content is obtained by the relation between the real density and the theoretical density at 0% volume content. Finally the void content is corrected using a lineal regression with the results of method 2 void content calculation.

The standard deviation of an indirect magnitude calculated from direct depended magnitudes is calculated as follow:

Being $z = q(x, y, \dots)$ then (APPENDIX D.1)

$$s(z) = \sqrt{\left(\frac{\partial q}{\partial x}\right)^2 s^2(x) + \left(\frac{\partial q}{\partial y}\right)^2 s^2(y) + \cdots} \quad \text{(APPENDIX D.2)}$$

D.1 Void content % standard deviation

The void content % calculated by method 1 is an indirect measurement obtained from the density of the specimens and the theoretical density.

D.1.1 Specimens density standard deviation

The specimen's density is calculated through the measurements of the inner diameter, the specimen's thickness, the specimen's length and specimen's weight.

Volume standard deviation

The inner diameter is stablished as a reference of the section, therefore the standard deviation is considered null. The standard deviations of the thickness and length are calculated

The outer diameter is calculated from the inner diameter and the thickness.

$$d_{out} = d_{in} + 2e \quad \text{(APPENDIX D.3)}$$

So the outer diameter standard deviation is:

$$S(d_{out}) = \sqrt{2^2 S^2(e)} \quad \text{(APPENDIX D.4)}$$

The specimen's volume is obtained using the following expression:

$$V = \frac{\pi}{4}\left(d_{out}^2 - d_{in}^2\right)L \quad \text{(APPENDIX D.5)}$$

Then the volume standard deviation is obtained,

$$S(V) = \sqrt{\left(\frac{\pi 2L}{4} d_{out}^2\right)^2 S^2(d_{out}) + \left(\frac{\pi}{4}\left(d_{out}^2 - d_{in}^2\right)\right)^2 S^2(L)} \quad \text{(APPENDIX D.6)}$$

Density standard deviation

The density deviation is calculated with the calculated volume and the measured density as follow,

$$\rho_{comp} = \frac{Mass}{Volume} \quad \text{(APPENDIX D.7)}$$

Then the standard deviation of the density is obtained as follow:

$$S(\rho_{comp}) = \sqrt{\left(\frac{1}{V}\right)^2 S^2(m) + \left(\frac{m}{V^2}\right)^2 S^2(V)} \quad \text{(APPENDIX D.8)}$$

D.1.2 Specimen's theoretical density standard deviation

The theoretical density of the specimens is obtained using the volume reinforcing fiber % calculated in the parameter characterization and the theoretical densities of Twaron and Polyamide 6 materials.

$$\rho_{th} = \rho Twaron * Vf\% - \rho PA6 * (1 - Vf\%) \quad \text{(APPENDIX D.9)}$$

The standard deviation of the theoretical density is caused by the Volume fiber % calculation.

$$S(\rho_{th}) = \sqrt{(\rho Twaron - \rho PA6)^2 S^2(Vf\%)} \quad \text{(APPENDIX D.10)}$$

D.1.3 Void content % standard deviation

Finally the void content % is calculated:

$$V\% = \frac{\rho_{specimens}}{\rho_{th}} \quad \text{(APPENDIX D.11)}$$

So the standard deviation is obtained using the expression:

$$S(V\%) = \sqrt{\left(\frac{1}{\rho_{th}}\right)^2 S^2(\rho_{specimens}) + \left(\frac{\rho_{specimens}}{\rho_{th}}\right)^2 S^2(\rho_{th})} \quad \text{(APPENDIX D.12)}$$

Reference

[1] Advani, Suresh G and Sozer, E. Murat, 2015, Adv. Thermoplastic Composite Manufacturing Processes. In: *Process modeling in composites manufacturing*. 1. New York: Marcel Dekker.

[2] Arhant, Mael, Davies, Peter, Burtin, Christian and Briançon, Christopher, 2015, Thermoplastic matrix composites for underwater applications: *20th International Conference on Composite Materials*. 2015.

[3] ASTM D2344, 2013, Short-Beam Strength of Polymer Matrix Composite Materials and their Laminates. *ASTM International. Standard test method*. 2013.

[4] ASTM D790, 2010, Flexural Properties of Unreinforced and Reinforced Plastics. *ASTM International. Standard test method.* 2010.

[5] ASTM D792, 2008, Density and specific Gravity of Plastics displacement. *ASTM International. Standard test method*. 2008.

[6] Bernet, N., Michaud, V., Bourban, P. E. and Manson, J. A.E., 1999, An Impregnation Model for the Consolidation of Thermoplastic Composites Made from Commingled Yarns. *Journal of Composite Materials*. 1999. Vol 33, no. 8, p 751-772. DOI 10.1177/002199839903300806. SAGE Publications

[7] Cadfil, 2015, Filament Winding Process. Cadfil® - Filament Winding Software & Technology. [online]. [Accessed 3 September 2015]. Available from: http://www.cadfil.com/filamentwindingprocess.html

[8] Cirino, M. and Byron Pipes, R., 1991, In-situ consolidation for the thermoplastic composite ring - residual stress state. *Composites Manufacturing*. 1991. Vol 2, no 2, p 105-113. DOI 10.1016/0956-7143(91)90187-l. Elsevier BV

[9] Colton, J. and Leach, D., 1992, Processing parameters for filament winding thick-section PEEK/carbon fiber composites. *Polymer Composites*. 1992. Vol 13, no 6, p 427-434. DOI 10.1002/pc.750130605. Wiley-Blackwell

[10] DIN 2089-T1, 1984, Zylindrische Schraubendruckfedern aus runden Dräten and Stäben: Berechnung und Konstruktion (Helical compression springs made of round wires and bars. Calculation and construction.). 1984.

[11] DIN 2089-T2, 1988, Zylindrische Schraubendruckfedern aus runden Dräten and Stäben: Berechnung und Konstruktion von Zugfedern (Helical compression springs made of round wires and bars: calculation and construction of tension springs). 1988.

[12] Figliola, R. S and Beasley, Donald E, 2000, *Theory and design for mechanical measurements*. New York: Wiley.

[13] Gennaro, R., Montagna, F., Maffezzoli, A., Fracasso, F. and Fracasso, S., 2011, On-line Consolidation of Commingled Polypropylene/Glass Roving During Filament Winding. *Journal of Thermoplastic Composite Materials*. 2011. Vol 24, no 6, p 789-804. DOI 10.1177/0892705711401849. SAGE Publications

[14] Grote, Karl-Heinrich and Antonsson, Erik K, 2009, *Springer handbook of mechanical engineering*. New York: Springer.

[15] Gruber, Mark B and Lamontia, Mark A, 2015, The fabrication and performance of ring-stiffened cylinders manufactured by a combined in situ automated thermoplastic filament winding and tape laying process. *Accudyne Systems Inc. white papers* [online]. 2015. [Accessed 25 September 2015]. Available from: http://www.accudyne.com/sites/default/files/JEC2004.pdf

[16] Henninger, F, Hoffmann, J and Friedrich, K, 2002, Thermoplastic filament winding with online-impregnation. Part B. Experimental study of processing parameters. *Composites Part A: Applied Science and Manufacturing*. 2002. Vol 33, no 12, p 1684-1695. DOI 10.1016/s1359-835x(02)00136-7. Elsevier BV

[17] Henninger, F. and Friedrich, K., 2002, Thermoplastic filament winding with online-impregnation. Part A: process technology and operating efficiency. *Composites Part A: Applied Science and Manufacturing*. 2002. Vol 33, no 11, p 1479-1486. DOIÂ 10.1016/s1359-835x(02)00135-5. Elsevier BV

[18] Hou, Meng, Ye, Lin and Mai, Yiu-Wing, 1995, Advances in processing of continuous fibre reinforced composites with thermoplastic matrix. *Plastics rubber and composites processing and applications*. 1995. Vol 23, no 5, p 279-293.

[19] Hulcher, A. B, Marchelo, J. M. and Hinkley, J. A., 1998, Correlation between double cantilever beam and wedge peel tests for automated tow placement. *Science of advanced materials and process engineering series*. 1998. Vol 43, p 1955-1965.

[20] Kim, Hee June, Kim, Sun Kyung and Lee, Woo Il, 1996, A study on heat transfer during thermoplastic composite tape lay-up process. *Experimental Thermal and Fluid Science*. 1996. Vol 13, no 4, p 408-418. DOI 10.1016/s0894-1777(96)00095-7. Elsevier BV

[21] Kim, S.K, Kim, G.M, Kim, H.J and Lee, W.I, 2002, An Experimental Study on the Thermoplastic Filament Winding Process Using Commingled Yarns. *Advanced Composite Letters*. 2002. Vol 11, no 2, p 67-71.

[22] Kremers, Marcus, Steuten, Bart, de Boer, Henk and Kanter, Jens de, 2015, Thermoplastic composite pipe; Operational experience in deepwater and technology qualification. *Airbone* [online]. 2015. [Accessed 16 September 2015]. Available from: http://airborne-oilandgas.com/

[23] Kyosev, Y, 2015, Chapter 10. Yarn winding operations in braiding. In: *Braiding technology for textiles*. 1. Woodhead PUB.

[24] Lamontia, Mark A. and Gruber, Mark B., 2002, Design, Manufacturing and Hydrotesting of Thermoplastic, Ring-Stiffened Composites for Deepsea Pressure Hulls. *Accudyne Systems, Inc*. 2002. Vol, Newark, DE.

[25] Lauke, B, Schone, A, Friedrich, K, Chandra, T and Dhingra, AK, 1993, High Performance Thermoplastic Composites Fabricated by Filament Winding. In: *ADVANCED COMPOSITES '93: INTERNATIONAL CONFERENCE ON ADVANCED COMPOSITE MATERIALS*. 1993. p 883-889.

[26] Lauke, B., Beckert, W. and Schneider, K., 1994, Interlaminar shear strength evaluation of curved composite samples. *Appl Compos Mater*. 1994. Vol. 1, no. 4, p. 267-271. DOI 10.1007/bf00568283. Springer Science + Business Media

[27] Lauke, B. and Friedrich, K., 1993, Evaluation of processing parameters of thermoplastic composites fabricated by filament winding. *Composites Manufacturing*. 1993. Vol 4, no 2, p 93-101. DOIÂ 10.1016/0956-7143(93)90076-k. Elsevier BV

[28] Little, John Eric, Yuan, Xiaowen and Jones, Mark Ian, 2012, Characterization of voids in fibre reinforced composite materials. *NDT & E International*. 2012. Vol 46, p 122-127. DOI 10.1016/j.ndteint.2011.11.011. Elsevier BV

[29] MACK, J and SCHLEDJEWSKI, R, 2012, Chapter 7. Filament winding process in thermoplastics. In: *Manufacturing Techniques for Polymer Matrix Composites (PMCs)*. 1. Woodhead Publishing.

[30] Mäder, E., Rausch, J. and Schmidt, N., 2008, Commingled yarns - Processing aspects and tailored surfaces of polypropylene/glass composites. *Composites Part A: Applied Science and Manufacturing*. 2008. Vol 39, no 4, p 612-623. DOI 10.1016/j.compositesa.2007.07.011. Elsevier BV

[31] Mantell, S.C, Wang, Q. and Springer, G.S., 1991, Thermoplastic tape laying. *36th International SAMPE Symposium*. 1991. Vol.36, p1763-1772.

[32] Martinez Miralles, Jordi and Puig Ortiz, Joan, 2003, *Chapter 3: Error en cadenes de mesura (Error in measure chains). Apunts d'assaig de màquines (Machine testing notes)*. [Barcelona]: J. Puig.

[33] Mazumdar, S. K. and Hoa, S. V., 1995, Manufacturing of Non-axisymmetric Thermoplastic Composite Parts by Tape Winding Technique. *Materials and Manufacturing Processes*. 1995. Vol 10, no 1, p 47-56. DOIÂ 10.1080/10426919508934997. Informa UK Limited

[34] Minnesota Rubber and QMR Plastics, 2003, Section 5. Plastic and Thermoplastic Elastomer Materials. *Copyrights ©2003 Minnesota Rubber and QMR Plastics. All rights reserved.* [online]. 2003. [Accessed 18 September 2015]. Available from: http://www.allsealsinc.com/05_Plastic-Thermoplastic.pdf

[35] NPTEL, 2015, Module 2. Measurement systems. Errors and calibration. [online]. 2015. [Accessed 20 September 2015]. Available from: http://www.nptel.ac.in/courses/108105063/pdf/L-10(SS)%20(IA&C)%20((EE)NPTEL)%20.pdf

[36] Ogale, Vinayak and Alagirusamy, Ramasamy, 2008, Structural analysis of Commingled yarns. *Department of textile technology, Indian Institute of technology. Delhi 10016, India*. 2008.

[37] Oster, F, Haupert, F and Friedrich, K, 2003, Advanced slide bearings: Thermoplastic filament winding combined with injection molding. *S.A.M.P.E. journal*. 2003. Vol 39, no 2, p 54-63.

[38] Perkin Elmer, 2015, *Frequently asked questions. Thermogravimetric Analysis (TGA)*. PerkinElmer.

[39] Peters, S. T., 2011, Chapter 6. Control of filament winding parameters. In: *Composite Filament Winding*. 1. ASM International. ISBN: 978-1-61503-722-3.

[40] Peters, S.T., 2011, Chapter 7. Filament winding technology learned. In: *Composite Filament Winding*. 1. ASM International. ISBN: 978-1-61503-722-3.

[41] Riba i Romeva, Carles, 1993, *Disseny i càlcul de molles (Design and calculation of springs)*. [Barcelona]: Edicions UPC.

[42] Riba i Romeva, Carles, 1994, *Disseny de màquines (Machine design)*. Barcelona: Edicions UPC.

[43] Rocher, J.-E., Allaoui, S., Hivet, G., Gillibert, J. and Blond, E., 2014, Experimental characterization and modeling of GF/PP commingled yarns tensile behavior. *Journal of Composite Materials*. 2014. Vol 49, no 21, p 2609-2624. DOIÂ 10.1177/0021998314551035. SAGE Publications

[44] Rogers, T.G., 1989, Rheological characterization of anisotropic materials. *Composites*. 1989. Vol 20, no 1, p 21-27. DOI 10.1016/0010-4361(89)90677-0. Elsevier BV

[45] Rosselli, Francesco, Santare, Michael H. and Güçeri, Selçuk I., 1997, Effects of processing on laser assisted thermoplastic tape consolidation. *Composites Part A: Applied Science and Manufacturing*. 1997. Vol 28, no 12, p 1023-1033. DOI 10.1016/s1359-835x(97)00072-9. Elsevier BV

[46] Schledjewski, R., 2009, Thermoplastic tape placement process in situ consolidation is reachable. *Plastics, Rubber and Composites*. 2009. Vol 38, no 9-10, p 379-386. DOIÂ 10.1179/146580109x12540995045804. Maney Publishing

[47] Schledjewski, Ralf and Miaris, A, 2009, Thermoplastic Tape Placement by Means of Diode Laser Heating. In: *Symposium; 54th, SAMPE*. Covina, CA. 2009. p 222.

[48] TEIJIN, 2015, Twaron a versatile high-performance fiber. [online]. 2015. [Accessed 4 September, 2015]. Available from: http://www.teijinaramid.com/wp-content/uploads/2012/02/1090308_Twaron-productbrochurefinal_051.pdf

[49] Thomann, Urs Ivan, 2003, *Direct Stamp Forming of Non-consolidated Carbon/Thermoplastic Fibre commingled Yarns*. Ph. D. Thesis. ETH Zurich. Swiss Federal Institute of Technology in Zurich.

[50] Toso, Yves Marcel Pierre, 2003, *Effective Automated Tape Winding Process with On-Line Bounding under Transient Thermal Conditions*. Ph. D. Thesis. ETH Zurich. Swiss Federal Institute of Technology in Zurich.

[51] W. Radford, Donald and M. Hedin, Kevin, 2015, Fused deposition technology applied to thermoplastic matrix placement and wetout in filament winding. In: *20th International Conference on Composite Materials*. 2015.

[52] Wagner, Matthias and Widmann, Georg, 2009, *Thermal analysis in practice*. Schwerzenbach: Mettler-Toledo.